# Self-assembling Phosphoramidate Pronucleotides: Enzymatic Regulation and Application Towards Therapeutic Delivery

A DISSERTATION
SUBMITTED TO THE FACULTY OF THE
UNIVERSITY OF MINNESOTA
BY

**Harrison Trent West**

IN PARTIAL FULFILLMENT OF THE REQUIREMENTS
FOR THE DEGREE OF DOCTOR OF PHILOSOPY

**Dr. Carston R. Wagner, Adviser**

**August 2019**

## ACKNOWLEDGMENTS

Completion of my graduate studies would not have been possible without the support and guidance of many people. Firstly, I would like to thank my advisor Dr. Carston (Rick) Wagner for accepting me into his research group and providing patient tutelage through my studies. His enthusiasm and support were essential to my progress in developing a new research focus in the lab and learning new skills and techniques well outside my comfort zone. Dr. Wagner has also strongly supported my activities outside the laboratory including internships with both the Economic Development Fellows Consulting Program and the Office of Technology Commercialization, both of which were essential in developing my career interest in pursuing commercialization of my own research. I would also like to thank past and present members of the Wagner laboratory for their mentorship and friendship throughout the years. Special thanks are owed to Dr. Cliff Csizmar for his expertise in Transmission Electron Microscopy which became an essential technique in the completion of my thesis work, and Dr. Jacob Petersburg for his friendship and inspiration to explore professional development opportunities, and Dr. Cody Lensing for his friendship and support throughout my graduate school career. I would also like to acknowledge Dr. Lakmal Rozumalski, Dr. Justine Delgado, Dr. Rachit Shah, Dr. Aniekan Okon, Ozgun Kilic, Alex Strom, Ellie Mews, Wang Yiao, Max Dillenburg, and Nicole Bentz.

## DEDICATIONS

Everything that I have achieved and everything that I will achieve, has been made possible only through the loving support of my family and friends. This thesis is dedicated to my parents Mark and Melanie, my sister Caroline, my grandparents, Susannah, Dan, and especially my partner, Victoria.

Thank you, and I love you all.

## ABSTRACT

Prior characterizations of the nucleoside phosphoramidate moiety have centered upon the ability of amine containing side-chains to mask the negative charge inherent to monophosphorylated nucleosides for the purpose of enhancing their passive movement across biological membranes. When used for the intracellular delivery of therapeutic nucleoside monophosphate analogs, these molecules are referred to as phosphoramidate "ProTides" and represent an important class of antiviral and anticancer prodrugs. The primary aim of this thesis to build upon these works and present the nucleoside phosphoramidate moiety as a multifunctional regulator of molecular self-assembly. Appendage of nucleoside phosphoramidates to molecules such as self-assembling peptides was shown to modulate the self-assembling properties of the molecules through alteration of the non-covalent interactions between individual monomers and nanostructure assemblies. Additionally, the nucleoside phosphoramidate moiety was found to impart enzyme responsive qualities. Histidine triad nucleotide binding proteins (Hints), an enzyme class that possesses phosphoramidase activity, were found to regulate the assembly of nucleoside phosphoramidate bearing nanostructures by inducing ionic interaction mediated crosslinking after enzymatic hydrolysis. Chemical modification of self-assembling peptides with nucleoside phosphoramidates bearing non-natural and therapeutic nucleosides was also achieved to effect the first ever demonstrated self-assembling phosphoramidate ProTides as one-component nanomedicines. The developed formulations are currently under investigation for localized delivery of cancer chemotherapeutic prodrugs.

## TABLE OF CONTENTS

## TABLE OF FIGURES

# CHAPTER 1: LITERATURE REVIEW

## 1.1. SELF-ASSEMBLING PEPTIDES AND THEIR DERIVATIVES

Chemistry is the science of atomistic and molecular transformation. As the traditionally regarded "central science", chemistry provides the critical framework for fundamentally understanding how atoms and molecules interact and change one another in natural processes, as well as in the development of new molecules.[1] Both inorganic and organic molecules are designed and synthesized by chemists for applications in all aspects of daily life, with molecular synthesis being the technique by which the manipulation of bonds between atoms is used to create desired changes in molecular structure.[2,3] The resulting orientation and arrangement of atoms within a molecular structure directly determines the physical, chemical, and biological properties of a particular molecule.[4,5]

The propensity of individual molecules to spontaneously associate together in ordered arrangements is one property governed by molecular structure.[6] While the forces holding atoms together within a molecule are largely covalent, the forces enabling intermolecular association are non-covalent.[7] Therefore, in the design and synthesis of self-assembling molecules, consideration must be paid not only to the covalent bonds between atoms, but also to the arrangement of atoms within a molecule to facilitate non-covalent interactions through space. Just as the arrangement of atoms within a molecule dictate structure, the three-dimensional arrangement of non-covalent forces between molecules in turn directly influences the structure of higher ordered molecular assemblies.[8]

Molecular self-assembly is ubiquitous across nature, synthetic chemistry, and materials development.[9] Indeed, biomolecular self-assembly contributes to the vast array

of biological matter consisting the extracellular matrix, cellular and subcellular membranes, and the cytoskeleton.[10] In synthetic chemistry and materials science, molecular self-assembly is readily utilized for the fabrication of nanomaterials and colloids, two-dimensional surface arrays, and mesoscopic to microscopic structures.[8,9,11]

Of significant interest to researchers and clinicians is the development of novel self-assembling materials for the treatment of disease. As with all self-assembling materials, the molecular subunits consisting supramolecular biomaterials may vary in size and chemical content (inorganic or organic), but must be applied to "support, enhance, or replace" diseased or damaged tissues and biological systems.[12–14]

Historically, biomaterials have included a range of materials such as bulk metals, ceramics, glass, and both natural and synthetic macromolecules.[15] Early biomaterials contributed to significant clinical advances in a range of medical fields such as orthopedic and dental implants, heart valve replacement, and surgical tools such as synthetic sutures.[15] The maturation of biomaterials science has led to the integration of the disciplines of clinical science, engineering, chemistry, and biology to effect the development of third generation biomaterials.[16] The goal of this next generation of materials is to move beyond enhancements in biocompatibility and demonstrate the potential to influence and guide biological interactions.[16] While traditional biomaterials maintain utility in a wide variety of biomedical applications, a desire to achieve the aims of third generation development has led researchers to investigate and develop materials with dynamic and tunable properties while also possessing biologically active moieties.[17–19]

**Figure 1.1 Characteristics of supramolecular biomaterials. Adapted from Webber et al.12**

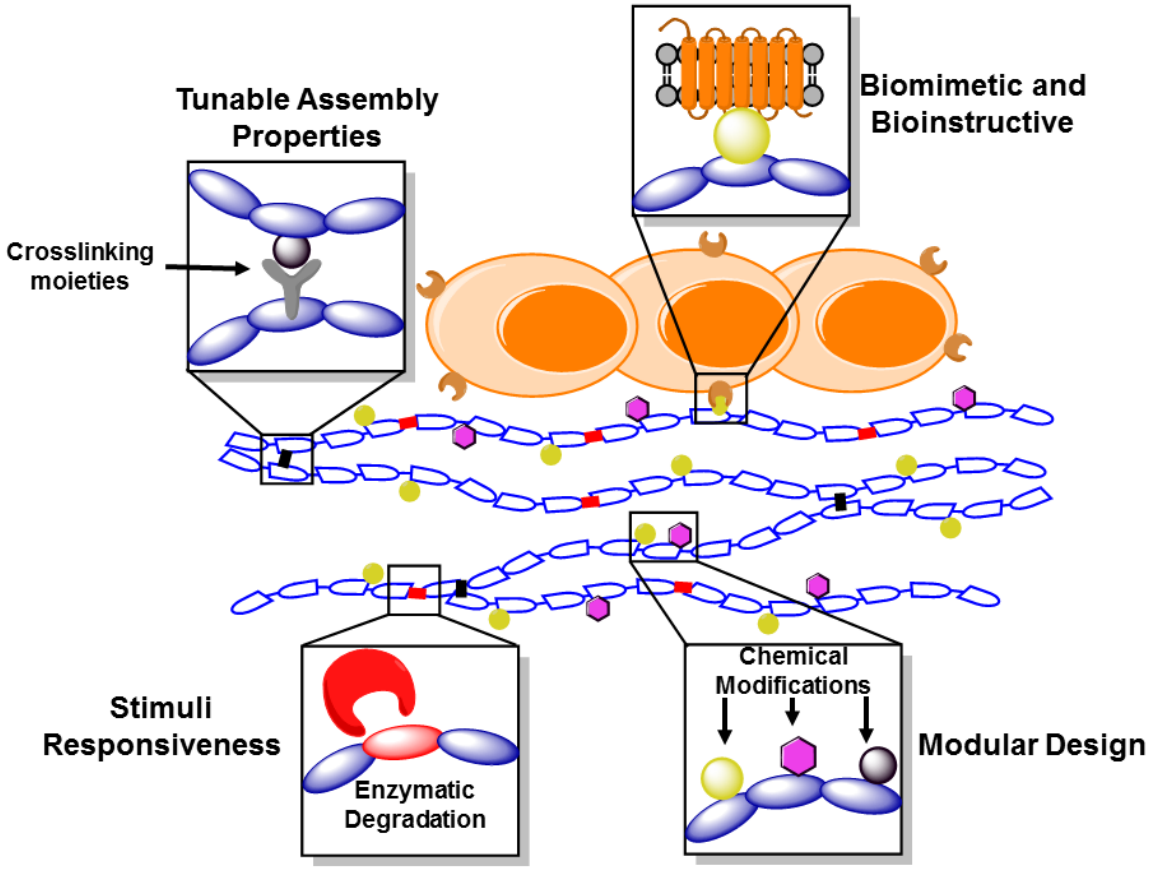

**Figure 1.2 Assembly formats of supramolecular biomaterials. Adapted from Webber et al.12**

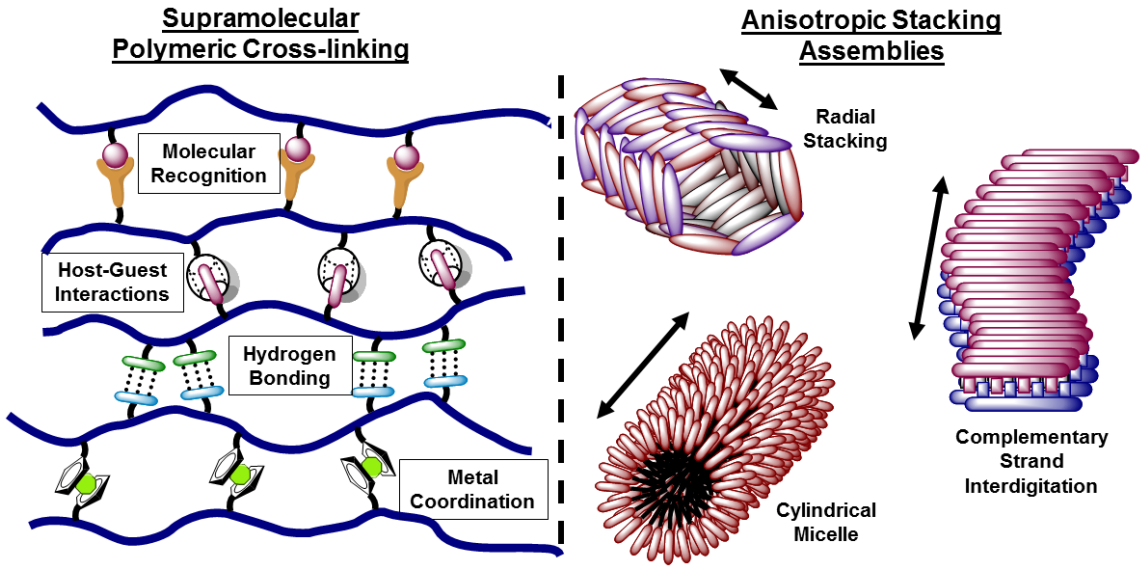

The fundamental properties of supramolecular biomaterials position them to be ideal in fulfilling the needs with which third generation biomedical materials have been tasked. Self-assembly relies upon combinations of non-covalent inductive and dispersive forces to achieve intermolecular cohesiveness.[20] Individually, these forces are small in magnitude and considerably weaker than covalent interactions. Nevertheless, these forces function in concert to confer mechanical properties to supramolecular materials approaching that of conventionally used cross-linked polymers and macromolecular systems.[12,13] Individually weak interactions between monomer units convey inherent sensitivity to stimuli as individual interactions may be modulated by biological, chemical, and physical cues to affect bulk properties.[21] This feature is currently being applied to achieve dynamic spatiotemporal control of biomaterials within living systems.[17,21] In addition, the chemical motifs driving molecular recognition and self-assembly are highly specific in their molecular recognition properties enabling rational design of supramolecular assemblies incorporating these motifs.[22] The highly ordered self-organization of the motifs enables modification of individual monomer units for the display of additional functional and responsive domains. The ability to combine multi-domain functional monomers into a single material further approaches the dynamic modularity displayed in biological systems and furthers the aim towards the development of biologically interactive and integrable therapeutic materials (**Figure 1.1**, adapted from Webber et al.).[12,22]

Two general assembly formats have been described for self-assembling biomaterials depending on the size of the molecules utilized and the non-covalent

interactions between them (**Figure 1.2**, adapted from Webber et al.).[12] Large linear polymeric molecules, otherwise unassociated except through chain entanglement, may be physically cross-linked through incorporated molecular recognition motifs.[12,13] Both synthetic and natural polymers traditionally lacking crosslinking moieties may be chemically modified with such crosslinking motifs along the length of the molecule to enable multiple association events to generate a supramolecular polymeric network. Utilization of "host-guest" interactions through incorporated macrocyclic hosts such as cyclodextrin and cucurbit[n]urils and a variety of hydrophobic guest ligands, complimentary hydrogen bonding moieties, and metal and chelating ligand combinations have been incorporated into supramolecular designs.[13,23–25] An alternative method to direct chemical incorporation of molecular recognition motifs is crosslinking polymer-nanoparticle interactions. In these systems crosslinking is achieved through complimentary chemistries on both the polymer and nanoparticle surface and can even be extended to the 3-D assembly of polymeric microgel particles.[26,27]

Low molecular weight organic molecules and peptides have been widely investigated for their self-assembling properties and for application as novel biomaterials.[28,29] In contrast to the cross-linking of linear polymers, these lower molecular weight molecules assemble into high-aspect ratio structures such as tubes, ribbons, and fibers (**Figure 1.2**, adapted from Webber et al.).[12] Non-covalent interactions leading to these assembly modes commonly include aromatic interactions and hydrogen bonding patterns between the peptide components leading to β-sheet, alpha-helical coiled-coil, and triple helix motif formation.[30] These interactions enable molecular stacking of individual

monomers into highly specific and ordered structures, eventually forming entangled matrices constituting supramolecular hydrogels.[31] In addition to conventional peptide monomers, chemical modification of peptides with alkyl chains has generated the seminal class of synthetic self-assembling molecules termed peptide amphiphiles.[32] The hydrophobic nature of the appended alkyl chains contributes to hydrophobic interactions between monomers which are stabilized by hydrogen bonds in the peptide block. Additional charged moieties in the peptide farthest away from the alkyl chain contribute to solubilization enabling the formation of cylindrical micelles or ribbon like nanofibers. In addition to lipophilic modification, biofunctionalities including nucleobases and synthetic moieties may also be used to direct monomer assembly alone or appended to peptides.[33,34] Engineered polypeptides are a similar class of self-assembling monomer that extends the functionality of small molecule peptide monomers to include high molecular weight macromolecules obtained through recombinant expression.[35] The resulting monomers may assemble into an array of structures dictated by the orientation of interacting interfaces and non-covalent interactions, but may also assemble into the oligomeric amyloid type assemblies exhibited by self-assembling peptides.[35]

As a class, supramolecular biomaterials hold significant therapeutic potential in applications such as drug and biologics delivery, tissue engineering and regeneration, imaging and diagnostics, immune therapy, synthetic biology, and bioelectronics to name a few.[31,36–42] The low molecular weight of monomers in this class of biomaterial enables high levels of control over chemical composition and heterogeneity as small molecules and peptides may be synthesized through conventional organic methods and even solid phase

synthesis.[28,29,43] The low molecular weight of these agents also facilitates biocompatibility including resistance to immunogenicity as small molecules do not generally induce an immune response without a carrier adjuvant. Moreover, the lack of exotic features in molecules such as self-assembling peptides consisting of short amino-acid sequence repeats further contributes to their lack of immune recognition.[38,39,44,45] Small molecules are also readily metabolized and cleared from tissues and systemic circulation and can be designed for degradation into biologically safe components by specific enzymes.[40,46] The ease of synthesis of these molecules further facilitates the incorporation of biological recognition motifs, signaling molecules, therapeutic moieties, and even components for material regulation (**Figure 1.3**).[32,33,47–49]

In this review, we aim to discuss recent advances in the biomedical application of self-assembling peptides and related derivatives with specific emphasis on rationally designed biological instructiveness, integrability, responsiveness, and *in vivo* regulation. Although the subject of intense investigation, self-assembling peptides and related molecules represent comparatively few clinically approved platforms.[18,39,50,51] It is our goal to highlight emerging areas of potential clinical success and to shed light on potential novel applications of these materials to address unmet medical needs. We begin the review with brief introductions of the general classes of self-assembling peptides and derivatives to facilitate later discussions regarding their specific application.

### 1.1.1 CLINICALLY USED SELF-ASSEMBLING PEPTIDES

**Figure 1.3 Characteristics of low molecular weight supramolecular biomaterials**

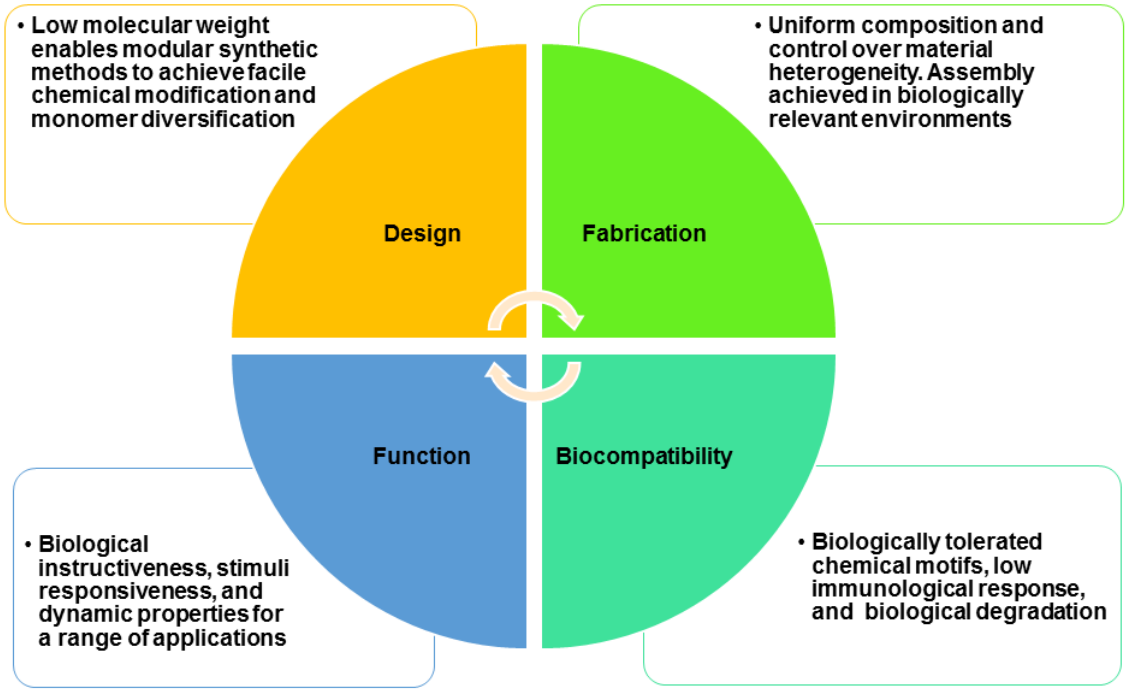

**Figure 1.4 Commercialized self-assembling peptides**

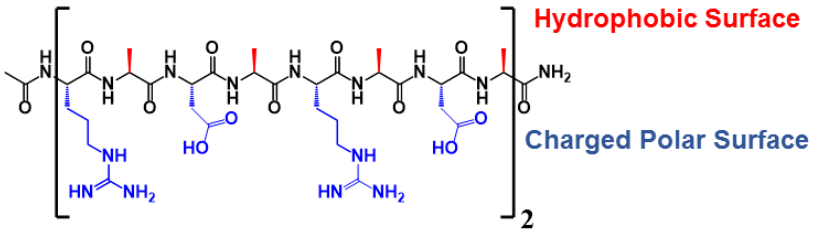


**RADA16-1 (Purastat)**

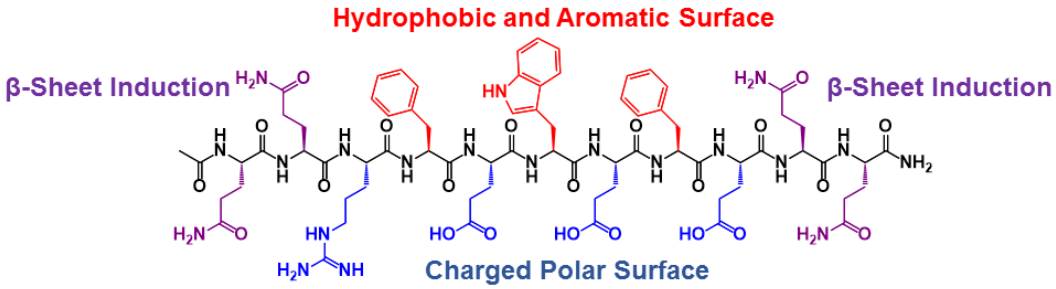


**$P_{11}$- 4 (Curodont)**

The discovery of the self-assembling protein sequence derived from zuotin, which contains a repeated sequence of the amino acids glutamic acid (E), alanine (A), and lysine (K) (n-AEAEAKAKAEAEAKAK-c) later termed EAK16-II, was a seminal observation in the field of self-assembling peptides.[49,52] The observation of self-complementary amino acid repeats within the sequence was originally investigated to determine the effects of ionic interactions within the highly charged oligopeptide as influencers of secondary structural characteristics. Serendipitously, the peptide was observed to undergo spontaneous self-assembly into nanofibrous structures in aqueous buffer of sufficient ionic strength. At the macroscopic scale, the nanofibrous structures formed membranes which were found to be thermally, chemically, and biologically stable. Curiously, the experimentally observed β-sheet secondary structure formed in the peptide assemblies was distinctly different from the computationally predicted α-helix.[52] The implications of this secondary structural motif driven by self-complementary ionic bridges and paired hydrophobic interactions provided the basis for expansion into synthetic derivatives based upon the same principles that have driven the field of self-assembling peptides for nearly three decades.[53]

These patterns of self-complementarity were readily utilized to design an entire class of *de novo* self-assembling peptides through careful balancing of the sequence and order of ionic and hydrophobic residues. Redesign of the EAK16-II peptide yielded changes in the length of oppositely charged blocks, as well as mix-and-matching of various ionic and hydrophobic amino acids to yield a plethora of derivatives.[54] One group of derivatives formed by through replacement of Glutamate with Aspartate, and Lysine with

Arginine, within the self-assembling peptide core generated the RADA16 series of self-assembling peptides. Important not only for their self-assembling properties and contribution to the basic understanding of supramolecular assembly, the RADA16 series of peptides realized successful commercial and clinical translation as hydrogels for tissue culture, as well as their clinical application as surgical aids, gels for regenerative medicine, and therapeutic delivery vehicles.[49,55] RADA16-I (RADARADARADARADA), commercially recognized as Purastat (3D-Matrix, Ltd.), is currently under clinical investigation as a hemostatic agent for endonasal, gastrointestinal, and hepatic surgeries (**Figure 1.4**).[56–58] The hemostatic properties of RADA16-I is proposed to result in part from the ionic strength triggered gelation mechanism of these peptides. Because of the ionic content of bodily fluids, the application of nanofiber solutions at sites of bleeding and hemorrhage rapidly generates gels to effect the hemostatic effect.[56–58] Purastat (RADA16-I) is clinically approved for its function as a hemostat in several countries and currently undergoing clinical trials in the USA.[39,49]

A transmembrane receptor domain of the IsK potassium channel was the inspiration of a series of self-assembled peptides that eventually became clinically used biomaterials for dental application. The 27 amino acid transmembrane domain was originally investigated in order to determine its β-sheet secondary structure character within lipid membranes through a series of biophysical studies.[59] Subsequent investigation of the peptide and a shortened 24 amino acid derivative revealed their ability to form organogels.[59,60] Like the previously mentioned families of peptides, hydrophobicity was found to play a key role in the ability of these peptides to become amphiphilic detergents

and thus not undergo gelation even in the presence of polar protic solvent.[59] Although increasing polarity was found to trigger the requisite structural transition for gelation, the studied peptides were found to be insoluble in water.[59]

To guide the *de novo* design of self-assembling peptides, Aggeli and colleauges developed a series of criterion which were used to instruct the development of gel forming peptide assemblies for biomedical application. The design of self-assembling peptides should incorporate (1) complementary ionic, hydrophobic, and hydrogen bond interactions among the side-chains, (2) lateral recognition between adjacent molecules to impart directionality and high aspect ratio features to the assemblies, and (3) hydrophilic surfaces to impart solubility in aqueous solutions through solvent interactions.[60] Consideration of the above guidelines led the group to synthesize a *de novo* oligopeptide referred to as DN1. Characterization of the peptide revealed its sequence (Ac-Gln-Gln-Arg-Phe-Gln-Trp-Gln-Phe-Glu-Gln-Gln-$NH_2$) imparted β-sheet forming character as well as linear assembly in aqueous environment.[60] The oppositely charged Arg and Glu residues contributed an antiparallel orientation of the β-sheet assembly, while a combination of hydrophobic interactions provided by the methylene units of the amino acid side chains and aromatic interactions between Trp and Phe residues aided inter-strand recognition.[60] The guiding principles of rational design leading to the DN1 were contrasted with a poly-Gln 11-mer peptide which similarly underwent assembly into β-sheet structures with adequate interstrand recognition, but formed insoluble aggregates in aqueous solution due to the lack of sufficient solvating polar residues.[60] In subsequent investigations, insertion and replacement of charged residues within the peptide was performed to determine the effect

on pH responsiveness. DN1's gelation capability was found to be significantly tied to pH, with gel phase formation at pH values lower than 5 and flocculated aggregates above pH 5 due to charge neutralization.[61] Subsequent replacement of Glu with a Gln residue yielded a singly ionizable peptide termed $P_{11}$-2 which formed a stable gel at pH values as high as 10 due to the ionization state of the Arg residue. A derivative of DN1 with sequence Ac-Gnl-Gln-Arg-Phe-Glu-Trp-Glu-Phe-Glu-Gln-Gln-$NH_2$ termed $P_{11}$-4, was determined to be highly sensitive to pH and ionic strength in terms of its assembly due to incorporation of one cationic residue (Arg) and three anionic residues (Glu). Similar to the $P_{11}$-2 peptide, $P_{11}$-4 formed self-assembled hydrogels at pH values between 5 and 7, but disassembled into isotropic solutions at pH values in excess of 7.2 (**Figure 1.4**).[61]

The ability to leverage the ionization state of $P_{11}$-4 in regulation of its assembling properties led to investigation of the peptide for skeletal tissue regeneration and engineering applications.[61–63] Similar to the self-assembling properties of RADA in response to ionic strength contributing to its function as a hemostat, the application of $P_{11}$-4 as a viscous solution at basic pH was envisioned as a delivery method to fill skeletal voids and undergo gelation as a result of *in situ* pH and ionic strength (**Figure 1.4)**.[61] Interestingly, the peptide was explored as a treatment technique for dental caries which are lesions characterized by reduced tooth enamel and mineralization, which affects the stability and mechanical properties of the tooth.[64] Application of the peptide solution and resulting self-assembly into nanotape structures was thought to potentially mimic the original extracellular matrix on which hydroxyapatite is deposited to generate the dental enamel. In the developing tooth, extracellular matrix is degraded as the tissue develops and

mineralizes, resulting in a lack of fibrous structures to allow remineralization in cases of later tooth disease or damage.[65] The supramolecular peptide scaffold of $P_{11}$-4 was found to contribute to deposition of hydroxyapatite crystals with its highly polar solvent exposed surfaces, high aspect ratio assembly, and high degree of order.[63] Compared to controls, application of $P_{11}$-4 peptide solution to teeth was found to reduce demineralization under acid conditions and contribute to remineralization at physiologic pH. $P_{11}$-4 gels were also able to form *de novo* hydroxyapatite in the absence of teeth, with areas of mineralization found throughout the gel structure which were absent in a comparative gelatin gel.[63] With these positive clinical results, the $P_{11}$-4 peptide has been commercialized as Curodont by the Swiss company Credentis and successfully translated into the clinic.[62,66] The agent has been approved in Europe for treating caries lesions and has also been applied for the treatment of sensitive teeth and enamel erosion protection.[67]

### 1.1.2 CLASSES OF SELF-ASSEMBLING PEPTIDES AND DESIGN CONSIDERATIONS

The previously mentioned examples comprise only a small portion of investigated self-assembling peptide platforms for biomedical applications. Numerous other β-sheet forming peptides have been investigated for their self-assembling properties which constitute one of the more well studied and diverse families of self-assembling molecules.[68–70] Other classes of self-assembling peptides have also been developed including α-helix forming peptides, aromatic peptides, and peptide amphiphiles. These are largely distinguished from one another by the non-covalent forces driving assembly and

their effect on resulting structural features of their assemblies. As these aspects have been reviewed elsewhere, we will only briefly introduce the various classes of investigated self-assembling peptides and considerations for their design and resulting morphology. [32,36,49,68,71]

#### 1.1.2.1. BETA-SHEET FORMING PEPTIDES

Following the discovery of the EAK and RADA classes of self-assembling peptides, understanding the thermodynamic and kinetic parameters and how they are affected by the non-covalent interactions leading to self-assembly became a primary goal of researchers in the field (**Figure 1.5**).[49] A fundamental investigation conducted following the discovery of EAK16-II sought to determine the effect of sequence modifications on resulting assembly properties.[54] A series of peptides consisting of alternating charged and hydrophobic residues were synthesized which varied in the identity of hydrophobic amino acid incorporated and number of repeated segments. As previous characterizations indicated assembly only in solutions of sufficient salt content, the effect of these modifications on the critical salt concentration for gelation were of primary interest as subsequent biomedical applications would later depend on this feature for *in situ* gelling derivatives. The peptides contained one of either Phe ($FKFE_n$), Ile ($IKIE_n$), or Val ($VKVE_n$) as the hydrophobic amino acids within the repeats.[54] Importantly, the hydrophobic content of the designed peptides was found to have significant consequences on the mechanical properties of resulting fibrous structures, a key feature taken into consideration for later prototype design for specific applications. Increasing side-chain hydrophobicity was found

to reduce the ionic strength dependence of gel formation, and the number of repeat amino acid segments affecting ionic strength dependence in a peptide length coordinated manner (**Figure 1.5**). Additionally, increasing the hydrophobic character of uncharged amino acids was found to result in an increase in self-assembly kinetics.[54]

**Figure 1.5. Structures of β-sheet forming self-assembling peptides**

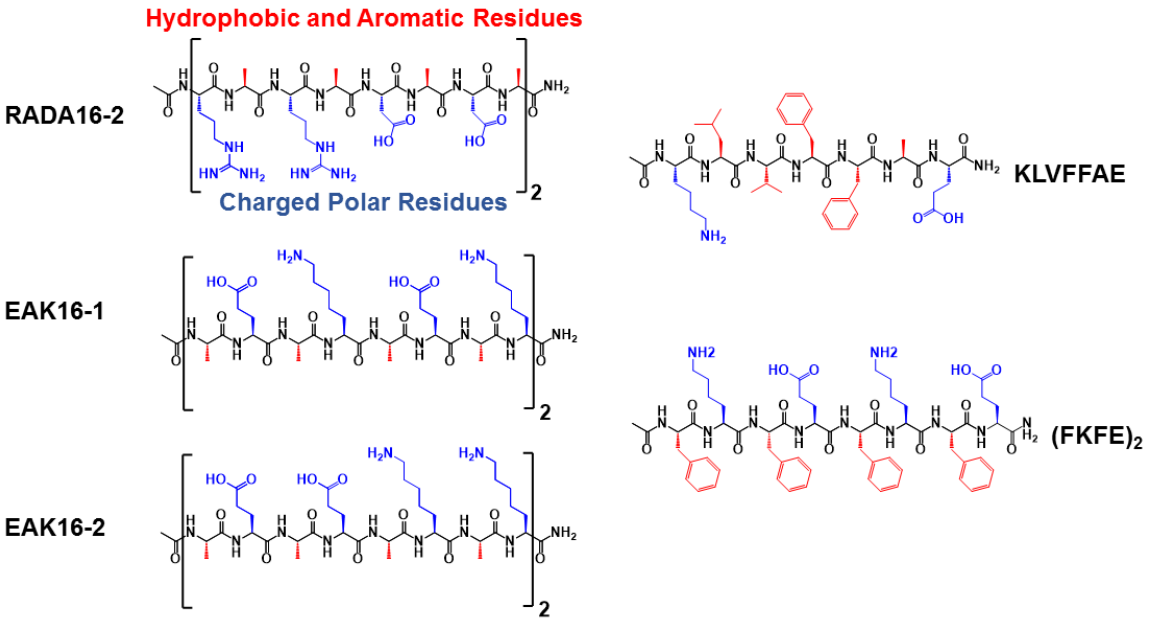

Kinetic enhancement of assembly was later explained by considering the balance of hydrophobic and charged residues within the peptide.[54,72] The energetic penalty for solvating the hydrophobic face of the peptides was determined to be counterbalanced by the charge repulsion experienced by the highly ionic hydrophilic faces. This interplay results in significant charge repulsion between peptides as the energetic barrier preventing the hydrophobic faces from associating at low salt concentrations, as previously demonstrated with application of DLVO theory to the assembly process indicating higher ion valence leading to lower peptide critical assembly concentrations.[72] Increasing ionic strength of the solution lowers the Debye length due to ionic screening, alleviating repulsion and enabling the hydrophobic faces to associate. [54]Furthermore, increasing the bulkiness of the hydrophobic side chain as in the case of the Phe containing peptides, increases the solvation penalty enabling assembly at lower salt concentrations than the respective Ile and Val containing amino acids.[54,72] In addition to the entropic penalty for solvation of the bulky Phe side-chains, association driven by enthalpic aromatic-aromatic interactions could also play a role in facilitating assembly, a thermodynamic factor important in multiple self-assembling peptide classes.[73,74]

Interestingly, the above experiments were performed at low pH where the lysine side chain residues, expected to be protonated, generate a highly cationic form of the peptide leading to the charge repulsion phenomenon.[54,72] Increasing the pH of the peptide solution to neutrality results in spontaneous assembly of the peptides into a fibrous gel matrix. This was further investigated through substitution of the negative Glu residues with uncharged Gln which produced two interesting effects. The first was increased requirement

for salt in solution at low pH, possibly due to reduced hydrogen bonding capability of Gln compared to Glu even in the uncharged state. The second was the ability to remain a viscous liquid at neutral pH and undergo assembly at increasing ionic strength. This is key for biomedical applications as addition of low pH solution is undesirable due to the potential for tissue damage.[54,72]

Substitution of the diphenylalanine residues in the amyloid-β 16-22 peptide (Ac-KLVFFAE-$NH_2$) with hydrophobic residues of varying steric bulk and aromaticity was performed to systematically characterize the effect of these side-chains on self-assembly (**Figure 1.5**).[75] Similar to hydrophobic interactions contributing to self-assembly in the FKFE peptides, the diphenylalanine core in amyloid-β is considered a key driving force in the fibrilization of the full length peptide and has been widely investigated in its own right as a self-assembling motif to be discussed in a later section.[76,77] Both phenylalanine residues were sequentially modified to either Ala, Tyr, cyclohexyl-Ala, or pentafluro-Phe, with the unnatural amino-acids providing key insights into the differing roles of hydrophobicity and aromaticity in driving self-assembly. Interestingly, both Ala and Tyr modification at the amyloid-β19 position prevented self-assembly of their respective peptides indicating that decreasing hydrophobicity was not tolerated at this position. In contrast, sedimentation studies determined that the cyclohexyl-Ala and Pentafluoro-Phe modifications significantly increased the assembly kinetics of their respective peptides.[75] The wild-type peptide exhibited a very slow self-assembly rate and took several weeks to reach an assembly equilibrium.[75] Conversely, the more hydrophobic synthetic modifications rapidly increased the assembly kinetics, reaching assembly equilibria in less

than an hour, with respective critical assembly concentrations for the cyclohexyl-Ala and pentafluoro-Phe modifications of 44 μM and 4 μM respectively.[75] Compared to the wild type peptide which possesses a critical assembly concentration of 33 μM, simple replacement at position-19 with the bulky cyclohexyl side chain is insufficient to recapitulate the aromatic-aromatic interactions present between Phe residues in β-strand oriented peptides and may even induce steric clash due to increased ring size.[75] In contrast, the cyclohexyl-Ala substitution at position-20 where Phe residues are predicted to participate in hydrophobic interactions with the Val residue resulted in a modest decrease of the critical aggregation concentration to 22 μM.[75] In both cases however, the pentafluoro-Phe modification made significant contributions to decreasing the critical aggregation concentration due to its retained aromatic character at position-19, and enhanced hydrophobicity contributed at both positions.[75] Interestingly, the enhanced assembly driving character of the pentafluoro-Phe could also be due to the high fluorous content of the side chain, which could contribute to non-covalent association.[75] Evident from this investigation is the wealth of assembly information that can be garnered from structure activity relationships investigating the role of individual amino-acid residues in promoting self-assembly. Careful tuning of intermolecular interactions through rationally designed amino acid substitutions can potentially play a significant role in guiding the dynamic assembly of peptides for functional benefit.

In addition to the identity of the amino acids, the number of amino acids within the peptide also plays a considerable role in regulating self-assembly. A previously mentioned investigation also looked beyond modifications to amino acid identity to observe the effect

of changing the number of KFE repeats within the self-assembling scaffold.[54] Interestingly, the study revealed a biphasic relationship between peptide length and salt dependence. Although initially decreasing the required salt concentration, continuing to increase the length of the peptide yields diminishing returns. With increasing peptide length, the hydrophobic surface area of the peptide increases faster than net charge, providing longer species and a greater driving force for association. Conversely, very long peptides carry an entropic penalty for self-assembly due to the long-range ordering of the molecules which counteracts the hydrophobic driving force without sufficient charge screening.[54]

These results have been further reflected in more theoretical investigations of peptide self-assembly. One study investigating the balance of enthalpic and entropic forces governing self-assembly of peptides with varying length correlated experimentally observed data with computational methods.[78] Interestingly, only peptides with five or greater residues were found to undergo self-assembly due to lack of enthalpically favored interactions between peptides to afford higher ordered association. Combining molecular dynamics simulations with experimental data revealed increasing peptide length results in sequential entropic penalties of approximately 11$k$ (where $k$ is the Boltzmann constant) per residue. This entropic penalty is associated with not only immobilization of the backbone but also the amino acid side-chains. Experimentally, increasing the peptide length from five to nine residues resulted in sequential decreases in the critical aggregation concentration (defined as the concentration of peptide required to trigger self-assembly) from 170 to 14 μM respectively. Similar to the results of Caplan et al., an eleven residue peptide possessed a critical aggregation concentration of 405 μM which was significantly

greater than the value of 14 μM found for the nine residue peptide.[54,78] Clearly an optimal sequence length is likely to exist in designing self-assembling peptides which is determined by the balance of associative interactions and the requirement for high degrees of peptide ordering.

Interestingly, the progression of monomer aggregation to elongated nanostructure can proceed through a series of transiently stable intermediate structures.[79] Evaluation of the self-assembly kinetics of the FKFEFKFE peptide found that by modulating the pH of the solution, the assembly kinetics could be slowed to allow visualization of time dependent structures using atomic force microscopy (AFM). Initial aggregation of the peptide after dissolution resulted in left-handed helical ribbons approximately 7.1 nm in width with a pitch of approximately 19 nm. After 2h, a second fibrillar species 8 nm in diameter began to form which continued to predominate at longer time points, eventually self-aggregating and forming interconnected fibrillar matrices. Molecular dynamics simulations were used to predict the arrangement and register of the β-strand interactions to explain the kinetic morphology transition. Interestingly, two different antiparallel and double helical arrangements were predicted to be stable with the morphological transition possibly due to continued collapse of the helices into more tightly packed nanofibers.[79]

Indeed, the molecular structure of the RADA16-I peptide was investigated through $^{13}C$ isotope labeling and subsequent solid-state NMR measurements. Unexpectedly, neighboring β-strands were found to be parallel in orientation enabling intermolecular ionic interactions between oppositely positioned Arg and Asp residues. Dipolar $^{13}C$-$^{13}C$

couplings between selectively labeled residues within the peptides provided the evidence for this assembly orientation.[55] $^{13}C$ isotope labeling within self-assembling peptides also has use in Fourier-Transform Infrared Spectroscopy (FTIR). In the study by Senguen et al., Isotope Edited FTIR (IE-FTIR) was utilized to study the orientation and pairing registry between neighboring amyloid-β derived peptides.[75,80] Amino acid residues Phe20, Ala21, and Leu17 were selectively $^{13}C$ labeled within the amyloid-β(16-22) peptide to probe for coupling between the isotopically labeled carbonyl carbons. $^{13}C$ is known to possess a lower vibrational frequency compared to $^{12}C$ which results in a 20 $cm^{-1}$ shift in the amide frequency when the $^{13}C$ labeled residue is alone in the peptide. However, greater shifts are expected when two isotopically labeled residues are in proximity, thus enabling, in the case of self-assembling peptides, the register of β-strand orientation to be determined. The study revealed that the peptide was assembled into an out of register antiparallel arrangement, offset by one amino-acid residue, evident from the enhancement in amide resonance shift observed between Leu17 and Phe20 labeled peptides regardless of the hydrophobic modification at position 19.[75]

Consideration of these studies for designing and modifying self-assembling peptides reveals an interesting point. The packing mode of β-sheet forming peptides is likely to be dependent on the sequence and resulting intermolecular interactions between peptides and not necessarily generalizable characteristics.[81] An examination of 30 self-assembling peptides derived from amyloid forming proteins such as insulin, the yeast prion Sup35, and Amyloid-β found a range of beta-sheet assembly orientations using x-ray crystallography techniques which indicated strong sequence dependence on structure.[81]

Interestingly, even the same peptide sequence can adopt variable packing modes and morphologies dependent on the environmental factors including the presence of metal cations and pH.[82–84]

**Figure 1.6 Considerations of register and peptide orientation in β-Sheet peptide assemblies**

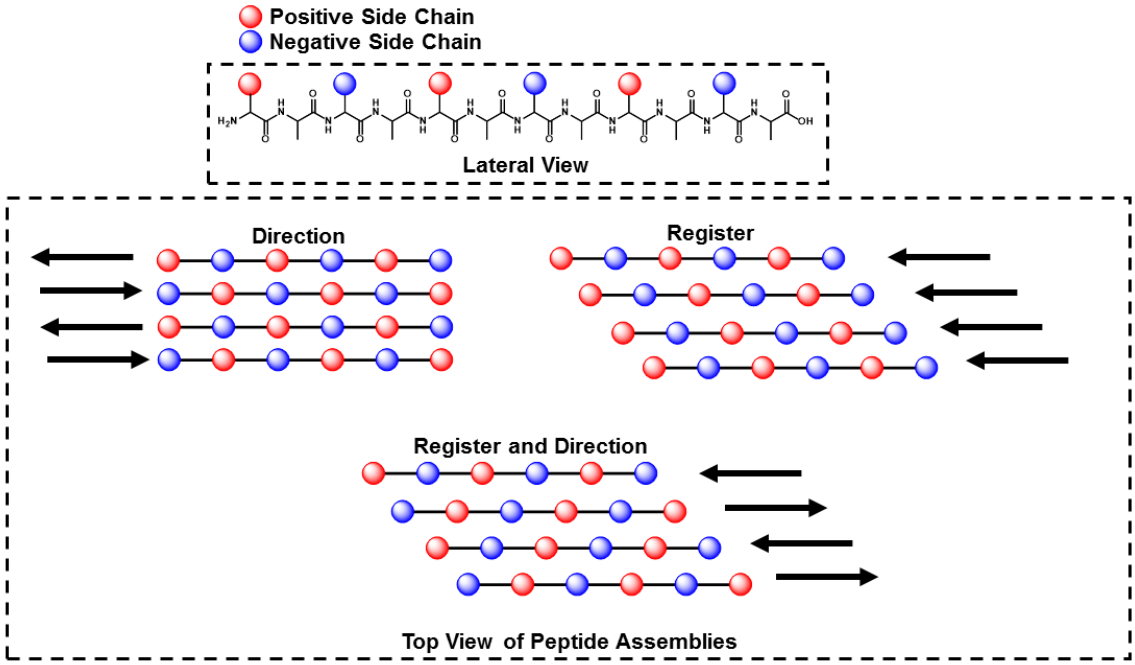

### 1.1.2.2 AROMATIC PEPTIDES

The diphenylalanine self-assembling motif, derived from residues 19 and 20 from the amyloid-β protein, has been widely used to drive self-assembly of a wide variety of peptide derivatives. Nanotubes formed from aqueous solutions of diphenylalanine were first observed and utilized as tools for the fabrication of metallic nanowires.[85] The rigid dipeptide nanotubes were distinctly different from the flexible amyloid fibers formed from longer peptides, although β-sheet character was observed in the assemblies from FTIR characterization (**Figure 1.7**).[85]

A combination of experimental and computational approaches were undertaken to investigate the molecular organization of the dipeptides within the nanotube formations. Interestingly, the peptides were ordered into hexagonal arrangements in a head to tail fashion with hydrated centers (**Figure 1.7**).[86] These results were later reaffirmed in computational analysis which predicted ring shaped organizations of the Phe-Phe peptide in which both side-chains are positioned on the exterior of the ring structures leading to T-shaped aromatic interactions.[87] T-shaped aromatic interactions have been observed between both aromatic amino acids and bases in nucleic acids and are thought to provide stabilizing interactions for molecular recognition (**Figure 1.7**).[88,89] Consecutive layering of the hexagonal ring structures into β-sheet arrangements is thought to form the basis for the Phe-Phe dipeptide nanotube formation.[88,89]

Most illustrative of the assembly driving force provided by the diphenylalanine motif is the observation that electrostatic interactions are expendable in the assembly of the

peptide into ordered nanotubes. Neutralization of both the N- and C-termini still was found to enable self-assembly into nanotubes.[85,90] This observation was supported by molecular dynamics simulations that predicted side-chain interactions are key to the early stages of the self-assembly process and electrostatic interactions between the termini contributing to ordering and stabilization of the peptide backbones.[90,91]

Neutralization of the N-terminal charge on the peptide has been shown to enable assembly of Phe-Phe, although nanofibrous structures are typically formed in contrast to nanotubes formed from the dually protected parental peptide (**Figure 1.8**).[91] Incorporation of hydrophobic and aromatic chemical modifications at the Phe-Phe N-terminus not only promotes self-assembly, but also gelation in aqueous solution. A range of hydrophobic and aromatic modifications at the N-termini of amino acids and short peptides were explored in early reports for their ability to induce and contribute to gelation in aqueous solution.[92–94] Among the most robust modifications was the polyaromatic fluorenylmethoxycarbonyl (Fmoc) group that was shown to generate rigid hydrogels and exhibited fiber morphology closely approximating those observed in traditional amyloid protein assemblies.[92] Typically utilized as a labile amine protecting group is solid phase peptide chemistry, the Fmoc group provides additional hydrophobic character to the peptides and is thought to potentially provide a larger interface for π-π interactions necessary to drive assembly.[95,96]

Evident through CD spectroscopic and FT-IR studies is the β-sheet character of Fmoc-Phe-Phe peptide assemblies.[97] Fluorescence spectroscopy showed that the N-terminal fluorenyl rings participate in aromatic-aromatic stacking interactions evident

through red shifting of the emission peak exhibited by Fmoc-Phe-Phe in comparison to Fmoc-Phe and the possible formation of J-aggregates evident from a significantly red shifted secondary fluorescence emission peak by Fmoc-Phe-Phe.[97] These observations were used as parameters for instructing molecular modeling interactions to investigate the packing mode of Fmoc-Phe-Phe. In the β-sheet assembly, two peptide backbones were hydrogen bonded and stacked atop one other, with fluorenyl groups zippered together with adjacent sheet assemblies. To maximize aromatic interactions between the fluorenyl rings, the sheet assemblies are twisted with respect to one another and form fiber structures with four peptides consisting the circumference of a tube-like fibril. The computationally predicted 3 Å diameter fibrils were observed to form even higher ordered structure using TEM imaging, forming ribbons of discrete widths consistent with the fibrils arranged lengthwise (**Figure 1.8**).[97]

A key feature of Fmoc-Phe-Phe is its ability to form rigid hydrogels in aqueous environments despite its high degree of hydrophobic character, in stark contrast to the careful balance of hydrophilic and hydrophobic residues necessary for self-assembly and gelation of other rationally designed peptide classes (**Figure 1.8**). The fabrication of Fmoc-Phe-Phe hydrogels is relatively facile and can be accomplished through initial solvation in organic solvent and subsequent dilution with water, or through modulation of pH.[92,94] The characteristic of Fmoc to drive assembly into hydrogels is not universal to all dipeptides. Comparing the gelation ability of Fmoc-substituted dipeptides demonstrated that Fmoc-Phe-Phe formed hydrogels under physiologic pH whereas other peptides required pH values below 4 to undergo gelation. Additionally, the location of Phe residues within

peptides can influence gelation as Fmoc-Phe-Gly forms gels in a pH dependent manner while Fmoc-Gly-Phe crystallizes in solution.[94] Despite being able to form gels under a variety of conditions, the mechanical properties of Fmoc-Phe-Phe hydrogels vary significantly from study to study and by fabrication technique. The final pH of prepared Fmoc-Phe-Phe gels was found to be a key parameter influencing mechanical properties with gel weakening. Diluting Fmoc-Phe-Phe from an initial organic solution with water was found to form rigid hydrogels due to the low pH of the resulting samples. Fmoc-Phe-Phe gels formed through pH titration demonstrate weaker mechanical properties at physiologic pH indicative of this pH influence. Buffers and presence of residual solvent also play a role in dictating the final rheological properties of Fmoc-Phe-Phe hydrogels.[98] Despite empirical characterization of these discrepancies, a fundamental understanding of the properties governing these molecular interactions is still not fully understood.

The charge state of Fmoc-Phe-Phe was demonstrated to play a key role in regulating observed assembly morphology. The pKa values of the C-terminal carboxylic acids of an N-terminally capped and uncharged peptides was shown to be approximately 3.5.[99] Above this pH, the negative charges of the peptides in solution should be expected to exhibit a repulsive effect, preventing the molecules from assembling into higher ordered structures. This effect was evident in the above-mentioned gelation studies of Fmoc-Phe-Phe where most of the studied peptides failed to form hydrogels at solution pH above this value. Nevertheless, Fmoc-Phe-Phe assembles into hydrogels at pH values close to neutral conditions as shown in the study and by others.[94]

The putative hypothesis behind this occurrence was suppression of Fmoc-Phe-Phe ionization, causing an increase in the carboxylic acid pKa enabling persistence of nanostructures at physiologically relevant pH. Although Fmoc-Phe-Phe is a singly ionizable molecule, titration curves of Fmoc-Phe-Phe surprisingly revealed two pH plateaus from 10.2-9.5 and 6.2-5.2.[100] These plateaus were taken as evidence of two possible pKa values associated with the peptide and its morphological transitions, and the pH titration data was correlated to structural characterization data. At pH values above the transition range of 9.5-10.2, the peptide formed clear solutions consistent with disperse monomers in solution. Decreasing the pH below 9 yielded a weak hydrogel consisted of paired nanofibers, associated along their length and consistent with previous characterization of Fmoc-Phe-Phe nanofibers.[92,97,100] The nanofiber assemblies only formed weak gels at this stage, possibly due to partial assembly with a distribution of monomers and higher assemblies present or the result of nanofiber charge repulsion. After the initial assembly transition, approximately two-thirds of the peptides were expected to remain ionized resulting in the partition of charged monomers from the assemblies. It is also possible that the bulk of monomers assemble into higher structures, inducing charge repulsion of the formed nanofibers preventing necessary fiber-fiber entanglements needed for the generation of robust gels. Continuing pH decrease to the second pKa transition at 6.8 would induce switch from a weak gel to a viscous solution, explained by reduction of overall nanofiber surface charge allowing the paired nanofibers to continue to associate along their long axis to form the ribbon-like assemblies previously described for Fmoc-Phe-Phe to form.[97,100]

A similar investigation on assembly pH dependence was undertaken for another aromatic dipeptide N-protected with a naphthyl moiety in lieu of the Fmoc protecting group.[101] N-terminal naphthalene modifications of dipeptides were originally investigated for their ability to drive self-assembly similar to Fmoc and were shown to enable self-assembly of dipeptides into a range of nanofibrous structures with varying morphologies dependent on the dipeptide sequence.[102] Prior to the study, glucono-δ-lactone (GdL) was realized as a tool to control the gelation kinetics of Fmoc-Phe-Phe due to GdL's slow hydrolysis which reduces solution pH and the ionization of the peptide.[103] This technique was further adapted to a NAP-Ala-Val peptide which was responsive to the pH modulation technique and formed gels below pH 5.[101] Interestingly, bromination of the naphthalene cap was found to enhance the gelation properties of the peptide through a putative increase of hydrophobic character.[101] Similar to Fmoc-Phe-Phe, the NAP-Ala-Val peptide possessed a carboxylic acid with a pKa of 5.9, a value significantly above the anticipated pKa. Spectroscopic data suggested assembly of the molecule into β-sheets with sufficient decrease in pH afforded by the addition of GdL. Chiral and linear dichroism spectroscopy results indicated chirality of the assembled naphthalene chromophores due to their ordered arrangement in the nanostructures. A biphasic assembly process was described beginning with initial deprotonation of the Nap-Ala-Val peptide at pH close to the pKa, which resulted in triggering assembly of the dipeptides into β-sheet assemblies. In the second phase, further deprotonation of the structures led to possible nanofiber entanglements and higher order lateral association of the fibers. The final rigidity and morphology of formed hydrogels was found to be independent of the amount of GdL added and resulting final pH.

Instead, rheological analysis pointed to a dependence on resistance to strain indicating that a combined effect of pH and assembly kinetics were regulating the crosslinking density of the nanofibers and not the underlying assembly interactions.[101]

From these studies of pH and its resulting effect on the self-assembly of short self-assembling, a similar set of parameters governing supramolecular association to that of larger lamellar β-sheet forming peptides is apparent. Firstly, a primary driving force of assembly is the hydrophobic association of the peptides through a combination of desolvation, methylene interactions from amino acid side chains, and π-π interactions afforded by the phenyl rings of Phe residues. This is exemplified by the propensity of Fmoc-Phe-Phe to self-assemble at pH values much higher than similar Fmoc protected hydrophobic peptides.[94] In addition to entropic desolvation of the hydrophobic side-chain, the enthalpic contributions of aromatic-aromatic interactions to the overall thermodynamic driving force of assembly seems universal. Using non-aromatic side chains in the NAP-Ala-Val peptide required additional hydrophobic character to be added to the naphthyl ring through bromination to facilitate self-assembly.[101] A second key feature is the charge state of the peptide. This is evident in pH titration studies showing a clear dependence of the ability of Fmoc-Phe-Phe and related peptides to self-associate as the C-terminal carboxylate becomes protonated.[100,101]

It is unclear why the carboxylate pKa of self-assembling peptides is increased compared to structurally related non-assembling peptides. A report investigating the assembly kinetics of N-terminally and C-terminally capped tetrapeptides bearing two Phe

and two Asp residues observed that the kinetic hurdle for fiber formation is the initial dimerization event of two peptides.[104] As GdL mediated decrease in pH neutralized the negative charge of the Asp side chains, the repulsive electrostatic effect between two peptides was removed.[104] Removal of this blocking effect enabled the both hydrophobic and aromatic residues of the peptide to drive assembly through the favorable desolvation of the bulky side groups and enthalpically favored aromatic-aromatic interactions.[104] The rate limiting step in the assembly of the peptides was determined to be dimer formation, evidenced by fluorescence data exhibiting a burst in fluorescence intensity provided by the more fluorescent dimer, followed by a decay period where higher oligomers possess decreased fluorescence.[104] The reason for the slower assembly kinetics of dimers and low oligomers directly from monomers was ascribed to the conformational restriction of the peptides in the organized assemblies in comparison to free monomers. As the peptides also generally initiated fibrillization at pH close to their pKa, partial ionization of the peptides could contribute to the higher energy barrier required for dimerization which would then be relieved by the more hydrophobic environment resulting in an environmentally specific increase in the pKa facilitating further protonation of the remaining residues. Following dimerization, association of the pre-ordered peptides into nanofiber assemblies was relatively rapid due to the low entropic barrier of assembling the already conformationally constrained peptides.[104]

**Figure 1.7 Radial assembly of Phe-Phe into hollow nanotubes**

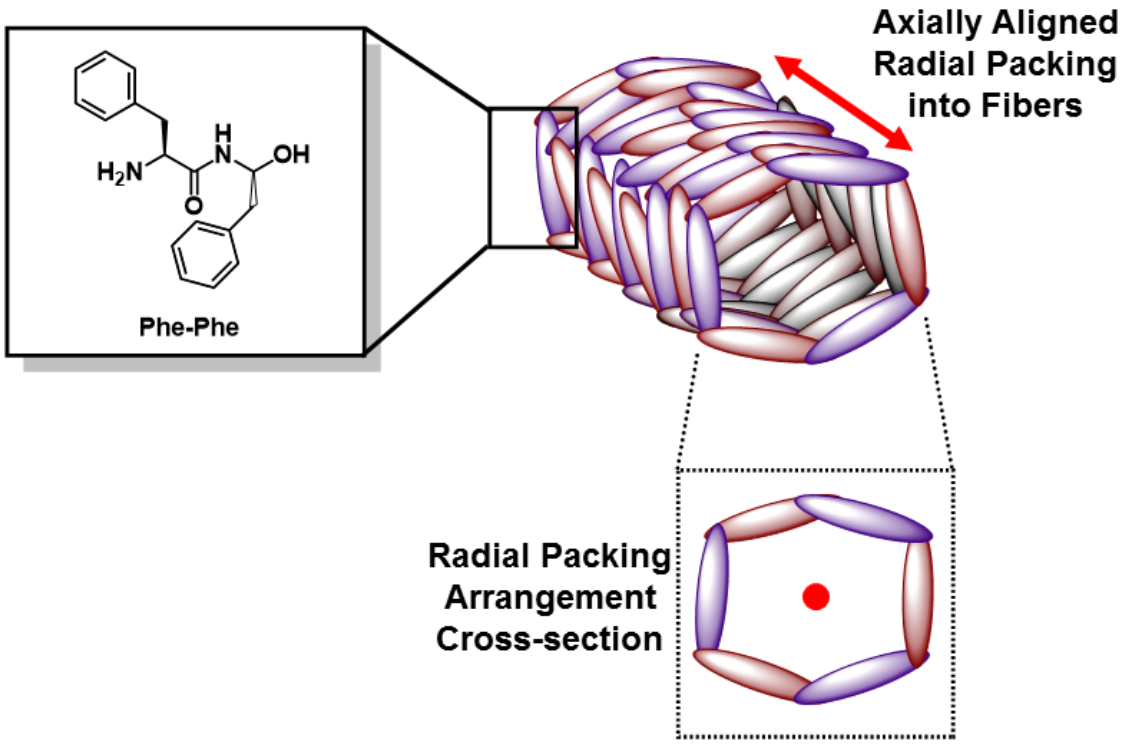

**Figure 1.8 Representation of Fmoc-Phe-Phe nanofiber assembly**

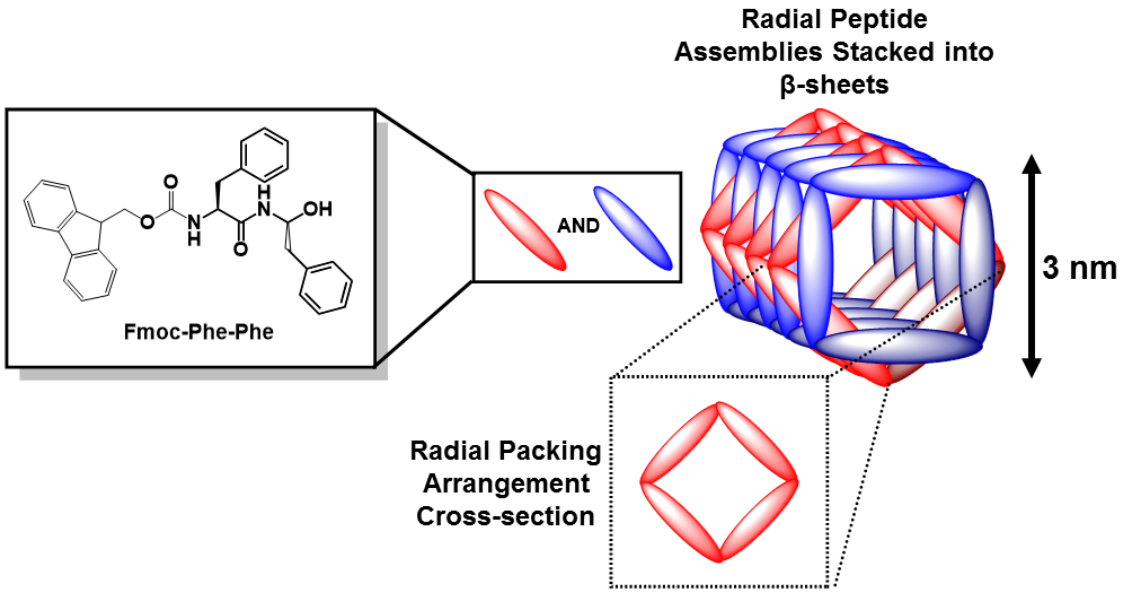

**Figure 1.9 Modifications of Phe-Phe dipeptide to yield aromatic self-assembling gelators**

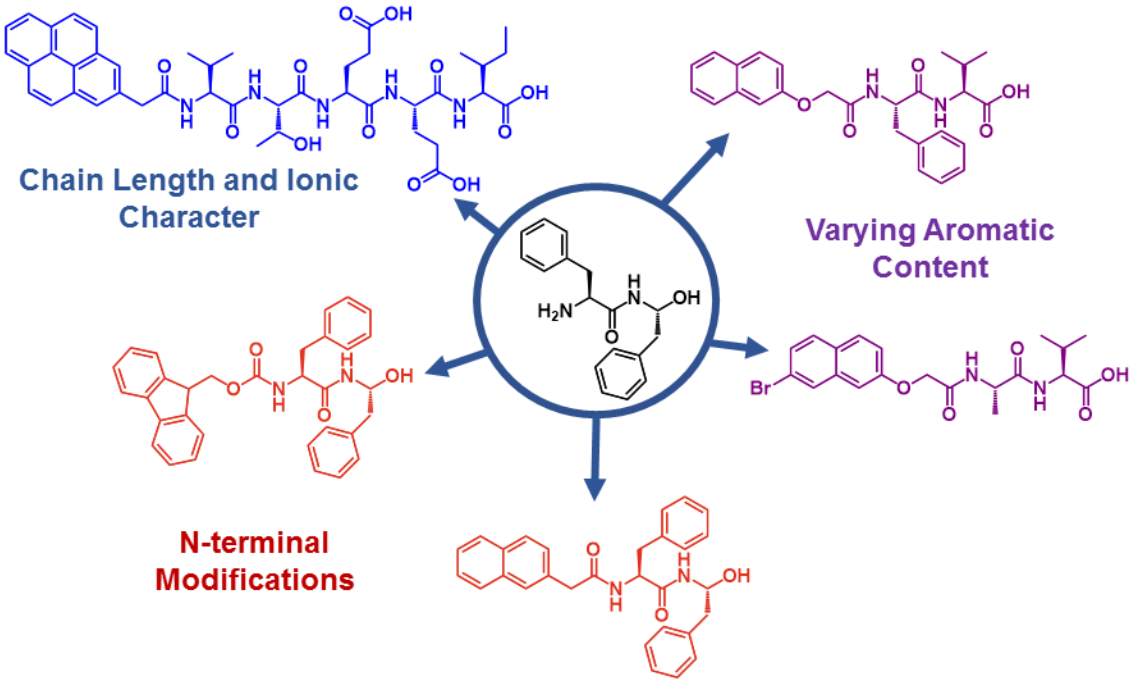

In designing supramolecular hydrogels of this class, care must be taken to ensure the optimal balance of hydrophobic, aromatic, and polar characteristics to ensure the formation of stable secondary structural characteristics and also assembled nanostructures that retain colloidal stability to prevent aggregation and precipitation (**Figure 1.9**). These features were considered in developing a simple model to explain the preferable formation of high aspect ratio structures in the gel state versus organization into 3D crystal arrangements.[105] It was found that the gel state consisting of nanofibrous structures could represent a thermodynamic minimum, stabilized by the amphiphilic nature of most self-assembling moieties which contribute to both association and nanostructure solvation. Subtle tuning of the strength of interactions between the simplified geometric monomer shapes could induce 1D or 3D organization, reminiscent of experimental observations where single amino acid changes could drastically alter the self-assembling and gelating properties of these molecules.[105]

A separate investigation attempted to correlate crystal structure packing to gelating capability of low molecular weight aromatic peptides to address the seemingly idiosyncratic nature of amino-acid substitutions either promoting or ablating gelating capability.[106] Peptides that formed crystals and not gels exhibited an increased propensity for aromatic interactions between N-terminal naphthyl groups which were found to abrogate the hydrogen bonding pattern present in gelating samples. Interestingly, crystals grown from gel samples lacked the aromatic π-π stacking typically associated with aromatic peptides indicating that the interactions may not be present or essential in all systems. Conversely, linearly organized water channels were found within the obtained

crystals indicating that internal hydration of nanostructures could also be a component of self-assembly.[106]

While computational simulations and analyses of crystal data have yielded valuable insight into the self-assembling properties of short aromatic peptides, correlation to actual gel structure and *a priori* molecule design from first principles remains largely out of reach. Structure-activity relationship studies and empirical observation remain a key technique in the design of optimal gelating peptides. Simple reorganization of aromatic residues within Fmoc protected tetrapeptides was found to alter the assembly kinetics, and simple substitution of amino acid residues within the core structure could prevent stable gelation.[107] Similar to design parameters adopted for designing β-sheet assemblies, general conclusions could be reached, such as increasing monomer aromatic character can, 1) accelerate assembly kinetics, 2) create more thermally stable structures, and 3) generate greater elastic character as determined by rheological analysis.[107]

In a systematic investigation of a varied peptide sequences and polycyclic aromatic N-terminal modifications, several of the derivatives failed to exhibit gel formation although most of the assembled structures did act as molecular gelators.[108] The peptide with the lowest side-chain hydrophobicity was unable to form gels with the smallest aromatic N-terminal substitution which consisted of a naphthyl group, but was able to gelate with Fmoc or pyrenyl modification.[108] A peptide bearing a Pro residue close to the N-terminus was not able to form gels with any N-terminal modification and instead formed precipitates, possibly indicating the molecular orientation of the peptide abrogated its ability to form

stable secondary structural characteristics in solution. Similarly, another peptide bearing Pro at the C-terminus failed to gel despite varied N-terminal modifications, indicating that the residue might universally prevent efficient packing and backbone reordering necessary for the formation of stable interstrand interactions.[108] Additionally, a lack of solubilizing polar groups can lower the solubility of N-terminally protected peptides with an excess of hydrophobic surface area. For example, pyrenyl modified VYGGG precipitating from solution while Fmoc and naphthyl modification formed stable gels.[108]

#### 1.1.2.3 PEPTIDE AMPHIPHILES

The power of covalent modifications was made evident in the N-terminally capped aromatic peptides as key drivers of self-assembly. Alternative to aromatic moieties are aliphatic chains which have been appended to peptide termini to generate linear amphiphilic molecules termed peptide amphiphiles. Lipidated peptides had previously been investigated for their ability to hydrophobically insert into biological membranes, and in the case of naturally derived lipoproteins, govern their underlying biological function.[109] Synthesis of fluorescent phospholipid conjugated peptides was achieved for the purpose of investigating the interactions of eukaryotic cells with immune cells.[110] In the course of the study, it was observed that oligomerization of the lipidated peptide assemblies occurred in the membrane and was suspected to result from associations between the membrane immobilized peptides.[110] Later investigations focused on the ability of synthetically lipidated peptides to form stable self-assembled nanostructures.[111]

**Figure 1.10 Peptide amphiphile design for hydroxyapatite deposition**

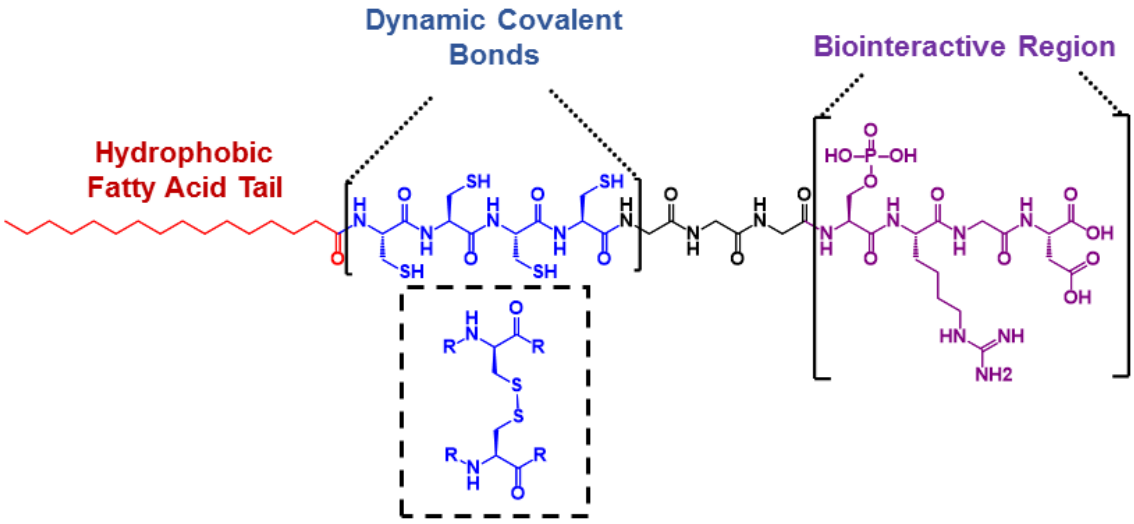

**Figure 1.11 Structures of peptide amphiphiles**

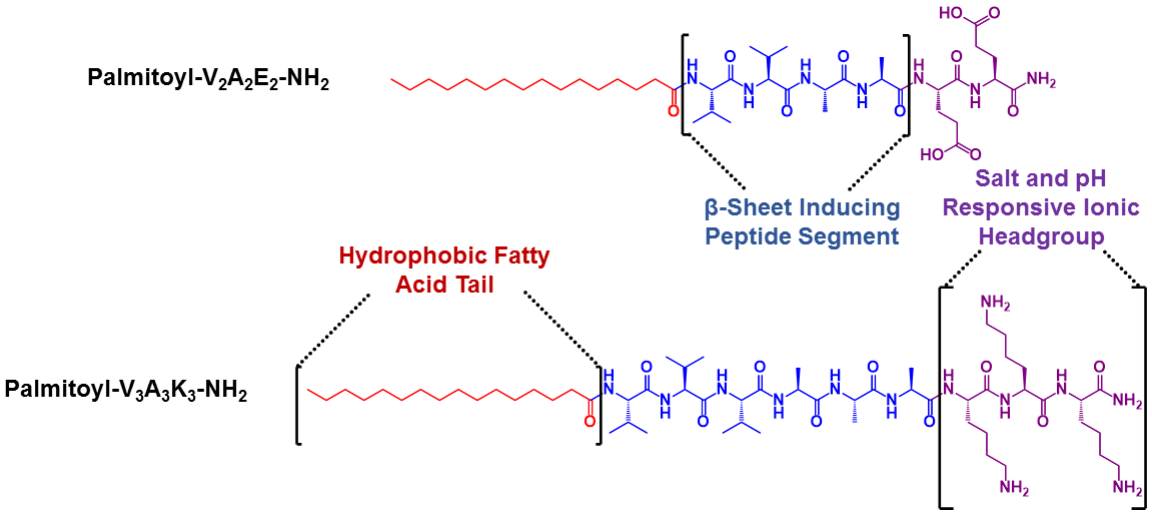

Extending the assembly of peptide amphiphiles from monolayers to high aspect ratio structures capable of forming hydrogels was achieved later in seminal work which cemented the peptide amphiphile as a key class of self-assembling hydrogelators.[112] In the study, linearly organized nanostructures with periodic display of negatively charged functional groups was desired to facilitate a functional and morphological mimic of bone, which consists of hydroxyapatite crystals deposited onto a collagen matrix substrate (**Figure 1.10**).[113] The peptide amphiphiles were able to be synthesized using standard solid phase techniques, with the N-terminal amine capped with fatty acid acyl chains.[112] Several components were incorporated into the molecular design of the peptide amphiphiles. The first was a block of Cys residues that were expected to provide mechanical stability by forming disulfide bonds with adjacent monomers.[112] Additionally, the dynamic nature of disulfide bonds was expected to enable reduction sensitive motifs that could be cyclically reduced then oxidized to generate tunable structures.[112] A second feature necessary for hydroxyapatite deposition was the inclusion of phosphorylated amino-acids into the peptide segment, thus mimicking highly phosphorylated proteins such as phosphophoryn which are highly anionic and contribute to mineralization of hard tissues such as dentin.[114] Thirdly, an Arg-Gly-Asp (RGD) sequence was incorporated at the C-terminus of the peptide to facilitate cell adhesion to the surface of the mineralized nanostructures formed by the peptide amphiphiles.[115] An alkyl chain of 16 carbons was used to modify the C-terminus to contribute a conical or triangular profile to the molecule, which is necessary for the packing of the peptide amphiphiles into high aspect ratio cylindrical micelles.[112] Cryo-TEM results confirmed assembly into 7-8 nanometer wide nanofibers, and

conventional TEM staining exhibited preferential binding to the negatively charged residues on the surface of the nanofibers versus the hydrophobic core, indicating the molecules within the cylindrical micelles were indeed oriented with the alkyl chains inward toward the center of the fibers and the peptide outward.[112] Interestingly, FTIR analyses suggested the peptides self-associated into β-sheet structures in possible combination with helical structures to effect the linear assembly of the molecules.[112] Due to the strong anionic character of the peptide segment, assembly of the structures was found to be pH dependent with assembly only observed at low pH values.[112]

Following this initial report, a significant body of work was put forth investigating the mechanistic details of the molecules self-assembly and their regulation by external stimuli. Similar to investigations demonstrating the pathway dependence of assembly on the resulting material properties of N-terminally capped aromatic peptides, different assembly protocols were found to induce varying morphologies in the resulting nanostructures.[116] Dissolution of palmitoyl-$Val_3Ala_3Asp_3$ in hexafluoroisopropanol (HFIP) resulted in soluble and unassociated monomers due to effective solvation of the lipophilic tail and effective polar interactions with the hydrophilic peptide segment (**Figure 1.11**). In the fully dissolved state, the peptide segments exhibited a random coil structure observed with CD spectroscopy.[116] In contrast, β-sheet formation was observed in predominantly aqueous HFIP co-solvent mixtures as a concentration of HFIP greater than 20% prevented assembly.[116] Intermediate co-solvent mixtures exhibited the random coil CD character of the peptide segment, but also demonstrated features of self-assembly. For example, a hypsochromic shift in the fluorescence of the solvatochromic probe Nile red bound to the

peptide domain was consistent with the possible presence of short oligomers.[116] Kinetic investigation of nanofiber assembly was undertaken to determine the role short oligomers may play in the assembly process. By injecting the amphiphile, which had been dissolved in HFIP, into water, a critical concentration of 20% HFIP was found to support β-sheet formation with the slowest rate of assembly also measured at this concentration. Higher concentrations of HFIP were found to only support random coil structures. Interestingly, a pathway dependent phenomenon was revealed in which the addition of peptide amphiphile and HFIP solvent resulted in different observed secondary structures. When the amphiphile was added directly to water and diluted to a 20% solution with HFIP, little effect on the kinetics of amphiphile assembly and the final β-sheet character was observable, consistent with the formation of highly metastable structures. Conversely, the addition of the amphiphile into an already high HFIP content solvent mixture resulted in only random coil structures although the final HFIP concentration was identical as before.[116] From these experiments a clear driving force for assembly is the hydrophobic alkyl chain which requires the entropy of desolvation to facilitate oligomer formation.[116] However, to generate stable high aspect ratio structures, aqueous conditions are required to stabilize the highly polar C-terminus of the peptide segment and reduce charge repulsion, as well as facilitate proper folding of the hydrogen bonding residues similar to the previously described β-sheet forming peptides such as RADA.[116]

Understanding of the thermodynamic landscape of the palmitoyl-$Val_3Ala_3Lys_3$ assembly was sought as it related dependence on ionic strength and pathway dependent structural transitions (**Figure 1.11**).[117] Similar to the energy wells and barriers relating to

protein folding and conformation, this study sought to determine whether energetically trapped assemblies of the peptide amphiphiles could be generated and whether the structures could dynamically interconvert with the generally regarded thermodynamically stable long cylindrical micelle structure.[117,118] A value of ionic strength determined to be 6 mM was found to control the formation of β-sheet structures among the peptide segments due to necessary Debye-screening effects between the cationic lysine residues.[117] Interestingly, this value could be achieved through added aqueous salt, or could derive from the charged peptide amphiphiles themselves. Dissolution of peptide amphiphiles below the critical ionic strength resulted in short nanofiber formation with the peptide segment having adopted a random coil structure due to the charged Lys residues. Conversely, the peptide amphiphile readily formed extremely long nanofibers in solutions above the critical ionic strength with the peptide segments arranged in β-sheets. Addition of salt to the low ionic strength peptide amphiphile solutions triggered significant morphology changes in the observed nanostructures with a transition to longer nanofibers possessing β-sheet peptide secondary structure.[117] This transformation took place on a rapid time scale indicating a low energy barrier to the transition. Conversely, the high ionic strength sample was diluted below the critical ionic strength without morphological change.[117] Thermal denaturation and reassembly was required to overcome the activation energy level required for transition to shorter random coil fibers. Modeling results further confirmed the molecular basis for the origin of the energy wells representing the differing nanofiber morphologies resulting from charge screening of the Lys residues.[117] The simulations predicted that a reduction in charge screening would favor randomly ordered

peptide segments with ill-defined micellar cross-sections, while the enabling of charge screening resulted in β-sheet formation and circular micellar cross-sections.[117] Interestingly, cell compatibility was found to be dependent on nanofiber morphology with long β-sheet nanofibers promoting cell attachment and survival while the shorter random coil nanofibers induced cell death.[117] These results imply that a correlation exists between the thermodynamic factors relating to nanofiber assembly and morphology and potential in biomedical applications.

In addition to transitions between structural morphologies, characterization of the molecular dynamics within a single nanofiber were investigated in an effort to bridge from computation molecular dynamics simulations to experimental results.[119] Self-assembling peptides have traditionally been designed and developed to generate specific morphologies and molecular orientations. Nevertheless, the results of experimental results have demonstrated that nanostructures can interconvert between different forms under varying conditions, thus conformational dynamics is likely to exist within nanostructured domains and within individual segments of molecules.[119] Modification of the different segments within model peptide amphiphiles with a spin-label nitroxide probe was achieved for the purpose of examining the dynamics with electron paramagnetic resonance (EPR) spectroscopy.[119] The molecular mobility of specific sites within the amphiphile characterized as rotational diffusion rates were plotted as a function of radial distance within the nanofiber cross-section.[119] Owing to the lipid nature of the interior of the micellar core, a liquid-like state was observed for this portion of the molecule indicating significant conformational flexibility.[119] In contrast, the peptide segment of the

amphiphiles exhibited solid-like character due to the β-sheet structures making up the exterior domain of the amphiphiles.[119] Interestingly, the β-sheet structures could be tuned through incorporating N-methyl amide residues that weaken the propagation of β-sheets throughout the structure.[119]

Inter-nanofiber dynamics were later investigated using super-resolution microscopy, which enabled the characterization of nanostructures using fluorescently labeled monomers.[120] With stochastic optical reconstruction microscopy (STORM), the authors characterized the dynamics between two orthogonally labeled nanofibers.[120] STORM enables visualization of structures below the diffraction limit of light using simple fluorophores commonly utilized in fluorescence microscopy.[121] Nanofibers conjugated to Cy3 and Cy5 were mixed and monitored for exchange of fluorophores between nanofibers.[120] A combination of monomer and oligomer exchange was observed between the nanofibers generating heterogenous distributions of the fluorophores along the nanofiber lengths. The heterogenous nature of fluorophore along the nanofiber lengths was attributed to locally stable β-sheet assemblies which were kinetically stable on the time course of the mixing experiment.[120] The results of the study indicate that though there is high cooperativity in the β-sheet assemblies dictating the high aspect ratio structure of the nanofibers. It was found, differentially ordered and stable peptide oligomers exist within the nanofibers that could potentially contribute different functional effects in mixtures of peptide amphiphiles affecting a range of parameters including their rheology, stability, and biological interactions.[120]

The roles of non-covalent intermolecular interactions in guiding peptide amphiphile assembly were investigated in a structure-activity relationship approach through synthesis of 26 derivatives bearing a number of assembly altering modifications.[122] A core cell adhesion motif was constructed at the C-terminus of all investigated peptide amphiphiles which bore the sequence Glu-Arg-Gly-Asp-Ser, with the last four residues comprising the integrin protein binding sequence and the addition of the anionic Glu residue to impart pH and ion responsiveness.[122] The other structural component of the peptide amphiphile held constant through the study was the hydrophobic alkyl chain at the N-terminus. of the peptide segment containing a 7-amino acid repeat of Gly residues.[122] To investigate the H-bond forming potential of different residues in the peptide segment, Gly residues were systematically replaced with sarcosines bearing N-methyl moieties. The modification of the Gly peptide backbone with N-methyl functionality was utilized to perturb the expected H-bonding pattern in the parent sequence, thus uncovering site specific contribution of specific residues to the overall stability of β-sheet assembly. In addition to N-Methyl scanning along the backbone of the peptide, the total N-methyl content was varied through incorporating multiple sarcosine residues through the sequence.[122] Subsequent biophysical and rheological characterization of the N-methyl peptide amphiphiles demonstrated a strong positional effect of H-bonding perturbation on assembly and stability.[122] The residues closest to the N-terminal alkyl chain were found to be the most important for guiding assembly as at least 4 uninterrupted Gly residues were required at the N-terminal portion of the segment to induce gel formation. Regardless of location, one N-methyl substitution among the 7 residue sequence still enabled nanofiber

formation, although modification of the first four residues disrupted the H-bonding pattern necessary to form mechanically stabilizing β-sheets.[122] Due to the low interaction of achiral Gly with circularly polarized light, Ala scanning was conducted through the 7-residue sequence to determine the contributions of each reside to the observed secondary structure.[122] Unsurprisingly, the first four residues adjacent to the alkyl tail exhibited strong β-sheet character. However, the next three residues and the constant Glu-Arg-Gly-Asp-Ser sequence present in all the peptides exhibited polyproline type II helical structure.[122]

Important design considerations are gleaned from integrating the above results into a structure-function schema (vide supra). First, complementing the results of the previously described EPR studies, the residues closest to the N-terminal alkyl chain are essential for propagating β-sheet formation through the cylindrical micelle nanofibers.[119,122] The resulting structural and conformational stability imparted by the secondary structural motif allows robust hydrogel formation under the required pH and ionic strength conditions. Secondly, the C-terminal portion of the peptide segment is not required to possess the β-sheet structural motif and can even form helical structures.[119,122] The flexibility afforded the C-terminal peptide secondary structure is important considering that biological recognition sequences may employ structures other than β-sheets.[123,124]

Computational simulations have also been performed to further understand the association mechanisms of peptide amphiphiles. Aside from the electrostatic forces providing repulsive or associative interactions dependent on effects of pH and ionic strength on charged residues within the peptide segment, the primary driving forces of

peptide amphiphile association are hydrogen bonding and hydrophobic interactions.[30] For the purpose of conducting simulations, a model amphiphile was constructed taking into account molecular structure and the intermolecular interactions leading to assembly.[125] Hydrophobic interactions in the absence of H-bonds drove association of monomers into monodisperse spherical micelles through a closed association mechanism.[125] Conversely, hydrogen bonding in the absence of hydrophobic interactions resulted in linear β-sheets assembled through step-wise aggregation in an open association yielding disperse assembly sizes.[125] A critical micelle temperature (CMT) was observed that regulated the effect β-sheet formation had on the overall assembly morphology.[125] Below the CMT, H-bonding amplifies the effect of hydrophobic forces due to local increases in hydrophobicity that facilitates the formation of amorphous aggregate structures.[125] However, linear assemblies of β-sheets formed along the outer surface of micelles above the CMT induce cylindrical micellization in order to avoid geometric curvature in the spherical assembly.[125] Analogous to experimentally determined Krafft temperatures, the hydrophobic parameter was found to play a direct role in determining the CMT value, and thus, the point below which formation of crystalline assemblies of surfactants is favored and the critical micelle concentration is nonexistent.[126]

Thermal transitions have been shown experimentally to regulate peptide amphiphile assembly morphology.[127] The peptide amphiphile palmitoyl-Lys-Thr-Thr-Lys-Ser possessed a Krafft temperature of 30°C, below which the amphiphile formed insoluble aggregates.[127] The phase transition was found to represent exchange between insoluble nanofibrous tapes and soluble spherical micelles.[127] Aggregation of the nanotapes was

determined to result from hydrophobic interactions which were stabilized through β-sheet hydrogen bonding interactions.[127] Heating was required to disrupt the intermolecular interactions and to overcome the entropic penalty for solvation in order to generate spherical micelles which were able to be characterized with solution NMR.[127]

In designing self-assembling molecules, especially those that exhibit properties of traditional surfactants such as the peptide amphiphiles, consideration must be made to the phase relationship of the molecules in relationship to temperature and concentration.[128] Although, intermolecular interactions may be incorporated into the H-bonding patterns of the peptide segment, colloidal stability of the high aspect ratio structures in solution may only occur under specific environmental conditions, thus presenting complications relating to material stability for potential biomedical application.[30,117] Additionally, incorporating biologically active motifs within the fibrous structures may require specific topologies for optimal presentation to achieve functional cellular interactions.[32] As with all materials, comprehensive integration of desired properties to meet the demands of the intended application environment is critical to generate systems that may be examined for specific purposes without interference from unintended material failure.

### 1.1.3 CHARACTERISTICS OF SELF-ASSEMBLING PEPTIDES AS BIOMATERIALS

Self-assembling peptides possess several characteristics that render them ideally suited to a range of biomedical applications. Firstly, the amide bonds contained within monomer peptide backbones are hydrolytically stable, indicating that they are robust

enough for bulk material application where temporal stability is necessary and will not chemically degrade to release problematic side products unlike hydrolytically labile polymers.[129] However, amide bonds are sensitive to endogenous and exogenous proteases which effect material degradation to release individual amino acid constituents which may be further metabolized or excreted.[129] Specific protease degradation sites may also be incorporated through the amino acid sequence present in the monomer which may confer responsiveness to matrix metalloproteinases, cathepsins, or plasmin as has been performed with polymeric materials crosslinked with enzymatically labile moieties.[130–134] The biodegradability of self-assembling peptides is an essential feature that enables *in vivo* deposition of material without later invasive removal.[129]

Secondly, self-assembling peptides are generally regarded to have low immunogenic potential which can be modulated depending on the incorporated sequences, their presentation to immune cells, and the morphology of formed nanostructures.[38] Generally, small molecules are regarded to be non-immunogenic, requiring chemical conjugation to larger macromolecular carriers to enhance their immunogenic potential. Termed haptens, such small molecules are not able to effect immune responses due to a lack of cross-linking capability between B-cell antigen receptors and undergo antigen presentation.[135] While self-assembling peptides themselves are small molecules consisting of natural amino acids, questions regarding the immunogenicity of their resulting self-assembled nanostructures has led to investigations of their immunogenic potential in preclinical models. After injection into test animals, the β-sheet forming EAKII peptide was shown to not elicit an inflammatory response at the injection site, nor to induce

observable tissue abnormalities.[136] Similar results have been observed for other β-sheet forming peptides which lack acute toxicity and facilitated formation of normal tissue.[137] Chemically modified self-assembling peptides bearing adhesion ligands, chemical functionality, or lipophilic modifications have been shown to exhibit low immunogenic potential.[33,138,139]

Despite the lack of observed immune response, only a few studies have investigated the immunogenic potential of self-assembling peptides for antibody production. The generation of IgG antibodies for a self-assembling polyglutamine peptide alone or modified with the integrin binding RGDS sequence was investigated to fundamentally characterize the peptide's immunogenic potential.[140] Although the peptide sequence was confirmed to be foreign to the mouse, only 1 mouse out of 5 generated a detectable response to the RGDS bearing peptide, while the unmodified peptide and a mixture of both peptides failed to generate any detectable antibody titer.[140] Thus, the results of this study are consistent with the conclusion that the peptides and their analogs exhibit low immunogenicity.

The context of the sequences presented in the self-assembling peptide appears to play a role in potential immune response. Although the structures of the unmodified and RGDS modified peptide nanostructures are approximately the same, an obvious difference in the immunogenic potential of the amino acid sequences exists.[140] Additionally, the degree of immune response can be different between modified peptides. Indeed, the RGD sequence has been previously observed to enhance the adjuvant activity of peptide vaccines delivered through nasal delivery.[141] Overall, while immunogenicity may be designed and

incorporated into self-assembling peptide sequences for specific applications such as vaccine delivery, a general assumption derived from the current body of literature is that self-assembling peptides are largely non-immunogenic. Nevertheless, the immunogenicity of self-assembling systems must be assessed on an individual basis, since the likelihood of a potential immune response is difficult to accurately predict for these systems.[140]

The amenability of self-assembling peptide systems to a range of chemical modifications is another feature ideal for application as biomaterials. Solid-phase chemistry enables rapid and divergent synthesis of chemically distinct self-assembling peptides bearing a range of modifications including fatty acids, reactive chemical moieties, unnatural amino-acids, ligands, and macromolecular modifications.[32,142–146] The mild reaction conditions afforded by solid-phase synthetic methods are tolerant to a wide range of chemical functionalities and well developed protecting group strategies greatly aid the chemist in developing synthetic plans.[96,147] Depending on the reagents and resin chemistry used, chemical modifications to stabilize peptides at termini for biomedical use may also be applied.[95,148]

Additionally, as previously mentioned, biological signaling sequences such as cell adhesion, growth factors, and other hormonal signals may be encoded into peptide sequences at the desired location to generate monodisperse and biofunctionalized monomers.[36] This is in contrast to polymeric systems where biological recognition motifs are often incorporated into polymeric systems post-polymerization yielding varying levels of functionalization throughout the material.[149–151] Modularity of self-assembling systems

is a feature not only of individual monomer units, but also of their combinations in self-assembling structures to develop multifunctional materials. Unmodified, modified, and mixtures of modified self-assembling peptides may be co-assembled into nanostructures at desired ratios.[144,152] Co-assembly has been achieved with a self-assembling peptides bearing cell adhesion motifs, bioactive drug molecules and imaging agents, nanostructure stabilizing motifs, modifications to chemically catalytic assemblies, as well as fluorescent moieties.[33,140,152–155] Modular assembly approaches pose a significant advantage to other systems as functional biomaterials as tight control of bioactive moiety concentration can be achieved, as the amount of functionally modified peptide will be the concentration added to the co-assembly.[47,48]

The ease of fabrication of peptide co-assemblies is also a desirable feature. Chemical modification of covalent polymers can have a significant effect on characteristics such as viscosity, solubility, and colloidal stability of formed nanostructures and can complicate processing.[156] While attachment of bioactive moieties to peptides can alter the balance of non-covalent interactions contributing to self-assembly, oftentimes the simple presence of the unmodified self-assembling peptide can lead to stabilization of the modified peptide within the assembled nanostructure. An extreme example was achieved by demonstrating co-assembly of full-length proteins into peptide nanofibers.[155] Fluorescent proteins could be recombinantly expressed bearing pro-fibril forming sequences termed "β-tails", which enabled favorable expression through fermentation in *Escherichia coli* without aggregation. In the presence of β-sheet forming peptides, multiple proteins were able to be incorporated into nanostructures with high levels of control.[155]

A fourth key characteristic of self-assembling peptide biomaterials is their ability to respond to stimuli in a dynamic manner. The non-covalent interactions governing assembly closely mimic the interactions leading to biomolecular assembly and molecular recognition present in living systems.[157] Although cooperativity in the non-covalent interactions leading to assembly convey significant structural stability to the assembled structures, the individually weak interactions enable sensitivity to a wide variety to stimuli that not only regulate assembly and disassembly, but also morphological transitions.[20] Responsiveness to both endogenous and exogenous stimuli has been engineered into self-assembling peptide systems to gain functional control over material characteristics after application within biological environments.[21,22] Early examples of dynamic responsiveness include the characterized self-assembly and gelation of β-sheet forming self-assembling peptides such as RADA and EAK after application to bodily fluids.[58] Additionally, the enhancement of rheological properties in the presence of endogenous divalent cations have also been demonstrated as a mechanism of responsiveness.[158]

Though these early examples have demonstrated clinical translatability, next generation mechanisms of responsiveness aim to exceed the spatiotemporal control offered by sensitivity to pH and ionic strength as little control over these environmental cues is possible within organisms. Enzymes have emerged as a powerful tool to regulate supramolecular assembly as they possess substrate specificity, are catalytic in effecting chemical transformations, and offer biocompatibility that is not present in other catalytic methods.[159] Thermal responsiveness is another stimulus that has been utilized with peptides to control their assembly. *De novo* designed β-hairpin peptides have long been

demonstrated to undergo assembly and gelation at temperatures above a lower critical solution temperature (LCST). Such hydrogels have been utilized for injectable delivery systems which undergo spontaneous self-assembly due to the increased temperature within an organism.[70,134,160] A thermally responsive moiety was constructed into self-assembling peptides through modification with the thermally responsive polymer poly(N-isopropylacrylamide) (PNIPAAm).[161] Similar to the β-hairpin peptides, PNIPAAm possesses an LCST and was shown to rigidify hydrogels formed from FEFEFKFK peptide.[161] Self-assembling peptides sensitive to other physical stimuli such as magnetic fields, ultrasound, and electromagnetic radiation hold promise for exploring biomedical application.[162–164]

In addition to environmental cues, self-assembling peptides may also be sensitive to the presence of ligands or complementary peptides. Self-assembly of D-Ala bearing peptides was triggered through addition of vancomycin, an antibiotic inhibitor of bacterial cell wall biosynthesis.[165] Similarly, completely cationic or anionic peptides have been shown to only assemble in the presence of the complementary ionic peptide as a mechanism to control gel formation through modulation of ionic interactions.[166] Biorthogonal chemistry has also been utilized to cross-link self-assembled peptide nanofibers, as well as conjugate neighboring monomers, in order to generate covalent polymers.[145,167]

## 1.2 SELECT BIOMEDICAL APPLICATIONS OF SELF-ASSEMBLING PEPTIDES

### 1.2.1 ANTIMICROBIALS AND BIOSURFACTANTS

Taking advantage of their amphiphilic nature, lipopeptides have increasingly been investigated for their surfactant properties in a variety of industries ranging from agriculture and biotechnology to medicine.[168,169] Similar to synthetically derived peptide amphiphiles, lipopeptides possess lipid moieties conjugated to a peptide sequence. Contrary, to the high aspect ratio organization of monomers into nanofibers by peptide amphiphiles, these molecules often form surfactant like spherical micelles.[170,171] Relevant to biomedical application, clinically used lipopeptides such as daptomycin and polymyxin b have demonstrated antimicrobial properties through disruption of bacterial membrane integrity (**Figure 1.12**).[172]

With growing interest in this mechanism of action, combined with the continued rise of resistant microbial strains and the dearth of new antibiotics, self-assembling peptides with antimicrobial characteristics have emerged as a promising therapeutic strategy to address this clinical need.[173] Antimicrobial peptides are ubiquitous across life with many organisms producing their own agents to defend against infection.[174,175] Interestingly, the phenomenon of self-assembly is now being recognized to play a role in the bioactivity of antimicrobial peptides.[176] For example, the human protein α-defensin 6 self-assembles into nanofiber networks upon binding to bacterial cell surfaces in the intestine, thus limiting pathogenic capability.[177] An additional human example is presented by the antimicrobial peptide dermicidin, which is secreted in human perspiration. Investigations into the mechanism of action have shown that $Zn^{2+}$ stabilizes the assembly of peptides into higher

ordered oligomers, neutralizing their respective charge and facilitating entry into pathogen membranes.[178] Recently, the cysteine-abundant antimicrobial peptide protegrin-4 was shown to form β-sheet fibrils which retained antimicrobial activity without demonstrating toxicity towards human cells.[179] In the development of antimicrobial peptides, self-assembly presents several advantages for therapeutic applications since higher ordered structures can impart greater selectivity for pathogen membranes, exhibit stimuli responsiveness to control activity, and demonstrate favorable pharmacokinetic properties in comparison to free monomers.[176]

Reminiscent of the lipopeptide antibiotics, peptide amphiphiles have been investigated as synthetic alternatives to naturally derived molecules. The peptide WMR, derived from the marine antimicrobial peptide myxinidin, was modified with alkyl chains to enable co-assembly with non-therapeutic peptide amphiphiles into nanofibrous structures.[180] Assembly into the higher ordered structures at the nanoscale enhanced the antimicrobial and antibiofilm activity of the peptide, possibly due to higher localized concentrations and greater proteolytic stability in the self-assembled form[180]. As cationic residues drive initial ionic interactions between antimicrobial peptides and the negatively charged bacterial membranes, a peptide amphiphile bearing the $(AKKARA)_2$ Cardin-Weintraub motif was synthesized and investigated for its efficacy against drug resistant bacterial strains.[181] In addition to the terminal cationic motif, the peptide amphiphile possessed an internal β-sheet forming domain adjacent to the fatty acid tail to stabilize the growth of linear nanofibers. Interestingly, addition of only a single AKKARA sequence at the C-terminus of the peptide corresponding to the solvent exposed region was tolerated

for self-assembly. Systematic investigation of the Cardin-motif peptide amphiphile's mechanism of action revealed the molecule possessed high binding affinity to lipopolysaccharides present in bacterial membranes, leading to membrane disruption. These effects were shown to lead to significant inhibition in the growth of methicillin resistant S*taphylococcus aureus* (MRSA) and multi-drug resistant *E. coli* compared to non-assembling counterparts and non-Cardin motif bearing amphiphiles.[181]

Complimentary to the membrane associative character of antimicrobial peptides, the nanostructure morphology dictating the presentation of these motifs to pathogen membranes has also emerged as a design consideration to maximize therapeutic potential.[182] A supramolecular structure-activity relationship study was undertaken to determine how morphological differences in formed nanostructures between similar peptide amphiphile sequences.[182] A panel of fatty acid modified poly-Lys peptide amphiphiles were synthesized that incorporated various fatty acid chain lengths and amino-acid modifications adjacent to the tails to influence propensity for intermolecular association between monomers leading to linear versus spherical assembly.[182] Surprisingly, spherical assemblies were found to have the greatest antimicrobial effect, exhibiting broad spectrum potency *in vitro* and in *Galleria mellonella* infection models.[182] The discrepancy between the antibacterial activity of differing morphologies was reasoned to be a product of the lower relative stability of spherical micelle assemblies compared to nanofibers and related linear structures.[182] Decreased stability in the spherical structures was likely to result in an increase of monomer release compared to nanofibers, essentially indicating that antimicrobial activity likely derives from released monomers and is only

secondarily related to morphology.[182] The use of such nanostructures as therapeutic delivery vehicles points to their behavior as therapeutic depots rather than bulky nanoparticles delivering many active moieties to a single cell.[182]

**Figure 1.12. Mechanisms of antimicrobial peptide biological activity**

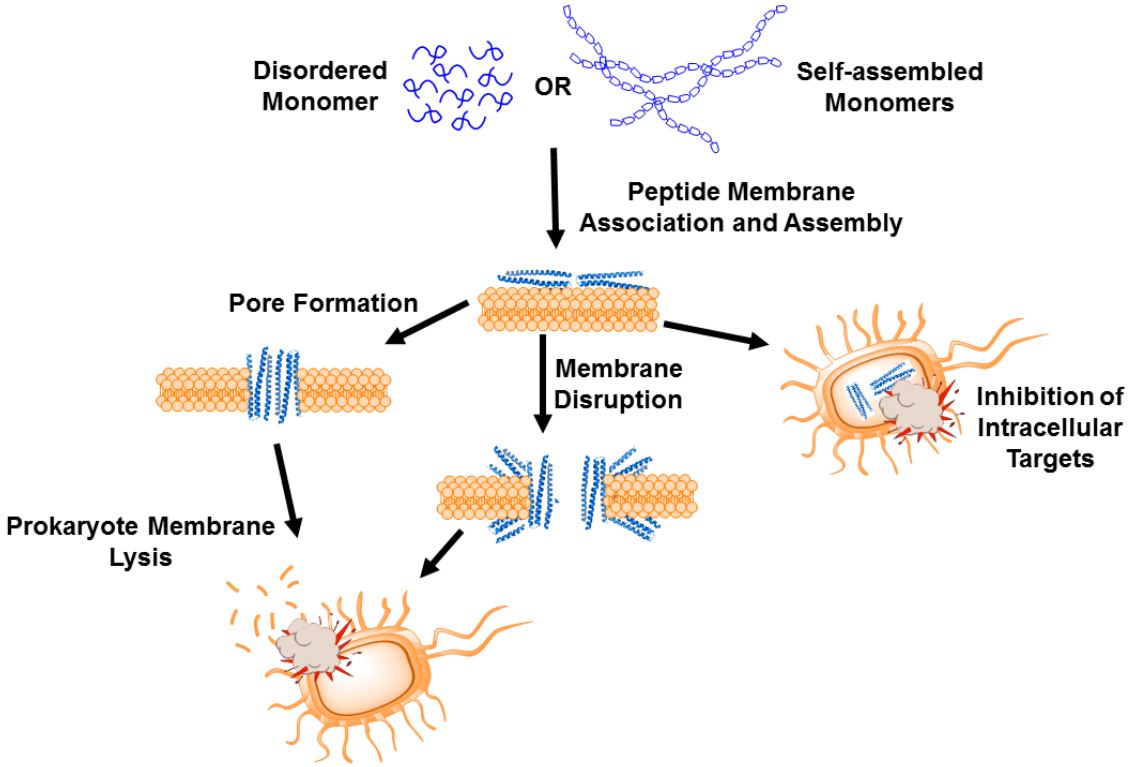

Further evidence of this phenomenon was provided in a study demonstrating that the thermodynamics of self-assembly directly relate to the antibacterial potency of self-assembling antimicrobial peptides.[183] Guanine nucleobase modified derivatives of magainin II and cecroin A-melittin, both biologically derived antimicrobial peptides, were investigated for their antimicrobial activity as a function of increasing guanine content. Due to the high self-association potential provided by guanine hydrogen bonding interactions, derivatives bearing high numbers of these residues possess high energetic barriers for dissociation and subsequent insertion into microbial membranes. This limits the free monomers available to exert a therapeutic effect and correlated experimentally to decreased potency.[183]

Longer synthetic self-assembling peptide sequences have also demonstrated antimicrobial activity against pathogenic organisms. A designed peptide sequence originating from BPIFA2, a protein secreted in human saliva, was found to have antibacterial activity after changing polar residues to cationic Lys residues.[184] The peptide termed GL13K and its D-enantiomer were investigated for the purpose of delineating biological activity between monomer and potential self-assembled structures.[185] Interestingly, the D-peptide derivative exhibited greater potency than the L-peptide derivative which was only partially attributed to differences in metabolic degradation.[185] Although both peptides eventually formed nanofibers as a thermodynamic product, the D-peptide underwent pathway dependent morphological transitions and possessed rapid assembly kinetics in comparison to the L-peptide. Additionally, a scrambled L-peptide consisting of the same amino acids demonstrated no activity and failed to assemble into

higher ordered structures.[185] These results were taken to indicate that the process of self-assembly was necessary for inhibitory activity due to the observed dependence on kinetics and morphology.[185]

*De novo* designed peptides that self-assemble into nanofibers were investigated with solid state NMR spectroscopy to address the monomer versus nanostructure antibacterial activity question.[186] In a block sequence design, the peptide D-W362 consisted of D-Lys residues at the termini to provide cationic character and the central block contained repeating Gln-Leu residues to drive assembly into β-sheets. Determination of minimum inhibitory concentration (MIC) values against gram negative bacteria provided evidence that peptide assemblies were responsible for activity as removal of monomers and oligomers through filtration and centrifugation did not alter activity.[186] Fluorescence microscopy and TEM were further utilized to characterize the inhibitory effect of the D-W362 as nanofibers were found to be associated with bacterial membranes and were predominantly associated with dead bacteria. Solid state NMR was used to investigate the membrane interactions of the peptide and confirmed that nanofibers preferentially interacted with liposomes over monomers and that exposed Leu residues may contribute to the membrane lytic activity.[186]

In addition to their membrane disruption function, endogenous antimicrobial peptides may also exert activity through immunomodulation, a feature that has inspired incorporation into potential therapeutics. The antimicrobial peptide LL-37 is one such immunomodulatory peptide whose dysregulation has even become associated with

autoimmune disorders such as atopic dermatitis and psoriasis.[187] LL-37 has been recognized to play a multifunctional role during inflammatory responses to infection.[188] While it possesses selective pathogen membrane lytic ability due to its highly cationic character, LL-37 can also lyse eukaryotic membranes at high concentrations, and even more surprisingly, forms supramolecular complexes with DNA to activate the innate immune system.[189,190] The mechanism by which LL-37 interacts with DNA is thought to derive from the high cationic character of the peptide, which has been observed to facilitate membrane transport of double stranded nucleic acids for presentation to Toll-Like Receptors (TLRs), as well as activation of the Type I interferon response through cytoplasmic sensing of DNA through the Stimulator of Interferon Genes (STING) pathway.[189,191] LL-37 was recently investigated for its roles in activating both TLR-9 and TLR-3 and found to generate protofibrils that complex with double stranded DNA forming a crystalline packing arrangement.[192] The ordered arrangement was shown to induce high avidity binding to TLR-9 resulting in induced cytokine release[192]. Importantly, the results of these studies provide a rationale for the design of antimicrobial peptide scaffolds capable of nucleic acid complexation and TLR activation through manipulation of spatial charge distribution along the assembled axis.[192] With the relevance of immunomodulation to diseases such as cancer and autoimmune disorders, this mechanism of immune modulation may lead to alternative classes of therapeutic agents.

### 1.2.2 HORMONAL SIGNALING MODULATION

Small molecule therapeutics are traditionally considered to induce monomeric interactions with their molecular target such as a single active agent inhibiting a pathogenic protein or endogenous signaling enzyme.[193] While significant bodies of work have investigated the role of bivalent and multivalent ligands in medicinal chemistry, the supramolecular presentation of bioactive therapeutic moieties is comparatively more recent due to growing interest nanomedicines since the discovery of self-assembling peptides.[49,194] Considered in this section are self-assembling peptides and related derivatives with direct biological action, either as monomer depots or in a supramolecular format. Agents chemically modified with therapeutically active moieties are discussed in a later section.

Peptide hormones are a class of biological signaling molecule that primarily exert their therapeutic function through ligand activity at extracellular signaling domains of cell surface receptors.[195] As signaling components of the endocrine system, peptide hormones are responsible for controlling a wide range of physiological function including food consumption. In particular, self-assembling peptide YY is a 36 amino acid peptide hormone that is released after meal consumption and regulates continued food intake and gastric mobility.[196] Despite its endogenous physiologic function, the clinical use of the peptide and its derivatives as therapeutics is limited by poor pharmacokinetic properties, since the peptides may be rapidly secreted and subject to metabolic deactivation.[197] Self-assembling derivatives of peptide YY functionalized with lipid chains have been investigated for their potential to decrease endogenous protease hydrolysis through micelle formation and binding to circulating albumin (**Figure 1.13**).[198] Palmitoylation was used to

lipidate peptide YY through different conjugation sites within the peptide to induce aggregation into micellar assemblies and form gels.[198] The location of the conjugation site was found to influence the self-assembling properties through modulation of the critical aggregation concentration, as well as nanostructure morphology.[198] The high sensitivity to the conjugation site was explained through substitution of cationic residues with the lipid modification, influencing the degree of charge screening and solution pH required to initiate assembly.[198] Self-assembly as a result of lipidation was found not only for the full-length protein, but also extended to lipid modified fragments of peptide YY. To facilitate synthesis and characterization, shortened derivatives of peptide YY were synthesized that consisting of the first 6 or 8 amino-acid residues from the N-terminus of the parent peptide, which were shown to self-assemble into micelle structures under solution conditions.[199] While the self-assembling properties of these molecules were characterized, correlation to biological activity was not reported.

Extending the self-assembly of signaling molecules to biological function, direct interaction of self-assembled nanostructures with the protein galectin-3 was recently investigated *in vitro* as a potential therapeutic strategy (**Figure 1.13**). Galectin-3 is a carbohydrate binding protein that is expressed in a variety of cell and tissue types, may be localized in various locations inside or outside of the cell, and has become associated with diseases such as fibrosis and cancer.[200] Galectin-3 naturally binds to saccharide moieties such as galactose and lactose which are not effective at inhibiting protein function due to very low affinity in the monomeric state.[201] Supramolecular presentation of monomeric binding ligands was investigated using n-acetylgalactosamine-β1,4-n-acetylglucosamine

(LacDinAc) modified β-sheet forming self-assembling peptides.[202] Nanofiber presentation of the ligand generated micromolar affinity for galectin-3 through increased avidity effects observed through binding in biochemical studies, although the results did not carry over to *in vitro* studies due to competition with serum components.[202] However, under low serum concentration conditions, the nanofibers were shown to inhibit galectin-3 mediated spontaneous apoptosis of T-cells.[202] Clearly, the multivalent presentation of bioactive ligands through decoration on supramolecular nanofibers presents a unique method of increasing the therapeutic potential of relatively weak interactions previously considered undruggable.

In addition to supramolecular presentation, conjugation of signaling hormones to self-assembling peptides has been shown to stabilize active conformations of shortened bioactive sequences. Synthetic short peptides, lacking the rest of the protein structure to stabilize active conformations, often form disordered coils in solution and lose binding efficacy.[203] Selective stabilization of a peptide derived from insulin-like growth factor 1 in a β-sheet conformation was achieved through conjugation to a short aromatic peptide.[203] Stabilization of this conformation was shown to more closely mimic the natural ligand presentation for binding as an α-helical derivative, while the non-stabilized peptide formed random coils and exhibited little activity.[203]

A similar phenomenon was reported in peptide amphiphile displayed ligands mimicking brain-derived neurotrophic factor which binds tyrosine kinase B receptors found in the CNS.[204] While the derivative peptide showed no activity alone, an

enhancement in downstream signaling was observed in primary cortical neurons and increased functional maturation was observed when the cells were cultured in ligand functionalized peptide amphiphile gels.[205] Signaling molecules need not be covalently linked to assembling monomers to confer stability. Supramolecular association of signaling growth factors such as transforming growth factor-β1 and bone morphogenetic protein 4 was achieved through non-covalent interactions with anionic self-assembling peptides enabling the fabrication of controlled release materials.[206]

**Figure 1.13 Supramolecular presentation biological signaling moieties**

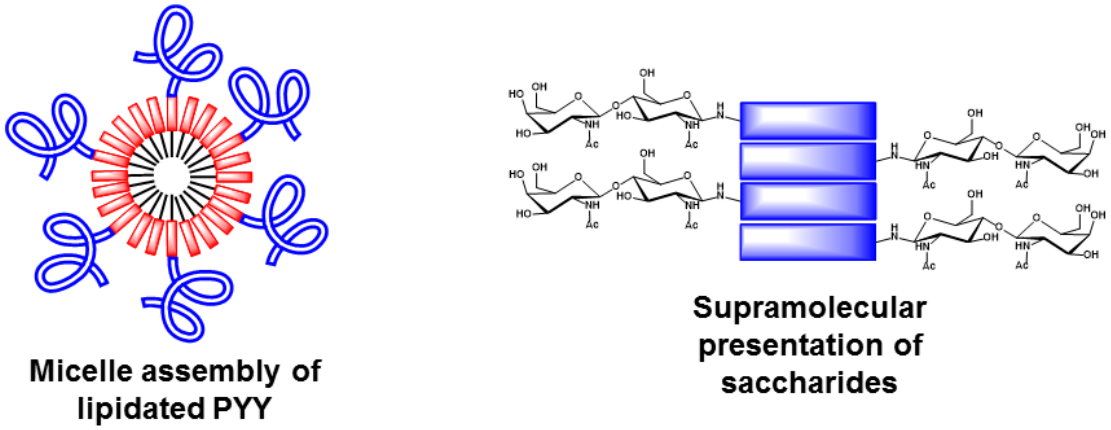


### 1.2.3 IMMUNOTHERAPY AND VACCINES

Supramolecular materials have proven to be invaluable for the advancement of vaccine development and immunotherapy.[207,208] As an alternative to existing vaccine strategies, self-assembling peptides have garnered interest as vaccine adjuvant materials to present disease associated antigens for recognition by the immune system (**Figure 1.14**).[208,209] Short aromatic peptides constructed from all D-amino acids were used to test

the generation of an immune response in mice against chicken egg albumin.[210] Immune response and resulting antibody titers were found to be dependent on the peptide charge state, since cationic derivatives exhibited greater immune stimulation than either a neutral or anionic peptide.[210] Interestingly, the formation of an immune response was not dependent on covalent attachment of the albumin to a self- assembling peptide, contrary to other adjuvant materials where direct attachment to the antigen is required.[211] Favorable humoral responses to adjuvants utilizing self-assembling peptides composed of D-amino acids rather than their L-configuration have been reported by others as well.[212] An antigen from chicken egg ovalbumin was conjugated to either L- or D-configured Phe-Lys-Phe-Glu-Phe-Lys-Phe-Glu self-assembling peptide and used to vaccinate mice. Although the generation of CD4+ effector T-cells was comparable between the stereochemically different peptides, higher antibody titers, and greater persistence of the vaccine material at the injection site were exhibited by the D-peptide.[212] Interestingly, greater stability at the injection site represents a plausible explanation for the favorable responses garnered through using unnatural D-peptides as adjuvant materials, since their degradation by extracellular proteases will be kinetically slower than their L-configuration counterparts.[212]

Direct attachment of antigens may also be achieved with self-assembling peptides due to the facile chemistry involved, thus facilitating opportunities for optimizing the presentation of antigens with differing morphologies and self-assembling moieties. An α-helix forming self-assembling peptide was used to present a clinically relevant antigen derived from epidermal growth factor receptor class III variant (EGFRvIII).[45] To enhance humoral immune response, peptides bearing T-cell selective epitopes were co-assembled

into the antigen nanofibers which induced favorable increases in antibody production and produced increased T-cell responses.[45] Additionally, the epitope bearing α-helical peptides were shown to be internalized by antigen presenting cells although the mechanism of uptake and importance of monomer versus nanoassembly uptake was not further characterized.[45]

**Figure 1.14 Self-assembling peptides for immunotherapy and vaccines**

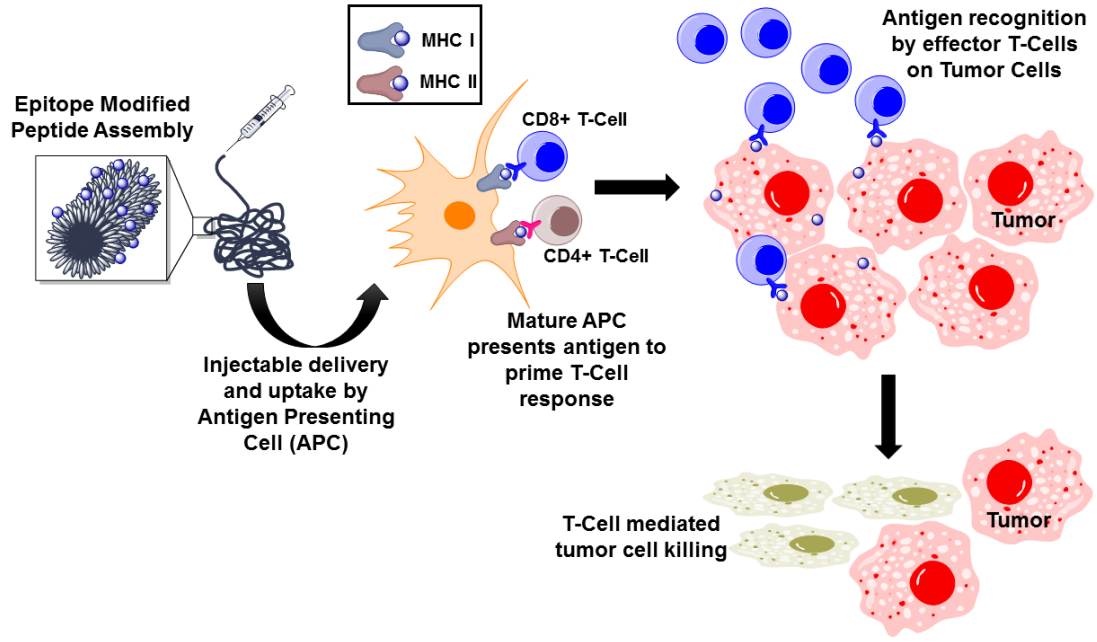

Immunization against tumor necrosis factor (TNF) was demonstrated in a similar system that also bore universal CD4+ T-Cell epitopes to promote humoral response.[44] In contrast to the previous example, this system utilized a β-sheet forming peptide which was able to generate significant T-cell responses to TNF indicating that the presentation morphology is not critical to the immunization process.[44] *In vivo* studies confirmed that immunization against TNF prevented lipopolysaccharide induced inflammation.[44]

A well characterized epitope of ovalbumin was conjugated to a dialkyl modified peptide amphiphile to investigate systemic antitumor effect of ovalbumin expressing tumor cells.[213] The unusual dialkyl modification was chosen to limit Toll-Like Receptor activation and observe tumor immunity arising from presentation of the peptide epitope alone.[214] Immunization against the ovalbumin expressing tumor cells was achieved and attributed to the peptide amphiphile facilitating dendritic cell uptake of the peptide epitope through hydrophobic insertion into dendritic cell membranes and stability enhancement of the peptide at the injection site.[213] Results of the study indicate that although some modified peptide derivatives and lipidated molecules can promote innate immune responses, adaptive responses may also be promoted by self-assembling adjuvant materials.

### 1.2.4 DRUG DELIVERY

Among the most investigated applications for self-assembling peptide materials is their use for the delivery of therapeutic agents. Traditional drug delivery materials for pharmaceutic applications generally involve non-covalent or covalent attachment to an excipient material which is used to control the disposition of the agent after dosing through

tissue targeting, limiting metabolism, and controlling release rate as examples.[215] Typically, these are polymeric materials that form gel like materials for localized delivery or micelles for systemic delivery.[216] Self-assembling peptides have been utilized in the same manner to form hydrogels for localized delivery either through stimuli-responsive drug encapsulation or through direct conjugation of therapeutic agents to self-assembling moieties.[47,217]

Self-assembled nanomedicines present an especially exciting class of delivery agents.[47,48] Direct conjugation of a self-assembling peptide to a bioactive agent essentially creates a one component drug delivery vehicle where the drug molecule is simultaneously both the therapeutic and delivery agent (**Figure 1.15**).[47] Oftentimes, the chemistry conjugating the drug molecule to the self-assembling moiety is designed to contain an effective prodrug of the active agent which would release the active moiety either within, or in proximity to a diseased cell.[218] Generally, the chemical modification to induce self-assembly of therapeutic molecules is hydrophobic in nature, and such modifications have been performed with a wide range of fatty acid, isoprenoid, and lipid functionalities for the purpose of triggering assembly into nanostructures and gels at the macroscopic scale.[48,217]

Additionally, self-assembled peptide nanomedicines for drug delivery have most commonly used hydrophobic aromatic peptides which possess multiple functions in the delivery platform: facilitating self-assembly, providing hydrophobic moieties that can facilitate cell entry, and providing metabolic stabilization and tissue retention of the active agent.[219] Conjugation of hydrophobic drugs is generally performed with agents that possess

poor pharmacokinetic properties or significant off-target toxicities, where direct application through an injectable formulation would be advantageous compared to systemic delivery. Two such agents are doxorubicin (DOX) and paclitaxel (PTX) which possess poor water solubility and significant off-target toxicities requiring novel formulations.[220,221] Both agents have been heavily investigated for *in situ* hydrogel delivery through self-assembling peptides due to their poor physiochemical properties as single agents, but high potency against cancer cells. DOX and PTX were both assembled into nanofiber hydrogels through direct chemical conjugation to an N-terminally capped aromatic peptide.[222] The peptide, also possessing phosho-Tyr residues, self-assembled in the presence of alkaline phosphatase resulting in removal of assembly blocking phosphate moieties and facilitating peptide-peptide interactions.[222] Interestingly, this method facilitates the assembly of hydrophobic drug-peptide conjugates as the phosphate groups solubilize the parent molecule and enable organization in the presence of catalyzing enzyme without precipitation from solution.[218,222]

Maintaining the stability of an injected supramolecular peptide drug delivery hydrogel is key to achieving a long-term release formulation without burst release kinetics that can lead to injection site toxicity and rapid metabolic deactivation and clearance of the chemotherapeutics.[218] N-terminally capped aromatic peptides with either D- or L-stereochemistry and possessing both phospho-Tyr and PTX modifications were self-assembled into drug carrying hydrogels in the presence of alkaline phosphatase.[222] The D-peptide modification was shown to be more hydrolytically stable to protease degradation compared to the L-peptide. Nevertheless, the D-peptide was still able to undergo catalytic

dephosphorylation to form hydrogels resulting in greater long-term potentialantitumor efficacy.

**Figure 1.15 Self-assembling peptides as single component nanomedicines for drug delivery**

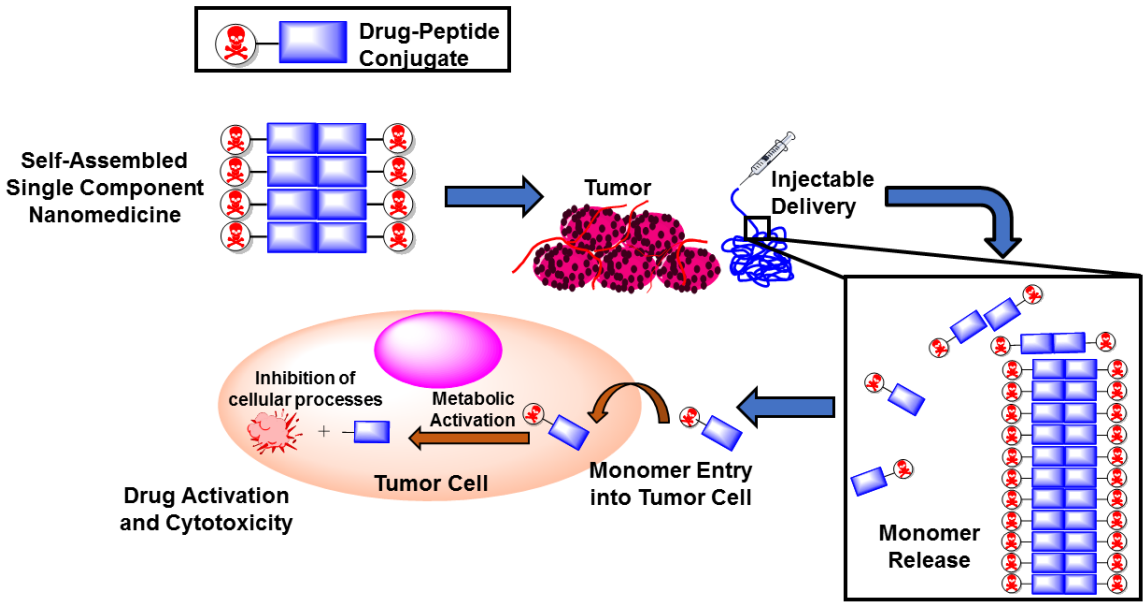

A similar enhancement of activity was observed for a self-assembling D-peptide for the delivery of cyclooxygenase-2 inhibitors to treat localized inflammation.[223] The NSAID naproxen was shown to possess increased potency for cyclooxygenase-2 when conjugated to the self-assembling peptide and with increased selectivity for its target over other isoforms.[223] Interestingly, the conjugation site of naproxen to the peptide was found to have a profound effect on the release kinetics of constituent monomers from the hydrogels indicating different conjugates possessed differing hydrogel assembly properties as well as critical aggregation concentration.[223]

Naproxen bearing hydrogelators were also combined with those bearing anti-HIV nucleoside based reverse transcriptase inhibitors to reduce inflammation at the site of injection and generate a prophylactic anti-HIV hydrogel.[224] Similar to the differing release rates observed for naproxen, the release of anti-HIV agents was shown to be dependent on the nucleoside therapeutic present as well as N-terminal modification again highlighting how modifications to molecular structure affect the thermodynamic properties guiding assembly.[224]

Additionally, prodrug self-assembly and delivery is not completely dependent upon *in situ* injection of a hydrogel solution for localized delivery. An interesting methodology to yield self-assembled nanomedicine within the tumor after systemic delivery was explored through phosphatase catalyzed hydrolysis of phosphor-Tyr residues.[225] A platinum(IV) prodrug of cisplatin was conjugated to a short aromatic peptide and administered systemically to mice, with self-assembly dependent upon overexpressed

phosphatases in the tumor microenvironment. Conjugation of the platinum agent to the self-assembling peptide resulted in increased tumor accumulation in biodistribution studies, decreased off-target toxicities compared to the free platinum agent, and maintained therapeutic antitumor efficacy *in vivo.*[225]

Peptide amphiphile conjugation has also been widely investigated as a method for generating drug delivery hydrogels. Hydrazone linkages are commonly used in therapeutic delivery vehicles due to their acid lability, leading to release of carbonyl containing therapeutics under the acid environment of the lysosome or in certain cellular microenvironments.[226] Acylhydrazine functionality was introduced into the peptide segment of a peptide amphiphile and used to generate a hydrazone linkage through condensation with the ketone of nabumetone, an NSAID pain reliever.[227] Release of the therapeutic agent was observed to occur in an initial burst followed by slower zero-ordered kinetics indicating hydrolysis of the linkage even under physiologic pH.[227]

Delivery of dexamethasone, a steroidal anti-inflammatory agent, was also achieved through a hydrazone linkage to a peptide amphiphile.[228] Dexamethasone was chosen for delivery to develop an anti-inflammatory hydrogel that could be used to treat autoimmune disorders and aid in cell transplantation therapies. Hydrolysis of the hydrazone linkage was controlled over several weeks and demonstrated efficacy in a mouse inflammation model where localized inflammation was suppressed without systemic effects.[228]

Therapeutic release from hydrazone linkages to peptide amphiphiles was systematically investigated through incorporation of a model fluorophore to different

locations within the peptide amphiphile structure.[229] Interestingly, the release kinetics of the agent was found to be dependent on the conjugation site in relationship to its effect on amphiphile packing into micelles as well as the ability to form β-sheet interactions between monomers.[229] These factors were predicted to influence the access of solvent to the hydrazone linkage with more solvent exposure leading to an increase in the rate of hydrolysis kinetics[229]. In addition to behaving as localized drug release depots, peptide amphiphile nanofibers have been investigated as active drug targeting formulations for systemic delivery.[230] Incorporation of an apolipoprotein A1 derivative sequence into the peptide segment of a peptide amphiphile and subsequent co-assembly with a non-targeting amphiphile generated soluble nanofibers capable of targeting atherosclerotic plaques.[230] The nanofibers were loaded non-covalently with a hydrophobic liver X receptor agonist to facilitate lesion reduction and antiatherosclerotic activity when targeted to sites of disease.[230]

A direct comparison of encapsulation versus covalent attachment to self-assembling peptides was investigated with opioid analgesic peptides derived from demorphin and endomorphin-2.[231] To develop a long-lasting opioid delivery formulation to treat chronic pain, a panel of analgesic peptides were conjugated to self-assembling peptides possessing natural amino acid sequences or metabolically stabilized peptides.[231] While the opioid agonist peptides possessed high levels of potency at the μ-opioid receptor (MOR), decreased potency was evident after self-assembling peptide conjugation.[231] Significantly reduced potency and in some cases altered pharmacological properties by the self-assembling peptide conjugation indicated that direct chemical incorporation into the

self-assembling structure afforded a level of safety from overstimulation.[231] Surprisingly, little difference was observed in the anti-nociceptive properties between the peptide hydrogel based methods indicating that monomer erosion from the fibrous hydrogels is the primary mechanism for therapeutic release instead of active proteolytic degradation.[231] However, proteolytic release of the active peptide agonist was still required for prodrug activation, since proteolytically stabilized conjugation resulted in decreased *in vivo* potency.[231]

The direct self-assembly of therapeutic agents has also led to injectable gel formulations, generally with peptide based drugs that represent true single component nanomedicines. Two such molecules have been approved as therapeutics. Lanreotide is a macrocycle somatostatin analog used in the treatment of acromegaly and certain neuroendocrine cancers.[232,233] In aqueous solution, lanreotide spontaneously assembles and forms hydrogels enabling its administration to patients in an injectable gel form. The self-assembly properties of lanreotide have been well investigated, revealing that the molecule forms highly defined nanotubes in aqueous environments, approximately 24 nm in diameter with a shell thickness 1.8 nm.[234] The injectable gel performs as a slow release depot, with released monomers antagonizing somatostatin receptors to decrease growth hormone production(**Figure 1.16**).[235]

A second clinically used peptide therapeutic gel is degarelix, which is a gonadotropin releasing hormone (GnRH) receptor antagonist that is used for the chemical castration of patients suffering from prostate cancer.[236] Degarelix self-assembles into

amyloid like fibers and exhibits a favorable safety profile and sustained hormonal castration for up to 50 days(**Figure 1.16**).[237] Additionally, self-assembly into amyloid like fibers has been investigated as a general property of GnRH receptor antagonists, with studies into enhancement of self-assembling properties under continued investigation.[238,239]

Other endogenous self-assembling peptides have been discovered and investigated as potential therapeutic hydrogels. A recent investigation characterized the gelating properties of hemopressin, a known self-assembling peptide with pharmacological action at cannabinoid receptors was undertaken to investigate formation of slow release depot.[240,241] The self-assembly of the peptide hydrogel was observed to be dependent on pH, was able to release both encapsulated macro- and small molecules, and was shown to be biocompatible.[240–242] Interestingly, hemopressin and related analogs have shown potency in reducing neuropathic pain in rodents presenting a possible clinical application.[242]

Universal among these peptides and their resulting self-assembled gels is a dependence of pharmacological activity upon slow and sustained release of monomer peptides. By extension, the thermodynamic parameters governing the self-assembly of peptides into higher ordered structures has a direct effect on the potential clinical utility of these agents.[183] Monomers must possess enough associative attraction to form temporally stable nanostructures to prevent burst release, and favorable non-covalent attraction between assembled nanostructures is required to provide macro-stability to the gel

formulation to prevent rapid material dissolution.[47,48] However, as monomers are generally the therapeutically active agents, the critical aggregation concentrations of the peptides must be sufficiently high in order to release pharmacologically relevant concentrations of the peptide.[182,231] Additionally, gel properties such as crosslinking density could also play an effect in controlling the release kinetics of monomers from therapeutic depot gels.[243] Clearly, further investigation is necessary to optimize the balance of physiochemical and material properties necessary for generating clinically translatable self-assembling peptide therapies.

**Figure 1.16 Structures of Lanreotide and Degarelix**

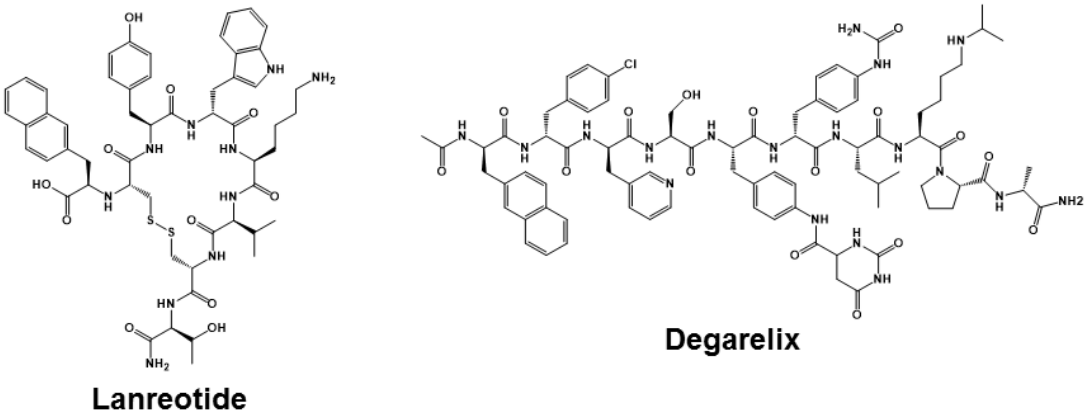

# CHAPTER 2: ENZYMATIC REGULATION OF SELF-ASSEMBLING NUCLEOSIDE PHOSPHORAMIDATES

## 2.1 INTRODUCTION

Portions of this chapter are adapted in a revised form from the published manuscript West et al., with the consent of all authors (HT West, CM Csizmar, and CR Wagner).[244] The manuscript was principally written by the author of this thesis, HT West.

Enzymatic regulation of self-assembly has emerged as a highly effective method of enabling spatiotemporal control over self-assembling materials.[159] Ubiquitous across nature, self-assembly in response to enzymatic activity is responsible for regulating many processes necessary for life and has been the subject of investigation for decades.[245,246] Among the most commonly recognized enzyme responsive assemblies is the assembly of tubulin into microtubules. Indeed, tubulin itself possesses guanosine triphosphate phosphorylase activity for its own self-regulation of dynamic supramolecular polymerization[247,248]. Additionally, recent studies have shown that a class of enzymes termed katanins can sever microtubules with implications for control over cell division.[249,250] In addition, the origins of the cellular cytoskeleton as a whole are thought to derive from primordial self-assembling enzymes.[251] The glycolytic enzyme phosphofructokinase 1 has also been shown to self-assemble into filamentous nanostructures from both purified extracts and within living cells.[252,253] Similar to tubulin, its activity is inherently tied to its own enzymatic activity with only catalytically active enzyme able to form higher ordered assemblies.[252]

Enzymatic post-translational modification of proteins can also influence self-assembly. One example is the regulation of protein cytoplasmic polyadenylation element binding protein (CPBE3) which has been associated with long term memory and synaptic

plasticity.[254,255] Key to its molecular function, CPEB3 is a transcriptional regulator with its activity state and self-assembly regulated by SUMOylation.[256] The covalent modification is removed in response to neural activity, enabling CPEB3 to self-assemble and undergo a functional switch to induce transcriptional activation.[256] Additionally, SUMOylation is responsible for solvating a number of other self-assembling proteins such as α-synuclein with SUMO groups preventing aggregation of the protein and decreasing associated cytotoxicity of molecular aggregates.[257] Enzymatic processing can also induce self-assembly through peptide backbone modification. Proteolytic cleavage of fibrinogen by the enzyme thrombin yields the self-assembling product protein fibrin.[258] Activation of fibrin self-assembly is a necessary step in clot formation after tissue injury and blood vessel damage to initiate the wound healing process.[259]

Central to the regulation of supramolecular assembly by enzymes is their ability to modulate non-covalent interactions between monomers through chemical transformation.[157,159] As can be seen from the above mentioned (*vide supra*), certain types of functionalities are able to prevent or promote self-assembly. As the self-assembly of biomolecules is highly specific and dependent on very defined associative interfaces, perturbation of these sequences with chemical modifications such as that achieved with SUMOylation can alter the pattern of hydrogen bonding, electrostatic, and hydrophobic interactions necessary for self-association.[256,257] Additionally, as in the case of fibrin, entire peptide blocks may be removed or joined together to either generate or degrade peptide sequences with self-assembling properties.[258,259] Such patterns of functional control with

enzyme responsive motifs have been extended to synthetic systems and widely investigated to generate functional and dynamic biomaterials.[159,260]

Diverse chemical transformations have been used to regulate a wide variety of self-assembling materials, though transformations are most commonly achieved through hydrolysis, condensation, and redox chemistries.[261–263] Enzymes achieve regulation of the self-assembly of peptides in the same manner that alterations to the amino acid sequences of self-assembling peptides can modulate assembly; through control of non-covalent forces between adjacent peptides as well as the interactions between the exposed surfaces of peptides and the solution environment. Hydrolysis is typically performed to remove assembly blocking moieties, which either prevent facial association of monomer peptides into organized linear assemblies or provide solubilizing handles that favor solvent interactions over monomer association.[159,260] In contrast, condensation reactions are typically used to complete self-assembling peptide sequences to achieve a complete self-assembling moiety.

Among the most widely investigated enzyme controlled assembly approaches is the phosphatase/kinase switch. In this system, phosphorylation at hydroxyl bearing residues interrupts the peptide binding interface presumably through a combination of charge repulsion and perturbation of the aromatic interactions and hydrogen bonding patterns between monomers (**Figure 2.1**).[262,264] To reverse the assembly blocking effect of the phosphate moiety, alkaline phosphatase activity hydrolyzes phospho-amino acids to yield inorganic phosphate and the unhindered self-assembling peptide[262,264]. As phosphate moieties may be appended to amino acids through kinase activity, cyclically dynamic self-

assembling systems have been demonstrated where self-assembling peptide gels can be repeatedly assembled and disassembled through sequential enzyme addition.[262] Additionally, a variety of chemical formats have demonstrated compatibility with the system including short aromatic peptides as well as peptide amphiphiles.[265]

**Figure 2.1 Kinase/Phosphatase Switch Regulation of Supramolecular Assembly**

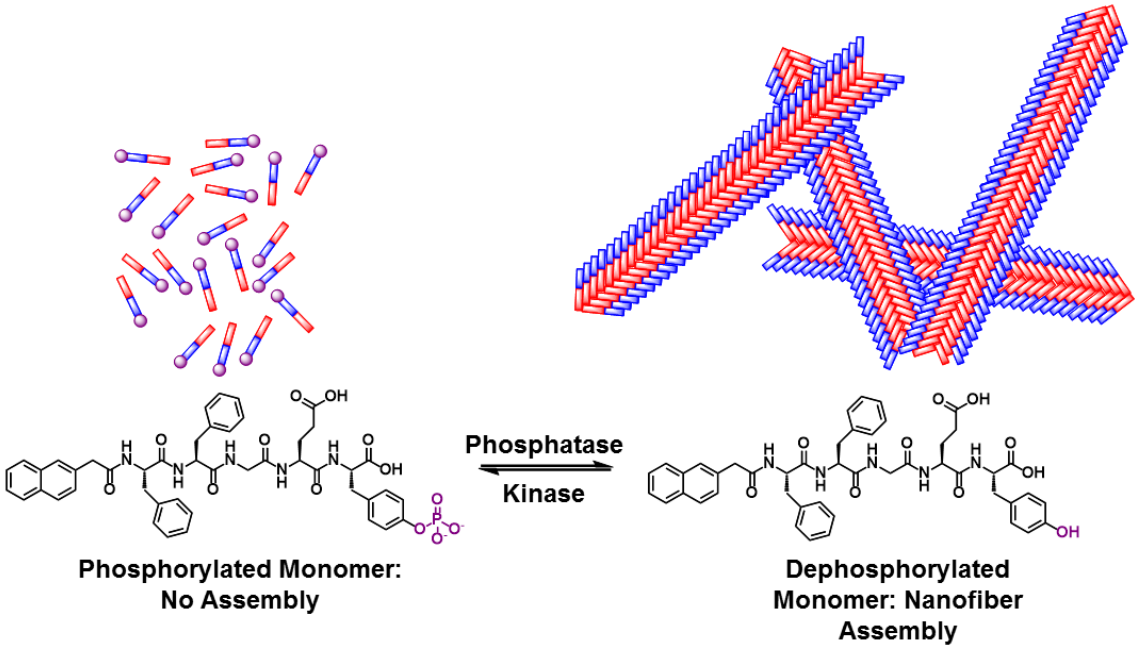

**Figure 2.2 hHint1 phosphoramidase activity and catalytic mechanism**

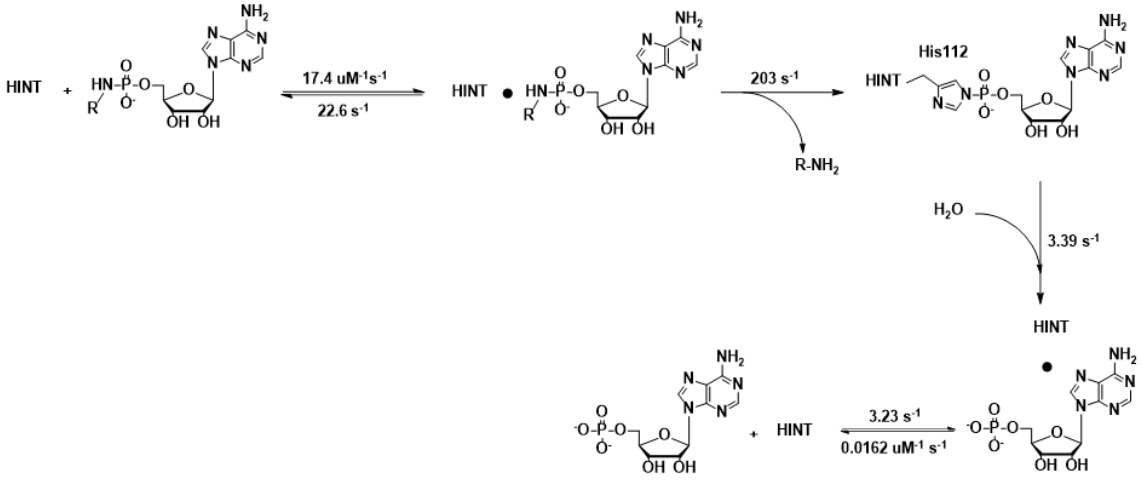

Key to the dynamic nature of their regulatory properties is the ability of enzymes to perform these transformations in real time and in aqueous solution. Additionally, enzymes possess desirable qualities for the regulation of self-assembling biomaterials including their high degrees of substrate specificity, catalytic versus stoichiometric activity, inherent biodegradability, and in the case of endogenous enzymes also biocompatibility.[159,260] Due to the utility of enzymatic activity in the regulation of self-assembling peptides, systems incorporating enzyme responsive motifs have been investigated for a wide variety of biomedical applications including drug delivery and imaging and diagnostics.[265,266]

Histidine Triad Nucleotide Binding Protein 1 (hHint1) is a human enzyme of the Histidine Triad superfamily of proteins characterized by the ubiquitous presence of a conserved triad of active site His residues which confer nucleotide binding capability and enzymatic activity.[267] Hint proteins are widely distributed across the kingdoms of life and are present in most sequenced genomes, with humans expressing three isoforms designated numerically as hHint1, hHint2, and hHint3.[267,268] Among the three enzymes, hHint1 has undergone the most thorough characterization in terms of its enzymatic activity and biological functions, with putative roles in transcriptional regulation and central nervous system function.[269–274]

Of clinical and therapeutic interest, hHint1 possesses unique phosphoramidase activity resulting in the phosphorus-nitrogen bond hydrolysis (**Figure 2.2**).[275–277] Nucleoside phosphoramidates are a class of synthetic prodrug that seeks intracellular delivery of monophosphorylated antiviral and anticancer therapeutics, thus bypassing

resistance mechanisms and the kinetic rate-limiting step of metabolic activation.[278] This prodrug methodology has contributed to clinically approved agents such as sofosbuvir, which is an anti-HCV agent shown to undergo intracellular activation by intracellular hHint1.[279]

hHint1's phosphoramidase activity is derived from a catalytic His112 residue, which performs nucleophilic attack upon the phosphorus atom of the phosphoramidate moiety, expelling the amine side chain and generating an active site nucleotidylated intermediate (**Figure 2.2**).[277] Subsequent hydrolysis of the intermediate releases the nucleoside monophosphate completing the catalytic cycle.[277,280] A number of synthetic substrates have been developed and assessed for hHint1 catalytic parameters revealing a preference for purine over pyrimidine substrates and ribose over deoxynucleotide and unnatural sugars.[275]

Noting the utility of enzymatic activity in the regulation of peptide self-assembly and combined with in depth knowledge of hHint1 enzymatic activity and substrate specificity, we sought to develop a hHint1 modulated self-assembly system. In our system, we specifically investigated how the assembly and gelation properties of self-assembling peptides could be modulated through covalent modification with nucleoside phoshoramidates, and how these properties change in response to hHint1 catalytic activity. To achieve this goal we developed a panel of self-assembling nucleoside phosphoramidate modified short aromatic peptides that were shown to undergo hydrogelation in the presence of hHint1. We also show that this mechanism of gelation results from an enzyme catalyzed morphological transition exhibited by supramolecular nanofibers. This work constitutes

the first report of self-assembling peptides modified with pronucleotide moieties, or phosphoramidate pro-gelators (PPGs), and the first report of hHint1 enzyme utilized for the regulation of material properties.

## 2.2 RESULTS

### Design, synthesis, and enzyme responsive properties of first generation nucleoside phosphoramidate progelators (PPGs)

In developing the hHint1 responsive gelating system, careful consideration was taken of how the nucleoside phosphoramidate moiety could be chemically incorporated into the monomer structure to achieve assembly and morphology control. Due to its chemical simplicity, robust self-assembling properties, and tolerance for a broad range of chemical modification, the short self-assembling peptide Nap-Phe-Phe (NAP-FF) was chosen as the base self-assembling moiety of the PPGs.[281] Additionally, derivatives of the molecule have found significant utility in the development of the phosphatase/kinase enzymatic switch for controlling peptide self-assembly providing further incentive for its incorporation into this system[262,264,265]. Our initial PPG design oriented the self-assembling peptide and nucleoside phosphoramidate moiety in a linear format, connecting the two moieties through a 1,3-diaminopropane linker. In our design, the nucleoside phosphoramidate was intended as an assembly blocking and solubilizing moiety, similar to phosphorylated amino acids in phosphate sensitive systems[262]. In response to hHint1 enzyme activity, it was expected that removal of the polar and anionic nucleoside phosphoramidate moiety would facilitate assembly of the released amine modified peptide. Two PPGs were synthesized in this design, NAP-FF-C3-AMP and NAP-FF-C3-CMP (**Figures 2.3, 2.4**). Interestingly,

NAP-FF-C3-AMP was observed to form weak hydrogels in aqueous buffer, as could be observed by visual inspection after attempted dissolution (**Figure 2.3**). In contrast, the less hydrophobic NAP-FF-C3-CMP molecule was observed to form clear solutions in aqueous buffer, indicating that the nucleoside phosphoramidate moiety may play a role in monomer self-association. Additionally, the PPG NAP-F-C3-AMP was synthesized which bore only a single Phe residue which was also observed to form clear solutions in aqueous buffer emphasizing the importance of the additional aromatic residue in promoting monomer self-association (**Figure 2.3**).

In contrast, the addition of hHint1 to NAP-FF-C3-CMP solutions resulted in clear and stable hydrogel formation (**Figure 2.4**). Gelation properties in the presence of hHint1 were further evaluated using small amplitude oscillatory rheometry (SAOR) which indicated a clear dependence of gelation kinetics on the quantity of enzyme added to the sample. SAOR is dynamic mechanical analysis technique that facilitates the investigation of soft materials such as hydrogels and viscous liquids. In the experiment, the material is sandwiched between two plates with one of the plates oscillating at a set frequency and amplitude. Through simultaneous recording of the torque and amplitude of the oscillation, a relationship between the applied stress and resulting deformation of the material yields values for the experimental parameters G' (elastic modulus) and G'' (loss modulus). The G' and G'' values correspond respectively to the contribution to sample rigidity from the solid and viscous liquid character of the material tested. As hydrogels are hydrated matrices, they possess both solid and liquid character, with the solid character (G') possessing a greater magnitude than the viscous liquid (G'') character due to the self-

supporting nature of rigid hydrogels.[282] The NAP-FF-C3-CMP sample containing 0.8 μM hHint1 failed to undergo gelation over the time course of the experiment indicated by the lack of increase in both G' and G''(**Figure 2.5a**). Increasing the concentration of hHint1 to 4 μM initiated gelation at approximately 8 minutes indicated by the rapid rise in both G' and G'', while further increase to 8 μM resulted in nearly instantaneous gel formation where G' and G'' increased at approximately time 0 (**Figure 2.5b,c**). Additionally, a strain sweep was performed where increasing the % strain or deformation of the material yielded a consistent linear region up to nearly 10 % (**Figure 2.5d**). As the linear region indicates non-dependence of both G' and G'' on the % strain value, the measure can be regarded as an indicator of the strength of the material in response to applied stress.[282]

Morphological investigation of hHint1 initiated gelation of NAP-FF-C3-CMP using transmission electron microscopy (TEM) revealed that a dense network of highly ordered nanofibers had formed in response to hHint1 activity (**Figure 2.6a**). The widths of the nanofibers were approximately 7-8 nm and the nanofibers were observed to form higher ordered arrangements through lateral fiber association. In contrast, samples without hHint1 activity exhibited few fibrous nanostructures with a predominance of amorphous aggregates indicating structural regulation in response to enzymatic activity occurred (**Figure 2.6b**). A downside to this first generation of compounds was that the synthesis was inefficient and resulted in poor yields, likely due to the mismatch in polarity between the nonpolar self-assembling peptide and the highly polar and zwitterionic nucleoside phosphoramidate amines (**Figure 2.3**). The diaminopropyl linker class was not further

pursued for these reasons and a more tractable and efficient synthesis was undertaken to facilitate development of a second generation of PPGs.

**Figure 2.3 Synthesis of NAP-F-C3-AMP and NAP-FF-C3-AMP**

Photograph on the left depicts an 11.2 mM solution of NAP-F-C3-AMP in buffer (right) and 11.2 mM solution of NAP-F-C3-AMP (left) with 10 uL of 3.86 uM hHint1. Flocculation was observed in the vial on the left due to enzyme activity while substrate only solution remained clear.

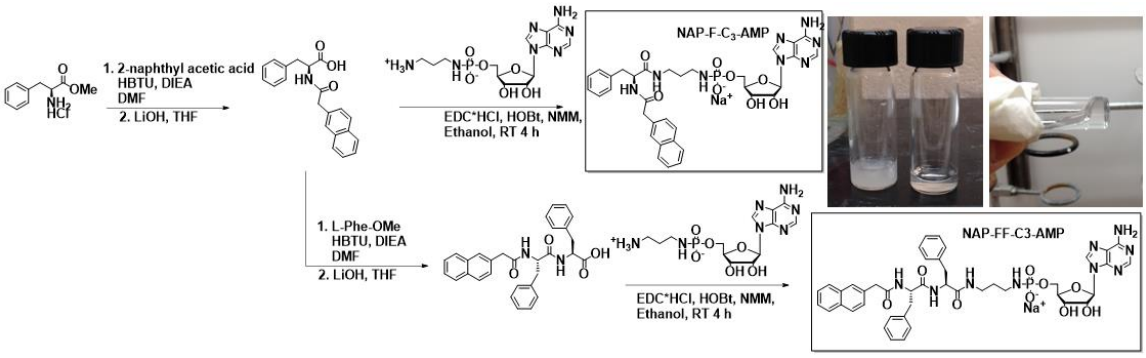

**Figure 2.4 Synthesis of NAP-FF-C3-CMP.**

Photograph shows 11.1 mM (1% by weight) solution of the phosphoramidate pro-gelator in buffer with gelation observed upon addition of hHint1 (4.1 μM final concentration)

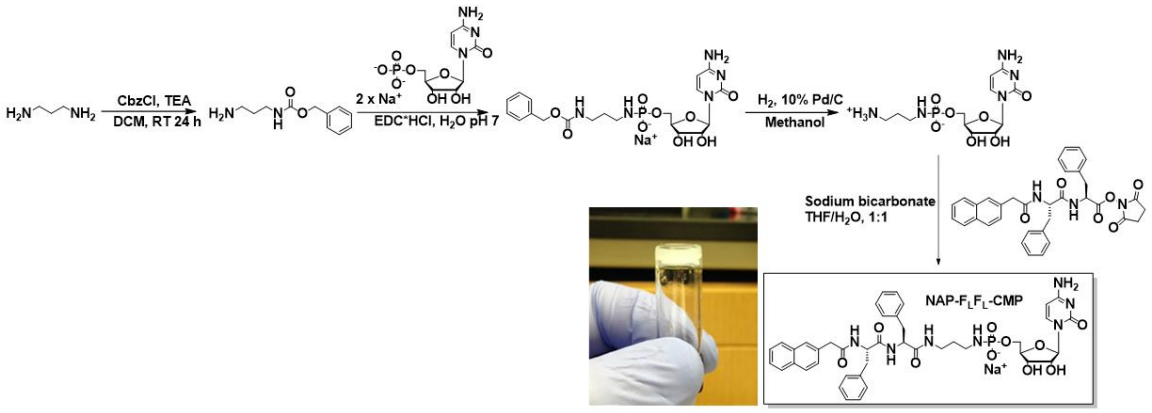

**Figure 2.5. Oscillatory rheometry of NAP-FF-C3-CMP**

(a) time sweep of 11.1 mM substrate solution with 0.8 μM hHint1 (b) 11.1 mM NAP-FF-C3-CMP with 4 μM hHint1; (c) 11.1 mM substrate with 8 μM hHint1; (d) strain sweep of hydrogel formed from c. to demonstrate linear viscoelastic region

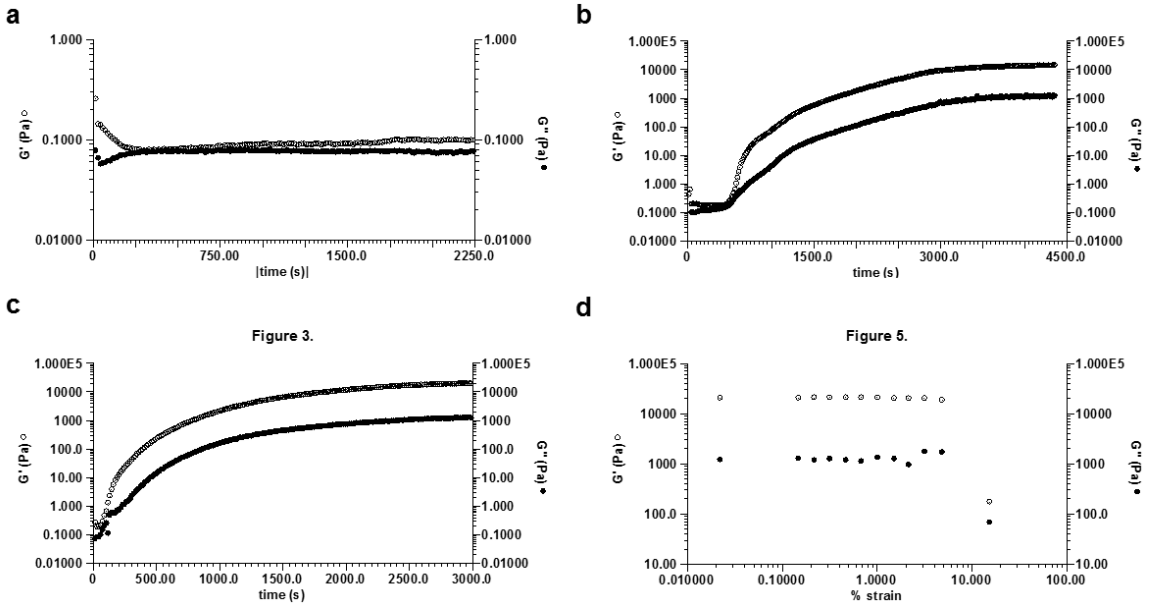

**Figure 2.6. Transmission electron microscopy of NAP-FF-C3-CMP**

(a) 1 wt/vol % substrate with 4 μM hHint1; (b) 1 wt/vol% substrate alone in buffer.

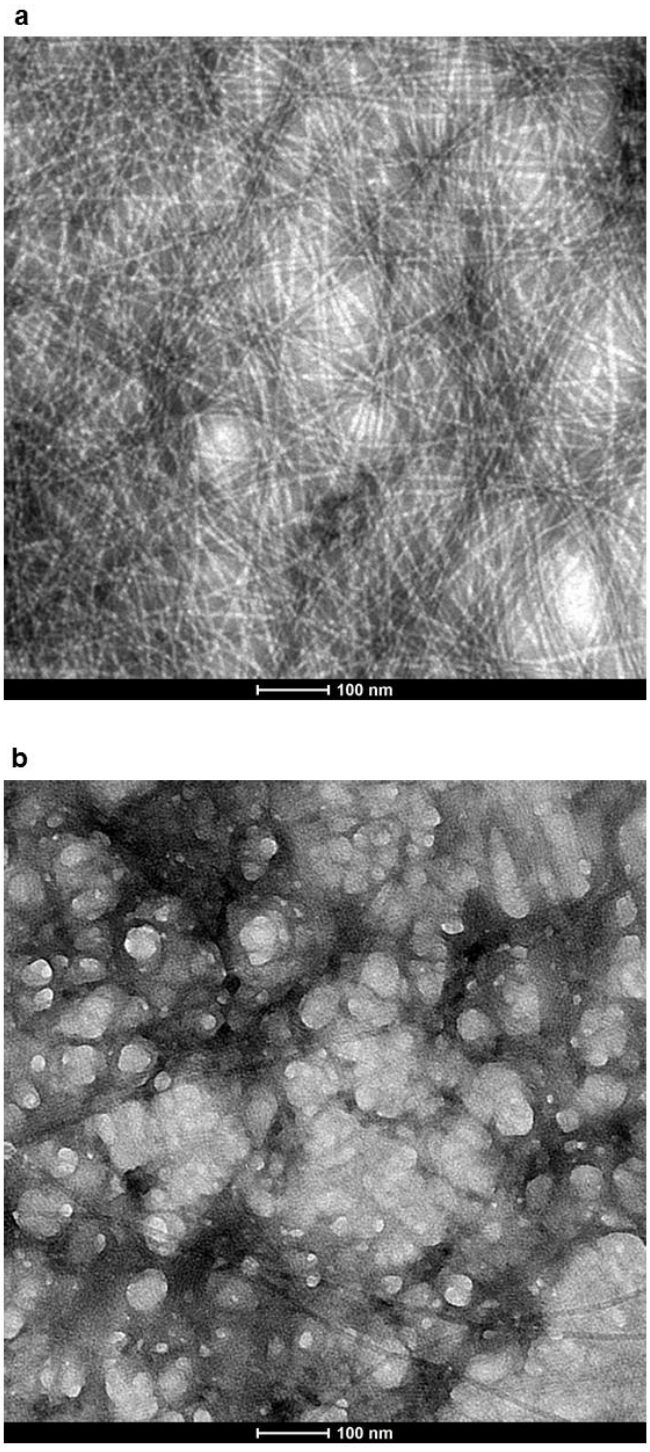

**Design, synthesis, and preparation of hydrogels from second generation PPGs**

Similar to the first generation PPGs a naphthyl N-terminal cap was incorporated into the peptide component for its chemical stability and propensity for driving assembly through aromatic interactions.[281] In contrast to the first generation PPGs, the diaminopropane linker was replaced with a short PEG linker to facilitate solubility of monomeric PPGs in the absence of hHint1. Additionally, the PEG linker incorporated bifunctionality with terminal primary amine and azide groups to facilitate click chemistry conjugation to suitably alkyne functionalized phosphoramidates to generate second generation PPGs. NAP-FF peptide obtained through standard Fmoc-solid phase synthesis, was coupled to an amino-$PEG_3$-azide linker yielding the azido-labeled self-assembling peptide **1**.[283] Nucleoside propargyl phosphoramidates were synthesized through the condensation of propargyl amine and the desired nucleoside monophosphates mediated by EDCI.[275] Azido-labeled peptide and corresponding propargyl phosphoramidates were coupled efficiently utilizing the copper catalyzed Huisgen cycloaddition reaction in the presence of Na Ascorbate and Copper (II) sulfate in 2:1 tBuOH/$H_2O$ as the solvent system to yield PPGs **2** (NAP-FF-AMP), **3** (NAP-FF-UMP), **4** (NAP-FF-GMP), and **5** (NAP-FF-CMP) (**Figure 2.7**).[284] Cation exchange chromatography with Dowex 50wx8 resin was performed to obtain the sodium salts of the respective PPGs.

The initial panel of second-generation PPGs was assessed for assembly properties and hHint1 enzymatic responsiveness. Each substrate was subsequently probed for its ability to self-assemble and form hydrogels in the presence of hHint1 using visual inspection. Solutions containing 0.9% wt/vol NAP-FF-AMP, NAP-FF-UMP, NAP-FF-

GMP, and NAP-FF-CMP (**2-5**) were prepared by dissolution of lyophilized PPG powder in hHint1 activity buffer (**SECTION 2.4 MATERIALS AND METHODS**). To investigate gel formation, hHint1 enzyme in activity buffer was added to generate solutions with final hHint1 concentration of 6 μM and 0.9% wt/vol substrate. Samples were briefly vortexed to ensure proper mixing and allowed to cure at room temperature. Samples were checked after 15 min., at which time vials were inverted. All four PPG alone samples were observed to remain viscous solutions in the absence of hHint1 (**Figure 2.8 insets**). During the same period, all four substrate solutions containing hHint1 underwent hydrogel formation (**Figure 2.8 insets**). Additionally, the four hydrogels remained stable for 24 hours after repeating the inversion test. Hydrogels originating from NAP-FF-AMP **2**, NAP-FF-GMP **4**, and NAP-FF-UMP **3** were all opaque in nature, with NAP-FF-CMP **5** forming translucent hydrogels.

**Assessment of morphology with Transmission Electron Microscopy**

Transmission electron microscopy (TEM) was utilized to investigate the nanostructures of both substrate and hydrogel samples after uranyl acetate negative staining and subsequent vacuum desiccation. Interestingly, structures ranging from amorphous aggregates to fibrous networks were observed in the absence of HINT1 (**Figure 2.8a-d**). Extensive fiber formation was observed in the NAP-FF-CMP **5** substrate sample with fibrous structures also evident in the NAP-FF-UMP **3** and NAP-FF-GMP **4** substrate samples. Within both the amorphous and fibrillar structures, portions of individual nanofibers could be resolved in samples of all for substrates and were determined to be 6-8 nm in diameter. Hydrogel samples presented clear and defined nanofiber formation for

all four substrates in the presence of hHint1(**Figure 2.8e-h**). In comparison to the substrate only samples, the fibrous networks formed from hHint1 activity were clearly defined with individual nanofibers possessing diameters between 7-8 nm. Not only were all hydrogel samples observed to exhibit nanofiber formation upon hHint1 activation, but much of the nanofiber content was contained within tightly packed nanofiber bundles suggesting a morphological transition may be responsible for the observed gelation. NAP-FF-AMP **2** and NAP-FF-GMP **4** exhibited extensive nanofiber association with NAP-FF-UMP **3** and NAP-FF-CMP **5** samples exhibiting fewer associated nanofibers and a prevalence of single nanofibers. Whether associated or existing as individual nanostructures, nanofibers in the hHint1 activated PPG gels retained similar diameters to non-enzymatically activated samples at 6-8 nm.

**Characterization of PPG nanostructure and hHint1 triggered hydrogel morphology and with cryogenic transmission electron microscopy (Cryo-TEM)**

Despite the observance of nanostructures in the enzyme free PPG samples through conventional TEM, it was difficult to discern how the observed structures correlated to the aqueous solutions of PPGs. Thus, Cryo-TEM was used for investigating the hydrated structures of the nanoarchitectures formed from the PPGs and their respective hHint1 formed hydrogels. This technique contrasts with conventional TEM which can affect nanostructure observation and characterization due to the necessity for extensive drying of the sample and sample staining with heavy metal salts which can introduce interfering artifacts and background staining.[285] Consequently, all four phosphoramidate pro-gelator substrates were analyzed by cryo-TEM, which revealed self-assembled fibrillar structures.

Consistent with the results of the TEM, solutions of all four substrates in HINT1 activity buffer were found to contain highly regular and continuous nanofibers approximately 7-8 nm in width (**Figure 2.9**). The nanofibers formed by all four pro-gelators are largely unassociated and likely only align with the lacey carbon of the cryo-TEM sample grid due to sample ice thickness variation. These results indicate the phosphoramidate pro-gelators form organized supramolecular structures in solution prior to hHint1 enzyme activation.

PPG hydrogels corresponding to each substrate formed from hHint1 were also examined with cryo-TEM. Hydrogel samples were prepared in hHint1 activity buffer at a concentration of 0.9% by wt/vol. with 6 μM hHint1 (**Figure 2.10a-d**). Clear nanofiber association was observed in all four hydrogel samples. Consistent with the results from TEM studies, this demonstrates cleavage of the nucleoside phosphoramidate moiety results in self-association of the nanofibers leading to hydrogel formation. Measurements of individual nanofibers present in both the substrate and hydrogel samples of NAP-FF-AMP **2**, NAP-FF-UMP **3**, NAP-FF-GMP **4**, and NAP-FF-CMP **5** were approximately identical and between 7-8 nm in diameter. Additionally, the nanofibers present in bundles were determined to be of equivalent diameter despite their induced assembly into dense association networks. Bundle diameters ranged from 14 nm to over 200 nm. The released peptide generated from hHint1 activity on the substrate nanofibers was also assessed for its gelation ability and nanostructure. NAP-FF-$NH_2$ (**Figure 2.11a**) was observed to form hydrogels at a concentration of 1% wt/vol in both water and PBS buffer. Addition of AMP at a concentration of 1% wt/vol also resulted in hydrogel formation. NAP-FF-$NH_2$ exhibited extensive ribbon-like structures exceeding 200 nm in width alone (**Figure 2.11b**).

Gels in the presence of AMP were observed to form a range of structures including individual nanofibers, twisted nanofiber ribbons approximately 35-55 nm in width, and larger ribbons (**Figure 2.11b**). Both gel structures contrast with the highly ordered monomeric substrate nanofibers and resulting structures formed from HINT1 activity.

**hHint1 triggered PPG hydrogelation determined with small amplitude oscillatory rheometry**

Small amplitude oscillatory rheometry (SAOR) has emerged as a key technique in examining the rheological properties of peptide based hydrogels and self-assemblies.[282] Time sweep experiments were used to examine the gelation kinetics resulting from enzymatic activity and resulting nanofiber association. A key observation in the gelation of PPGs triggered by hHint1 is their syneretic behavior, complicating the use of oscillatory rheometry by decreasing the observable time scale for measurement due to loss of geometry adhesion. Although all four PPGs were observed to form hydrogels under various conditions, reproducibility of final plateau moduli and gelation kinetics was complicated by the syneretic behavior of the hydrogels leading to loss of sample adhesion to rheometer geometries due to liquid-gel phase separation (**Figure 2.12**). These effects were especially pronounced in characterization of the purine substrates which were observed to have unstable time dependent moduli.

To mitigate problems associated with sample syneresis, adhesive sandpaper was used to enhance gel adhesion to geometries. Although syneresis led to unpredictable loss of sample adhesion after gelation occurred, determination of gelation time was enabled by this modification. The kinetics of NAP-FF-AMP **1** hydrogelation were found to be closely

tied to the amount of enzyme used to formulate samples, similar to the previously investigated NAP-FF-C3-CMP molecule (**Figure 2.13**). In the presence of 6 μM hHint1, rapid increases in both storage and loss moduli were observed at approximately 100 s. In contrast, NAP-FF-AMP **1** underwent gelation by 3 μM HINT1 resulting in increases of both G' and G'' at an average time of 238 ± 30 s (**Figure 2.13**). However, hydrogels formed from this substrate exhibited marked syneresis and loss of geometry adhesion over extended time sweep experiments. Two concentrations of hHint1 were also utilized to investigate NAP-FF-UMP **3** gelation kinetics (**Figure 2.14**). At a concentration of 6 μM, hHint1 was able to induce hydrogel formation from 0.9% wt/vol of NAP-FF-UMP **3** at an average time of 157 ± 67 s. Reducing the concentration of hHint1 to 3 μM resulted in significantly delayed gelation to an average time of 458 ± 130 s ($p = 0.0041$, two-tailed student's t-test). Due to its ability to exhibit stable moduli over extended time courses, different concentrations of NAP-FF-UMP **3** were also investigated for their ability to form hydrogels in response to hHint1 activity. Although decreasing the concentration of PPG resulted in concomitant decreases in plateau moduli as expected due to fewer monomers participating in assembly, gelation was observed at concentrations of NAP-FF-UMP **3** as low as 0.23 wt/vol% (**Figure 2.15a**).

**Role of hHint1 catalysis in triggering gelation of PPGs**

To elucidate the role of hHint1's active site in initiation of hydrogelation, additional time course experiments were performed in the presence of a competitive hHint1 small molecule competitive inhibitor, HNTI-3a ($K_d$ = 230 nM, structure in **Figure 2.15b**).[44] Samples of 0.9% NAP-FF-AMP **2** and NAP-FF-UMP **3** were prepared in HINT1 activity

buffer containing 2% DMSO alone or with 6 mM HNTI-3a. hHint1 was added to the solutions at a concentration of 6 μM and moduli were monitored over time courses to observe the occurrence of hydrogel formation. HNTI-3a was found to completely ablate hydrogelation of NAP-FF-UMP **3** for over 26 min. In contrast, clear hydrogel formation was observed in the absence of inhibitor and in the presence of DMSO only (**Figure 2.15b**). Consistent with the reversibility of inhibition of hHint1 by HNTI-3a, over the course of 24 h, hydrogelation was eventually observed. In contrast, although activation of NAP-FF-AMP **2** by hHint1 was inhibited by HNTI-3a, the kinetics of hydrogel formation were less severely affected. In comparison to the DMSO only control which exhibited instantaneous gelation at this hHint1 concentration, HNTI-3a resulted in a delay of substrate activation with sharp increases of moduli occurring at an average time of 346 ± 39 s in the presence of the inhibitor (**Figure 2.15c**). These results likely reflect the greater substract specificity of hHint1 for purine over pyrimidine phosphroamidates.[275]

Additional time sweep experiments were conducted in the presence of a hHint1 H112N active site mutant to confirm that the enzyme catalytic activity is the initiator of hydrogelation (**Figure 2.15d**). This mutant retains high binding affinity for nucleoside phosphoramidates but lacks the histidine residue necessary for nucleophilic catalysis[280]. In the presence of 11 μM H112N mutant, NAP-FF-AMP **2** or NAP-FF-UMP **3** demonstrated only weak hydrogel formation with moduli never rising above 0.2 Pa. Consequently, consistent with the inhibition studies, hydrolysis of the phosphoramidate moieties by the hHint1 active site along the substrate nanofibers result in hydrogel formation through non-covalent crosslinking of supramolecular nanofibers.

**Figure 2.7. Synthesis of second generation PPGs (2-5)**

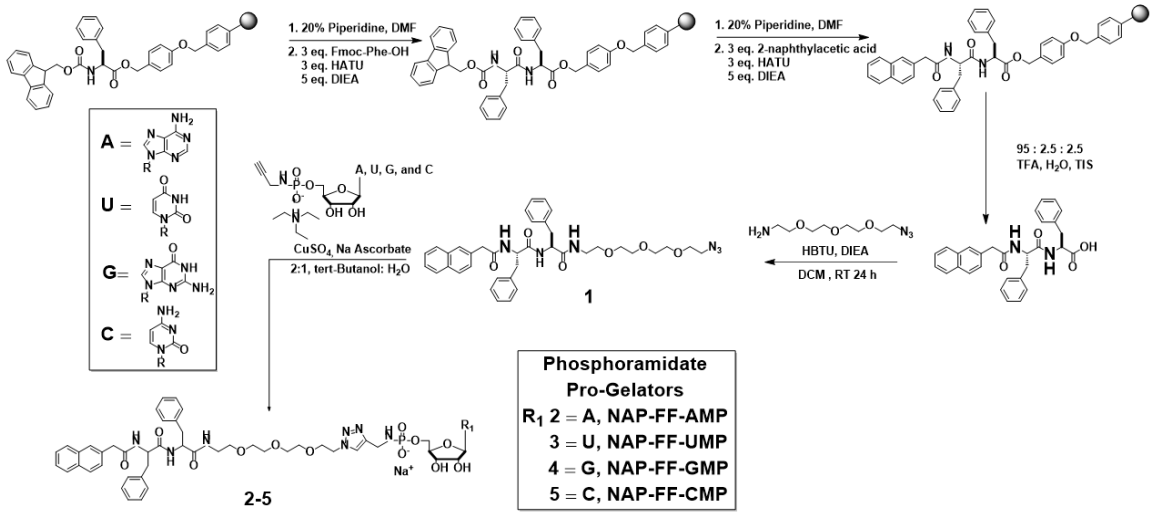

**Figure 2.8. Transmission Electron Microscopy of Hydrogels and Substrates**

Top Panel: Transmission electron microscopy (TEM) of substrate nanofiber solutions in the absence of hHint1 (scale bars represent 200 nm) (a). NAP-FF-AMP, (b). NAP-FF-GMP, (c). NAP-FF-UMP, and (d) NAP-FF-CMP. Bottom Panel: TEM of hHint1 formed hydrogels (scale bars represent 100 nm) (e). NAP-FF-AMP, (f). NAP-FF-GMP, (g) NAP-FF-UMP, and (h) NAP-FF-CMP

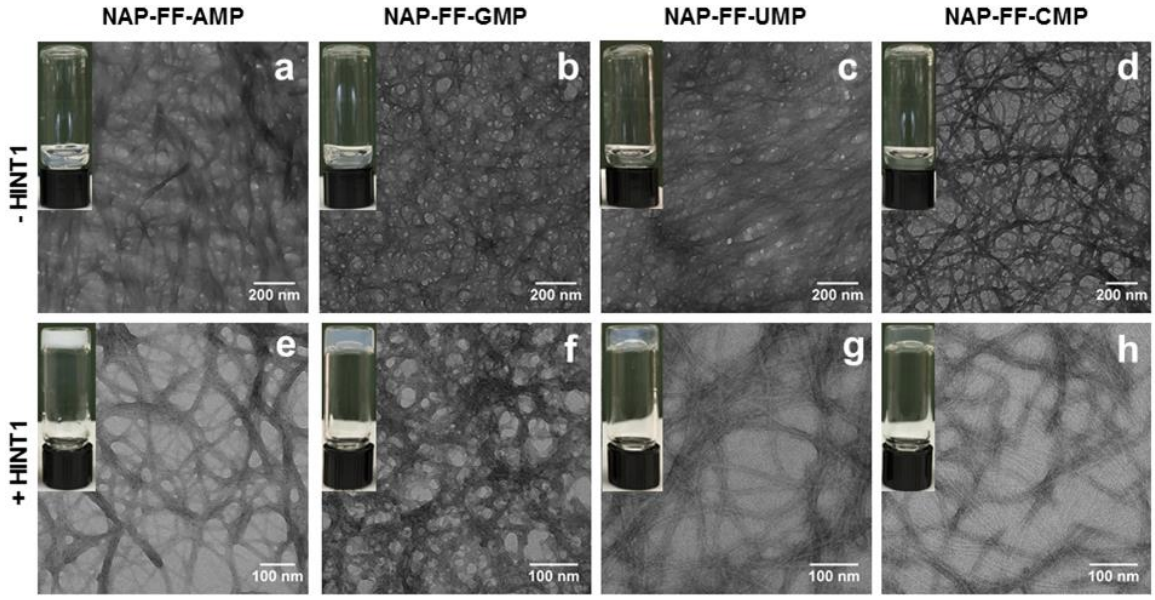

**Figure 2.9 Cryo-TEM Substrates**

PPG Nanofibers in Buffer (a) NAP-FF-AMP, (b) NAP-FF-UMP, (c) NAP-FF-GMP, (d) NAP-FF-CMP. (All scale bars represent 0.15 μM)

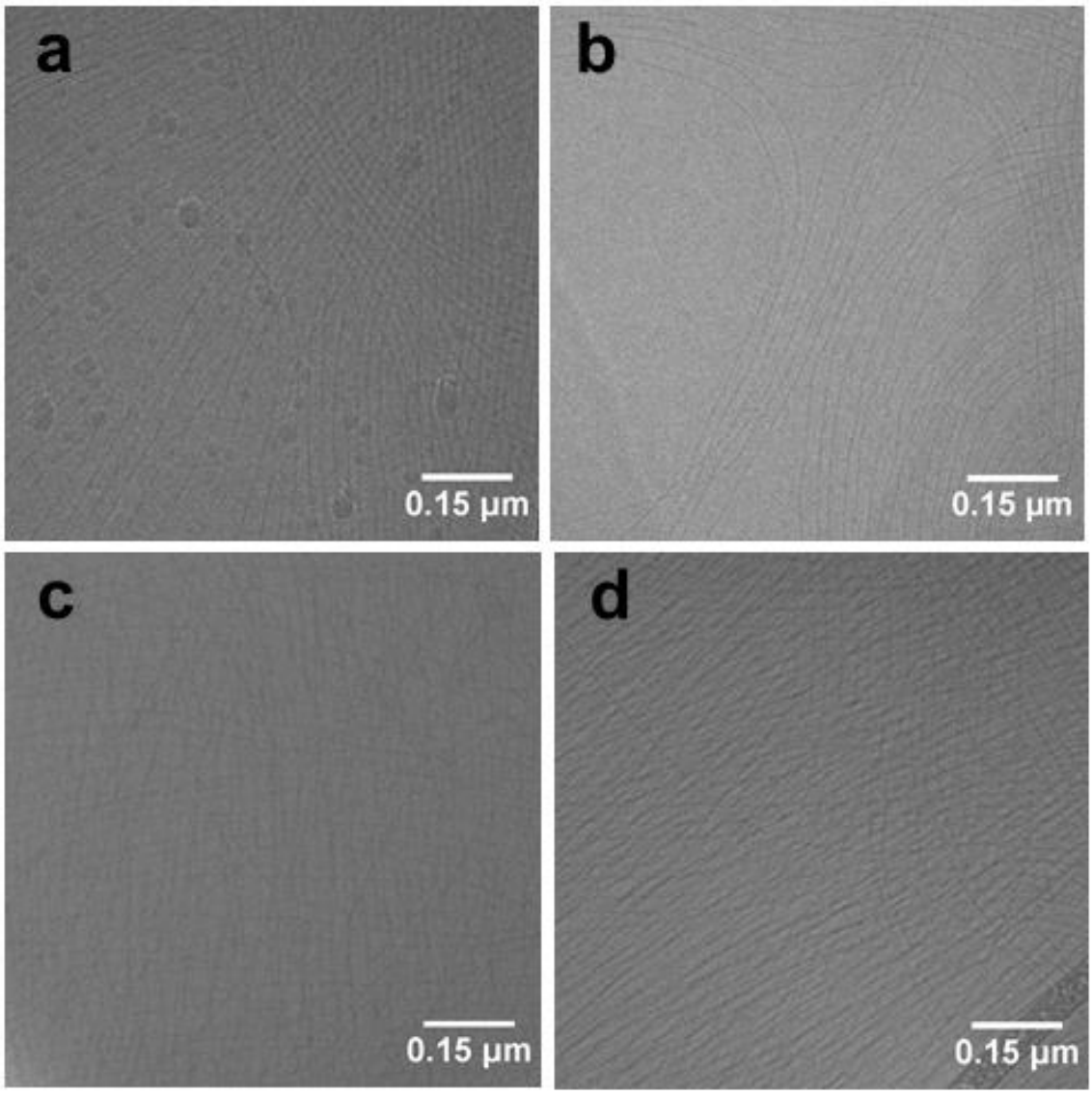

**Figure 2.10. Cryo-TEM of Hydrogels**

Hydrogels formed in the presence of hHint1 (a) NAP-FF-AMP, (b) NAP-FF-UMP, (c) NAP-FF-GMP, (d) NAP-FF-CMP (All scale bars represent 0.15 μM)

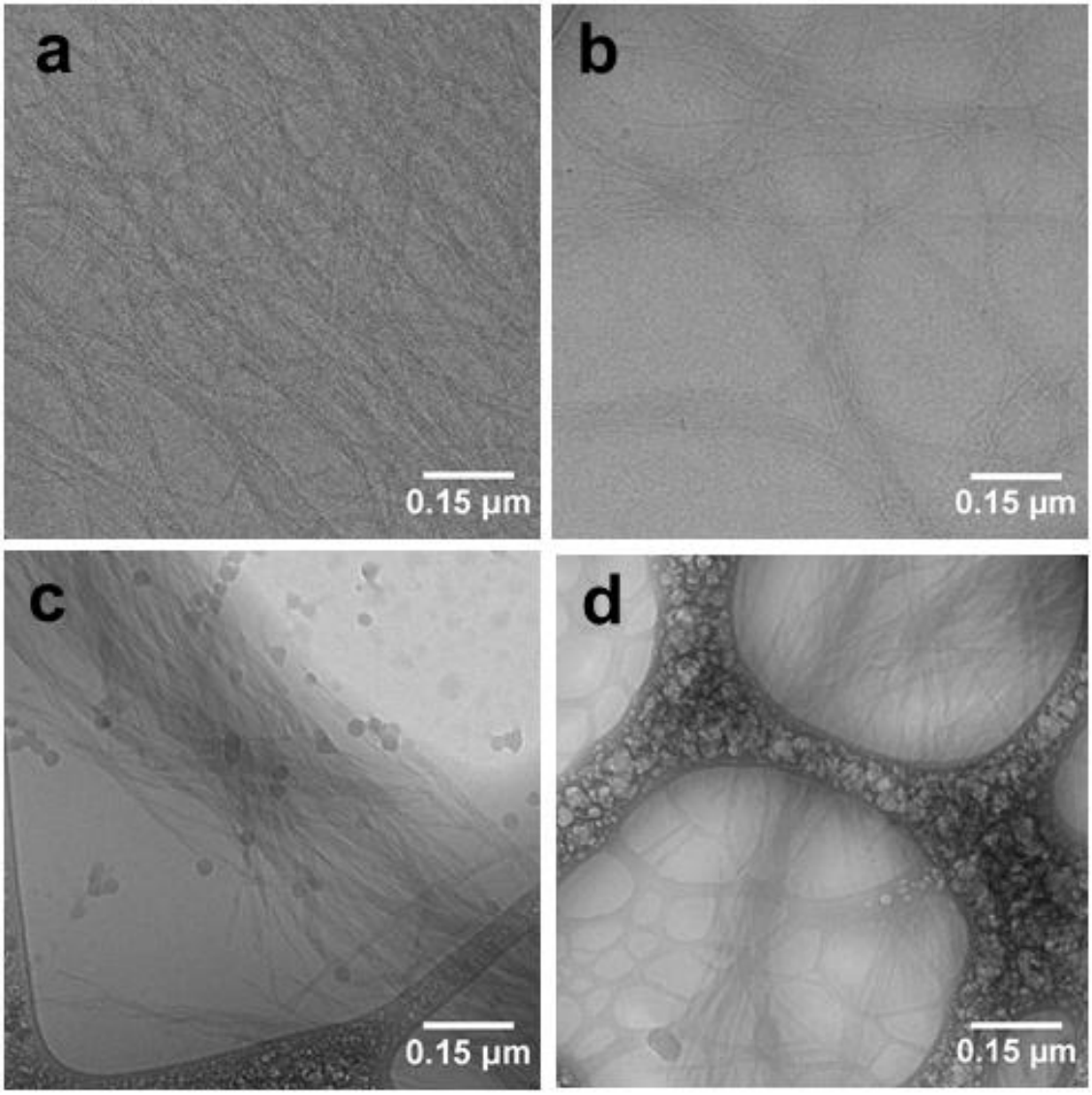

**Figure 2.11 Cryo-TEM of Free Peptide and Nucleoside Monophosphate**

(a) NAP-FF-NH2 structure in the presence of PBS only, (b) and in the presence of AMP. (All scale bars represent 0.15 μM)

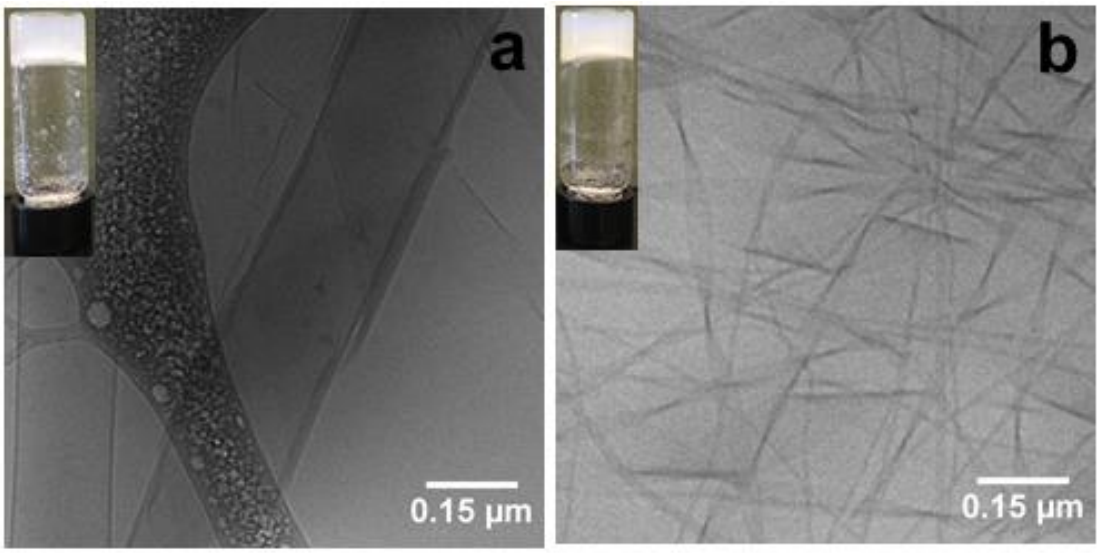

**Figure 2.12. hHint1 induced gelation of PPGs measured with SAOR.**

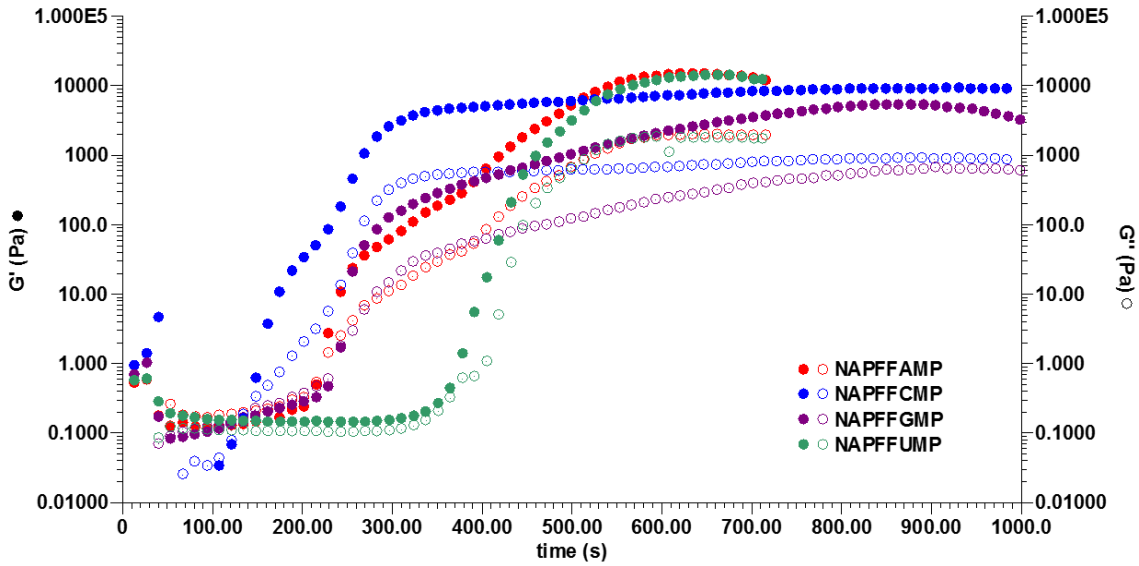

**Figure 2.13. NAP-FF-AMP gelation in the presence of hHint1.**

Red curves represent both G' (filled shapes) and G'' (open shapes) in the presence of 6 μM hHint1. Blue curves represent both G' (filled shapes) and G'' (open shapes) in the presence of 3 μM hHint1. Data shown is of three replicate experiments for each concentration of enzyme. Gelation points are indicated by black arrows.

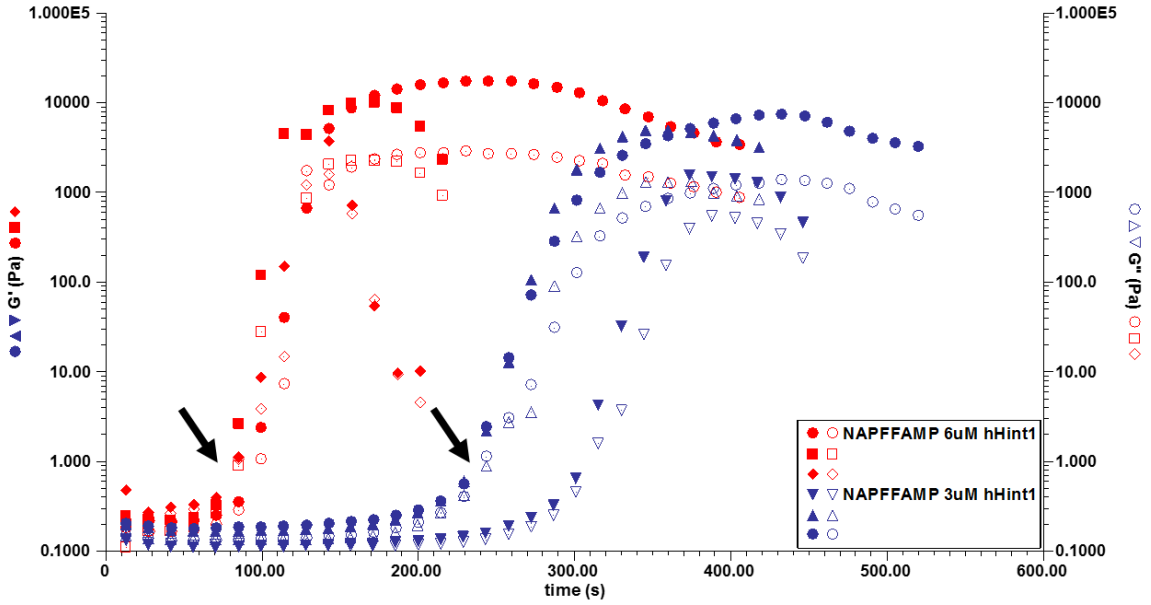

**Figure 2.14 NAP-FF-UMP gelation in the presence of hHint1.**

(a) Red curves represent both G' (filled shapes) and G'' (open shapes) in the presence of 6 μM hHint1. Blue curves represent both G' (filled shapes) and G'' (open shapes) in the presence of 3 μM hHint1. Each pair of G' and G'' curves represent a single time course measurement. 5 replicate experiments are shown for each concentration. Display of replicate data is shown to demonstrate the clear effect hHint1 has on gelation kinetics despite the variability in the data. (b) Scatter representation of gelation time points. Statistical significance (**) determined from student's t-test (p = 0.0041, two-tailed)

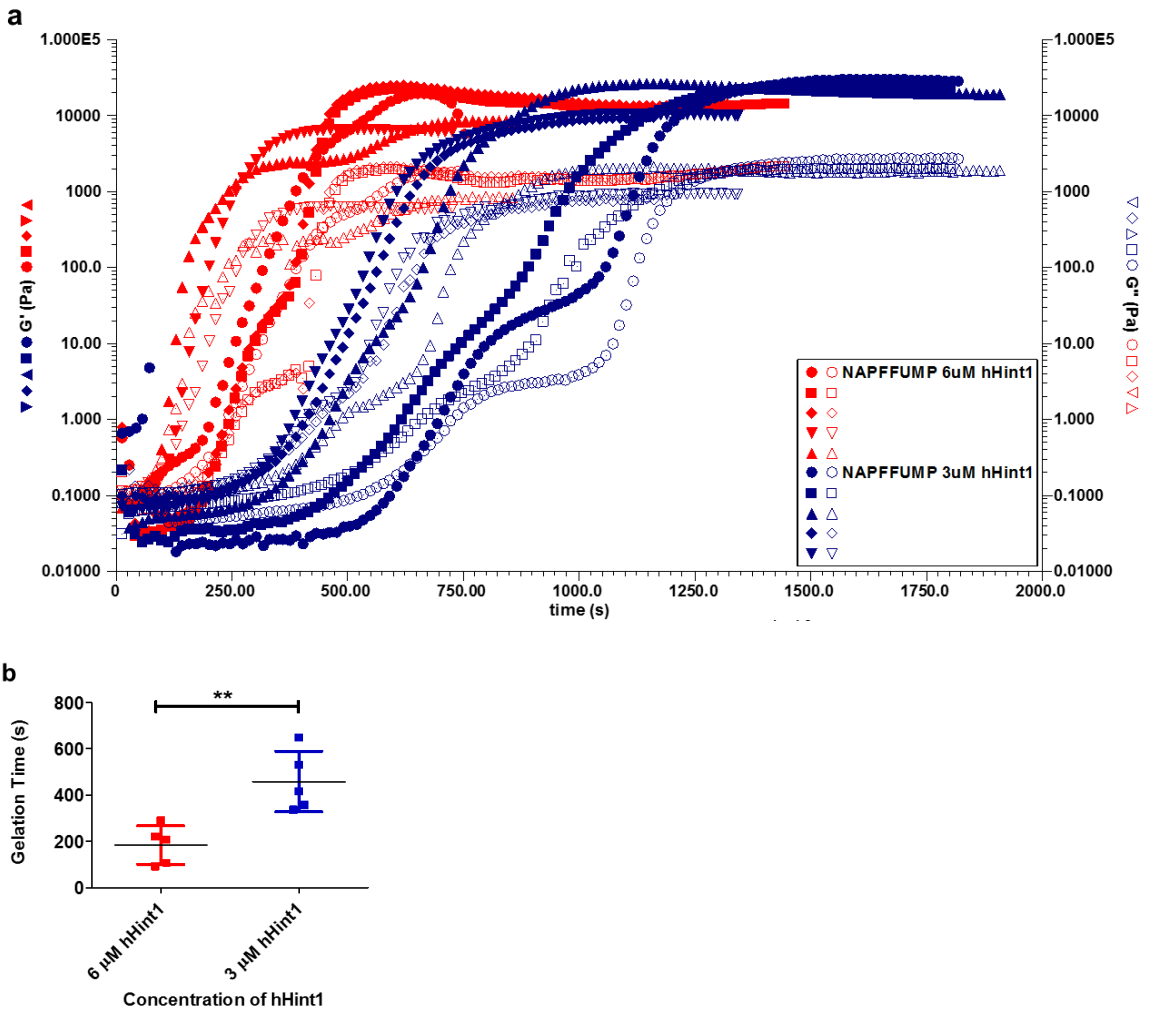

**Figure 2.15 Concentration, inhibitor, and mutant enzyme gelation experiments**

(a) Time sweeps at 0.45% and 0.23% wt/vol concentrations of NAP-FF-UMP with 6 μM hHint1 (b) NAP-FF-UMP and NAP-FF-AMP in the presence of H112N mutant (c) NAP-FF-UMP with hHint1 inhibitor or DMSO control (d) NAP-FF-AMP with hHint1 inhibitor or DMSO control

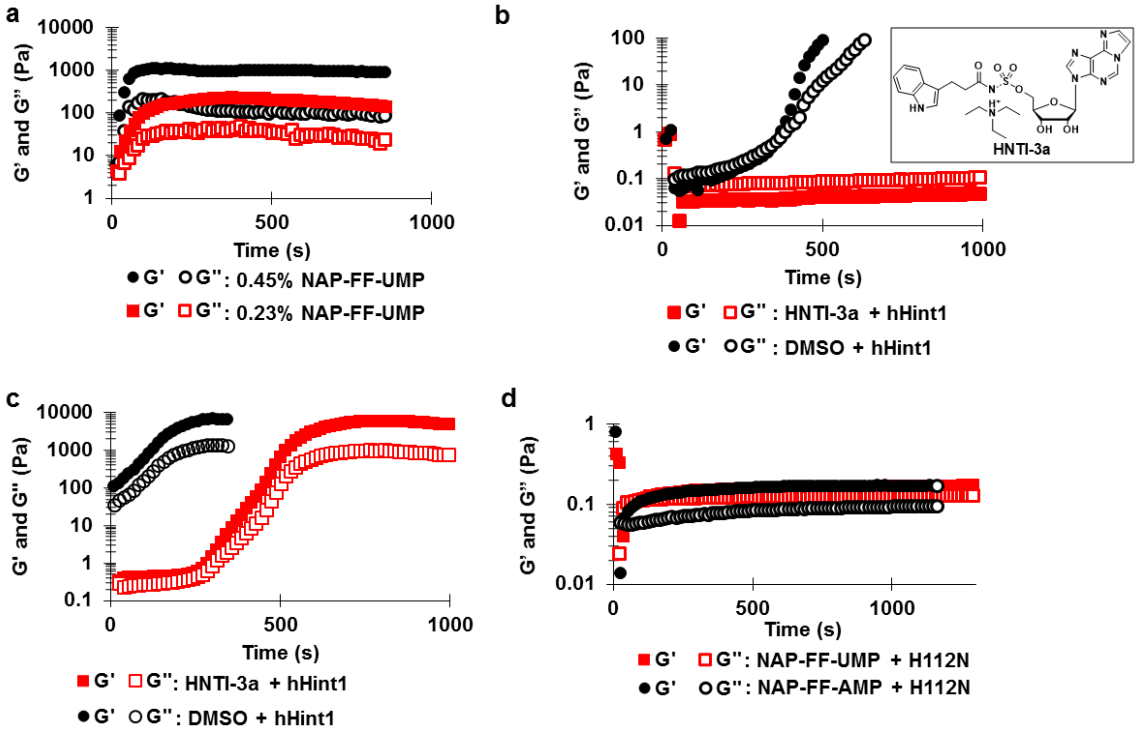

To further determine whether hHint1 catalytic activity was occurring in the gelation process, $^{31}P$ NMR experiments were performed demonstrating that rapid hydrolysis of NAP-FF-AMP **2** to AMP and NAP-FF-UMP **3** to UMP occurred within minutes of hHint1 addition (**Figure 2.16**). Examination of hHint1 formed gels with HPLC was performed to further investigate the relative proportion of PPG substrate remaining in the gels. It was determined that the percentage of NAP-FF-AMP **2** remaining within hHint1 formed hydrogels after 24 hours was less than 1% (**Figure 2.17**).

**Model substrate to probe hHint1 induced gelation with $^{1}H$ NMR**

To further understand the required substrate parameters of PPGs for hHint1 activation, an inverse linker substrate (NAP-FF-Inv-UMP, **6**) was synthesized where uridine monophosphate was functionalized with the amino-$PEG_3$-azide and the NAP-FF peptide was functionalized with propargyl amine at its free carboxyl terminus. Resulting copper catalyzed click chemistry effectively yielded a molecule with switched orientation of the linker compared to the PPGs **2-5**. To observe if the molecule in fact performed as a functional PPG in response to hHint1 activity SAOR was utilized to determine its gelation capability. Analogous to PPGs **2-5**, the inverse linker PPG **6** readily formed hydrogels in the presence of hHint1 with an average gelation time of 178 ± 38 s in the presence of 6 μM hHint1, similar to NAP-FF-UMP **3** (**Figure 2.18a**). Additionally, cryo-TEM was utilized to investigate the morphology resulting from PPG assembly and resulting hHint1 enzyme activation. Also similar to the other PPGs, the inverse linker PPG **6** also assembled into highly regular nanofibers approximately 7-8 nm in diameter. In the presence of hHint1, the

nanofibers were observed to undergo lateral association into nanofiber bundles (**Figure 2.18b)**.

To further investigate hHint1 catalytic activity on inverse linker PPG **6**, NMR was utilized to monitor the reaction trajectory in the conversion of phosphoramidate to monophosphate and to estimate the concentration of visible nucleoside monophosphate. NAP-FF-Inv-UMP **6** was dissolved in $D_2O$ at a concentration of 1 wt/vol % (≈ 9.4 mM) and 6 μM hHint1 was used to initiate the gelation reaction in the NMR tube. Both $^{1}H$ and $^{31}P$ nuclei were monitored over time with MeCN utilized as an internal standard for $^{1}H$ experiments to estimate the concentration of generated UMP (**Figure 2.19a,b**). In $^{32}P$ experiments, a clear conversion from the substrate phosphoramidate to UMP was observed in response to hHint1 addition as expected. However, $^{31}P$ NMR experiments provided no information about the state of the PPGs, released peptide, or UMP in regards to their higher ordered assembly and whether aggregates or soluble monomers were observed. Interestingly, $^{1}H$ NMR spectra of inverse linker PPG **6** exhibited broadened and upfield shifted peaks in response to increasing concentration indicative of a decrease in relaxation times resulting from aggregate assembly (**Figure 2.19c)**. $^{1}H$ NMR analysis of hHint1 induced gelation revealed complete disappearance of peptide associated peaks overtime with gradual increases in peaks associated with released UMP, indicating the formation of NMR invisible aggregate peptide structures and soluble nucleoside monophosphate. Estimation of the concentration of released UMP over time using MeCN as an internal standard revealed less than 10% molar equivalent (≈ 800 μM) of monophosphate was released in the gel forming reaction (**Figure 2.19b**).

**Figure 2.16 $^{31}$P NMR of 4.5 mM NAP-FF-AMP in the presence of 6 µM hHint1 in activity buffer.**

Qualitative experiment indicates a clear transition from PPG to nucleoside monophosphate product

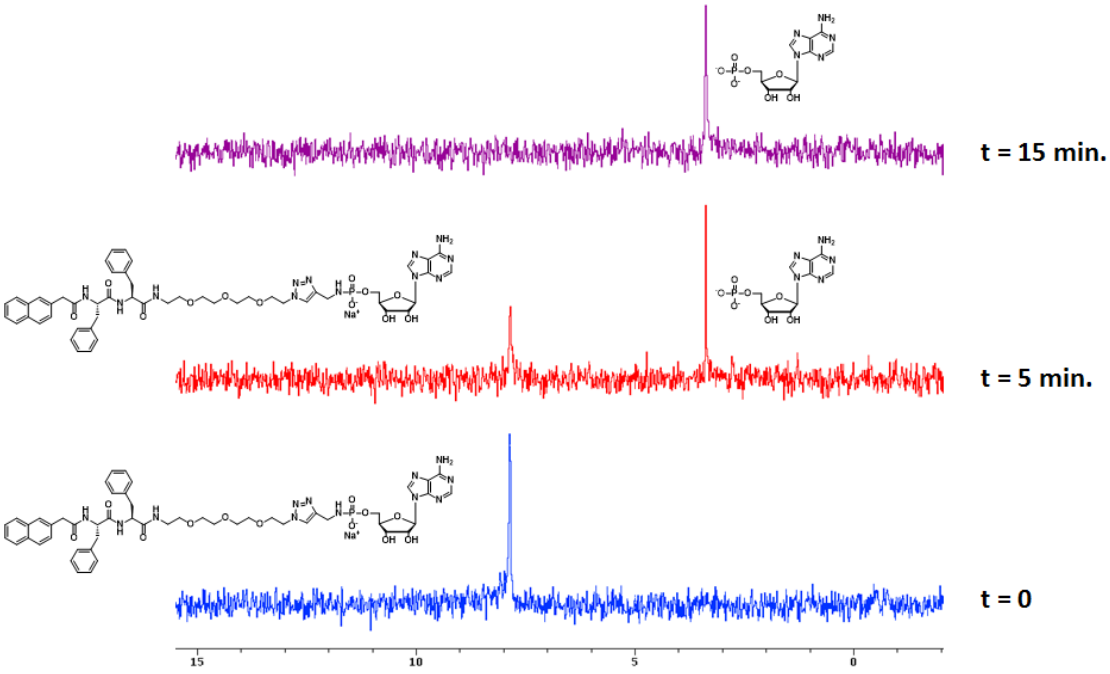

**Figure 2.17 Catalytic Turnover of NAP-FF-AMP by HINT1:**

A representative HPLC time course of HINT1 induced degradation of NAP-FF-AMP at time points 10 min, 30 min, 2.5 h, 5 h, 20 h and 24 h. The percent remaining NAP-FF-AMP after 24 h was determined to be 0.8±0.1 % within HINT1 formed hydrogels.

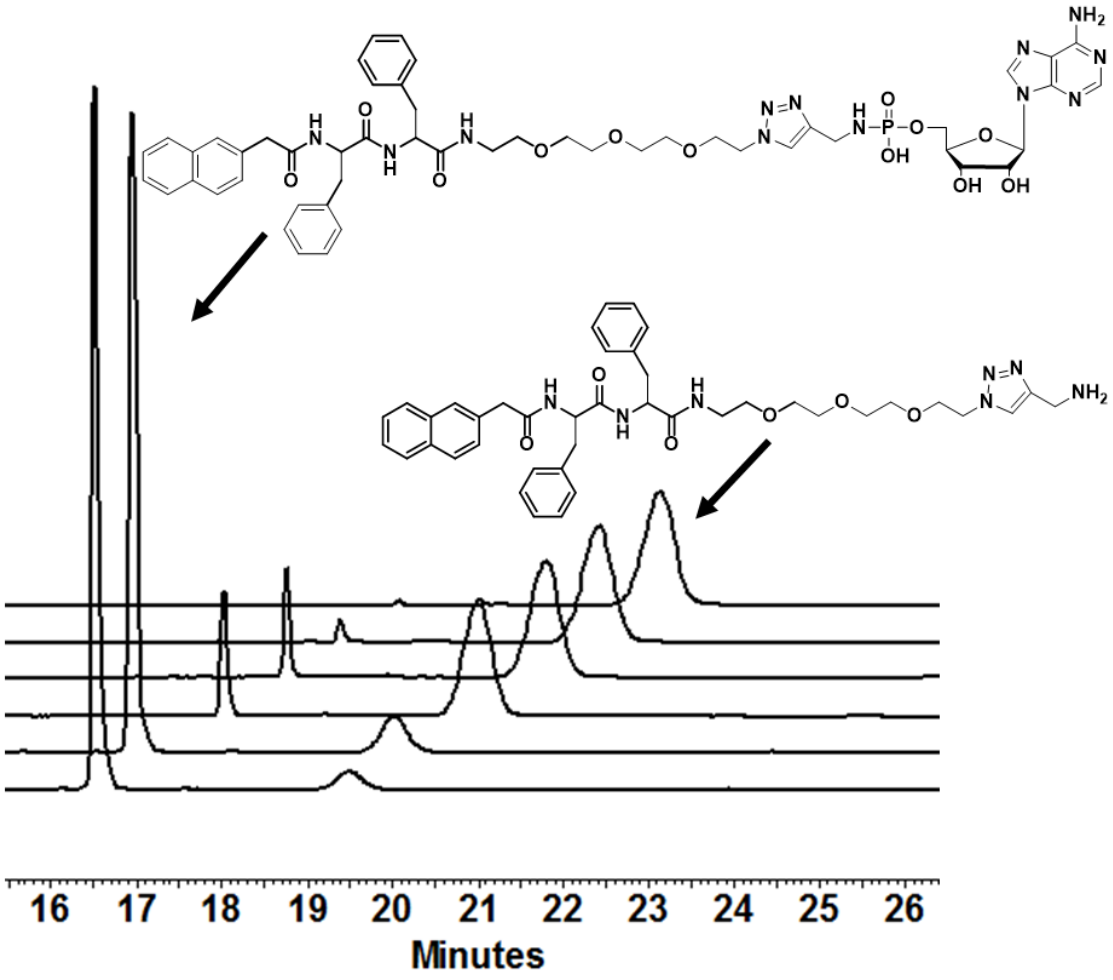

**Figure 2.18 hHint1 activated gelation of NAP-FF-Inv-UMP 6**

(a) SAOR time sweep in the presence of hHint1 (b) Cryo-TEM of NAP-FF-Inv-UMP (c) Cryo-TEM of NAP-FF- Inv-UMP in the presence of hHint1 (d) Synthesis of **6**

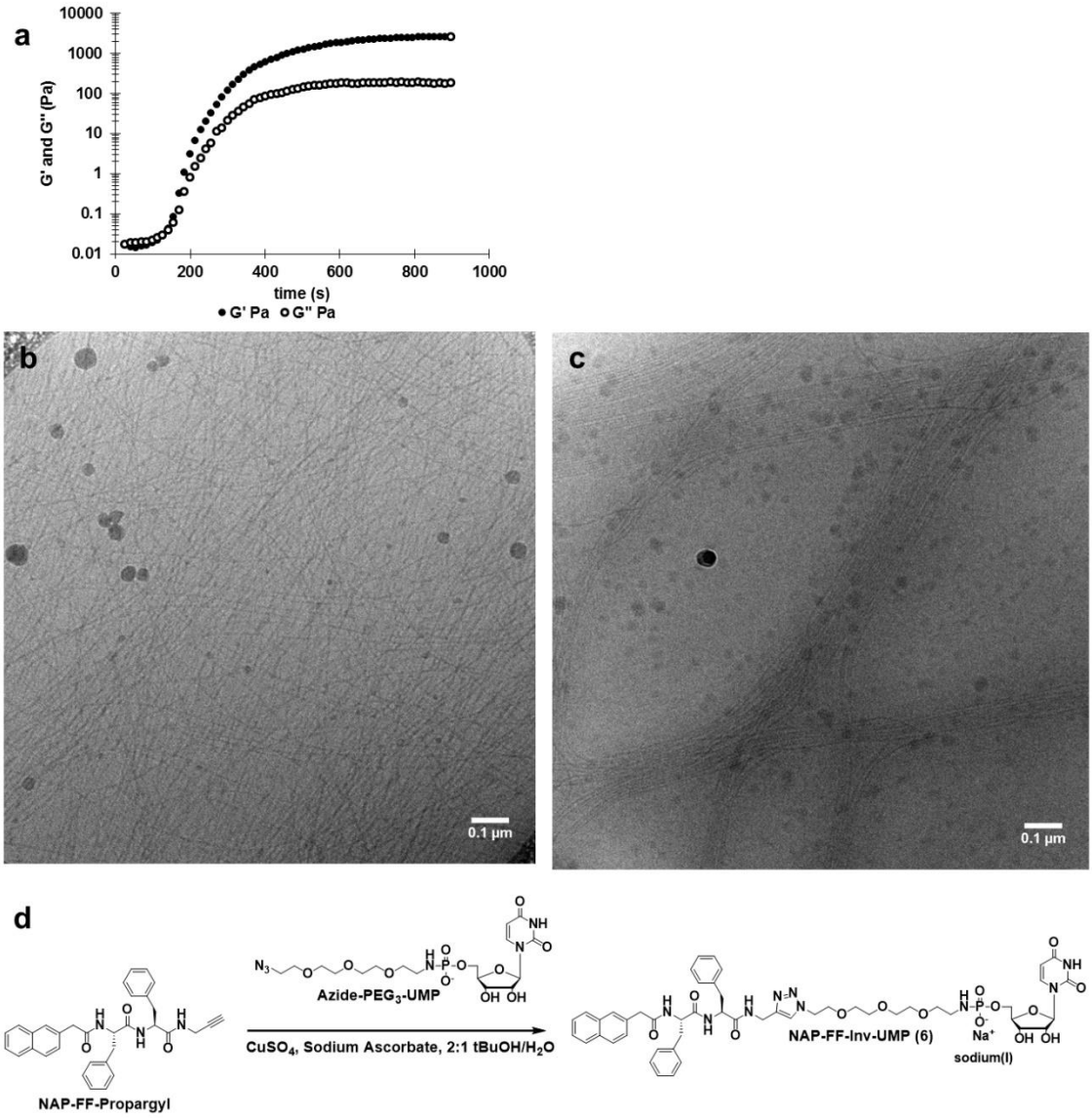

**Figure 2.19 NMR characterization of NAP-FF-Inv-UMP (6)**

(a) $^{31}$P NMR of hHint1 hydrolysis of **6** in blue and formed phosphate in red (b) $^{1}$H NMR of nucleobase proton at ring position 6 in PPG **6** in blue and UMP in red (c) concentration dependence on signal 1% wt/vol to 0.01% wt/vol, red box around aromatic region

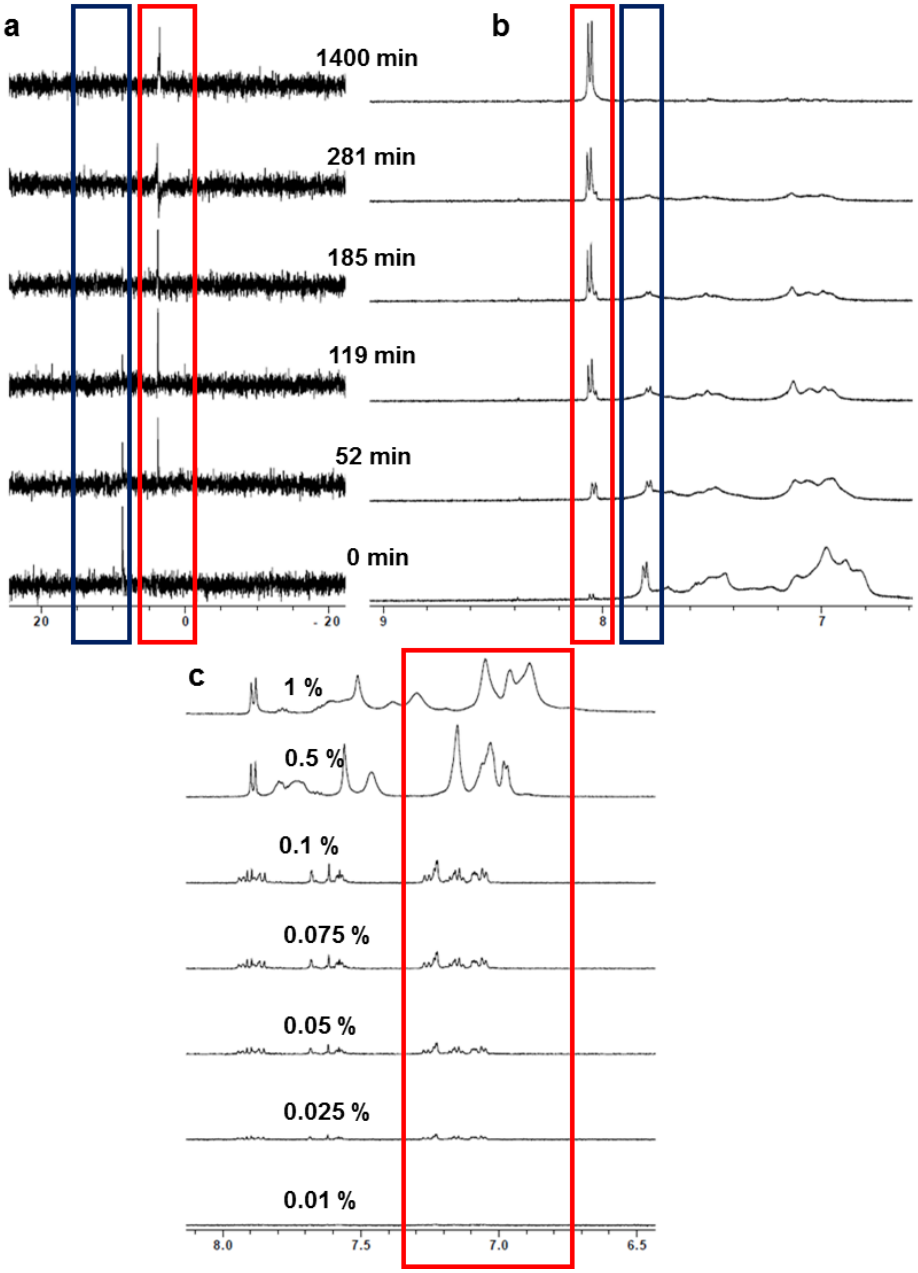

**Figure 2.20 Studies regarding nucleoside monophosphate retention in hHint1 formed gels**

(a) comparison of competitive release of UMP from hHint1 formed gels of PPG **6** determined from $^{1}H$ NMR due to supernatant presence of $D_2O$ alone or with 10 mM Sodium phosphate (b) schematic illustrating monophosphate sequestration in hHint1 formed gels

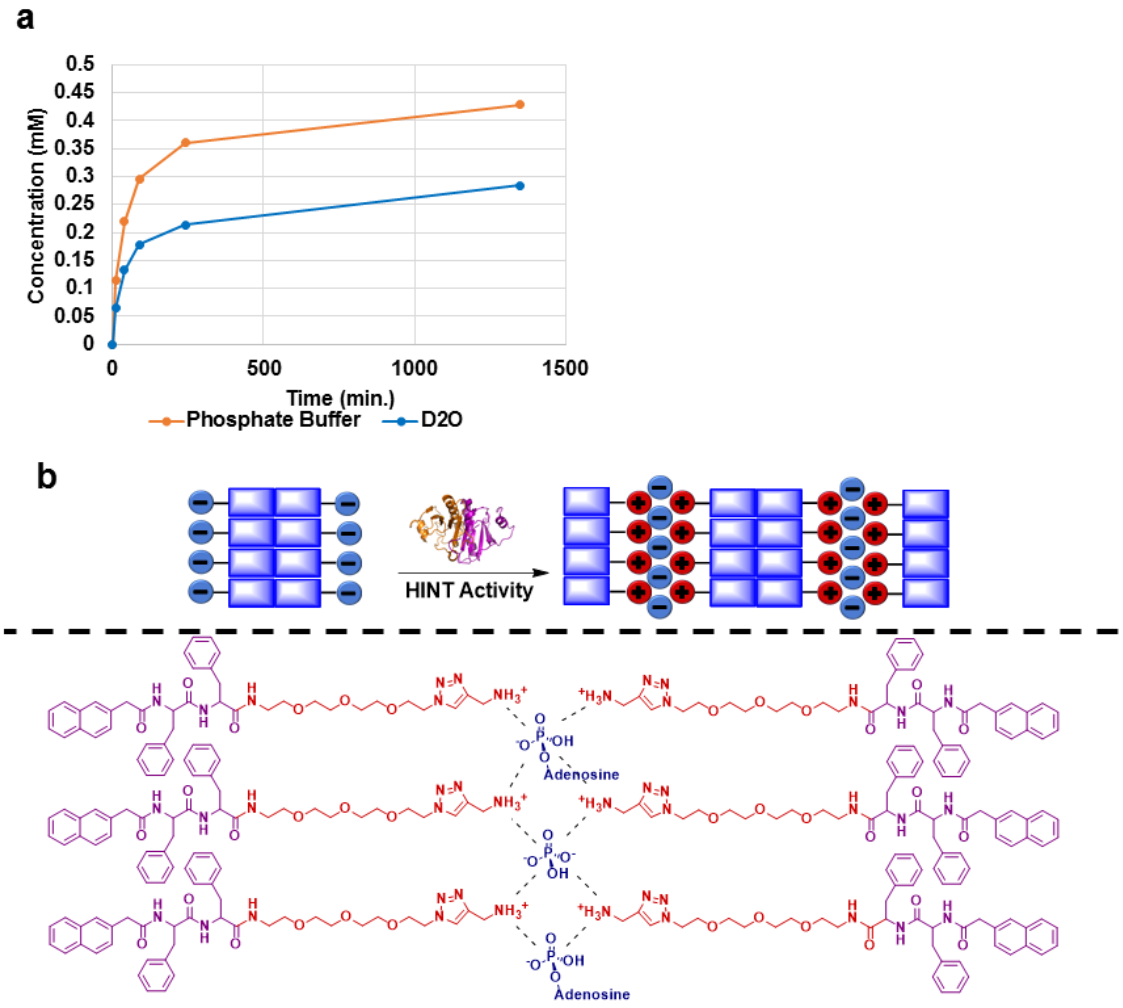

**Figure 2.21 NAP-FF-EtAd hHint1 kinetics assay**

(a) representative velocity curves for individual concentrations of PPG (pseudo-burst phase indicated by black arrow). (b) Schematic of hHint1 activity and generated fluorescence from hHint1 phosphoramidase activity

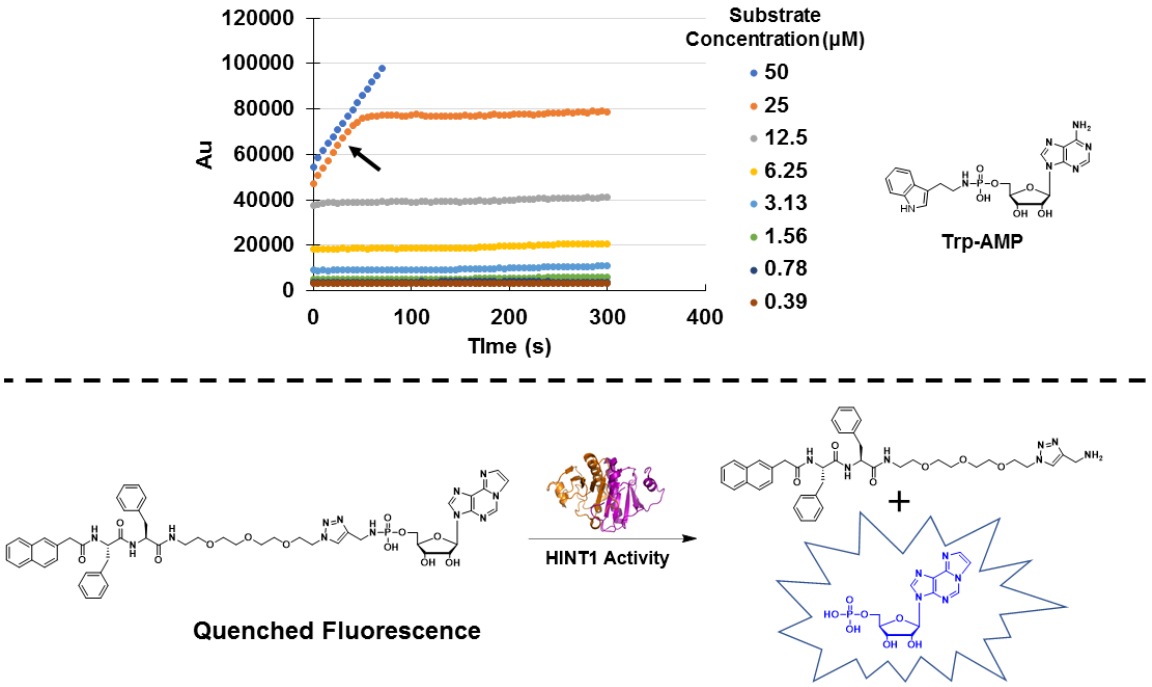

**Figure 2.22 Time dependent release of ethenoadenosine monophosphate from hHint1 gels formed from PPG 7**

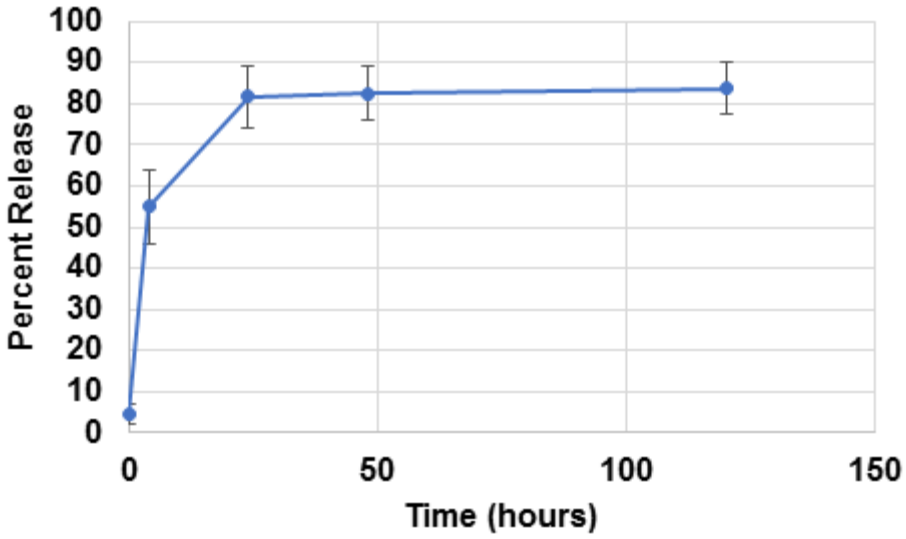

Previous determinations have shown that nearly all phosphoramidate is turned over in response to hHint1 catalytic activity and further experiments were carried out investigating the possibility UMP was becoming immobilized within nanofibers resulting in fractional release. NAP-FF-Inv-UMP hydrogels were formed in $D_2O$ using hHint1 and allowed to equilibrate overnight. The next day either additional $D_2O$ or $D_2O$ containing 10 mM sodium phosphate were layered on top of the gels and aliquots were removed at different time points to determine whether phosphate ion could replace nucleoside monophosphate in the forming gel and induce greater release of UMP over equivalent time periods (**Figure 2.18a**). Compared to addition of $D_2O$ alone, $D_2O$ containing additional phosphate ion resulted in greater release of UMP indicating possible ionic substitution in the formed gel structure due to competition for cationic nanofiber binding with inorganic phosphate. In such an assembly mechanism, the positive charges present on the self-assembled peptide nanofibers could coordinate multivalent anions such as the released nucleoside monophosphate and inorganic phosphate, leading to cross-linking of the nanofibers through ionic interactions (**Figure 2.20b**).

**Model fluorogenic substrate to determine hHint1 catalytic parameters of PPG activation**

Although hHint1 catalytic hydrolysis of PPGs could be monitored through the above-mentioned studies, the techniques are unable to provide catalytic parameters related to hHint1 enzyme activity for comparison to known and characterized substrates. To determine whether hHint1 catalytic activity could be monitored in a continuous assay format, the fluorogenic PPG NAP-FF-EtAd (**7**) was developed which bears the unnatural

fluorescent nucleoside 1,$N^6$-ethenoadenosine in lieu of traditional nucleosides.[286] Interestingly, conjugation of the unnatural nucleoside phosphoramidate to the self-assembling NAP-FF peptide resulted in significant quenching of fluorescence. Upon hHint1 hydrolysis, a rapid increase in the nucleoside fluorescence was observed. Steady state kinetic analysis at concentrations well below the expected critical aggregation concentration (CAC) revealed $K_m$ and $k_{cat}$ values of 4.8 ± 1.2 μM and 33 ± 13 $s^{-1}$ respectively (**Figure 2.21**). These kinetic parameters compare favorably to previously characterized nucleoside phosphoramidates such as Trp-AMP which possesses a $K_m$ 0.13 ± 0.02 and $k_{cat}$ 2.1 ± 0.1.[275] Interestingly, a pseudo burst-phase was observed in hHint1 kinetics experiments with higher concentrations of NAP-FF-EtAd **7**. A possible explanation for the occurrence is that hHint1 acts upon oligomeric assemblies at a faster rate due to the localized high concentrations of phosphoramidate, with equilibrium steady state reached upon turnover of these assemblies. Further investigations into enzyme activity upon self-assembled structures is clearly warranted.

NAP-FF-EtAd **7** was also utilized as a model probe to investigate the release of ethenoadenosine monophosphate from hHint1 formed gels in phosphate buffer. Over 24 hours, over 80% of the generated monophosphate was released from hHint1 formed gels. Interestingly, an equilibrium was reached after that time where only limited additional ethenoadenosine monophosphate was released over several days. Although the gelation reaction and supernatant were both DBPS, it appears that nearly a fifth of generated monophosphate is retained in hHint1 gels under physiologically relevant pH and salt concentrations at equilibrium (**Figure 2.22**)

## 2.3 DISCUSSION

The first-generation of PPGs provided key evidence that hHint1 responsive elements could be incorporated into self-assembling peptides to gain spatiotemporal control over their gelating properties. Additionally, the first-generation series of compounds also established that the NAP-FF peptide's robust self-assembling character would provide a useful model self-assembling peptide for further chemical modification to impart hHint1 responsiveness. Clearly evident was the need for a second phenylalanine residue in the peptide to generate stable gel assemblies rather than flocculated aggregates in contrast to other reports of hydrogels formed from singly Fmoc-protected amino acids.[287,288] Such discrepancy could be derived from the observed pathway dependence of hydrogelation on preparation procedure for short aromatic amino acids and peptide derivatives, as well as reduced aromatic surface area provided by the naphthyl N-terminal cap compared to the N-terminal Fmoc group to stabilize linear assembly[98].

The $PEG_3$ linker was found to readily enable dissolution of the second generation PPGs, regardless of conjugated nucleoside monophosphate, to obtain viscous solutions in aqueous buffer, presumably through enhanced solvation due to favorable water-ethylene glycol interactions.[144] As anticipated, addition of hHint1 to aqueous PPG solutions yielded hydrogels which were stable on the bench top for days. Conversely, PPG solutions without enzyme remained viscous solutions over the same period of time. The presumed mechanism of enzyme induced gelation centered on the potential assembly blocking characteristics of the polar nucleoside phosphoramidate moiety which was anticipated to promote monomer solubilization along with the extended PEG linker, until removal by

hHint1. Analogous mechanisms of gelation have been widely promoted in the literature with similarly functionalized short-aromatic self-assembling peptides. Short aromatic self-assembling peptides were previously shown to be functionalized in linear orientations with C-terminally conjugated linkers connecting the self-assembling peptide to hydrophilic solubilizing moieties such as taurine or nucleotides.[289,290] Interestingly, these reports indicated a lack of monomer assembly alone in solution, with both supramolecular association and hydrogelation dependent on treatment with esterase in the case of the taurine bearing monomer and alkaline phosphatase for the adenosine monophosphate monomer.

Conventional TEM studies revealed that discrete numbers of nanofibers formed bundles through lateral association resulting from hHint1 enzymatic activity. Due to its presence in all PPGs analyzed and uniformity within inspected samples, we regarded this structural feature as the primary driver of hHint1 induced PPG gelation. Laterally associated nanofibers were previously described in hydrogels formed from the self-assembly of Fmoc-Phe-Phe in response to decreasing pH, indicating this may be a general feature of hydrogels formed from short aromatic self-assembling peptides.[100] However, less clear from our studies was the nature of assembly in the PPG solutions without enzyme, as a range of structures were observed ranging from amorphous aggregates to fibrous networks. Additionally, due to the need for uranyl acetate staining and sample dehydration, it was not clear whether the observed structures were formed in solution prior to staining and drying or produced as a result of the sample preparation.

Given the indeterminate nature of the TEM studies, cryo-TEM proved crucial for gaining further insight into the mechanism of hHint1 induced hydrogelation. Cryo-TEM enables visualization of soft materials and nanostructures in the solvated state without interference from artifacts derived from staining and drying.[285] Surprisingly, all four PPG solutions formed monodisperse and unassociated nanofibers. However, samples treated with hHint1 readily formed nanofiber bundles generated from lateral nanofiber association as observed from conventional TEM. Additionally, the unconjugated self-assembling peptide formed distinctly different nanostructure morphologies than those observed from the PPGs indicating pathway dependent organization of monomer assembly originating from the nucleoside phosphoramidate moiety. From combined conventional and cryo-TEM results, it was presumed that hHint1 catalyzes the transition between PPG nanofibers and their higher ordered assembly into bundles. Presumably, the mechanism of hydrogelation results from hydrolysis of the phosphoramidate moieties present along assembled substrate nanofibers, allowing the "deprotected" nanofibers to self-assemble.

Inorganic phosphate and other polyanionic molecules have been previously observed to initiate association of primary amine containing supramolecular structures through charge coordination of self-assembled nanofibers.[291,292] Hydrogelation of the nanofibers would not be predicted after treatment with hHint1, since the surface of the nanofibers would switch from anionic to cationic, unless compensating ionic interactions are present. Consequently, it is possible the nucleoside monophosphate product is responsible for cross-linking the poly-cationic self-assembled nanofibers and may contribute additional non-covalent interactions through nucleobase hydrogen bonding and

aromatic interactions (**Figure 2.20**). Ionic cross-linking is ubiquitous in supramolecular polymer and low molecular weight hydrogelation, which is evidenced by examples such as the $Ca^{2+}$ dependent cross-linking of alginate, organic phosphate cross-linking of chitosan, and the inorganic phosphate cross-linking of cationic peptide nanofibers.[291–294] Nucleobases have long been investigated as self-assembling motifs and have been incorporated into a wide variety of synthetic and biologically sourced polymers to impart their hydrogen bonding propensity into higher ordered structures.[295,296] Interestingly experiments investigating whether nucleoside monophosphates could be competitively released from hHint1 formed hydrogels revealed that the addition of inorganic phosphate containing buffer accelerates the release of nucleoside monophosphate from the hydrogels. Presumably, inorganic phosphate could replace nucleoside monophosphate in the charge coordinated hHint1 gel while maintaining multivalent interactions and effectively cross-linking the primary amine containing nanofibers (**Figure 2.20**). Further investigation of this cross-linking mechanism could confirm the unique mechanism of gelation in which the enzymatically released moiety is the mediating unit of nanofiber crosslinking and hydrogel formation.

Dependence on hHint1 for triggering gelation of PPGs was evident in SAOR studies where increased gelation kinetics were observed in response to increased hHint1 concentration. Additionally, differences in the kinetics of gelation were observed with the purine substrate NAP-FF-AMP **2** demonstrating more rapid gelation with equivalent enzyme concentration than NAP-FF-UMP **3**, reflecting hHint1 specificity preference.[275] Interestingly, even in the assembled state with concentrations of monomer at saturating

levels orders of magnitude above typical nucleoside phosphoramidate $K_m$ values, hHint1's preference for purine substrates is still evident.[275]

Additionally, hHint1 inhibitor and catalytically dead H112N mutant confirmed that both access to the active site and catalytic activity were necessary for initiating the gelation reaction. Preference for the purine substrate was again evident in SAOR time sweeps of NAP-FF-AMP **2** and NAP-FF-UMP **3** with hHint1 preventing gelation of the pyrimidine substrate for at least 30 min, while the purine substrate was still able to form hydrogels despite delayed gelation kinetics in comparison to samples without inhibitor. The difference in response is likely explained by the higher affinity of the unnatural purine base in the inhibitor substrate mimic, which more effectively blocks pyrimidine access to the active site than the more comparable NAP-FF-AMP substrate.[286] Importantly, due to the known binding of the HNTI-3a ligand in the active site of hHint1 and demonstration of reduced gelation kinetics for both PPGs **2** and **3** albeit to different degrees, hHint1 triggered gelation appears to be occurring through interactions of PPGs and the enzyme's active site. Dependence on catalytic activity as the sole driver of hydrogelation was further confirmed through incubations with the catalytically dead hHint1 H112N mutant which was found to be unable to initiate gelation for either NAP-FF-AMP **2** or NAP-FF-UMP **3**.

hHint1 enzymatic activity was found to be very efficient in the gelation of NAP-FF-AMP **2** with less than 1% of the PPG substrate remaining in the hydrogel after 24 hours. Due to the preassembly of PPGs into nanofibers, and the high turnover of PPGs to the amine containing peptide and nucleoside monophosphate, hHint1 likely performs its phosphoramidase activity on PPGs contained within nanofibers. To monitor this reaction

in real time, inverse linker PPG **6** was monitored in the presence of hHint1 using both $^{31}$P and $^{1}$NMR. As expected, a clear conversion of phosphoramidate to monophosphate was observed using $^{31}$P NMR as observed in the hydrolysis of NAP-FF-AMP **2**. Additionally, monitoring of $^{1}$H NMR over the same time frame demonstrated production of UMP and gradual disappearance of peptide associated resonances due to the assembly transition from soluble nanofibers to NMR silent gel structures. Surprisingly, although the concentration of substrate PPG in the sample tube was quite high, only a small amount of UMP was observed over 24 hours, much less than the expected stoichiometric equivalent.

A possible explanation for the low observed concentration of released UMP upon treatment of NAP-FF-Inv-UMP **6** with hHint1is the sequestration of the nucleoside monophosphate as a cross-linking ion pair agent between cationic nanofibers (**Figure 2.20**). Competition experiments were performed to observe if solutions containing inorganic phosphate could competitively release UMP from the hHint1 formed gels. Indeed, the addition of $D_2O$ containing phosphate resulted in an increased release of UMP compared to addition of $D_2O$ alone indicating that the released nucleoside monophosphate potentially mediates nanofiber cross-linking. Due to the effectively high concentration of released nucleoside monophosphate in the vicinity of nanofibers resulting from hHint1 activity, the nucleoside monophosphate is likely preferentially immobilized between nanofibers compared to other ions. However, slow substitution could occur as an equilibrium is reached with the surrounding solution similar to other ionically cross-linked hydrogels.[291,292]

To further probe the importance of the hHint1 released nucleoside monophosphate on hydrogelation, nucleoside monophosphate retention studies were carried out with the fluorogenic PPG NAP-FF-EtAd. After incubation in phosphate buffered saline for 24 hours, approximately 80% of ethenoadenosine monophosphate molar equivalents were released from the hHint1 formed gel. Since 20% of the nucleoside monophosphate remained in the gel, it appeared an equilibrium was reached in which, despite total supernatant changes, the remaining monophosphate appears to be locked into the gel and unable to be released. Thus, the majority of nucleoside monophosphate is likely initially immobilized in surface exposed areas where exchange with solvent anions is likely achieved rapidly. However, approximately 20% of monophosphate appears to be buried within the nanofiber bundles and sequestered from solvent exposed areas, with multivalent ionic interactions that are not readily susceptible to competition with solvent ions.

Additionally, efforts were undertaken to compare the phosphoramidase activity of hHint1 on PPGs compared to previously characterized nucleoside phosphoramidates, to determine how the bulkier self-assembling peptide conjugation would affect catalytic parameters. Interestingly, the fluorogenic substrate exhibited only a 40 fold increase in $K_m$ compared to known purine substrates but possessed a higher $k_{cat}$ value by 10 fold indicating that the PPG substrates remain efficient substrates of hHint1 despite the bulky linker and peptide.

Due to the distance separation of the nucleoside phosphoramidate and self-assembling peptide, it is likely that the conjugation strategy could be applied to other peptides, as well as synthetic and natural bio-polymers to impart hHint1 responsiveness for

regulation of supramolecular assembly and nanostructure morphology. Ionic cross-linking is ubiquitous in mediating supramolecular interactions between self-assembling peptides, peptide amphiphiles, and polymers.[291–294,297] Cationic lysine containing self-assembling peptides were shown to be sensitive to the presence of inorganic phosphate which induced crosslinking of nanofibers and hydrogelation[291]. The gelation mechanism was demonstrated with other polyanionic species such as suramin, trypan, heparin, and clodronate[292]. Chitosan, a biopolymer derived from chitin, was shown to undergo gelation in the presence of 6-phosphogluconic acid mediated by ionic cross-linking between primary amines on the polymer and the negatively charged groups of 6-phosphogluconic acid.[294,297] Nevertheless, such methods of cross-linking rely on stoichiometric quantities of cross-linker to effect the gelation reaction. The gelation of such molecules is also inherently sensitive to subtle changes in solution pH and ionic strength complicating their production and application. In comparison, small quantities of hHint1 enzyme catalyze similar transitions with nucleoside phosphoramidate functionalized self-assembling peptides or polymers in solution media with physiologic relevant salt concentrations and pH in a selective manner at sub-stoichiometric concentrations of the counter ion. In addition, cross-linking is generated by a human enzyme and the cross-linking agent itself is an endogenous biomolecule indicating potential biocompatibility in comparison to systems where co-solvents and synthetic cross-linkers can have associated toxicities.[298] We hope to further develop such systems for application as *in situ* formed biomaterials for drug delivery or regenerative purposes.

## 2.4 MATERIALS AND METHODS

**Materials and General Methods**

Commercially available chemicals were utilized without additional purification. Fmoc-Phe-OH, nucleoside-5'-monophosphates, propargyl amine, 2-naphthylacetic acid, $CuSO_4 \cdot 5xH_2O$, Na Ascorbate were purchased from Sigma-Aldrich. The amide coupling reagents 1-ethyl-3-(3-dimethylaminopropyl)carbodiimide (EDC), (1-[Bis(dimethylamino)methylene]-1H-1,2,3-triazolo[4,5-b]pyridinium 3-oxid hexafluorophosphate (HATU), and (2-(1*H*-benzotriazol-1-yl)-1,1,3,3-tetramethyluronium hexafluorophosphate (HBTU) were purchased from Oakwood Chemical. Fmoc-Phe pre-loaded Wang resin was purchased from Bachem. Amino-$PEG_3$-Azide was purchased from Quanta Biodesign. Diisopropylethylamine, tert-butanol, and piperidine were purchased from Sigma-Aldrich. All bulk solvents were sourced from Fisher Scientific and were of high pressure liquid chromatography (HPLC) grade. hHint1 wild type (WT) and H112N mutant were expressed and purified as previously described.[280] Normal and reverse phase chromatographic separations were performed on a Teledyne Isco CombiFlash system. Analytical HPLC was performed on an Ultimate 3000 System (Agilent) and Higgins Analytical Targa C18 5 μm column with 50 mM triethylammonium bicarbonate (TEAB) buffer and acetonitrile (30%-100% Acetonitrile). hHint1 enzymatic activity studies were monitored by HPLC at wavelength 280 nm. Quantitative experiments were performed by diluting hydrogel samples (0.9% phosphoramidate pro-gelator Substrate, 6 μM in hHint1, in Dulbecco's phosphate buffered saline (DPBS)) 10x by volume in dimethylsulfoxide (DMSO) after 24 h. Aliquots were taken from the DMSO solutions and diluted 10x with 50 mM TEAB Buffer for HPLC injection. Electrospray Ionization Mass Spectrometry

(ESI-MS) was performed on an Agilent MSD SL system and high resolution MS was performed on an LTQ Orbitrap Velos (Thermo Scientific). Dowex 50wx8 cation exchange resin was sourced from Sigma-Aldrich. Nuclear magnetic resonance imaging (NMR) of all compounds was performed at 25°C utilizing an Ascend 500 MHz Bruker spectrometer ($d_6$-DMSO, Cambridge Isotope Laboratories). $^{31}$PNMR to observe hHint1 catalysis was performed using 5 mM phosphoramidate substrate in hHint1 activity buffer (20 mM HEPES, 1 mM $MgCl_2$, pH 7.3) with 6 uM hHint1 and 5% $D_2O$.

**General procedure for synthesis of (1)**

Standard Fmoc-based solid phase chemistry was utilized to obtain the NAP-FF peptide. Example Synthesis: Fmoc-Phenylalanine pre-loaded Wang Resin (1.0 mmol) was swelled in dichloromethane for 15 minutes and washed three times with DMF. The resin was suspended in 20% Piperidine in DMF with agitation provided $N_2$ bubbling for three minutes. The resin was washed with 20% Piperidine in DMF and again agitated for 18 additional minutes to ensure complete removal of Fmoc protecting group. After three washings with DMF, the resin was suspended in DMF and to the reaction vessel was charged Fmoc-Phenylalanine (3 eq., 1.16 g), HATU (3 eq., 1.9 g), and DIEA (5 eq., 870 uL). The coupling solution was agitated with $N_2$ bubbling for 45 minutes. Following the coupling reaction, the resin was again washed three times with DMF and deprotected with the same procedure as the pre-loaded resin. Following Fmoc deprotection, naphthyl acetic acid (3 eq., 558 mg), HATU (3 eq., 1.14 g), and DIEA (5 eq., 870 uL) were charged to the reaction vessel and agitated with $N_2$ for 45 minutes. Following the coupling reaction, the resin was washed 3 times with DMF and 3 additional times with DCM. The resin was dried

*in vacuo* overnight. Following resin drying, the resin was treated with 95:5 TFA/$H_2O$ for 2 hours to effect peptide cleavage. The cleavage cocktail was agitated by shaking during this time. Resin particulates were filtered away and the filtrate was concentrated to a clear gum. The crude peptide residue was purified via flash chromatography to provide NAP-FF in good yield (Yields: 62-79%). $^1$H NMR spectrum (DMSO-$d_6$): 2.73 (q, 1H), 2.93 (m, 1H), 3.00 (dd, 1H), 3.07 (dd, 1H), 3.53 (q, 2H), 4.46 (q, 1H), 4.58 (m, 1H) 7.85 (8.28 (d,1H), 8.34 (d, 1H), 12.77 (s, 1H).

Purified NAP-FF-OH peptide was charged to a round bottomed flask containing a solution of 3,6,9-trioxa-1-azidoundecamine (1.2 eq.) in anhydrous DCM. HBTU (2 eq.) and DIEA (1.5 eq.) were added to the solution and allowed to stir overnight at room temperature. The reaction solution was diluted in DCM and washed with 0.1N HCl (100 mL) and brine (2 x 100 mL). The organic layer was dried over magnesium sulfate and concentrated to a clear gum which was purified with normal phase chromatography (DCM/MeOH 0-15%) (70-98%). $^1$H NMR spectrum (DMSO-$d_6$): 2.69 (q, 1H), 2.81 (q, 1H), 2.97 (dd, 2H), 3.16 (m, 1H), 3.22 (m, 1H), 3.34 (d, 1H), 3.37 (t, 2H), 3.48-3.49 (m, 14H), 4.47-4.55 (m, 2H), 7.15-7.25 (m, 10 H), 7.47 (m, 2H), 7.61 (s, 1H), 7.75 (d, 1H), 7.79 (d, 1H), 7.85 (d, 1H), 7.96 (t, 1H), 8.13 (d, 1H), 8.27 (d, 1H)

**General Synthesis of Phoshoramidate Pro-Gelators (2-5)**

5'-Nucleoside-monophosphate (2.5 mmol) was charged to a round-bottomed flask and suspended in minimal de-ionized water (≈ 500 uL). To the suspension was added propargyl amine (5 eq.) and the pH was adjusted to ≈ 7 with 6N HCl. EDCI (4 eq.)

wasadded to the red solution which was magnetically stirred. Reaction progress was monitored with $^{31}P$ NMR which indicated reaction completion within 30 minutes. The reaction solution was concentrated to a red gum and the crude material was partially purified through reverse phase chromatography. The resulting nucleotide propargyl phosphoramidate (2.0 eq) in $H_2O$ (2 mL) was added to a suspension of **1** (0.325-0.366 mmol) in 4 mL of t-BuOH. To this mixture was added 0.1 eq. of $CuSO_4$ x $5H_2O$ and 0.2 eq. of Sodium ascorbate. The reaction vessel was purged with Argon and allowed to stir at room temperature overnight in the dark. The suspensions were then purified with reverse phase chromatography to obtain the TEA salts of the phosphoramidate pro-gelators. Sodium salts were obtained of final compounds through cation exchange chromatography with Dowex 50wx8 resin ($Na^+$ form). $^1H$-NMR spectra and HPLC chromatograms are located in **Appendices**.

NAP-FF-AMP (2): Yield 33.2%, $^{31}P$ NMR (DMSO-$d_6$): 6.296 ppm, HRMS (ESI-): Calculated 1063.4191, Found 1063.4174. ((2R,3S,4R,5R)-5-(6-amino-9H-purin-9-yl)-3,4-dihydroxytetrahydrofuran-2-yl)methyl ((1-((4S,7S)-4,7-dibenzyl-1-(naphthalen-2-yl)-2,5,8-trioxo-12,15,18-trioxa-3,6,9-triazaicosan-20-yl)-1H-1,2,3-triazol-4-yl)methyl)phosphoramidate

NAP-FF-UMP; (3): Yield 25.8%, $^{31}P$ NMR (DMSO-$d_6$): 6.226 ppm, HRMS (ESI-): Calculated 1040.3919, Found 1040.3905. ((2R,3S,4R,5R)-5-(2,4-dioxo-3,4-dihydropyrimidin-1(2H)-yl)-3,4-dihydroxytetrahydrofuran-2-yl)methyl ((1-((4S,7S)-4,7-dibenzyl-1-(naphthalen-2-yl)-2,5,8-trioxo-12,15,18-trioxa-3,6,9-triazaicosan-20-yl)-1H-1,2,3-triazol-4-yl)methyl)phosphoramidate

NAP-FF-GMP (4): Yield 62.7%, $^{31}$P NMR (DMSO-$d_6$): 6.314 ppm, HRMS (ESI-): Calculated 1079.4140, Found 1079.4125.((2R,3S,4R,5R)-5-(2-amino-6-oxo-1,6-dihydro-9H-purin-9-yl)-3,4-dihydroxytetrahydrofuran-2-yl)methyl ((1-((4S,7S)-4,7-dibenzyl-1-(naphthalen-2-yl)-2,5,8-trioxo-12,15,18-trioxa-3,6,9-triazaicosan-20-yl)-1H-1,2,3-triazol-4-yl)methyl)phosphoramidate

NAP-FF-CMP (5): Yield 28.0%, $^{31}$P NMR (DMSO-$d_6$): 6.289 ppm, HRMS (ESI-): Calculated 1039.4079, Found 1039.4071. ((2R,3S,4R,5R)-5-(4-amino-2-oxopyrimidin-1(2H)-yl)-3,4-dihydroxytetrahydrofuran-2-yl)methyl ((1-((4S,7S)-4,7-dibenzyl-1-(naphthalen-2-yl)-2,5,8-trioxo-12,15,18-trioxa-3,6,9-triazaicosan-20-yl)-1H-1,2,3-triazol-4-yl)methyl)phosphoramidate

**Synthesis of Inverse Linker NAP-FF-Inv-UMP Phosphoramidate Pro-Gelator (6)**

NAP-FF-Propargyl: Solid components NAP-FF-OH (423 mg, 0.88 mmol) and HBTU (667 mg, 1.76 mmol) were charged to an oven dried round bottomed flask and suspended in dry DCM. Under $N_2$ atmosphere, propargyl amine (140 μL, 2.19 mmol) and DIEA (303 μL, 1.76 mmol) were added to the suspension which stirred overnight at room temperature. The reaction solution was diluted in DCM and washed with 0.1N HCl (100 mL) and brine (2 x 100 mL). The organic layer was dried over magnesium sulfate and concentrated to a clear gum which was purified with normal phase chromatography (DCM/MeOH 0-15%) Yield 81%, $^{1}$H NMR spectrum (DMSO-$d_6$): 2.74 (t, 1H), 2.82 (m, 1H), 2.96 (m, 1H), 2.99 (m, 1H), 3.15 (s, 1H), 3.48-3.593(q, 2H), 3.86 (s, 2H), 4.48-4.56 (m, 2H), 7.15-7.23 (m, 10H),

7.47 (m, 3H), 7.602 (s, 1H), 7.75 (d, 1H), 7.79 (d, 1H), 7.86 (d, 1H), 8.18 (d, 1H), 8.25 (d, 1H), 8.32 (t, 1H)

Azide-$PEG_3$-UMP: Uridine monophosphate (1.1 g, 3.4 mmol) was added to a scintillation vial and suspended in 2 mL of $H_2O$. 3,6,9-trioxa-1-azidoundecamine (600 mg, 2.75 mmol) was added to the suspension and the solution was neutralized with 1N HCl dropwise. EDCI (2 grams, 10.5 mmol) was added to the suspension which stirred for 4 hours. At this time the crude solution was diluted in 50 mM TEAB and was partially purified through reverse phase chromatography. LRMS (ESI-) 523.2, calculated 523.4, $^{31}$P NMR (DMSO-$d_6$): 6.258 ppm. Residual EDCI urea salt was present in the partially purified phosphoramidate however the product was carried to the next step without additional purification.

NAP-FF-Inv-UMP; (6): Preparation was performed as for PPGs 2-5. Yield $^{31}$P NMR (DMSO-$d_6$): 6.679 ppm, HRMS (ESI-): Calculated 1040.3919, Found 1040.3904. ((2R,3S,4R,5R)-5-(2,4-dioxo-3,4-dihydropyrimidin-1(2H)-yl)-3,4-dihydroxytetrahydrofuran-2-yl)methyl (2-(2-(2-(2-(4-(((S)-2-((S)-2-(2-(naphthalen-2-yl)acetamido)-3-phenylpropanamido)-3-phenylpropanamido)methyl)-1H-1,2,3-triazol-1-yl)ethoxy)ethoxy)ethoxy)ethyl)phosphoramidate

**Synthesis of Fluorogenic NAP-FF-EtAd Phosphoramidate Pro-Gelator (7)**

Preparation was achieved through generating the propargyl phosphoramidate derivative of the fluorescent monophosphate followed by click chemistry to the azido peptide **1**. Ethenoadenosine monophosphate was prepared as previously described in the literature.[299] The propargyl phosphoramidate derivative was synthesized through EDCI mediated

coupling to the monophosphate and subsequent partial purification through reverse phase. Subsequent click reaction conditions and purification were identical to that described above in the synthesis of PPGs **2-5**.

NAP-FF-EtAd; (7): Preparation was performed as for PPGs 2-5. Yield $^{31}$P NMR (DMSO-$d_6$): 6.299 ppm, LRMS (ESI-): Calculated 1087.4, Found 1087.6 ((2R,3S,4R,5R)-3,4-dihydroxy-5-(3H-imidazo[2,1-i]purin-3-yl)tetrahydrofuran-2-yl)methyl ((1-((4S,7S)-4,7-dibenzyl-1-(naphthalen-2-yl)-2,5,8-trioxo-12,15,18-trioxa-3,6,9-triazaicosan-20-yl)-1H-1,2,3-triazol-4-yl)methyl)phosphoramidate

**General preparation of phosphoramidate pro-gelator solutions and hHint1 formed hydrogels**

Precursor and gel samples were prepared as follows: Lyophilized foams of each phosphoramidate pro-gelator were weighed into scintillation vials and dissolved in hHint1 activity buffer resulting in 1% wt/vol solutions. Samples were mixed with vortexing to ensure complete dissolution of the material. Final working solutions of 0.9% wt/vol concentration were obtained by mixing 450 μL of each 1 % wt/vol pro-gelator solution with 50 additional μL of hHint1 activity buffer. Hydrogel samples were generated in a similar manner by adding 50 μL of hHint1 in activity buffer to 450 μL of 1% wt/vol pro-gelator solution to generate samples containing 6 μM concentrations of enzyme and 0.9% wt/vol.

**Conventional and Cryo-Transmission Electron Microscopy**

Imaging was performed using an FEI Technai Spirit Bio-Twin instrument. Conventional TEM hydrogelation samples contained 0.9% by wt/vol phopshoramidate pro-gelator and 19 μM HINT1 in activity buffer except NAP-FF-AMP which contained 36 uM HINT1. Gelation samples cured on grid for 10 minutes before blotting and staining. Substrate only samples contained 0.9% by wt/vol phosphoramidate pro-gelator in activity buffer. Conventional TEM samples were stained with 2% uranyl acetate for negative imaging.

Hydrogel samples of **2-5** analyzed with Cryo-TEM contained 0.9% by wt/vol phosphoramidate pro-gelator and 6 μM HINT1 in activity buffer. The gel forming reaction was allowed to proceed for at least 10 minutes before vitrification. Substrate only samples contained 0.9% by wt/vol phosphoramidate pro-gelator in activity buffer. Inverse linker substrate **6** was analyzed similarly with 3 μL of 1 % wt/vol PPG in DPBS applied directly to the sample grid followed by 0.5 μL of hHint1 solution for a final enzyme concentration of 50 μM in the gel sample. PPG alone sample consisted of 3.5 μL of 1% wt/vol PPG. Cyro-TEM of 1% wt/vol NAP-FF-$NH_2$ in DPBS was performed with or without 1% wt/vol adenosine monophosphate.

**Small Angle Oscillatory Rheometry**

Rheological experiments were performed on a TA Instruments AR-G2 Rheometer. The 25 mm geometry was utilized with upper and lower geometries modified with 600 grit sandpaper to aid in sample adhesion. All samples were 500 μL in volume and were prepared by combining 450 μL of 1% wt/vol substrate in HINT1 activity buffer with up to 10 μL of Enzyme (Final Concentration in Sample 6 μM), and 40 uL of HINT1 activity

buffer to maintain constant volumes between samples. The Peltier temperature was set to a constant temperature of 23ºC. Time course experiments were performed at 0.1% strain and 1 rad/s for all experiments with both values within the linear viscoelastic range. Experiment time lengths were kept to a minimum to observe sample curing while avoiding evaporation, the effects of which were mitigated by use of humidity chamber lined with moistened paper towels. In samples demonstrating a clear sol-gel transition with G' becoming greater than G'', gelation times are defined as the time point at the crossover. For samples where G' was greater than G'' for the entire time course, a time point was estimated by constructing linear curves before and after the G' increase and determining the time point at which both linear functions possessed equal values to estimate the inflection point. All reported gelation time points are averages of at least 3 individual experiments.

**NMR Experiments with NAP-FF-Inv-UMP**

Concentration experiments were performed by making 0.005%, 0.01%, 0.025%, 0.05%, 0.075%, 0.1%, 0.5%, 1% wt/vol solutions of NAP-FF-Inv-UMP **6** in $D_2O$. Experiments monitoring the catalytic activity of hHint1 were performed in $D_2O$ without $H_2O$ co-solvent to enhance $^1H$ signal from the PPG and released monophosphate, and to delay hHint1 enzyme kinetics to enable monitoring over extended time periods. The concentration of NAP-FF-Inv-UMP was 1% wt/vol with MeCN as an internal standard due to its miscibility with $D_2O$ and presence of a single peak not overlapping with any region of the PPG. The concentration of UMP generated was determined using the equation $A = \frac{Area_A \times S}{Area_S}$ where A is analyte concentration, S is the concentration of MeCN, and the Area

is the integrated signal for a characteristic peak. The peak monitored from UMP was the position 6 proton of the nucleobase. UMP release experiments from hHint1 formed gels were performed by making hydrogels from 3.9 μM hHint1 and 1 % wt/vol PPG with a total volume of 610 μL. Gels were cured at room temperature overnight, and the next day 610 μL of either $D_2O$ or $D_2O$ with 10 mM Sodium phosphate (both monobasic and dibasic for final pD of 7.4) were added to the top of the gels and incubated for different time periods. The cumulative release of UMP was determined using the equation above and MeCN as an internal standard.

**NAP-FF-EtAd Fluorescence Assays**

hHint1 enzyme kinetic assays were performed as previously described[275]. Deviation from the published method was only used with respect to the fluorophore excitation and emission which were achieved at 305 nm and 415 nm respectively. Non-linear regression with built in Michaelis-Menten model in GraphPad Prism was used to determine catalytic parameters. Ethenoadenosine monophosphate release was performed by first generating 50 μL hydrogels from NAP-FF-EtAd with 0.9% wt/vol concentration of the PPG in DPBS. The hydrogels cured overnight and at different time points, 450 uL of additional DPBS were layered onto formed gel. At time points, the buffer was removed, replaced with equivalent volume of fresh buffer, and analyzed with Cary Eclipse Fluorimeter using an ethenoadenosine monophosphate standard curve to determine the concentration of released monophosphate. Experiment was performed in triplicate.

# CHAPTER 3: SELF-ASSEMBLY OF NUCLEOSIDE PHOSPHORAMIDATE MODIFIED PEPTIDES AND NUCLEOBASE DEPENDENT GELATION

## 3.1 INTRODUCTION

Since their serendipitous discovery, various chemical modifications of self-assembling peptides have been made to modulate their self-assembling and functional properties beyond making changes in their peptide sequence.[49,145,300] Among the earliest performed and most basic of chemical modifications has been the addition of lipophilic moieties such as fatty acids to generate peptide amphiphiles or lipopeptides.[49,71,111] In addition to promoting membrane association and anchoring, aliphatic modifications promote self-assembly of peptides themselves into micellar structures through hydrophobic collapse.[117] The broad utility of peptide amphiphiles is reflected in the robustness of their self-assembly in a wide variety of formats, driven by the unique balance of non-covalent interactions that lead to assembly at low concentrations and with remarkable stability.[32,117] Additionally, peptide modification is not limited to a single fatty acid chain as diglycerides have also been used to generate supramolecular vaccine adjuvants.[213]

N-terminal aromatic modification of short peptides has proved invaluable as synthetic peptide modifications to drive assembly and gelation. The addition of a Fluorenylmethoxycarbonyl (Fmoc) group to the N-terminus of diphenylalanine peptides sparked the development of a wide variety of low molecular weight gelating molecules investigated for use in applications ranging from cell culture substrates to drug delivery vehicles.[92,97] Alternative N-terminal aromatic modifications include various naphthalene and pyrene derivatives, as well as simple protecting groups such as benzyloxycarbonyl moieties (**Figure 3.1**).[101,108] In addition, functional molecules such fluorescent dyes and

therapeutics bearing aromatic character have been used as N-terminal aromatic modifications.[301,302] Despite the varied modifications that have been demonstrated, the commonality among these moieties is the promotion of self-assembly through hydrophobic collapse and stabilization of peptide association through aromatic and complementary steric interactions.[75,100,107,108]

Additional modifications have sought modulation of assembly properties such as gelation, rheological enhancement, or colloidal stabilization.[144,161,303] Conjugation of a short PEG unit to Fmoc-pentafluorophenylalanine was found to enhance response to shear when co-assembled with the unmodified amino-acid into a supramolecular gel.[144] Favorable solvation of the nanostructure surface was thought to play a role in promoting stability of the nanofibers in a liquid-like state under shear forces until re-establishment of the entangled gel network could occur.[144] Thermoresponsive polymer segments have been conjugated to the C-termini of self-assembling peptides to influence their gelation properties in response to an increase in temperature.[161] Co-assembly of the polymer-peptide conjugates with unmodified peptide yielded supramolecular hydrogels with enhanced rigidity due to enthalpically favorable intra-fiber interactions between the conjugated poly(N-isopropylacrylamide) polymer and peptide nanofiber although gelating properties were unaffected by increasing temperature.[161] Native chemical ligation has also been used to enhance the mechanical properties of self-assembled peptide hydrogels.[303] The conjugation technique was utilized to form covalent amide bonds between self-assembled β-sheet forming peptides to effect assembly cross-linking.[303]

**Figure 3.1 Structures of PPGs 2-5 and NAP-FF-OH with N-terminal aromatic modification**

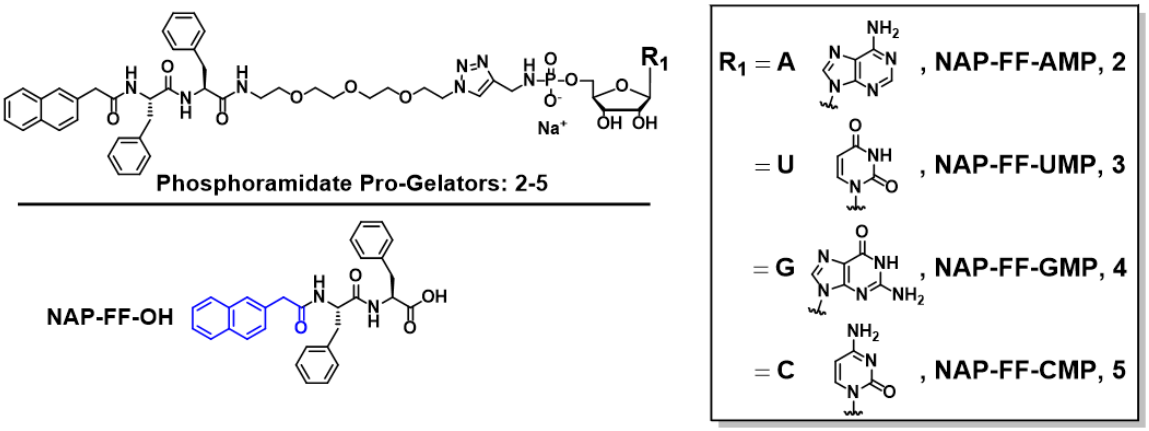

**Figure 3.2 Growth factor immobilization on peptide nanofiber through streptavidin sandwich**

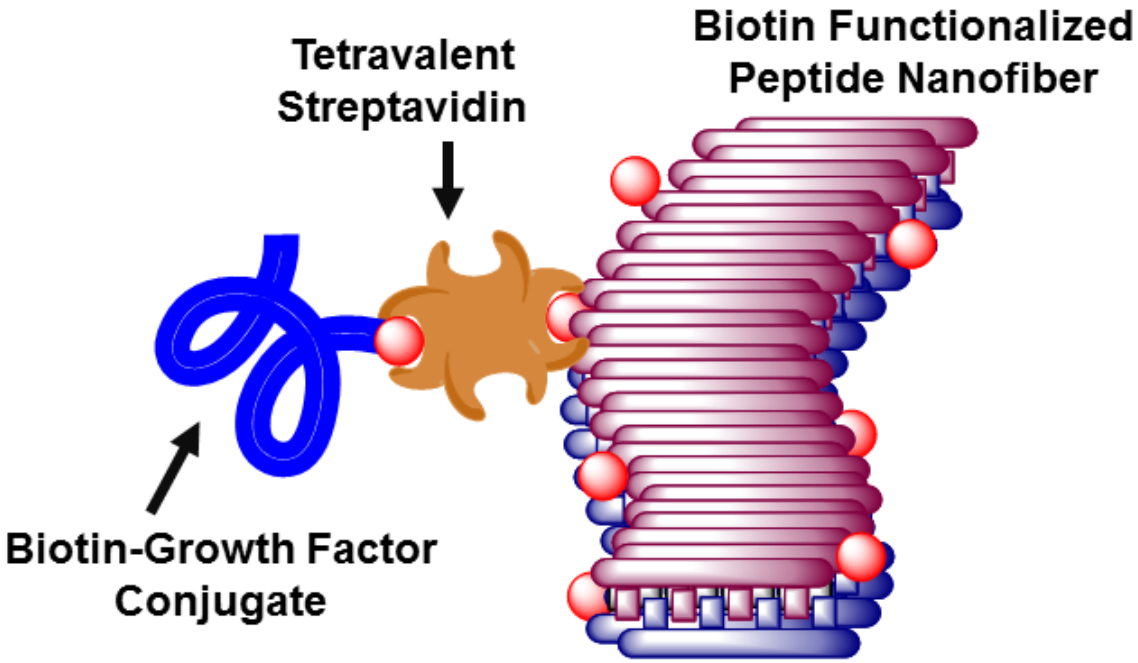

**Figure 3.3 Strategies of self-assembling nucleopeptide design**

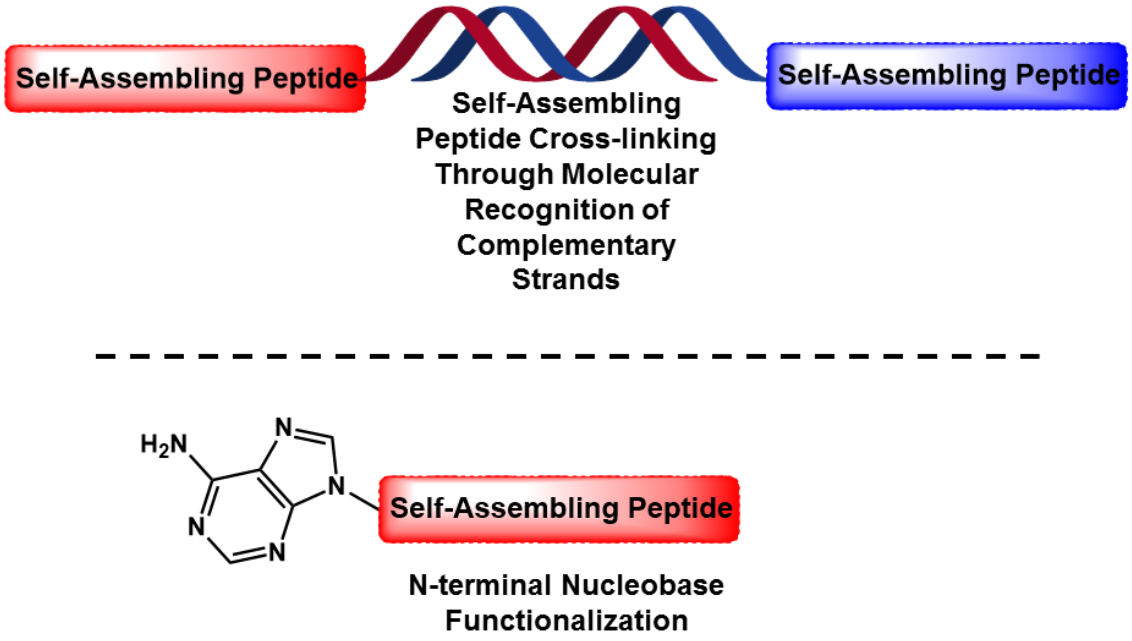

**Figure 3.4 G-tetrad hydrogen bonding pattern**

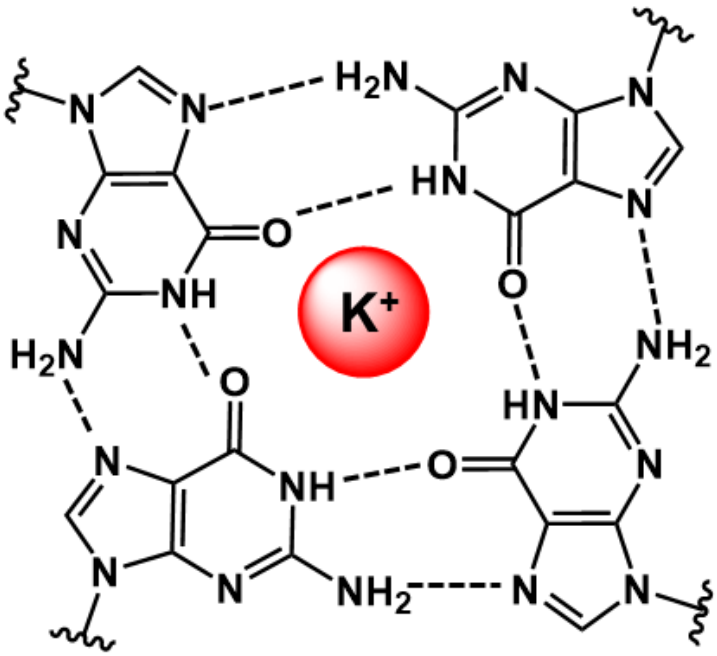

**Figure 3.5 Nucleopeptides formed through click chemistry conjugation of peptide and nucleoside**

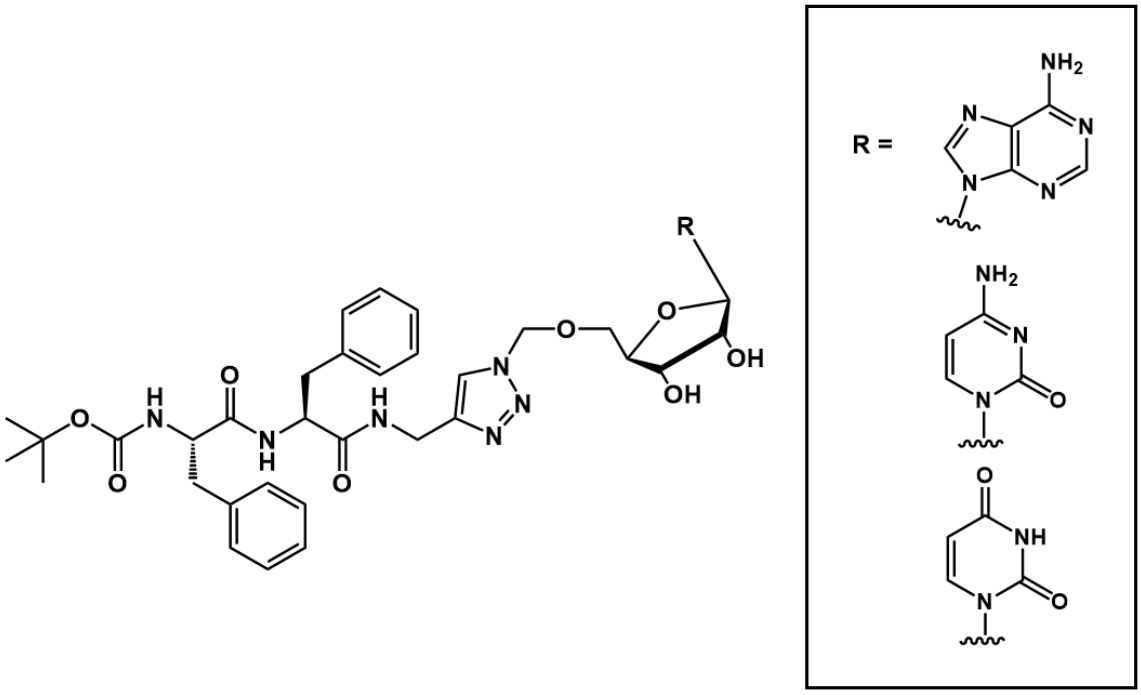

Functional modification of self-assembling peptides has been achieved through conjugation to a wide variety of synthetic and biological molecules to impart characteristics useful in a wide range of applications.[33,49,304,305] One method of functionalization is through chemical conjugation of self-assembling peptides in the synthetic stage prior to material self-assembly, either alone or in co-assembly with unfunctionalized peptide to maintain predictable assembly morphology and mechanical properties.[33,155] Among the first explored modifications was the conjugation of biotin to a RADA class self-assembling peptide for the purpose of growth factor delivery to damaged myocardial tissue. In the design, biotinylated insulin-like growth factor 1was immobilized onto the also biotinylated peptide nanofibers through the multivalent interactions provided by streptavidin (**Figure 3.2**). [33] Fully folded proteins were co-assembled into self-assembling peptides through modification of the protein sequence to include a β-sheet forming motif through recombinant expression. In the system, peptide nanofibers were modified with green fluorescent protein without aggregation and loss of fluorescence in the assembled state.[155] The above examples are obviously not comprehensive of the vast array of modifications reported, but clearly illustrate the breadth of modifications possible.

Post-assembly covalent modification has also been utilized as a method to influence the gelation and functional properties of self-assembling peptides and peptide amphiphiles.[306] A major hindrance to the addition of functional moieties to self-assembling peptides is the tendency for modification to perturb the delicate balance of intermolecular and monomer-solvent interactions that contribute to association, either disrupting assembly or preventing it entirely. Post-assembly modification using click chemistry was

investigated as a way to append small molecules and proteins to self-assembled nanofibers.[306] Similar formats have sought to cross-link self-assembled peptide nanostructures after assembly to enhance their gel rigidity. Peptide amphiphile nanofibers bearing multiple Lys residues in the peptide segment were cross-linked with glutaraldehyde through Schiff base formation, significantly increasing their elastic moduli and resistance to shear. An interesting approach to post-assembly modification was demonstrated where peptide amphiphiles bearing dienes in the aliphatic tail were cross-linked with ultraviolet light. Introduction of covalent cross-linked induced ordering of peptides repulsed by electrostatics from random coil to β-sheet configurations, stabilizing the assemblies and inducing nanofiber strand growth.[167]

Incorporating elements of both application focused functionality and enhancement of assembly properties, nucleo-peptides have proven to be among the most valuable of covalent modifications in self-assembling peptides. The most simplistic nucleo-peptides have incorporated nucleobases as biologically derived aromatic moieties for N-terminal modification of short self-assembling peptides, with reported hydrogen bonding capability to nucleic acids although the molecular orientation and mechanism of this interaction is unclear (**Figure 3.3**).[34,307–309] Conjugation at the C-terminal end of short aromatic peptides has also been demonstrated with possible enhancement of solvent exposure contributing to the ability of modified gel forming peptides to achieve functional interactions with a range of nucleic acids.[53] Similar modifications have also been achieved through incorporation of peptide nucleic acids into surface exposed domains of peptide amphiphiles, enabling sequence selective duplex formation with oligonucleotides exhibiting stabilities rivaling

that of corresponding DNA duplexes (**Figure 3.3**).[154,310] Peptide-nucleic acid modification of a self-assembling peptide was also shown to enable the cross-linking of supramolecular peptide nanofibers through biomolecular recognition achieved through a complementary oligonucleotide sequence. Inclusion of the cross-linking moiety was shown to enhance the rheological properties of gels formed from peptide nucleic acid modified in terms of elastic modulus and frequency response.[311]

Derivatives of nucleosides and nucleotides have long been investigated as self-assembling moieties capable of forming gels in either organic or aqueous solvent.[312] Generally, nucleosides and nucleotides are modified with aliphatic moieties such as alkyl chains to promote their assembly and impart gelating properties to overcome the high degree of solvation imparted by the sugar and phosphate.[312–314] Although monomeric Watson-Crick hydrogen bonding interactions may readily promote assembly in organic media, addition of coordinating moieties may also be necessary to trigger hydrogelation through further non-covalent interactions which has been achieved with metal salts and cationic surfactants.[315,316] The most robust class of nucleoside and nucleotide based hydrogelators are based on guanosine, taking advantage of its unique ability to form tetrads in the presence of alkali cations in aqueous solution (**Figure 3.4**).[317] Simple triacetylation of guanosine hydroxyl groups and addition of a methoxy group at the 8 position of the guanosine ring yielded simple hydrogelator capable of supporting the growth of cells.[318] Additionally, diol modification of the guanosine ribose ring with borate generated robust gelators capable of assembling in the presence potassium salt and high elastic moduli due to cross-links provided by the borate modification.[319] However, a common limitation of

guanosine derived hydrogels is their eventual aggregation and crystallization from solution as formed gels result from metastable assemblies not represented by thermodynamic minima.[312] Additionally, due to the relatively small area of intermolecular interaction between nucleoside units, the rheological properties of formed gels are generally poor which limits potential application.[320] Enhancing the rheological properties and gel stability of these gels generally includes addition of polymers or small molecule stabilizers of G-tetrads.[318,320,321]

Compared to nucleobase incorporation, relatively few investigations have sought to incorporate nucleosides or nucleotide derivatives into self-assembling peptides. Recently, click chemistry was used to click nucleosides to self-assembling peptides (**Figure 3.5**).[322] Interestingly, the modification triggered assembly into spherical nanostructures, capable of encapsulating dyes enabling monitoring of long-term release.[322] Additionally, adenosine monophosphate was conjugated to short aromatic peptides to impart alkaline phosphatase sensitivity to generate a responsive gelation system. The monophosphate was conjugated through the exocyclic amine of the nucleobase, facilitating presentation of the mono-phosphoester for phosphatase hydrolysis.[323]

We previously demonstrated the synthesis and self-assembly of nucleoside phosphoramidate functionalized peptides into monodisperse nanofibers in aqueous solution.[244] Our previous investigations sought to establish the nucleoside phosphoramidate motif as an enzyme responsive moiety for controlling the spatiotemporal gelation properties of self-assembling peptides.[244] However, it has not escaped our

attention that the nucleoside phosphoramidate moiety can potentially play a role in influencing the self-association of functionalized peptides, as well as inter-fiber cross-links leading to phosphoramidate driven gelation. The nucleoside phosphoramidate moiety represents a fascinating peptide modification as it simultaneously imparts elements of hydrophobicity, aromaticity, polar solvating groups, ionic charge, and nucleobase driven hydrogen bonding interactions. Primarily, we have found guanosine phosphoramidate functionalization as a driver of nanostructure association and gelation in solutions of suitable ionic strength. In reporting our preliminary findings here, we hope to provide insight into the potential applications of nucleoside phosphoramidates as modulators of supramolecular assembly which can be applied to self-assembling systems based on peptides and macromolecules.

## 3.2 RESULTS

### Critical aggregation concentrations of phosphoramidates 2-5

A surprising observation in our previous development of hHint1 responsive self-assembling molecules was the spontaneous assembly of nucleoside phosphoramidate functionalized self-assembling peptides into highly ordered and monodisperse nanofibers. Despite the high polarity imparted by the functionalization through the hydrophilic diol of the ribose sugar and negative charge provided by the phosphoramidate moiety, monomer solvation was disfavored under the investigated experimental conditions, instead favoring the nanostructure assembly.

**Figure 3.6 Critical aggregation concentration (CAC) determination of self-assembling phosphoramidates 2-5 determined with nile red fluorescence and sedimentation by ultracentrifugation**

(a) representative nile red assay readout for critical aggregation determination of NAP-FF-AMP **2** (b) calculated CAC for compounds **2-5** determined from nile red assay and sedimentation for **2** and **3**. Values represent mean and ± standard deviation for at least three separate experiments.

a

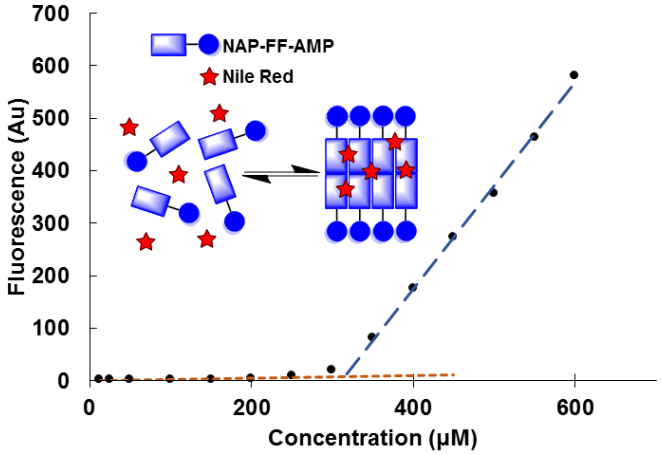


b

| Compound | Nile Red CAC (μM) | Sedimentation CAC (μM) |
|---|---|---|
| NAP-FF-AMP | 319 ± 3 | 267.6 ± 1.8 |
| NAP-FF-UMP | 419 ± 6 | 451 ± 42 |
| NAP-FF-CMP | 411 ±7 | NA |
| NAP-FF-GMP | 328 ± 24 | NA |

To further understand the assembly properties of the nucleoside phosphoramidate functionalized peptides **2-5**, investigation of the critical aggregation concentration (CAC) for each molecule was performed using a Nile red fluorescence assay (**Figure 3.6**). Nile red is a solvatochromic dye with well characterized fluorescence in hydrophobic environments leading to its widespread use as a phospholipid membrane imaging dye as aqueous quenching of fluorescence is relieved in lipid environments.[324] In addition to functioning as a imaging probe for membranes, Nile red has widely been used as a staining agent for detecting amyloids and characterizing self-assembled nanostructures.[167,325] The assay was performed with each phosphoramidate **2-5** by incubating varying concentrations of monomer with an identical 50 μM Nile red across all samples. Upon mixing, each sample was heat denatured and reannealed at room temperature overnight in the dark to ensure proper measurement of the assembly equilibrium. The critical aggregation concentration represents an equilibrium threshold below which monomers predominate, and above which self-assembled nanostructures are present. Therefore, in the Nile red assay, at concentrations below the CAC, only baseline fluorescence will be observed due to quenching of fluorophore in aqueous solvent. However, as the concentration of phosphoramidate exceeds the critical aggregation concentration, Nile red can become immobilized within the nanostructures thus relieving quenching by solvent and enabling fluorescence readout. Interestingly, the two purine bearing conjugates NAP-FF-AMP **2** and NAP-FF-GMP **4** exhibited CACs of 319 μM and 328 μM respectively (**Figure 3.6**). In contrast, the pyrimidine modified phosphoramidates NAP-FF-UMP **3** and NAP-FF-CMP

**5** exhibited greater CAC values compared to the purines of 419 μM and 411 μM respectively (**Figure 3.6**).

Because critical aggregation concentration determination using Nile red is a secondary measurement of self-assembly, we sought to corroborate these values using sedimentation experiments. Sedimentation through ultracentrifugation is a useful technique for investigating the monomer and assembly equilibria of amphiphiles and self-assembling molecules.[75] High-speed centrifugation of phosphoramidate solutions enabled separation of self-assembled nanostructures and oligomeric species which collapsed onto the bottom of centrifuge vessels generating a clear pellet, with free monomer remaining in solution measured with HPLC. CAC values using the technique were found to closely approximate those determined from the nile red assay with respective values for NAP-FF-AMP and NAP-FF-UMP of 267 μM and 451 μM indicating the same trend between purine and pyrimidine modified peptides (**Figure 3.6b**).

**Spontaneous gelation of phosphoramidate conjugates 2-5 investigated with SAOR**

Previously, we found that phosphoramidates **2-5** formed viscous solutions at 0.9 % wt/vol in 20 mM HEPES and 1 mM $MgCl_2$ through visual inspection aided by the inversion test. In this test, liquid like material behavior is exhibited through flow and the lack of a self-supporting structure, and gel character is indicated by the converse in both aspects. A limitation of the technique is the difficulty in distinguishing weak gels from viscous solutions as the yield stress of weak gels can be so low as to induce flow upon simple inversion in small vessels.

**Figure 3.7 SAOR investigation of gel forming phosphoramidate NAP-FF-GMP 4**

(a) strain response of elastic (G') and loss (G'') moduli indicating linear region from 0.10% to approximately 10% where hydrogel mechanical properties are independent of applied stress and resulting strain (b) angular frequency of applied stress response of elastic (G') and loss (G'') moduli across a wide range of frequencies indicating broad linear response region (c) Cyclic strain experiments indicating shear thinning properties. Shaded regions represent the application of high strain to induce gel reversion to liquid like state indicated by higher loss (G'') moduli than elastic (G') moduli. All figures represent single experiments representative of data collected in at least three separate experiments.

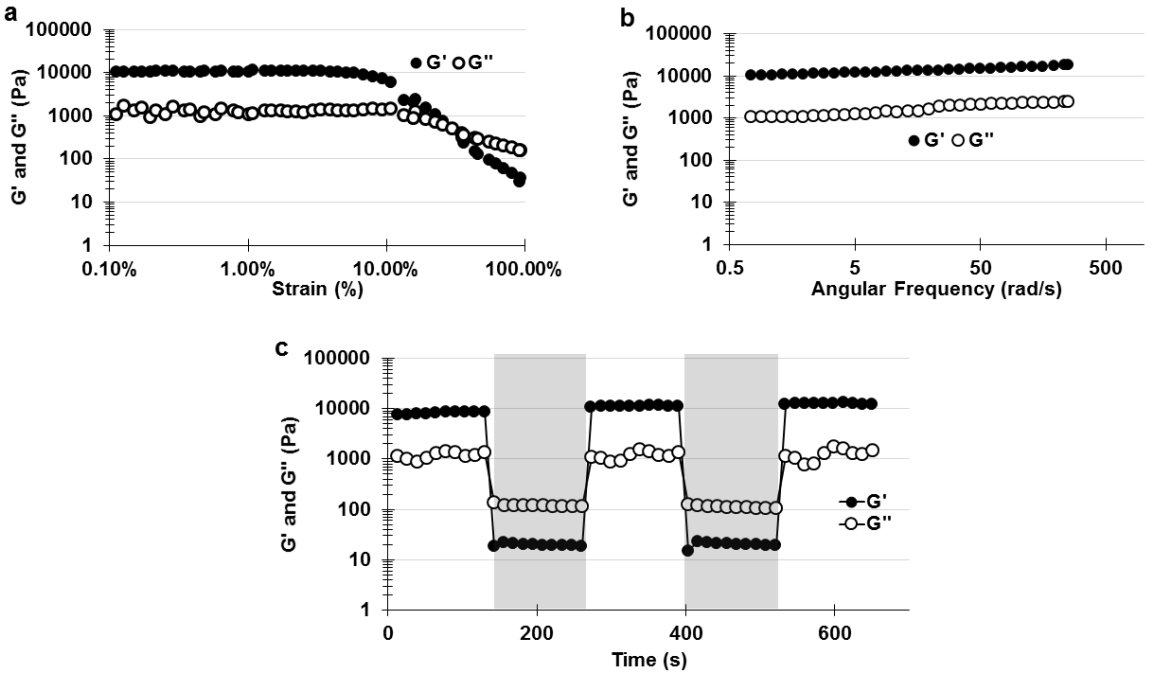

**Figure 3.8 SAOR characterization of NAP-FF-GMP 4 gelation in the presence of varying ionic strength**

(a) strain sweeps and (b) frequency sweeps of 2.5 % wt/vol **4** in 10 mM Sodium phosphate with 75 mM NaCl (black circles, G' filled and G'' open) and 55 mM NaCl (blue squares, G' filled and G'' open) (c) time sweep of 2.5 % wt/vol **4** in 10 mM Sodium phosphate with 35 mM NaCl. The very low moduli measured for these samples indicate no gel character. All figures represent single experiments representative of data collected in al least three separate experiments.

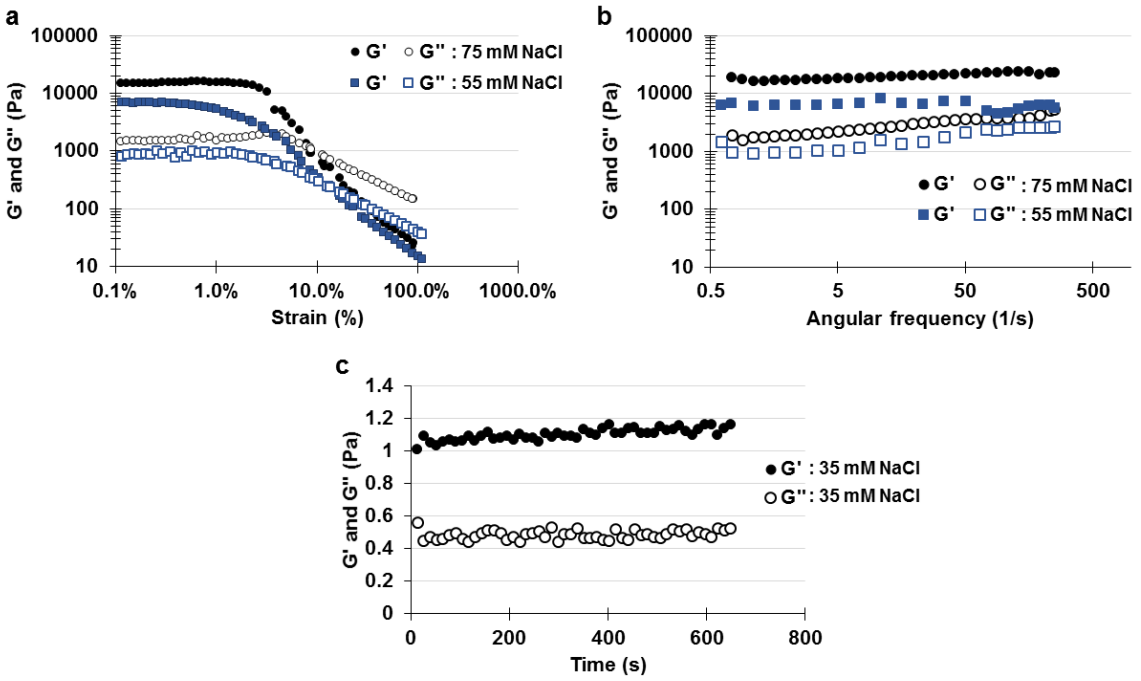

Solutions of phosphoramidates **2-5** prepared in DPBS were investigated using small amplitude oscillatory rheometry (SAOR) to determine possible weak forming gel properties due to higher concentration and increased ionic strength. Despite these changes, NAP-FF-AMP **2**, NAP-FF-UMP **3**, and NAP-FF-CMP **5** demonstrated only weak gel character, at 2.5 % wt/vol with measured elastic moduli on the order of 10 Pa which borders on the detection limit of the instrument. The weak mechanical properties of phosphoramidate nanofibers formed from **2**, **3**, and **5** was evident upon sample application to the rheometer geometries as deposited material rapidly collapsed into spreading solutions.

In contrast, NAP-FF-GMP **4** formed robust hydrogels at a concentration of 2.5 % wt/vol in DPBS signified by significantly higher elastic moduli (G') than loss moduli (G'') in the linear viscoelastic region, where changes in magnitude and frequency of applied stress do not affect material rigidity (**Figure 3.7a,b**). The hydrogels possessed elastic moduli on the order of 10 kPa (9.4 ± 4.6 kPa) with a gel-sol transition at 30% strain (**Figure 3.7a**). More interestingly, cyclic strain experiments revealed the shear thinning properties of the gels. Significant decreases in moduli and liquid like character were observed at strains greater than the yield strain, which rapidly reversed upon return of strains within the viscoelastic region (**Figure 3.7c**). Cycling between high and low strain could be repeated several times without loss of peak moduli over time further indicating the stability of the hydrogels and recovery properties (**Figure 3.7c**).

**Salt concentration dependent gelation of NAP-FF-GMP 4 determined with SAOR and effect of phosphoramidate mixing**

As NAP-FF-GMP **4** is expected to be negatively charged in aqueous solution at physiologic pH, the gel forming character of the molecule was investigated in buffers of varying ionic strength to investigate a dependence of gelation on ionic screening, a factor possibly contributing to only weak gel formation in previously characterized samples. Ionic screening above a critical salt concentration is generally required to achieve self-assembly and gelation of charged peptides and peptide amphiphiles, and it was expected that similar character would be exhibited in this system.[72,117] Three different solutions buffered with 10 mM sodium phosphate and possessing sodium chloride concentrations of 75 mM, 55 mM, or 35 mM were used to prepare samples of **4** at concentrations of 2.5 % wt/vol. In the high salt sample elastic moduli were comparable to the hydrogel prepared in DPBS with an average elastic modulus of approximately 15 kPa (14.9 ± 2.0 kPa) over the linear viscoelastic region (**Figure 3.8a,b**). In comparison, hydrogels of **4** prepared in buffer with 55 mM NaCl exhibited significantly reduced moduli, with plateau moduli over the linear viscoelastic region approximately 6.5 kPa (6.5 ± 1.9 kPa) (**Figure 3.8a,b**). However, both gels possessed wide linear ranges in response to both increasing strain and frequency. In comparison, **4** prepared in buffer containing 35 mM NaCl possessed exceedingly weak gel like character with moduli never exceeding 10 Pa indicating a clear dependence on ionic strength for gel forming character (**Figure 3.8c**).

**Stability of NAP-FF-GMP 4 hydrogels and monomer release kinetics**

The observation of NAP-FF-GMP **4** gel formation spurred further investigation into characterizing the stability of the gels over time. Monomer erosion was assessed for 2.5 % wt/vol gels formed in DPBS where an additional supernatant layer was added to the top of cured gels after 24 h. Aliquots of supernatant were removed from samples at time points over several days. The gels exhibited remarkable stability over this time period with less than 10% of total monomers lost from the gel over 10 days (**Figure 3.4**).

Determination of supernatant monomer content over time also enabled the determination of kinetic rate constants for the release of monomers from formed hydrogels and corresponding half-life release profiles. A study investigating the pharmacological release profile of somatostatin-14 monomers from self-assembled nanostructures produced an empirical hybrid first order and zero order release equation to describe the system's erosion phenomenon.[326] Minimization through least squares non-linear regression revealed that the zeroth order rate constant was not necessary in the fitting of the release experimental data for NAP-FF-GMP **4** and that a modified version of the first order rate equation,

$$C_R = CAC \times (1 - e^{-k_1 t})$$

where $C_R$ is the percentage release of monomer from the total sample, CAC is the equilibrium percentage of released monomer expected based on the critical aggregation concentration, $k_1$ is the first order rate constant, and t is time closely fit experimental data. Additionally, model fitting of the data produced a predicted first order rate constant of 2.65 ± 0.10 x $10^{-4}$ $min^{-1}$ corresponding to equilibrium half-life of 2.62 ± 10 x $10^3$ min or 43 h

(**Figure 3.9**). Monomer release experiments were not performed with non-gelling phosphoramidates **2**, **3**, or **5** due to difficulty of maintaining nanofiber separation from added supernatant solutions without high speed centrifugation, which was expected to affect monomer release kinetics through the dense nature of formed pellets.

**Characterization of assembly formation with NMR**

Monomer erosion experiments provided key evidence of the strength of intermolecular interactions leading to both monomer assembly and inter-fiber cross-links in the NAP-FF-GMP **4** phosphoramidate gels. Additionally, although both purines have similar CACs, the aforementioned techniques provide little insight into the differences the two nucleosides play in the early stages of assembly. $^{1}$H NMR experiments were performed to further characterize monomer association to generate supramolecular assemblies. Using MeCN as an internal standard, the concentrations of NMR visible NAP-FF-GMP **4** and NAP-FF-AMP **2** was determined with molecules dissolved in either $D_2O$ or $D_2O$ with 10 mM sodium phosphate and 50 mM NaCl (**Figure 3.10a,b**). As expected, samples in $D_2O$ with no salt generated linear responses of observed signal to increasing concentrations indicating that NMR silent aggregates were not forming and only soluble aggregates and monomer were likely observed. In contrast, NAP-FF-GMP **4** prepared in $D_2O$ with 10 mM sodium phosphate and 50 mM NaCl demonstrated a striking lack of monomer signal. At 0.0625 % wt/vol, the observed signal of the aromatic region of **4** significantly deviated from linearity resulting in no significant increase in the observed signal compared to 0.03125 % wt/vol. Furthermore, no significant increase in the observed signal was found

by further increasing the sample concentration from 0.125 % wt/vol to 0.25 % wt/vol. Since 0.0625 % wt/vol corresponds to approximately 567 μM, slightly higher than the anticipated CAC, we observed that **4** quickly transitions from monomer to NMR invisible aggregate structures. Indeed, gel-like character was observed in the two highest concentrations at 0.125 % wt/vol and 0.25 % wt/vol. Similar trends were observed with samples of NAP-FF-AMP in $D_2O$ or $D_2O$ with phosphate buffered saline (**Figure 3.10b**). Linear increases with concentration were observed in the $D_2O$ only sample with flattening of the concentration response above 0.0625 % wt/vol. The results show a clear dependence of assembly for both purine phosphoramidates on the ionic strength of solution but fail to point to a mechanism indicative of NAP-FF-GMP's gelating properties in comparison to NAP-FF-AMP. Although both phosphoramidates lost significant concentration response to relative integration above the expected CAC, the nature of the formed assemblies could be of a different nature, differing in size and intermolecular associations between assemblies.

**Small angle x-ray scattering**

Previous cryo-TEM studies confirmed the self-assembly of phosphoramidates **2-5** into highly monodisperse nanofibers, approximately 7-8 nm in width and with lengths on the order of microns.[244] However, TEM spectroscopic studies limit sample visualization to localized regions suitable for image generation. Small angle x-ray scattering experiments were performed to gain information about sample wide nanostructure morphology.[327] In contrast to x-ray crystal analysis where crystallized samples produce distinct diffraction

patterns which give precise information about atomic structure, x-ray scattering analysis of solution phase samples produces radially smeared scattering patterns, which are azimuthally averaged to produce 1D scattering profiles.[328] We sought to initially investigate the phosphoramidates at concentrated levels in $H_2O$ (**Figure 3.11**). Surprisingly, strong diffraction peaks were observed at q-values 2.7 x $10^{-2}$ to 3.7 x $10^{-2}$ $A^{-1}$ in 5 % wt/vol samples of NAP-FF-GMP **4** and NAP-FF-AMP **2**. Conversion of the q-values to characteristic distances revealed the sharp peaks corresponded to distances between 17 nm and 22 nm. In scattering experiments, the presence of sharp peaks generally corresponds to high levels of sample wide uniformity in nanostructures mimicking crystalline features. As the measured diameter of nanofibers is approximately 7-8 nm as observed from cryo-TEM studies, and the length of nanofibers is on the order of microns, the characteristic scattering peak was attributed to long range ordering of the nanofibers. Such long-range ordering has been observed in other self-assembling peptide systems where charge repulsion due to ionized residues limits the packing of nanofibers at high concentrations, leading to a characteristic inter-nanofiber distances represented by sharp scattering peaks resulting from hexagonal packing.[329] Interestingly, the characteristic peak from NAP-FF-GMP **4** was less sharp than the other phosphoramidates indicating less degree of sample wide homogeneity in terms of nanofiber packing, possibly due to nanofiber cross-links and associations.[330,331] Additionally, the scattering peak was deemed to be concentration dependent as samples examined at lower concentrations failed to reproduce the sharp peak, but retained features in the low-q region indicative of inter-particle repulsion.

**Figure 3.9. Monomer erosion from NAP-FF-GMP 4 gels.**

Vertical axis corresponds to the percent release of monomer over time from the total original amount. The blue curve corresponds to a first order release equation fit to the data through non-linear least squares regression which enabled determination of observed half-life of release. Calculated values correspond to mean and standard deviation of three separate experiments.

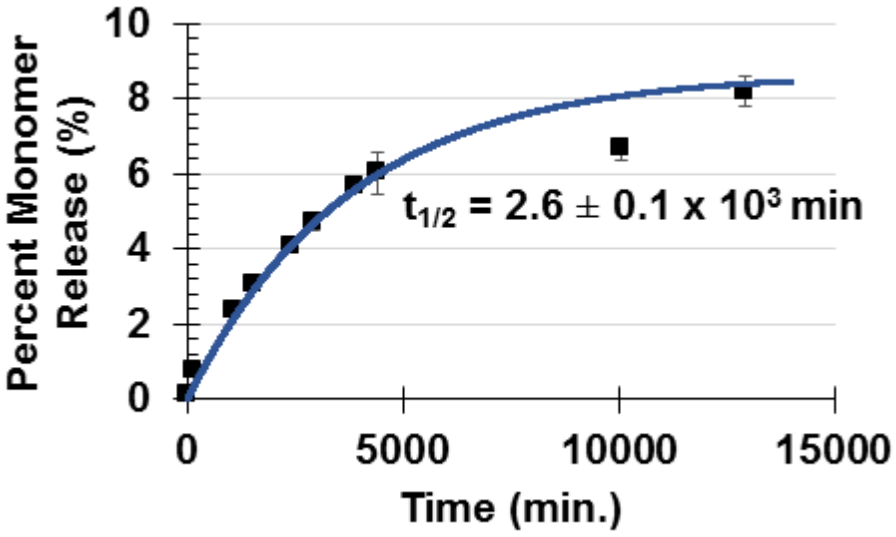

**Figure 3.10. $^{1}$H NMR studies with signal intensity studied as a concentration of phosphoramidate NAP-FF-AMP 2 or NAP-FF-GMP 4**

(a) $^{1}$H NMR spectrum of NAP-FF-GMP **4** at the indicated % wt/vol concentrations in $D_2O$ (left) and $D_2O$ with 10 mM sodium phosphate and 50 mM NaCl (right). Blue (left) and black (right) boxes represent the aromatic region consisting the phenyl side-chains and naphthyl ring. Spectrum are not on the same vertical scale due to increased scaling on the right as only weak signals were produced in the gel forming samples. (b) Relationships of aromatic region signal integration to increases in concentration. Linear relationships are evident in samples without added salt, but clear loss of linearity is evident in samples of phosphate buffered saline.

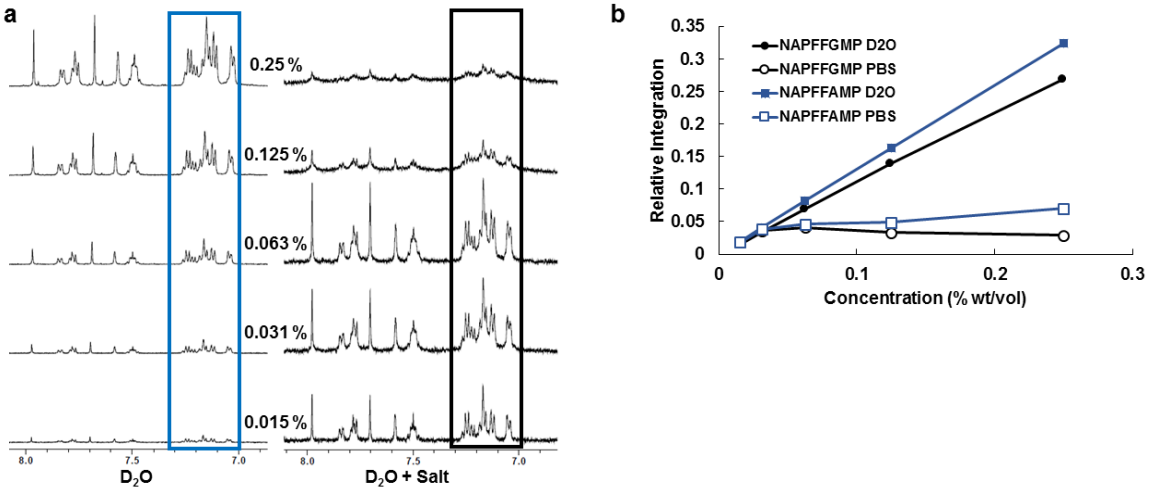

**Figure 3.11. SAXS scattering profiles of NAP-FF-AMP and NAP-FF-GMP**

NAP-FF-AMP 2 (blue) and NAP-FF-GMP 4 (black) in $H_2O$ at concentrations of 5 % wt/vol. Sharp peaks are evident at corresponding d-spacings between 17-22 nm. Sharp peaks are indicative of sample wide nanofiber alignment into hexagonal close packing arrangement due to charge repulsion of the anionic fibers.

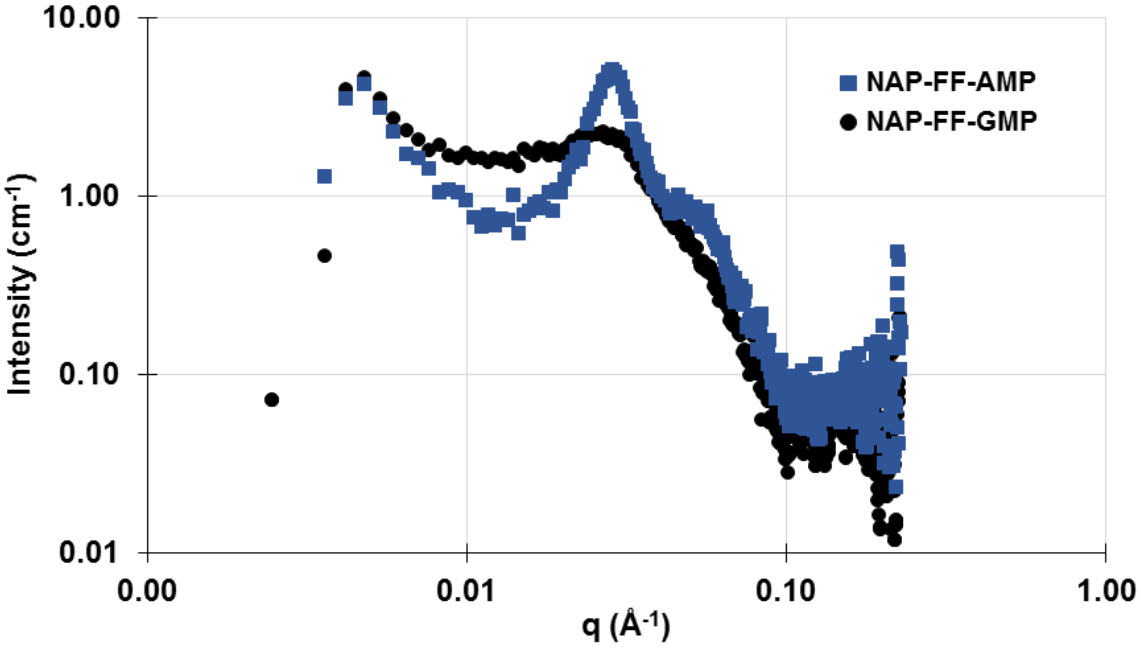

**Figure 3.12. SAXS scattering profile of 2.5 % wt/vol NAP-FF-GMP in DPBS**

Experimental data (blue) in DPBS buffer and theoretical model fitting of the data (red). Experimental curve represents background, intensity beam, and transmission corrected data. The model curve corresponds to the built-in cylindrical form factor in the fitting software SASVIEW. Best fits were achieved with cylindrical radii approximately 3.5 nm. Inset shows the slope of the low q-region corresponding to -1, indicative of cylindrical structure.

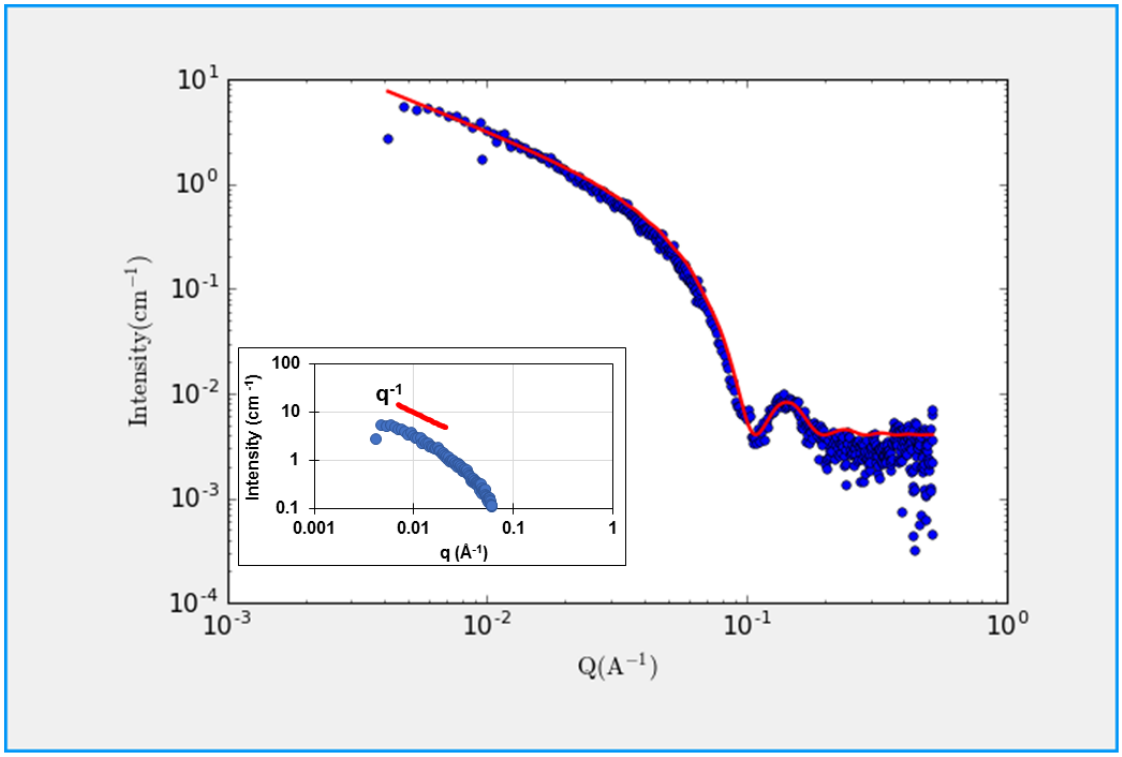

Due to the high degree of nanofiber alignment, fitting of the data to form factor models was deemed infeasible with samples in $H_2O$. As solution ionic strength can limit charge repulsion in self-assembly, scattering experiments were performed with NAP-FF-GMP **4** as a 2.5 % wt/vol solution in DPBS. The 1D scattering profile was modeled to theoretic form factors in SASVIEW software using the built-in cylinder form factor model, which closely approximated the experimental data with cylinders bearing radii approximately 3.5 nm (**Figure 3.12)**. Additionally, the slope of the data in the low q region is close to -1 indicative of cylindrical structure.[327–329,331] The model also predicted exceedingly long nanofibers, longer indeed than the resolution range of the SAXS detector (≈ 100 nm), further confirming the assembly of phosphoramidate-conjugates into very long cylindrical nanofibers.

**Isothermal titration calorimetry**

To gain further insight into the thermodynamic parameters defining assembly of phosphoramidates **2** and **3**, isothermal titration calorimetry (ITC) was performed to determine the enthalpic and entropic contributions to the free energy of assembly. ITC is an indispensable technique for investigating molecular recognition events contributing to intermolecular association, and has been widely applied in the investigation of amphiphile assembly.[332] In preliminary studies, NAP-FF-AMP was investigated by titrating concentrated phosphoramidate into empty buffer, enabling visualization of the heat of disassembly. Fitting of the enthalpies as a function of concentration using a general sigmoidal dose response model enabled determination of the CAC of 420 ± 8 μM

represented by the midpoint of the sigmoidal curve. It was anticipated that an increase in the CAC would be observable during the titration experiments at 30°C. Enthalpies of dissociation were determined from linear curves representing the top portion of the sigmoidal and calculating the respective enthalpy at the concentration corresponding to the CAC. The enthalpy of dissociation was determined to be 22.0 ± 0.4 kJ/mol with the corresponding enthalpy of association being the negative of the same value. As the CAC represents a thermodynamic equilibrium between monomers and assemblies, the thermodynamic relationship (**Equation 1**)

**Equation 1:** $\Delta G_a = RT \times \ln(CAC')$

in which the Gibb's free energy of association is proportional to the natural logarithm of the mole fraction of CAC' in buffer solution.[332,333] Determination of the Gibb's free energy of association enabled the corresponding calculation of the entropy of association, thus providing a TΔS of 8.4 ± 0.4 kJ/mol. Clearly both the favorable enthalpic and entropic forces of NAP-FF-AMP **2** contribute to its high propensity for self-association, although the enthalpic contribution to assembly is dominate (**Figure 3.13**).

**Investigation of co-gel rheological properties**

Because of the propensity for nucleobase modified materials to undergo Watson-Crick hydrogen bonding interactions, we investigated the gel forming properties of NAP-FF-GMP **4** and NAP-FF-CMP **5** co-gels (**Figure 3.9**). Surprisingly, mixing of NAP-FF-CMP with NAP-FF-GMP had a detrimental effect on gel rigidity indicating a decrease of inter-fiber cross-linking interactions contributing to stable gel formation evidenced by the

decreased values of G' and G''(**Figure 3.14a**). Samples that contained 2.25 % wt/vol **4** and 0.25 % wt/vol possessed elastic and loss moduli approaching that of pure gel forming NAP-FF-GMP and exhibited shear recovery in cyclic strain experiments indicating potential injectability (**Figure 3.14b**). However, a sample containing 1.67 % wt/vol **4** and 0.83 % wt/vol NAP-FF-CMP exhibited significantly reduced moduli than **4** alone with G' lower than 1 kPa (**Figure 3.14a**). Above the ration of the NAP-FF-CMP **5**: NAP-FF-GMP **4** ratio was not pursued as a loss of gel formation was observed indicating the significance of the G-base in driving gelation.

As the phosphoramidates are anionic, we also sought to form gels through addition of cationic polymers and divalent metal cations. A polyethylene imine (PEI) solution (50% in $H_2O$, $M_w$ 600,000-1,000,000) was diluted in DPBS to generate a ≈ 5 % wt/vol solution which was added at different ratios to the non-gel forming NAP-FF-CMP **5** to generate samples with final concentrations of 2 % wt/vol **5** and 1 % wt/vol PEI or 1.67 % wt/vol **5** and 1.67 % wt/vol PEI (**Figure 3.14c**). Although the phosphoramidate alone failed to form a gel, addition of PEI was found to trigger gel formation in both samples. Interestingly, the 2:1 **5** to PEI concentration sample formed the more robust hydrogel with an elastic modulus (G') greater than 1 kPa, while the 1:1 concentration sample of **5** to PEI exhibited markedly reduced rigidity with an elastic modulus approximately 250 Pa. Additionally, the gels exhibited shear thinning propensity and were able to recover their plateau moduli after application of high strain (**Figure 3.14d**).

**Figure 3.13. NAP-FF-AMP ITC Results.**

Data represents enthalpy of dissociation as a function of concentration for NAP-FF-AMP **2** background subtracted to account for thermal events associated with instrumental setup. Data was fit to built-in sigmoidal three parameter dose response model in GraphPad Prism to obtain the midpoint of the curve corresponding to the CAC to produce ΔG of association. Enthalpies were determined by generating linear curves approximating the top of the sigmoidal and calculating the magnitude at the CAC.

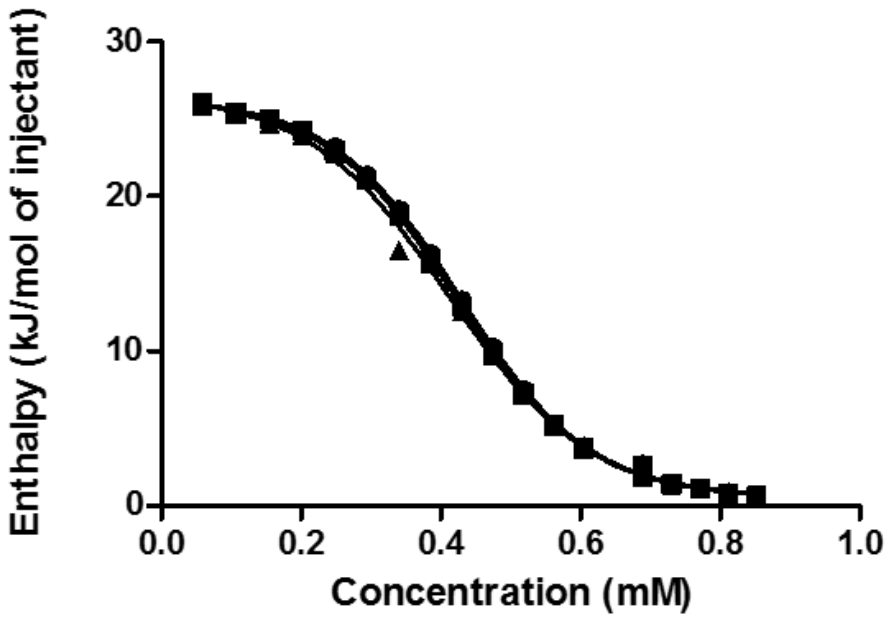


| Temperature (°C) | ΔH (kJ/mol) | ΔG (kJ/mol) | TΔS (kJ/K) | CAC (uM) |
|---|---|---|---|---|
| 30 | -22.0 ± 0.4 | -30.41 ± 0.49 | 8.4 ± 0.4 | 420 ± 8 |

**Figure 3.14. SAOR of co-gel formulations**

(a,b) Strain sweep and cyclic strain of NAP-FF-GMP and NAP-FF-CMP at ratios of 9:1 and 2:1 for total % wt/vol concentrations of 2.5 % for both materials. (c,d) Strain sweep and cyclic strain of NAP-FF-CMP and PEI co-gels at 2:1 and 1:1 ratios at total % wt/vol concentrations of 2.5 % for both materials

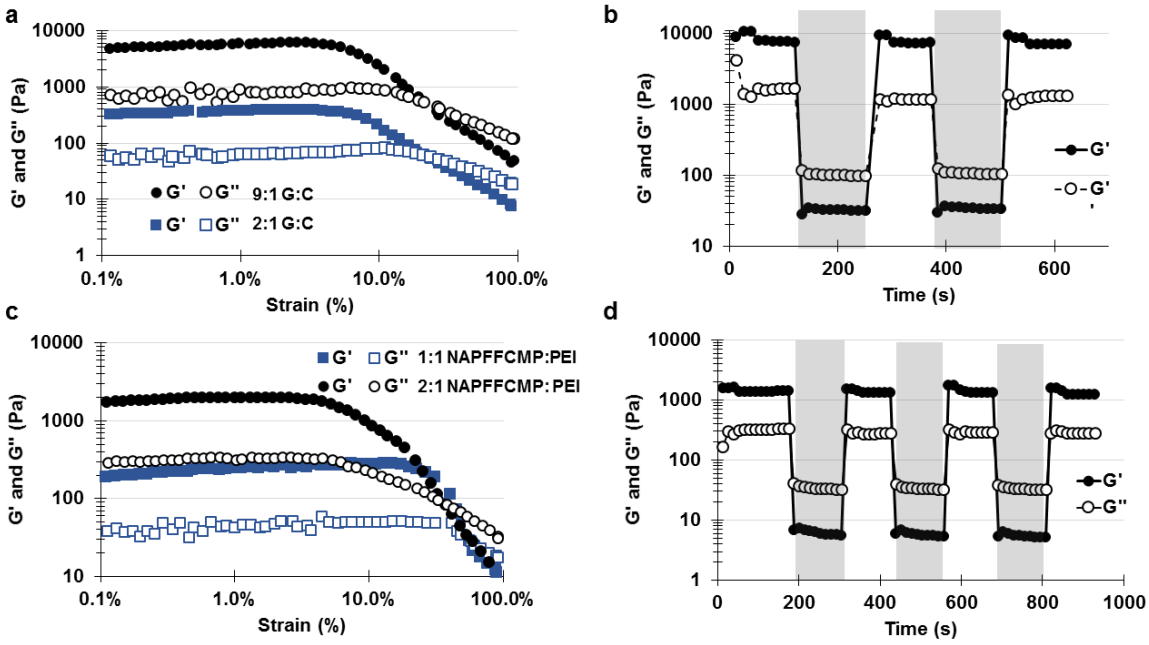

## 3.3 DISCUSSION

The primary aim of this study was to gain fundamental understanding of the nucleoside phosphoramidate moiety relating to its ability to be used as a chemical modification for the regulation of peptide self-assembly. Our surprising observations that nucleoside phosphoramidate modified peptides **2-5** spontaneously assemble into highly monodisperse nanofibers immediately spurred curiosity as to whether macroscale assembly could be achieved with the nanofibers under untested conditions.[244] Despite their assembly into micron sized nanofibers, phosphoramidate conjugates **2**, **3**, and **5** failed to form self-supporting gels indicating that despite their significant size, little entanglement or cross-linking of the nanofibers was achieved. As the phosphoramidate moiety is negatively charged, we hypothesized that increasing the ionic strength of the solution would reduce charge repulsion between nanofibers and promote nanofiber entanglements and possible gel formation. However, despite dissolution into high ionic strength buffers such as DPBS, these molecules failed to form self-supporting hydrogels.

In contrast, the phosphoramidate conjugate **4** modified with guanosine monophosphoramidate, readily formed self-supporting hydrogels with robust moduli under the same conditions. Additionally, hydrogels of **4** exhibited shear thinning properties and complete moduli recovery after application of high strain indicating the intermolecular and inter-assembly interactions contributing to gel formation could be readily broken and reformed in response to the application of stress. The gels also exhibited large linear viscoelastic regions to both changes in the magnitude and frequency of applied stress indicating the stability of gel inducing non-covalent interactions. The ability of **4** to form

hydrogels was found to be context dependent, as a decrease in the solution ionic strength below a critical threshold resulted in an inability to form gels.

Based on these results, we hypothesized that two primary factors regulate the supramolecular self-assembly of the nucleoside phoshporamidates. The anionic character imparted by the phosphoramidate moiety, which results in high negative surface charge density along the nanofibers, prevents cross-linking and entanglement resulting in a lack of gel formation in phosphoramidate conjugates **2**, **3**, and **5**. Although NAP-FF-GMP **4** is also negatively charged, its ability to utilize the privileged self-associating properties of the guanine nucleobase are likely responsible for its gel formation capability.[312,318–321] Self-assembling molecules based upon guanine, guanosine, and guanosine monophosphate represent one of the most widely studied classes of self-assembling molecules.[312] The primary driver of self-association in this class is the propensity for guanine bases to undergo Hoogsteen hydrogen bonding to form G-tetrads or quadruplexes.[312,318,320] Such interactions are typically used to order small molecule nucleoside and nucleotide derivatives into fibrillar high aspect ratio structures.[312,319–321] However, in the context of the self-assembling phosphoramidate system, the aromatic peptide NAP-FF is the primary driver of monomer assembly into high aspect ratio nanofibers.[281] As all four phosphoramidate modified conjugates were previously observed to form fibers of equivalent morphology, we posit that the guanosine phosphoramidate moiety drives inter-fiber interactions through G-quadruplex formation instead of driving monomer association. Consequently, the presence of guanine base in the phosphoramidate moiety is able to overcome the negative charge repulsion and nanofiber surface solvation and drive

association and nanofiber cross-linking in solutions of sufficient ionic screening.[329,334] Evidence for this hypothesis was provided by experiments combining the non-gelling C-base modified **5** with **4** and investigating gel formation with SAOR. Although complementary Watson-Crick interactions were expected to enhance the rheological properties of co-gel mixtures, a concentration dependent decrease in the moduli of co-gels compared to NAP-FF-GMP alone was observed. It is possible that complementary base-pairing between C and G bases is not favored in the system over solvation of the nanofiber surface and formation of G-tetrads. Although C and G base pairs possess three hydrogen bonds in the interaction, a Hoogsteen base-paired G-tetrad would possess eight interactions, and provide a planar aromatic surface to promote further tetrad formation, as well as providing a coordinating environment for alkali metal cations.[317,335]

To improve the rheological properties of non-gelling phosphoramidate conjugates various methods were investigated including addition of divalent cations and cationic polymers to aid in ionic cross-linking of the anionic nanofibers. Poly-L-Lys (PLL) was added to nanofiber solutions but resulted in non-thermoreversible aggregates rather than gel formation. However, addition of high molecular weight and branched PEI to nanofiber solutions resulted in thermoreversible gel formation when mixed with NAP-FF-CMP at 2:1 and 1:1 % wt/vol ratios. Interestingly, the 2:1 phosphoramidate to PEI gel exhibited higher moduli than the 1:1 sample indicating an optimal stoichiometry might exist between the cationic polymer and phosphoramidate nanofibers. Additionally, the 5% aqueous solution of PEI used to form samples possessed no gel forming character and exhibited similar viscosity to buffer alone indicating no structure was formed by the polymer alone.

The gels also exhibited shear thinning capability indicating the crosslinks were readily broken and reformed in response to applied shear. Although the mechanism of this interaction is unknown, it is expected that the high molecular weight and branched nature of the polymer prevents high degrees of nanofiber ordering, instead promoting specific nucleation sites where nanofibers become cross-linked at specific locations. Further investigation into mixing of non-gel forming phosphoramidate conjugates with polymer and rheological additives could generate hybrid materials with interesting functional properties for various biomedical applications.

The effect of the nucleoside phosphoramidate moiety on the propensity of functionalized NAP-FF monomers to associate was investigated by CAC determination and NMR experiments. CAC were determined by Nile red fluorescence assay, which measures oligomer formation through the increased fluorescence of the immobilized solvatochromic dye within growing nanostructures.[324] The two purine functionalized molecules NAP-FF-AMP **2** and NAP-FF-GMP **4** possess CACs nearly 100 μM lower than the pyrimidine functionalized molecules NAP-FF-UMP **3** and NAP-FF-CMP **5**, although when compared, little difference was observed among the purines and pyrimidine functionalized molecule. As hydrophobic collapse is a likely a primary driver of self-association in molecules **2**-**5**, the larger nucleobase ring system present in the purine conjugates could potentially increase the hydrophobic character of molecules **2** and **4** leading to their association at lower concentrations. Sedimentation experiments were performed to exclude differential affinity by the aggregates for the Nile red dye as an explanation for the discrepancy observed between purines (NAP-FF-AMP **2**) and

pyrimidines (NAP-FF-UMP **4**). Indeed, the phosphoramidates exhibited similar respective CAC values as those obtained using the Nile red fluorescence assay for NAP-FF-AMP **2** and NAP-FF-UMP **3**. Furthermore, the similarity in CACs between purine conjugates **2** and **4** indicate that the gel forming propensity of **4** is not reflected in the initial association of monomers, but rather is an event independent of initial association and likely resulting from post-assembly association of the nanofibers. Similarly, $^{1}$H NMR investigation of NAP-FF-AMP **2** and NAP-FF-GMP **4** revealed little differences in the association of the respective monomers in response to increasing concentration or ionic strength. Samples of **2** and **4** prepared in $D_2O$ exhibited strong linear responses in the signal intensity of the aromatic region of the molecules' peptide portion to increasing concentration, indicating neither phosphoramidate conjugate self-assembled into appreciable NMR silent aggregate in these conditions although assembly into soluble oligomers could not be discounted. In contrast, samples of **2** and **4** prepared in $D_2O$ buffered with 10 mM sodium phosphate with 50 mM NaCl (pD ≈ 7.2) demonstrated clear loss of linearity above concentrations of 0.03125 % wt/vol, with little gain in signal intensity upon further increase of monomer concentration. As 0.03125% wt/vol and 0.0625 % wt/vol correspondingly represent concentrations below and above the expected CACs, further addition of monomer to obtain concentrations above 0.03125% wt/vol does not result in continued increase in signal intensity due to monomer sequestration in NMR invisible aggregates. This data corroborates the determined CAC values for these molecules, since the monomer concentration should remain static above the CAC even with further increase of the phosphoramidate concentration. A caveat of this technique is that observed signal cannot

distinguish between monomer, soluble oligomers, or monomers in equilibrium with the nanostructures when the on and off rates are faster than the NMR time scale. Further investigation into relaxation times could reveal differences between the two phosphoramidates in terms of the nature of oligomeric assemblies formed just above the CAC. As assemblies of NAP-FF-GMP **4** readily form gels, association of formed assemblies would result in significant shortening of the $T_2$ relaxation time due to the negative linear relationship of the parameter with molecular size. As NAP-FF-AMP **2** does not undergo gelation, oligomeric assemblies formed above the critical aggregation concentration are not expected to further associate with one another potentially exhibiting $T_2$ relaxation times longer than **4**.[336]

We also sought to characterize the release of phosphoramidate monomers from formed assemblies through erosion experiments. Initial experiments with non-gelling phoshoramidate conjugates **2**, **3**, and **5** demonstrated dispersal of nanofibers into added supernatant complicating the detection of monomers. However, NAP-FF-GMP **4** gels remained stable at the bottom of microcentrifuge tubes for weeks enabling continual monitoring of monomer concentration present in added buffer supernatant. The release of NAP-FF-GMP from gels was found to be exceedingly slow, with less than 10 % of the monomer released after nearly 10 days. Fitting of the erosion data with a modified first order rate equation that considers the CAC of **4** enabled determination of a release half-life of approximately 43 h. The slow release of monomer from hydrogels of **4** can be attributed to the combination of non-covalent guanosine specific interactions resulting in gel formation. In addition to being immobilized within nanofibers due to anticipated aromatic

interactions and hydrogen bonding, Hoogsteen hydrogen bonding between monomers of cross-linked nanofibers could further reduce solvent accessibility and monomer mobility within the gel matrix. Additionally, the release profile appears to be highly dependent upon the CAC as the value represents an upper bound on the maximal concentration of monomer present in solution. Thus, the release profile of monomer from the phosphoramidate hydrogel appears to depend on both the thermodynamics of assembly, as well as the associative factors between nanofibers leading to gel matrix formation. This system exemplifies the highly controlled release profile achievable with single-component nanomedicine gels, and potentially guides the future development of drug delivery formulations.[47]

Analysis of nanofiber morphology was investigated with SAXS experiments to correlate observations made previously in cryo-TEM experiments. Previous characterizations of the nanofibers revealed highly monodisperse nanostructure populations, consisting of fibers approximately 7-8 nm in diameter and of lengths on the scale of microns. The advantage SAXS presents as a complimentary technique to cryo-TEM experiments is that scattering creates a solution averaged profile representative of nanostructure morphology, while TEM enables visualization of small localized regions of material. Our initial scattering investigations utilized phosphoramidate conjugates dissolved at high concentrations in $H_2O$ to maximize the potential for scattering above background level. Surprisingly, samples analyzed in $H_2O$ at 5 % wt/vol concentrations revealed intense scattering peaks at d-spacings of approximately 20 nm. As this characteristic feature is more than double the diameter of nanofibers, and orders of

magnitude smaller than the length, we hypothesized that the characteristic peak is likely the distance between nanofibers. Similar observations have been made in the literature where highly charged peptide-amphiphile nanofibers underwent solution ionic strength and amphiphile concentration dependent long range ordering due to the high degree of nanofiber ionic repulsion.[329] Due to the expected surface exposure of the anionic nucleoside phosphoramidate moiety in phosphoramidate-conjugate assemblies, the nanofiber surface is expected to be highly charged which would contribute significant charge repulsion between nanofibers and induce long range ordering, especially at high concentrations where nanofibers are forced into tightly packed arrangements. These results further confirm that charge repulsion between the nanofibers is a significant hurdle to nanofiber entanglement and association, as liquid crystalline ordering is more favorable in solutions of low ionic strength. These results also corroborate previous cryo-TEM observation of nanofiber alignment in phosphoramidate-conjugate samples, where variations in ice thickness induced nanofiber accumulation along the lacey carbon matrix of the formvar grid, although the nanofibers themselves maintained a characteristic distance between them.[244]

Additionally, differences in the peak intensity were observed between NAP-FF-AMP **2** and NAP-FF-GMP **4** nanofibers. Although both phosphoramidate samples possessed peaks at equivalent q-values, the peak generated by the sample of **2** was much more pronounced indicating that a higher degree of sample wide order was present than in **4**. Investigation of nanofiber morphology within the samples in $H_2O$ was precluded by this high range ordering as accurate model fitting would require the incorporation of structure

factor parameters to account for the observed liquid crystalline character of the nanofibers.[327] Scattering experiments were performed with NAP-FF-GMP **4** dissolved in DPBS at a concentration of 2.5 % wt/vol to investigate the nanoscale morphology of the nanofibers. Using the scattering analysis program SASVIEW, data from this experiment was fit using a built-in cylindrical form factor model which indeed confirmed the cylindrical nature of the nanofibers, as well as their high aspect ratio dimensions. The calculated radii of the nanofibers closely approximated experimentally observed dimensions at approximately 36 Å or 3.6 nm. Fitting of the data was most robust using nanofiber lengths on the order of hundreds or thousands of nanometers which correlates with the experimental observation of exceedingly long nanofibers and a high aspect ratio. Additionally, the slope of the low q-region was approximately -1 further indicating cylindrical fiber morphology.

The results of our combined investigations into the morphology of the nanofibers formed by phosphoramidate conjugates closely mirrors previous investigations into the morphology of nanofibers formed by similar aromatic self-assembling peptides.[100] Fmoc-FF was previously shown to self-assemble into nanofibers approximately 3 nm in diameter, with lateral assemblies of the nanofibers contributing to gel formation in solutions of sufficiently low pH.[100] Due to the structural similarities between Fmoc-FF and the self-assembling peptide in our system NAP-FF, the dimensions of fibers and orientations of phosphoramidate conjugate monomers should closely approximate that of Fmoc-FF. Moreover, as the C-terminal ends of the peptides in Fmoc-FF are solvent exposed on the surface of nanofibers, the PEG linker and nucleoside phosphoramidate moiety would

provide added thickness to the surface of the nanofibers by more than doubling the molecular length of monomers within the fibers. A possible structural model would consist of the NAP-FF portion of the molecule assembling into a peptide nanofiber core analogous to Fmoc-FF, with increased observed nanofiber width due to the PEG-nucleoside phosphoramidate shell on the nanofiber surface. This presents an exciting opportunity for future structural modeling experiments to corroborate this hypothesis.

Despite our characterizations of nanofiber formation, gelation, and morphology, none of the techniques described above provide specific information as to the thermodynamic parameters guiding assembly and disassembly apart from CAC determination which can be used to calculate the free energy of association.[332] The disassembly of NAP-FF-AMP **2** due to the injection of concentrated nanofiber solution into buffer generated an endothermic response similar to ITC analysis performed with other self-assembling peptides in the literature.[337] In response to increasing concentration, the observed enthalpy followed a negative sigmoidal relationship which enabled fitting of the data to extrapolate at the equilibrium point the CAC value of 420 μM. As CAC determination of **2** using techniques at room temperature yielded values around 300 μM, a slight increase in the observed CAC at higher temperature is expected. In addition, extrapolation of enthalpies of association at the CAC revealed enthalpically favorable monomer association indicating specific molecular recognition events between monomers contributing to assembly. Interestingly, comparison of the magnitudes of the enthalpic and entropic contributions to assembly indicated enthalpically driven association although the entropic contribution was also favorable. A caveat of this technique is that the high CAC

values of the phosphoramidates in solution mean at equilibrium, the injected solution is a mixture of nanofibers and monomers, meaning that exothermic dilution of the monomer in buffer is likely to cause an underestimation of the endothermic enthalpy of dissociation. Minimization of this effect can be achieved through generation of non-equilibrium samples, where concentrated stocks of phosphoramidate are diluted to the working ITC concentration without thermal denaturation and annealing. However, the higher CAC values of pyrimidine phosphoramidates resulted in noisy baseline data and the gel forming propensity of NAP-FF-GMP precluded its analysis with this technique. Alternative techniques such as differential scanning calorimetry (DSC) could potentially be used to observe the thermal transitions associated with disassembly as analysis of micellization is also customarily carried out with this method.[338,339]

In conclusion, we have undertaken fundamental characterization of the self-assembling properties of phosphoramidate modified peptides and determined the factors that lead to nanofiber cross-linking and gel formation. The anionic nature of the nucleoside phosphoramidate moiety, combined with favorable solvation provided by the PEG linker and ribose hydroxyl groups contribute substantial colloidal stability to the nanofiber assemblies of all four phosphoramidate conjugates. Nevertheless, ionic screening is necessary to prevent long-range nanofiber ordering in solution due to charge repulsion between the highly anionic phosphoramidate nanofibers. Additionally, the high solvation of the nanofibers likely contributes to a lack of cross-linking and entanglement between nanofibers formed from NAP-FF-AMP **2**, NAP-FF-UMP **3**, and NAP-FF-CMP **5** which precludes gel formation even at high concentrations and in solutions of physiologic ionic

strength. However, nanofibers formed from NAP-FF-GMP **4** readily cross-link, likely due to the high propensity of guanosine to self-associate through Hoogsteen hydrogen bonding in aqueous solution. The conformational flexibility afforded by the PEG linker could enable a variety of intra- and inter-fiber G-tetrad cross-links to form, and when combined with the high degree of solvation of the nanofiber surface, enables the colloidal instability commonly associated with G-tetrad assembled low molecular weight gelators to be overcome.[312,318–321] The nucleobase moiety of the phosphoramidate conjugates also plays a role in driving monomer assembly, as the larger ring systems of the purine bases promote assembly at lower concentrations than their pyrimidine counterparts. Additionally, the gelation induced by the guanosine base of **4** appears to be separated from the propensity of the phosphoramidate-conjugate to self-assemble into nanofibers and is instead a product of post-assembly interactions. We hope these fundamental studies spur further interest in the development of nucleoside phosphoramidate functionalized materials, especially self-assembling small molecules and peptides where exciting opportunities lie in the development of single component nanomedicines.

## 3.4 MATERIALS AND METHODS

Synthesis of NAP-FF-AMP **2**, NAP-FF-UMP **3**, NAP-FF-GMP **4**, and NAP-FF-CMP **5** was performed at previously described.[244] All bulk solvents were purchased from Fisher Scientific and were of high pressure liquid chromatography (HPLC) grade. Analytical HPLC was performed with an Ultimate 3000 System (Agilent) and Higgins Analytical Targa C18 5 μm column with 50 mM triethylammonium bicarbonate (TEAB) buffer and acetonitrile (30%-100% Acetonitrile). Nuclear magnetic resonance imaging

(NMR) of all compounds was performed at 25°C utilizing an Ascend 500 MHz Bruker spectrometer ($d_6$-DMSO and $D_2O$, Cambridge Isotope Laboratories).

**Nile red fluorescence assay and sedimentation experiments**

Phosphoramidate-peptide conjugates were dissolved in DPBS to generate stock solutions of 5 mM. Concentrated stock solutions were thermally denatured on heating block for 10 minutes at 70°C to ensure dissolution and allowed to cool to room temperature. Sample solutions ranging from 0-600 μM for purine conjugates and 0-700 μM for pyrimidine conjugates were made by diluting stocks in DPBS. Nile red was prepared by dissolving 2.5 mg in 2 mL of methanol and sonicating. A 200 μM solution was made by diluting the methanol stock in DPBS, with this solution added to phosphoramidate-conjugate to generate a final concentration of nile red in each sample of 50 μM. The samples were thermally denatured at 70°C for 10 minutes and reannealed at room temperature overnight. After 24 hours, the samples were analyzed on a Cary Eclipse Fluorimeter with excitation wavelength of 550 and emission scan of 615-670 with emission and detector slits at 5 nM. The instrument was zeroed with nile red added to DPBS without phosphoramidate. Maximal absorbance was recorded for each sample and plotted against the concentration to generate two linear curves, one below the anticipated CAC and one above. The intersection of the two lines was taken as the CAC value. Each concentration was measured in triplicate for each phosphoramidate with CAC values representing the mean and standard deviation of the three experiments. Sedimentation experiments were performed by generating standard curves via HPLC detection at 280 nm, and subsequent determination of monomer concentrations present in supernatants. Sedimentation was

performed with 1 mM phosphoramidate conjugates at a volume of 8 mL in 10 mL polycarbonate ultracentrifugation tubes with a spin protocol of 100,000 x g for 30 minutes at 22°C on a Beckman Optima XPN100 ultracentrifuge. Samples were heat denatured at 70°C for 10 minutes and equilibrated at room temperature overnight prior to centrifugation.

**Small amplitude oscillatory rheometry (SAOR)**

Rheological experiments were performed on a TA Instruments AR-G2 Rheometer. The 25 mm geometry was utilized for all experiments with peltier temperature control maintaining a constant temperature of 23°C. A humidity chamber was lined with moistened laboratory tissue paper and placed over the sample to mitigate evaporation of water. All samples were analyzed with a gap distance of 1 mm. Time sweep experiments were performed with strain % and frequency values within the linear viscoelastic region (0.5% strain and 1 rad/s). Strain sweep experiments were performed with a constant oscillatory frequency of 1 rad/s and frequency sweep experiments were performed with constant strain of 0.5%. Cyclic strain experiments were performed with 2 min application of 100% strain, followed by a 2 min re-conditioning step before re-analysis for 2 min at 0.5% strain. Samples of all four phosphoramidate conjugates were prepared in Dulbecco's Phosphate Buffered Saline solution at concentrations of 2.5 % wt/vol. Salt concentration analysis samples were prepared in 10 mM Sodium phosphate buffer with either 75 mM, 55 mM, or 35 mM NaCl at pH 7.4. All reported values are the average of at least three separate experiments. Time sweeps of NAP-FF-CMP and PEI co-gels were performed at 1% strain and 1 rad/s angular

frequency, with cyclic strain experiments performed with 1% strain and 90% strain at a 1 rad/s frequency.

**Monomer erosion and release kinetics from NAP-FF-GMP 4 hydrogels**

Experiments were performed in an adapted protocol described in the literature.[326] Hydrogel samples of NAP-FF-GMP **4** were prepared in DPBS within microcentrifuge tubes at a total volume of 100 μL and concentration of 2.5 % wt/vol. The gel samples cured overnight at room temperature, and the next day, 500 μL of additional DPBS was layered onto the gel to act as a supernatant or sink for released monomers. At timepoints over ten days, 100 μL aliquots were removed from the supernatant, promptly replaced with equal volume of identical buffer, and analyzed via HPLC to determine concentration via previously made standard curves. All reported values are the average of at least three separate experiments.

**Small angle x-ray scattering (SAXS)**

Samples were prepared in either Millipore purified water or DPBS at the concentrations specified. Analysis was performed on a SAXSLAB Ganesha instrument with the sample contained within a sandwich cell holder sealed with Kapton film, equipped with a Pilatus detector enabling measurements in the WAXS, MAXS, and SAXS configurations with detector distances of 100, 450, and 1050 mm respectively. Experiments were performed with 50kV and 0.3 mA energy source. Corrections for transmission and incident x-ray beam were made and background scattering was subtracted from sample data by measuring buffer or water only sealed within sandwich cells. Fitting was performed in SASVIEW software with built in cylindrical form factor model.

**Isothermal titration calorimetry (ITC)**

ITC experiments were performed on a MicroCal Auto-ITC200 system (Malvern Panalytical). Samples of concentration 1-5 mM prepared in DPBS were titrated into DPBS in 2 μL aliquots with spacing of 250 s. Titrations were performed at a temperature of 30°C. Integrated raw data was converted to kJ/mol and plotted against concentration of phosphoramidate. Sigmoidal curve fitting was performed in GraphPad Prism software with the built in variable slope three parameter function to obtain the CAC. Enthalpies of disassembly were determined by generating linear functions of the top portions of the sigmoidal curve representing high degrees of disassembly at low concentrations of peptide, and correspondingly calculating the enthalpy at the concentration corresponding to the CAC. Determination of the enthalpy of disassembly and the CAC afforded determination of the free energy of assembly as well as the associated entropy as described in the results section.

**$^{1}$H NMR characterization of NAP-FF-AMP 2 and NAP-FF-GMP 4 self-assembly**

Samples were prepared in either $D_2O$ or $D_2O$ with 10 mM Sodium Phosphate and 50 mM NaCl. The phosphate buffered saline solution was prepared using both monobasic and dibasic phosphate salts to generate a solution with corresponding pD of 7.2. Phosphoramidates were dissolved at a concentration of 0.25 % wt/vol and serial dilutions were made to generate samples of 0.125, 0.0625, 0.0313, and 0.0156 % wt/vol, corresponding to concentrations both above and below the anticipated CAC. MeCN was used as an internal standard to obtain relative integration values of the aromatic region of

the phosphoramidate conjugates, the portion of the molecule which drives assembly. T2 experiments were performed with the T2 CPMG experiment in Bruker TopSpin. Samples were degassed using freeze-pump method to remove dissolved oxygen.

# CHAPTER 4: PRONUCLEOTIDE DELIVERY THROUGH SUPRAMOLECULAR DESIGN

## 4.1 INTRODUCTION

Since the commercialization and approval of 6-Mercatopurine in 1953, there have been over 30 nucleobase, nucleoside, and nucleotide analogs clinically approved as anti-cancer or anti-viral agents by the U.S. Food and Drug Administration (FDA).[340,341] In general, the molecules within this class exert their therapeutic effect as antimetabolites, or mimics of endogenous molecules that inhibit the biochemical processes of disease, such as nucleic acid synthesis.[340–342]

Nucleoside antimetabolites have proven to be clinically useful for the treatment and prevention of viral infections.[340] The success of these agents is highlighted by the widespread use of nucleoside reverse-transcriptase inhibitors in treatment regimes for HIV infection and the blockbuster success of Sovaldi as a curative agent for Hepatitis-C infection.[279,343] The clinical efficacy of these anti-viral nucleoside antimetabolites (VNAs) is due in large part to their potent selectivity for viral processing enzymes over mammalian homologs. VNAs act through inhibition of either viral RNA or DNA synthesis without impairing the host's nucleic acid metabolism. These features impart a significant therapeutic index which results in dose regimens designed to limit viral persistence through mutation with limited toxicity concerns.[344]

Comparatively fewer nucleoside antimetabolites have been developed for the treatment of cancer.[340,341] Rather than gaining favorable therapeutic indices through specificity for viral enzymes, anti-cancer nucleoside antimetabolites (CNAs) rely on the proliferative nature of tumor cells over healthy tissues to maintain a therapeutic safety

profile.[345] CNAs exert their therapeutic effect by taking advantage of the cancer cell's reliance on high rates of proliferation that require production of nucleic acids. Inhibition of DNA and RNA synthesis, as well as disruption of the salvage pathway in which nucleic acid degradation metabolites are reused for RNA and DNA synthesis have been key targets for CNAs.[341]

Despite their clinical success and widespread clinical use, CNAs are subject to the serious limitations of therapeutic resistance by tumor cells and off-target toxicities.[345–347] While generally well tolerated, their lack of specificity to cancer cells leads to dose limiting side-effects, and in severe cases, causes serious life-threatening conditions.[346] Resistance to CNAs is largely a result of the modification of the biochemical steps required for intracellular metabolism to an active form (**Figure 4.1**).[348]

The polar nature of CNAs necessitates their facilitated transport across the plasma membrane by equilibrative and concentrative nucleoside transporters.[349] Inside the cancer cell, nucleobase analogs must be ribosylated and nucleoside analogs must undergo an initial phosphorylation step.[350,351] Two subsequent phosphorylation steps by monophosphate and diphosphate kinases yield the active triphosphate forms of CNAs that are incorporated into growing strains of DNA to initiate chain termination.[352,353] Cellular sensing of CNA induced DNA damage initiates a cascade of responses which can result in cell death.[354,355] Clinical mechanisms of resistance to CNAs include both the downregulation of drug activating enzymes and upregulation of deactivating enzymes. Downregulation of nucleoside transporters and activating kinases, as well as upregulation

of deactivating enzymes, limit the accumulation of intracellular CNAs available to progress along the kinase activation pathway. Modifications to the activity of molecular targets such as DNA polymerases and proteins involved in the apoptotic response may also act as resistance mechanisms to CNAs.[356]

Of the CNAs developed as antineoplastic agents, only Gemcitabine (dFdC) and 5-Fluorouracil and its related derivatives are currently clinically approved and effective in the treatment of solid tumors.[345] As a representative CNA, dFdC has demonstrated significant clinical efficacy in treating a variety of metastatic or advanced cancers including those of the breast, lung, and ovaries.[345] Additionally, it is one of the few agents demonstrating utility in treating advanced or metastatic pancreatic cancer.[357] Nevertheless, dFdC suffers from the serious drawbacks of chemotherapeutic resistance, dose-limiting toxicities, and metabolic inactivation which contribute to limited clinical use for specific indications.[346,348,357,358] Characterized resistance mechanisms to dFdC, resulting in loss of clinical efficacy include downregulation of intracellular transport (human equilibrative nucleoside transporter 1, hENT1), downregulation of intracellular monophosphorylation (deoxycytidine kinase, dCK), downregulation of secondary targets (ribonucleotide reductase, RRM1), upregulation of inactivating deamination (cytidine deaminase, CDA), and upregulation of phosphatases (cytosolic-5'-nucleotidase II, cN-II).[356] While dFdC is generally well tolerated, serious off-target complications from treatment include pulmonary, neurological, and vascular toxicities.[346,358] Additionally, dFdC is rapidly converted to its inactive dFdU form by both plasma and hepatic cytidine deaminases after intravenous administration.[359] Indeed, at least 75% of dFdC undergoes deamination and is

excreted in urine after 24 h which significantly limits free drug available and tumor up take.[359] Consequently, enhancing the clinical efficacy of CNAs has been an area of intense research and is generally pursued through a combination of enhanced drug accumulation at the site of disease, avoidance of metabolic drug inactivation, bypass of clinical resistance mechanisms, and avoidance of dose mitigating off-target toxicities.[313,360–364]

The selective targeting of anticancer agents to tumor cells with antibodies has seen clinical success with the approval of several agents and could provide an avenue for enhancing therapeutic efficacy and minimizing off-target toxicities[365]. Non-antibody based targeting ligands such as aptamers and peptides selective for tumor cell surface markers have been conjugated to CNAs to investigate therapeutic efficacy *in vivo* resulting in significant advances in the potential enhancement of therapeutic index of CNAs.[363,366,367] Pharmacological combination of dFdC with potential enhancers of CNA activity, including inducers of nucleoside kinase activity to increase dFdC entry into the intracellular activation pathway, have also been investigated.[368] Pronucleotide or ProTide strategies, similar to the ones successfully used for VNAs, have been developed that can overcome transport and kinase based resistance have also been explored.[278,340,369,370]

Pronucleotide strategies present a fascinating method for enhancing therapeutic efficacy of CNAs as they simultaneously overcome the need for active transport across cellular membranes, bypass the initial phosphorylation step, and avoid clinical traditional resistance mechanisms of CNAs.[278,340] In the pronucleotide strategy, monophosphate derivatives of the nucleoside drug are synthesized with chemical functional groups

appended to the phosphate to mask the negative charges inherent to the free acid (**Figure 4.2**). Masking these charges increases the hydrophobicity of the drugs enabling passive diffusion of the molecules across the cellular membrane. Once inside the cell, a variety of chemical and enzymatic release mechanisms may be incorporated into the pronucleotides to enable intracellular removal of the phosphate masking groups to reveal the monophosphate form.[278,340]

Nucleoside phosphoramidates are one such pronucleotide and achieve phosphate masking through appendage of amine containing side chains to the phosphorus atom, where the nitrogen atom of the side chain replaces an oxygen atom of the phosphate moiety. The phosphoramidate strategy reduces the net negative charge on the molecule and facilitates membrane permeability through enhanced hydrophobic character presented by the amine containing side chain and phosphate masking.[278,340,371–374] Intracellular removal of the amine containing side chain is performed by a family of nucleoside phosphoramidases referred to as Histidine Triad Nucleotide Binding Proteins (Hints).[267,375–377] Humans express three Hint isoforms designated numerically as hHint1, hHint2, and hHint3, with hHint1 of particular interest due to its role in the metabolic activation of the clinically approved anti-HCV phosphoramidate prodrug sofosbuvir to achieve intracellular delivery of the 5'-monophosphorylated form of 2'-deoxy-2'-α-fluoro-β-*C*-methyluridine.[378]

In addition to antivirals, phosphoramdiate pronucleotides are under investigation for the intracellular delivery of CNAs. The phosphoramidate pronucleotide NUC-1031 (Acelarin) which is a ProTide derivative of dFdC monophosphate is under clinical

investigation for the treatment of biliary tract cancer, ovarian cancer, pancreatic cancer, and other advanced solid tumors (**Figure 4.3**).[379] NUC-1031 was found to result in higher concentrations of the active triphosphorylated form of dFdC and circumvented conventional resistance mechanisms associated with transport of the nucleoside by hENT1 and phosphorylation by dCK.[364,379]

Despite the clinical success of phosphoramidate pronucleotides for antiviral treatment and their promise for anticancer treatment, there are no clinically approved agents in this class for the treatment of cancer. Sofosbuvir is dosed orally enabling rapid metabolic activation of the ProTide in the liver, which fortuitously is also the site of HCV infection.[380] Alternatively, anticancer ProTides such as NUC-1031 are dosed intravenously to limit hepatic clearance and metabolic inactivation.[364,379] To overcome the challenges associated with dosing, administration, and off-target toxicities, novel delivery methods for dFdC are under investigation including drug loaded liposomes, polymer-based nanoparticles, and inorganic nanoparticles.[361,381–384] These delivery systems largely rely on non-covalent immobilization methods such as encapsulation and surface adsorption to facilitate transport of the active agent as delivery vehicles in systemic delivery. Alternatively, covalent modification of dFdC has resulted in promising formats for enhancing the stability of dFdC transport relative to non-covalent particle immobilization, since adsorption and encapsulation techniques may result in poor drug retention. [385] Pegylation has been shown to increase tumor retention, circulating half-life, and prevent deamination if conjugation of dFdC is performed through its N4 exocyclic nitrogen.[362] Additionally, lipophilic groups such as squalene, isoprenoids, and fatty acids may be

appended to dFdC to enhance its lipophilicity and limit metabolic deactivation.[386–388] Interestingly, these chemical modifications have also been utilized as drivers of molecular self-assembly to generate dual function drug/drug-carrier nanoassemblies (**Figure 4.4)**.[314,360]

Supramolecular hydrogels consisting of low molecular weight organic molecules are characterized by the assembly of monomeric units into a hydrated network of nano- to microscale structures that physically entrap aqueous solution to form solid-like hydrated materials.[28] Direct self-assembly of drug-like molecules into supramolecular hydrogels constitutes an innovative method for the controlled delivery with several clinically approved single component nanomedicine hydrogels already in existence.[233,237] Self-assembling therapeutics achieve favorable drug carrier properties such as shear thinning gel formation, while maintaining highly controlled drug loading as each self-assembling unit is itself a drug molecule.[47,48] Additionally, localized therapeutic delivery is advantageous as it presents high concentrations of therapeutic directly to the diseased tissues, without systemic presentation to non-diseased tissues, thus limiting off-target toxicities and metabolic clearance.[389]

Chemical modification of dFdC has been used to trigger assembly of the modified derivatives into supramolecular hydrogels for delivery.[152,313,387,390] Chemical modification of the 5'-OH and N-4 positions of dFdC with acyl chains through ester, amide, carbamate, and urea linkages yielded a panel of dFdC derivatives that formed hydrogels in mixed organic/aqueous solution and retained cytotoxic activity against *in vitro* cancer cell lines.[313]

Triggered gelation of dFdC derivatives has been explored to achieve functional control over the assembly properties of drug laden gels.[390] Schiff base formation between the N4 amino group of dFdC and an aldehyde functionalized peptide triggered self-assembly of the chemically generated monomer into supramolecular hydrogels.[390] Additionally, conjugation of dFdC to Fmoc-Gly yielded a monomer which could be co-assembled with N-terminally capped aromatic self-associating peptides to generate drug immobilized nanofibers.[152]

Inspired by examples of nucleoside based supramolecular assemblies, we proposed to extend the utility of self-assembling dFdC derivatives through the development of self-assembling therapeutic phosphoramidate pronucleotides. Previously, we examined the utility of the nucleoside phosphoramidate moiety as a regulatory motif in small molecule self-assembly.[244] Aromatic peptides functionalized with nucleoside phosphoramidates were found to self-assemble into highly regular supramolecular nanofibers which were substrates for hHint1. The hydrolysis of the nanofiber nucleoside phosphoramidate moieties by hHint1 triggered a structural transition at the nanoscale through nanofiber association and bundling.[244] Utilizing the same self-assembling molecular scaffold, we have substituted the natural nucleoside moiety within the nucleoside phopshoramidate motif with dFdC to generate potential ProTide therapeutic bearing supramolecular nanofibers. The dFdC ProTide nanofibers were found to be highly monodisperse, possessing widths of 7-8 nm, and lengths on the order of microns. The *in vitro* cytotoxic properties were investigated in cancer cell lines originating from malignancies commonly treated with dFdC clinically. Our studies indicate that the self-assembling dFdC

pronucleotides are potentially able to circumvent clinical mechanisms of dFdC resistance due to avoidance of the need for active transport and bypass of the rate limiting initial phosphorylation step. This work presents the first demonstration of a self-assembling phosphoramidate ProTide derivative as a potential injectable therapeutic delivery at the site of disease.

**Figure 4.1. Metabolic activation of CNAs.**

Example shown is representative case of Gemcitabine (dFdC). NMPK (Nucleoside Monophosphate Kinase) and NDPK (Nucleoside Diphosphate Kinase)

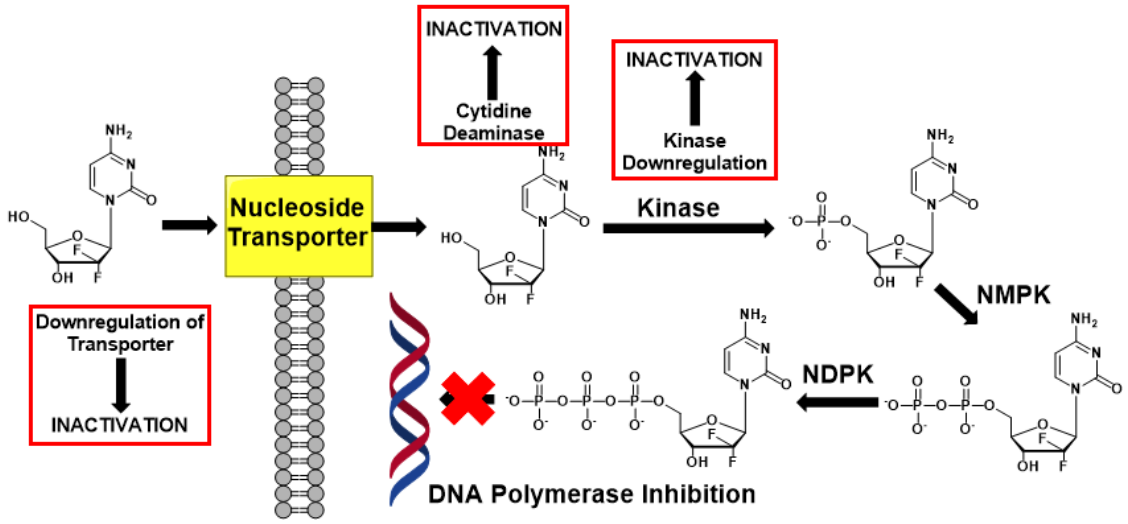

**Figure 4.2 Phosphoramidate ProTide cell entry and metabolic activation**

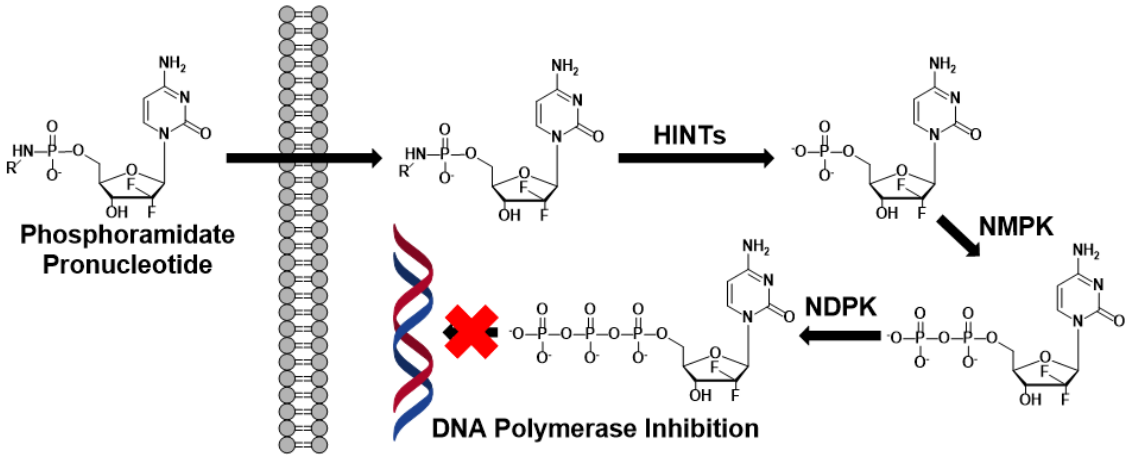

**Figure 4.3 Structure of phosphoramidate ProTide Nuc-1031 (Acelarin)**

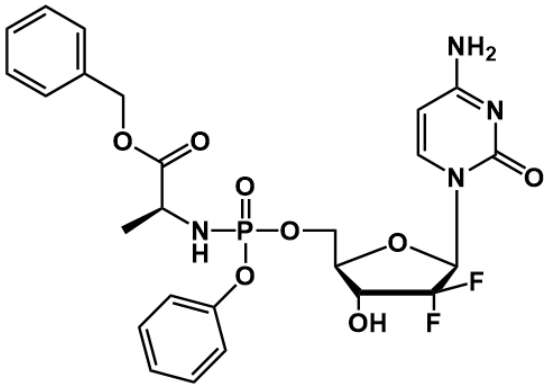


Nuc-1031 (Acelarin)

**Figure 4.4 Chemically modified Gemcitabine (dFdC) derivatives**

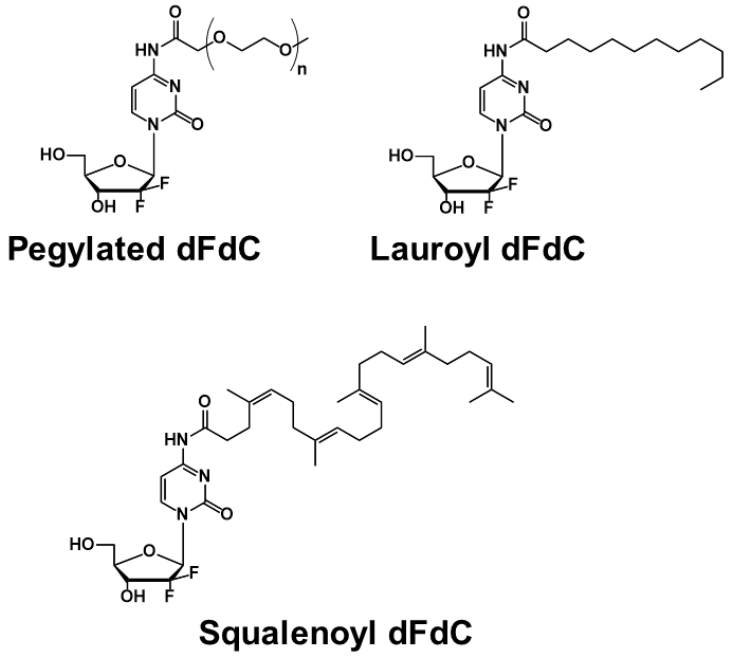

## 4.2 RESULTS

### Synthesis of NAP-FF-GEM

We chose to approach the synthesis of the dFdC phosphoramidate through Atherton-Todd (AT) chemistry, where the reactive 5'-nucleoside phosphorochloridate intermediate is generated *in situ* through the oxidation of a diester H-phosphonate species (**Figure 4.5**).[391–393] A global silyl protecting group strategy was employed through protection of the N-4 exocyclic amine with 2-(trimethylsilyl)ethyl carbamate (TEOC) functionality, protection of the 3'-OH with a tert-butyldimethylsilyl ether (TBDMS), and protection of the free acid of the phosphoramidate monoester with 2-(trimethylsilyl)ethyl ester.[394] Sequential protection of the exocyclic amine and 3'-OH of dFdC with TEOC and TBDMS groups enabled selective phosphonylation of the 5'-OH. Esterification of the free phosphonate acid with 2-(trimethylsilyl)ethanol, followed by *in situ* oxidation to the propargyl phosphoramidate under AT conditions, yielded the fully protected dFdC phopshoramidate diester. Deprotection of the fluoride sensitive groups under mild conditions with tetrabutylammonium fluoride (TBAF) yielded the propargyl phosphoramidate monoester which was coupled to azido-functionalized self-assembling peptide under copper catalyzed click chemistry conditions as previously described to yield the final self-assembling phosphoramidate NAP-FF-GEM **8** (**Figure 4.5**).[244]

### Characterization of NAP-FF-GEM Self Assembly

Previous investigations of the self-assembling properties of self-assembling phosphoramidates revealed a dependence of critical aggregation concentration (CAC) on

the conjugated nucleoside (**Chapter 3**). More specifically, purine nucleobases were observed to induce assembly at lower concentrations of monomer in comparison with pyrimidines, possibly due to the greater hydrophobic imparted by the larger purine rings. We sought to characterize the self-assembly of NAP-FF-GEM **8** using the same assay conditions previously used to establish CACs utilizing Nile red as an assembly probe.[324] Briefly, the assay operates on the principle that the fluorescence of Nile red increases when immobilized within supramolecular nanostructures in comparison to the molecules quenched fluorescence in aqueous solution.[117,325] Surprisingly, the CAC of NAP-FF-GEM **8** was significantly decreased in comparison to the pyrimidine bearing phosphoramidates, with the unnatural nucleoside resulting in a CAC of 340.7 ± 0.6 μM, compared to CAC values for NAP-FF-UMP **3** and NAP-FF-CMP **5** of 419 μM and 411 μM respectively. Interestingly, this value more closely approximates the CACs observed with the purine bearing phosphoramidates NAP-FF-AMP **2** and NAP-FF-GMP **3** (**Figure 4.6**).

The solvated nanostructure of NAP-FF-GEM was investigated with cryo-TEM imaging as well as SAXS. Previous investigations revealed self-assembling phosphoramidates formed highly monodisperse self-assembled nanofibers 7 nm in diameter and possessing lengths on the order of microns. Cryo-TEM imaging of NAP-FF-GEM **8** prepared in DPBS at a concentration of 0.5 % wt/vol revealed morphology identical to that observed with phosphoramidate conjugates modified with natural nucleosides (**Figure 4.7**). Additionally, the fibers were found to be largely unassociated with each other except through long range ordering along the lacey carbon grid, likely due to negative charge repulsion combined with the limiting thickness of the ice and excessive lengths of

the nanofibers. SAXS measurements were performed on samples of NAP-FF-GEM 5 % wt/vol in both $H_2O$ and DPBS. Interestingly, significant long-range ordering of the nanofibers was evident in samples prepared in deionized $H_2O$ indicating significant charge repulsion between nanofibers due to the high density of anionic charges on the nanofiber surface and high degree of solvation contributed by the PEG linker and polar ribose moiety (**Figure 4.8a**). The characteristic scattering peak was evident at q-values corresponding to approximately 20 nm which is indicative of the distance between the centers of tightly packed nanofibers. NAP-FF-GEM prepared in DPBS also possessed this feature but with significantly reduced intensity indicating a lower degree of nanofiber alignment due to electrostatic repulsion (**Figure 4.8b**). Despite observed nanofiber repulsion, comparison to a cylindrical form factor model with a radius of 3.5 nm and length of 1000 nm was performed to correlate the nanofiber morphology to the observed cryo-TEM nanostructures. A close approximation to the theoretic model was achieved, albeit with deviations from the model at low q-values corresponding. The discrepancy is likely due to long-range ordering of the nanofibers which would necessitate both structure and form factor incorporation in future model fitting to obtain accurate model fits.[328,331]

Concentration dependence studies on the observed $^1$H NMR signal in the aromatic region of the NAP-FF-GEM **8** was used to further characterize supramolecular assembly, since the aromatic peptide segment NAP-FF is hypothesized to be predominately responsible for driving monomer association.[395] Samples were prepared in either $D_2O$ or $D_2O$ with 10 mM sodium phosphate and 50 mM NaCl to investigate the dependence of salt concentration on assembly. In samples prepared without added salt, a clear dependence of

observed signal on concentration was observed indicating that large NMR invisible aggregates were not predominate in the sample (**Figure 4.9**). In contrast, samples prepared in $D_2O$ with phosphate buffered saline indicated a loss of linearity at concentrations above the expected CAC with added monomer no longer contributing to visible NMR signal (**Figure 4.9**). These results are consistent with the formation of higher ordered oligomeric species forming resulting in NMR silent aggregates, or in this case, nanofiber networks. Significant peak broadening is indicative of higher ordered assembly in the presence of additional salt contributing to significant reductions in the $T_2$ relaxation time.[336] Although higher ordered association is likely occurring in the $D_2O$ sample, oligomeric species could be smaller in comparison to the $D_2O$ with PBS sample due to increased charge repulsion. In addition, an increased CAC in $D_2O$ compared to buffer also cannot be ruled out.

Interestingly, experiments assessing the rheological properties of 2.5 % wt/vol NAP-FF-GEM **8** in DPBS revealed that like previously investigated pyrimidine phosphoramidates, no gel forming character was evident with low elastic moduli recorded on the order of 10 Pa. Lack of gel forming character in the self-assembled phosphoramidates is consistent with high nanofiber surface solvation and lack of cohesive non-covalent interactions leading to nanofiber cross-links.

**Biological activity of NAP-FF-GEM**

To determine if the conjugated dFdC pronucleotide contained within the NAP-FF-GEM phosphoramidate imparted biological activity, *in vitro* growth inhibition was assessed against human cancer cell lines. Dose dependent antiproliferative effects of NAP-

FF-GEM **8** against MDA-MB-231 triple negative breast cancer cells, H460 non-small cell lung cancer, and U87 glioblastoma were observed, with higher concentrations of NAP-FF-GEM **8** exhibiting greater antiproliferative effect (**Figure 4.10**). Although the highest concentration of NAP-FF-GEM examined was 1 mM which is well above the CAC value, toxicity was still observed at this concentration indicating that assembly of monomers into higher ordered structures does not preclude activity. Concentration dependent growth inhibition of NAP-FF-GEM **8** was compared to NAP-FF-CMP **5** which bears the natural nucleoside cytidine to compare the extent of growth inhibition derived from the peptide-phosphoramidate conjugate alone. Interestingly, NAP-FF-CMP **5** also exhibited toxicity at higher concentrations, albeit to a lesser degree than NAP-FF-GEM **8**, indicating that the peptide portion of the phosphoramidate may possess modest growth inhibitory activity. Growth inhibition against MDA-MB-231 cells revealed an $IC_{50}$ value for NAP-FF-GEM **8** of 2.6 ± 2.0 μM. In comparison, fitting of growth inhibition data for NAP-FF-CMP was not possible due to the modest growth inhibition even at 1 mM. Indeed, NAP-FF-CMP **5** only approached 50% growth inhibition at the highest concentrations dosed. Similar trends were observed against U87 and H460 cell lines, with NAP-FF-GEM **8** exhibiting greater growth inhibition at higher concentrations than NAP-FF-CMP (**Figure 4.10b,c**). The biological activity of NAP-FF-GEM **8** was also observed to be comparable to a 5-fold lower concentration of dFdC indicating a modest decrease in toxicity of the phosphoramidate conjugate relative to the free drug. Overall, NAP-FF-GEM **8** possesses greater antiproliferative properties than NAP-FF-CMP **5**, indicating that the cytotoxic nucleoside enhances the biological activity of phosphoramidate-peptide conjugate.

**Figure 4.5 Synthetic procedures for NAP-FF-GEM 8.**

(a) i. HMDS and cat. $(NH_4)SO_4$ ii. TEOC-ONp and NMI iii. TEA in MeOH (b) DMTrCl, pyridine (c) 5% DCA in MeOH/DCM (d) Phosphorous acid, Pivaloyl chloride (e) 2-(trimethylsilyl)ethyl alcohol, Pivaloyl chloride (f) $CCl_4$, propargyl amine, TEA (g) TBAF (h) $CuSO_4$, Sodium ascorbate, Compound 1 (NAP-FF-$PEG_3$-$N_3$)

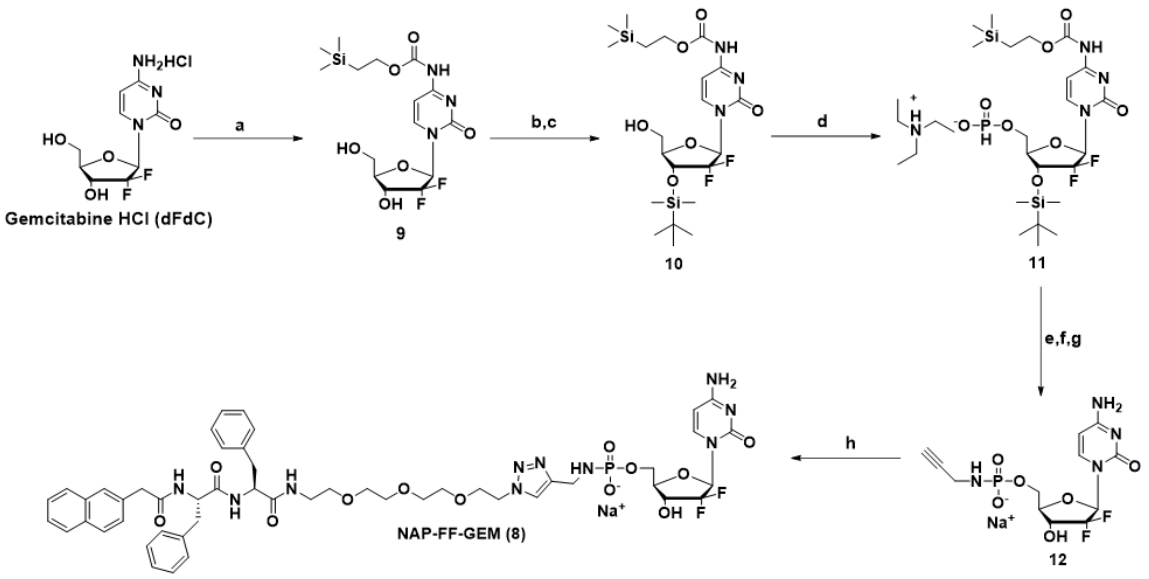

**Figure 4.6 Nile red critical aggregation fluorescence assay NAP-FF-GEM 8.**

Vertical axis corresponds to fluorescence readout and horizontal axis corresponds to concentration of self-assembling phosphoramidate NAP-FF-GEM **8.** Curves were constructed using data points representing the two linear regions of pre-assembly and post-assembly response with the intersection of the two curves used to determine the CAC. Data shown is averaged with visible error bars representing ± standard deviation. CAC value represents average and ± standard deviation of n = 3 experiments. Graphic depicts the immobilization of nile red into oligomeric nanostructures resulting in fluorescence.

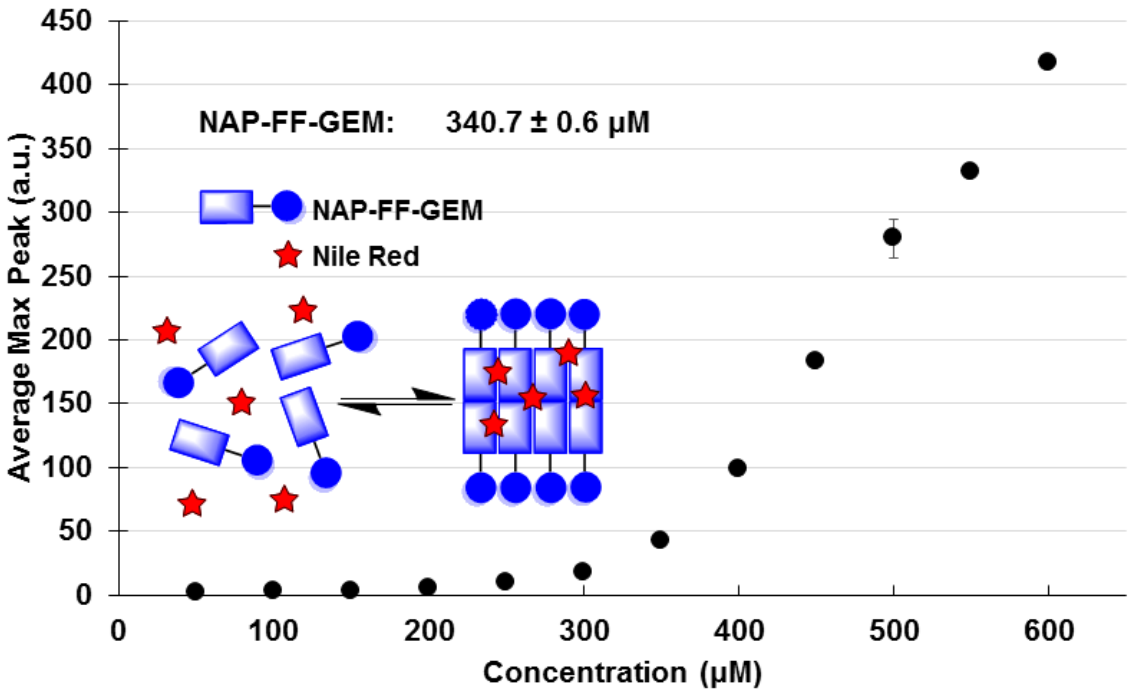

**Figure 4.7 Morphological characteristics of nanostructures formed from NAP-FF-GEM 8**

(a) Cryo-TEM images at 0.5 % wt/vol concentration in DPBS. Scale bars represent 150 nm or 0.15 microns (b) SAXS profile of phosphoramidate at 5 % wt/vol concentration in DPBS. Blue points represent experimental data with green curve representing theoretical model fit using built in cylindrical form factor model within SASVIEW software with cylinders bearing radii of 3.5 nm and lengths of 1000 nm. Deviation from theoretical model is attributed to concentration dependent ordering of the nanofibers rather than random orientation (c) SAXS profile of phosphoramidate at 5 % wt/vol concentration in $H_2O$. Distinct scattering peak corresponds to the inter-fiber distance resulting long range nanofiber packing due to high concentration and anionic repulsion.

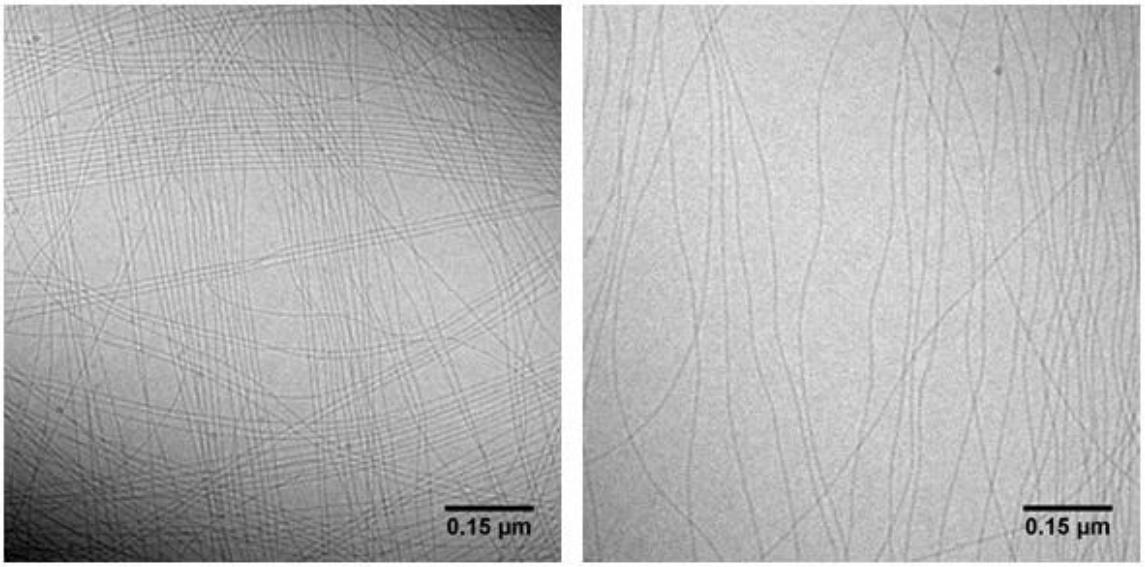

**Figure 4.8 SAXS of NAP-FF-GEM 8**

(a) SAXS profile of phosphoramidate at 5 % wt/vol concentration in $H_2O$. Distinct scattering peak corresponds to the inter-fiber distance resulting long range nanofiber packing due to high concentration and anionic repulsion. (b) SAXS profile of phosphoramidate at 5 % wt/vol concentration in DPBS. Blue points represent experimental data with green curve representing theoretical model fit using built in cylindrical form factor model within SASVIEW software with cylinders bearing radii of 3.5 nm and lengths of 1000 nm. Deviation from theoretical model is attributed to concentration dependent ordering of the nanofibers rather than random orientation

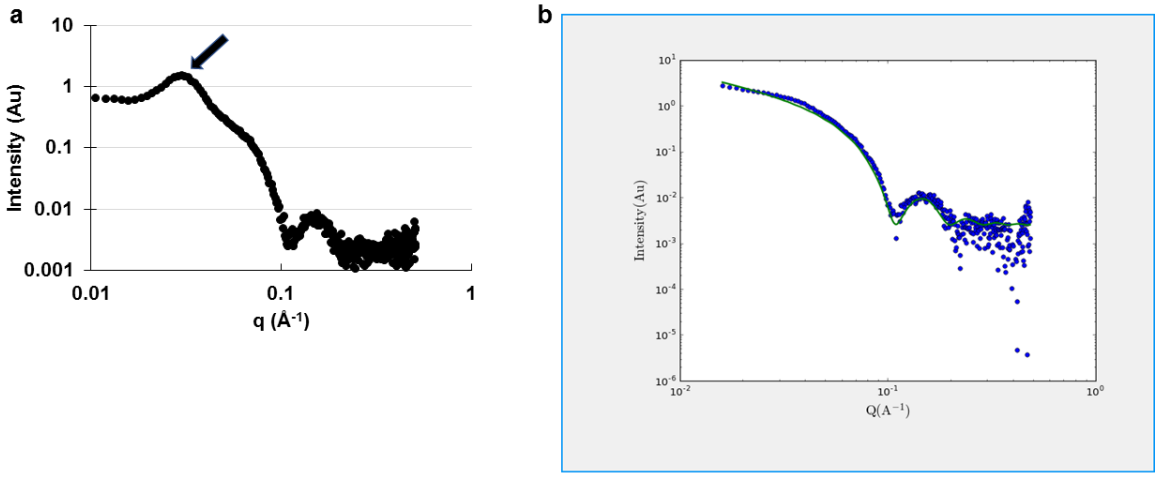

**Figure 4.9 Concentration dependence of observable NMR signal resulting from the aromatic region of NAP-FF-GEM 8.**

Boxed regions correspond to the aromatic region of phosphoramidate in $D_2O$ alone (left, blue) and $D_2O$ with 10 mM Sodium phosphate and 50 mM NaCl, pD 7.2. The sample in $D_2O$ shows concentration dependent increase in observed signal. Sample in buffer shows concentration dependent increase until concentration 0.063%, which is above the CAC. Broadening of peaks indicates decrease in T2 relaxation time indicating assembly into higher ordered oligomeric species.

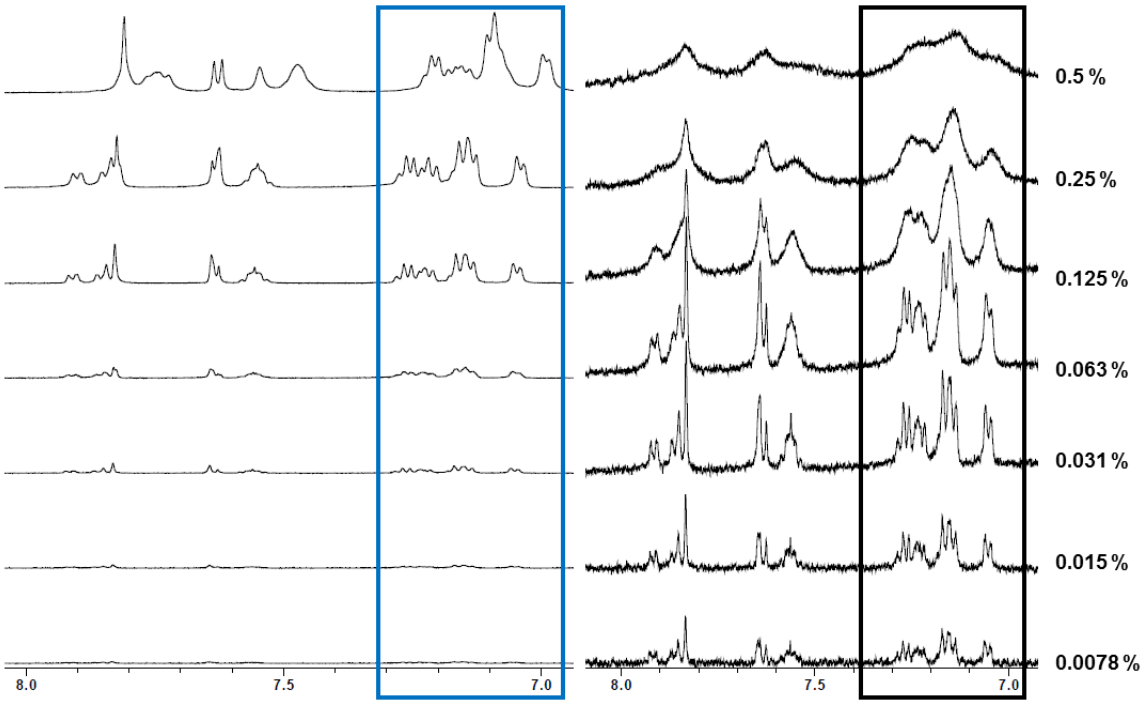

**Figure 4.10 Anti-proliferative activity of NAP-FF-GEM assessed with MTS assay**

(a) NAP-FF-GEM (blue) compared to NAP-FF-CMP (black) in MDA-MB-231 cells at 48 h with 5,000 cells per well. Data shown represents average of n =4 (NAP-FF-GEM) and n =3 (NAP-FF-CMP) independent experiments with error bars representing ± standard deviation. NAP-FF-GEM IC50 against MDA-MB-231 was determined to be 2.6 ± 2.0 μM (mean ± standard deviation, n = 4) using the three parameter sigmoidal dose response inhibition model in GraphPad Prism. IC50 determination for NAP-FF-CMP was not possible due lack of 50% cell killing at high concentrations. Vertical axis corresponds to viability relative to cell only control. Stars represent one-tailed t-test significance ($p < 0.05$) (b) Concentration dependent antiproliferative activity of NAP-FF-GEM (blue) and NAP-FF-CMP (black) against U87 cells at 48 h with 5,000 cells per well. Data shown represents mean and standard deviation of triplicate data points from a single experiment (c) Concentration dependent antiproliferative activity of NAP-FF-GEM (blue), NAP-FF-CMP (black), and Gemcitabine (light brown) against H460 cells at 48 with 5,000 cells per well. Concentrations of phosphoramidate are 500, 50, 5, and 0.5 μM with concentrations of Gemcitabine 5-fold lower at 100, 10, 1, and 0.1 μM. Data shown represents mean and standard deviation of triplicate data points from a single experiment.

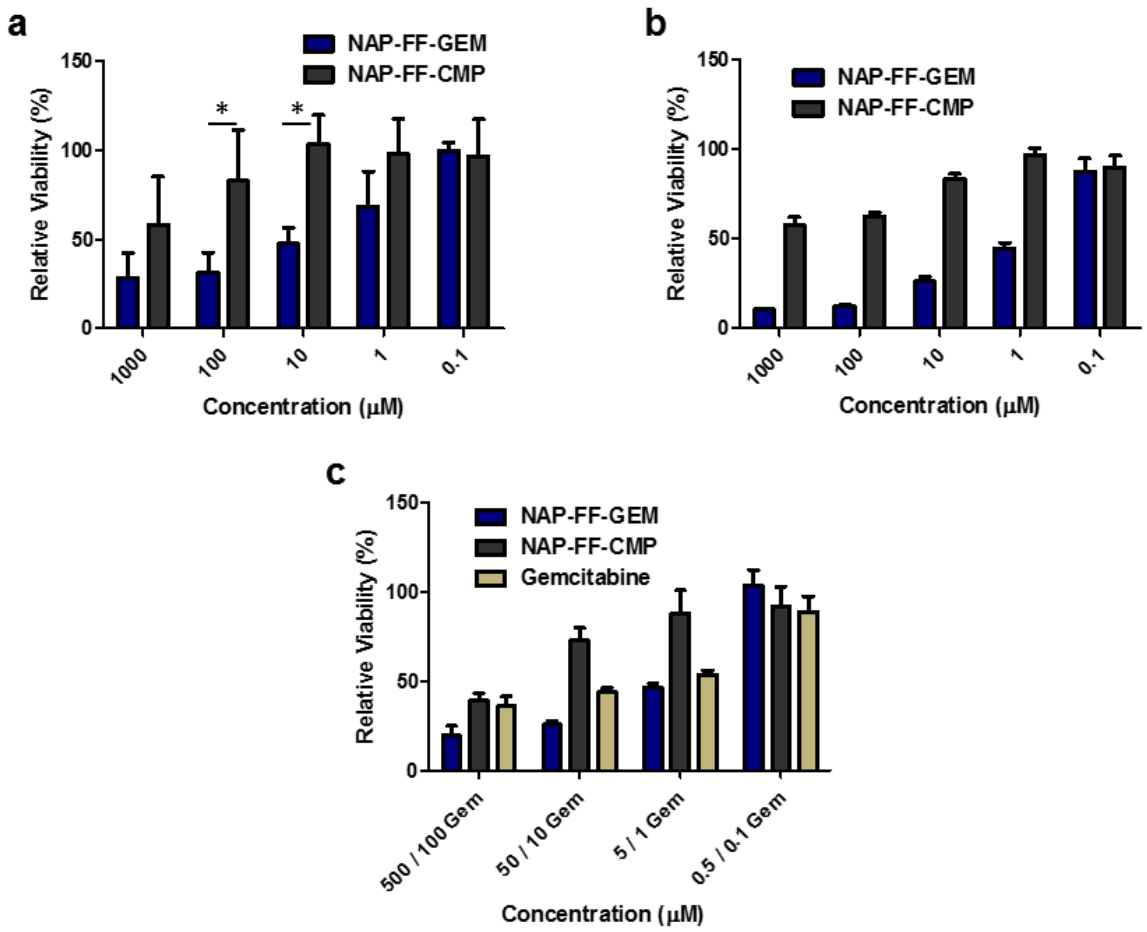


## 4.3 DISCUSSION

Previous characterizations of phosphoramidate conjugated self-assembling peptides revealed no perturbation of the nanofiber structure as a result of changing the nucleoside appended through the phosphoramidate moiety.[244] These results were corroborated through cryo-TEM and SAXS analysis of the nanostructures formed by NAP-FF-GEM **8**. Highly monodisperse and high aspect ratio nanofibers with diameters of 7 nm and lengths on the order of microns were observed in cryo-TEM images of samples prepared in aqueous buffer. Additionally, SAXS analysis revealed solution ionic strength dependent long-range ordering of the long cylindrical nanofibers, similar to analyses

performed on phosphoramidate nanofibers of NAP-FF-AMP **2** and NAP-FF-GMP **4** (**Chapter 3**). Overall, the identity of the nucleoside appears to have little effect on nanostructure morphology with the NAP-FF peptide driving assembly into cylindrical nanofibers and the PEG-linker and anionic phosphoramidate moiety imparting colloidal stability and nanofiber solvation. The nucleoside moiety does appear to have an effect in the early stages of monomer association apparent in the lower CAC value of NAP-FF-GEM **8** in comparison to the natural pyrimidine nucleoside phosphoramidate conjugates NAP-FF-CMP **5** and NAP-FF-UMP **3**. NAP-FF-GEM's **8** CAC more closely approximated that observed for the purine conjugated phosphoramidates indicating that the geminal 2'-difluoro- modification of the dFdC nucleoside is likely imparting greater hydrophobic driving force or fluorous interactions in promoting monomer assembly. Importantly, these results indicate that a variety of CNAs and VNAs could potentially be used to generate therapeutic phosphoramidate conjugates without significantly altering their ability to self-assemble. Additionally, relative trends of CAC based on the chemical modification possessed by the therapeutic nucleoside moiety could enable rational design of drug releasing nanofibers with predictable monomer release properties and assembly.

Interestingly, the self-assembling phosphoramidate NAP-FF-CMP **5** demonstrated antiproliferative effects at high concentrations against *in vitro* human cancer cells. As the cytidine nucleobase is a non-toxic endogenous molecule present at high concentrations within the cell, the biological activity of the conjugate is likely derived from the peptide portion of the molecule.[396] Cytotoxic effects of enzyme activated gelation have been well demonstrated with phosphate and ester modified self-assembling peptides.[397] In these

systems solvating chemical modifications are removed by endogenous enzymes which enable monomer self-assembly into fibrous nanostructures.[262,289] The formation of such structures within and around cancer cells *in vitro* was shown to disrupt cell physiology and homeostasis contributing to cell death.[398] A similar mechanism could be occurring with NAP-FF-CMP **5** as previous studies demonstrated the ability of hHint1 to induce gelation of soluble NAP-FF-CMP nanofibers through phoshoramidate hydrolysis. As hHint1 is an intracellular enzyme, accumulated intracellular monomer could be converted from the phosphoramidate conjugate to free gelating peptide. Activation of internalized monomers could lead to the assembly of gelating peptides into oligomeric species that could inhibit cellular processes, since the peptides likely possess lower CAC values than the nucleoside phoshoramidate conjugates.

When comparing the activity of NAP-FF-GEM **8** and NAP-FF-CMP **5**, NAP-FF-GEM **8** was found to have enhanced antiproliferative activity compared to NAP-FF-CMP **5** due predominantly to the replacement of cytidine with the cytotoxic CNA dFdC.[10,21] This observation is consistent with the uptake of monomers of NAP-FF-GEM **8** and intracellular conversion by hHint1 releasing the peptide and 5'-dFdC-monophosphate, thus operating as a gemcitabine ProTide for dFdC monophosphate. These results may indicate that NAP-FF-GEM **8** could indicate the potential of the associated nanofibers to circumvent clinical resistance mechanisms to dFdC, enabling greater inhibition of DNA polymerase and ribonucleotide reductase.[348,359] The antiproliferative effects of phosphoramidate monoester modified CNAs were previously demonstrated to result from intracellular release of the

monophosphate after internalization and hHint1 phosphoramidase activity, with NAP-FF-GEM presumably operating under the same mechanism.[372–374,376,377]

This study represents the first demonstration of a self-assembling therapeutic phosphoramidate pronucleotide. Previous investigations of self-assembling dFdC derivatives explored their use for localized chemotherapeutic delivery, although the lipophilic modifications required co-assembly with other self-assembling molecules or organic solvent for colloidal stabilization.[313,387] In our system, self-assembly of NAP-FF-GEM is readily achieved without co-assembly and in physiologically relevant aqueous solutions. Although localized hydrogel delivery formulations of dFdC have been investigated, small molecule drug delivery is complicated by non-optimal release kinetics with simple encapsulation leading to drug burst release, and covalent polymeric conjugation requiring matrix degradation or macromolecule internalization to achieve therapeutic release.[47]

Achieving self-assembly of the therapeutic moiety conveys significant control over the release of therapeutic monomer as an upper bound on free-monomer exists in the CAC and the kinetics of release are directly dependent on the extent of non-covalent interactions between monomers and cross-links between nanofibers.[326] We envision using NAP-FF-GEM in localized chemotherapeutic formulations in combination with immunotherapies to enhance therapeutic response. The utility of localized dFdC delivery in promoting immune checkpoint inhibitor efficacy was demonstrated, recently, in syngeneic mouse models of cancer by promoting a pro-immunogenic phenotype in the tumor microenvironment.[399] We

hope to further examine the utility of our system for localized modulation of the tumor microenvironment to promote systemic anticancer effect, as well as explore this approach for the delivery of other anticancer and antiviral nucleotides.

## 4.4 MATERIALS AND METHODS

### Materials and General Methods

Commercially available chemicals were utilized without purification and were of the highest quality available. Gemcitabine HCl (dFdC) was purchased from Carbosynth. Other chemical reagents were sourced from Sigma-Aldrich, Acros Organics, Oakwood Chemical, or Chem-Impex. N-methylimidazole, triethylamine, and pyridine were purchased from Sigma-Aldrich in sure-seal bottles as dry solvents. Bulk solvents were purchased from Fisher and were of HPLC quality. Flash chromatography as well as reverse phase separation were performed using a Teledyne Isco CombiFlash system. Analytical HPLC was performed using an Ultimate 3000 System (Agilent) and Higgins Analytical Targa C18 5 μm column. Mobile phase for analytical HPLC was 50 mM triethylammonium bicarbonate (TEAB) buffer and acetonitrile (30%-100% Acetonitrile). Low resolution Electrospray Ionization Mass Spectrometry (ESI-MS) was performed on an Agilent MSD SL system. Nuclear magnetic resonance imaging (NMR) of all compounds was performed at 25°C utilizing an Ascend 500 MHz Bruker spectrometer ($d_6$-DMSO or $D_2O$, Cambridge Isotope Laboratories). $^{31}P$ spectra were recorded with proton decoupling.

### Cryo-TEM

A 0.5% wt/vol of NAP-FF-GEM was prepared in Dulbecco's Phosphate Buffered Saline (DPBS). 3 μL of the NAP-FF-GEM solution was applied to a lacey Formvar/carbon grid (Ted Pella, Inc.; Cat: 01883) in the humidified chamber of a Vitrobot Mark IV (FEI). The samples were blotted and vitrification was achieved through rapid plunging into liquid ethane. Grids were imaged on a Tecnai Spirit G2 BioTWIN (FEI) equipped with an Eagle 2k CCD camera (FEI) under a high tension of 120 kV. Images were processed and analyzed in ImageJ using the TIA reader plugin.

**Small Angle X-ray Scattering (SAXS)**

Samples were prepared in either Millipore purified water or DPBS at the concentrations specified. Analysis was performed on a SAXSLAB Ganesha instrument with the sample contained within a sandwich cell holder sealed with Kapton film, equipped with a Pilatus detector enabling measurements in the WAXS, MAXS, and SAXS configurations with detector distances of 100, 450, and 1050 mm respectively. Experiments were performed with 50kV and 0.3 mA energy source. Corrections for transmission and incident x-ray beam were made and background scattering was subtracted from sample data by measuring buffer or water only sealed within sandwich cells. Fitting was performed in SASVIEW software with built in cylindrical form factor model.

**Nile Red Assay**

Solutions containing varying concentrations of NAP-FF-GEM and 50 μM Nile Red were made in Dulbecco's Phosphate Buffered Saline Solution, heated to dissolution, and cooled to room temperature. The samples were left in the dark for 24 h before measurement.

Solutions were analyzed on a Cary Eclipse Fluorimeter with excitation wavelength of 550 nm and emission scan from 600 to 670 nm. Nile red is a solvatochromic dye and its fluorescence is quenched in aqueous environments. Critical aggregation concentration was determined from solving for the cross-point for the two linear regions of the plot below and above the critical aggregation concentration.

**NAP-FF-GEM NMR Concentration Experiments**

Experiments were performed using a Bruker Avance 500 MHz NMR with data workup and analysis performed in Bruker TopSpin software. Samples were prepared in either $D_2O$ or $D_2O$ with 10 mM Sodium Phosphate and 50 mM NaCl. The phosphate buffered saline solution was prepared using both monobasic and dibasic phosphate salts to generate a solution with corresponding pD of 7.2. Phosphoramidates were dissolved at a concentration above the critical aggregation concentration and serially diluted to concentrations both above and below the anticipated CAC. MeCN was used as an internal standard to obtain relative integration values of the aromatic region of the phosphoramidate conjugates, the portion of the molecule which drives assembly.

**MTS Proliferation Assay**

Relative proliferation at 48 h of U87 human glioblastoma cells; MD-MB-231 human triple negative breast cancer cells; and H460 human non-small cell lung cancer cells were determined after treatment with NAP-FF-GEM (**8**), NAP-FF-CMP (**5**), and Gemcitabine (dFdC). Cancer cells were grown in 96 well plates overnight at a cell density of 5,000 cells per well after trypsinization from culture flask. The next day, media was removed and

replaced with the desired concentration of compound in Dulbecco's Modified Eagle Medium (Gibco) supplemented with 5% FBS and Pen/Strep (Gibco) antibiotic solution. Gemcitabine was added to media as a DMSO solution and the final concentration of DMSO in dosed and control wells was 0.4%. After 48 h, AQueous One MTS kit(Promega) was used to assess relative viability of control and dosed cells. Raw data was fitted in GraphPad Prism to a variable slope three parameter sigmoidal dose response inhibition model to obtain IC50s.

**Synthesis of NAP-FF-GEM (8)**

Compound 9: Gemcitabine HCl (1 gram, 3.3 mmol) was added to an oven dried round bottomed flask and suspended in a 50:50 mixture of hexamethyldisilazane and dioxane (20 mL). Catalytic ammonium sulfate (50 mg) was added, and the white suspension was subjected to reflux conditions for 4 hours. Over this time period, the white suspension transitioned to a clear solution. The reaction solution was cooled to room temperature and concentrated *via* rotary evaporation to a white residue with repeated co-evaporation with toluene. The resulting white solid was dissolved in anhydrous DCM and N-methylimidazole (836 μL, 1 mmol) and 4-nitrophenyl-(2-trimethylsilyl)ethyl carbonate (2.3 g, 8.3 mmol) were added to the solution which was stirred overnight at room temperature under $N_2$ atmosphere. The reaction solution was concentrated *via* rotary evaporation and resuspended in 20% TEA in MeOH (20 mL) and stirred for 1 hour. The solution was adsorbed onto silica and purified via flash chromatography to obtain compound 9, 80%. $C_{15}H_{23}F_2N_3O_6Si$. LRMS (ESI+) 408.1. $^1$H NMR spectrum (DMSO-$d_6$):

0.04 (s, 9H), 1.00 (m, 2H), 3.67 (m, 1H), 3.80 (dt, 1H), 3.88 (m, 1H), 4.21 (m, 3H), 5.29 (t, 1H), 6.16 (t, 1H), 6.30 (d, 1H), 7.10 (d, 1H), 8.20 (d, 1H), 10.82 (s, 1H).

Compound 10: Compound 9 (1.085 grams, 2.66 mmol) was dissolved in anhydrous pyridine (15 mL). To the clear solution was added dimethoxytrityl chloride (2.35 g, 7 mmol) and triethylamine (445 μL, 3.2 mmol). The solution was stirred at room temperature overnight under $N_2$ atmosphere. The next day, methanol was added to the reaction and allowed to stir for 1h. The clear yellow solution was concentrated to a yellow residue and purified by normal phase chromatography. (yield 1.85 grams, impurity gives over 100%). The obtained impure residue was dissolved (1.85 grams, assumed 2.66 mmol with impurity) in 50 mL of anhydrous DMF. To the clear solution was added 2.5 eq. of tert-butyldimethylsilyl chloride and 5 eq. of imidazole. Overnight stirring gave complete turnover of starting material. The solution was concentrated utilizing rotary evaporation and the residue was diluted in EtOAc and washed with sat. bicarb, brine, and water. The organic layer was dried over magnesium sulfate and adsorbed onto silica for normal phase chromatography. Product containing fractions were pooled dried to remove solvent, and then treated with 10% MeOH/DCM containing 5% dichloroacetic acid in 10 mL. The reaction was stirred for 6 hours and the solution was adsorbed onto silica and purified by flash chromatography to obtain compound 10, 73% over three steps. $C_{21}H_{37}F_2N_3O_6Si_2$. LRMS (ESI+) 522.2. $^1$H NMR spectrum (DMSO-$d_6$): 0.02 (s, 9H), 0.06 (s, 3H), 0.07 (s,3H), (d, 0.83 (s, 9H), 0.91 (q, 2H), 3.57 (m, 1H), 3.77 (d, 1H), 3.86 (m, 1H), 4.17 (t, 2H), 4.34 (q, 1H), 5.28 (d, 1H), 6.14 (t, 1H), 7.08 (d, 1H), 8.13 (d, 1H), 10.79 (s, 1H)

Compound 11: Compound 10 (1 gram, 1.9 mmol) was dissolved in pyridine (10 mL) and added to an ice-water cooled round bottomed flask containing phosphorous acid (474 mg, 5.8 mmol). Trimethylacetyl chloride (356 μL, 2.9 mmol) was added dropwise to the solution and warmed to room temperature. The solution was stirred overnight and concentrated to a yellow oil via rotary evaporation. The crude product was purified with reverse phase chromatography, 100%-0% 50 mM triethylamine bicarbonate (TEAB) buffer in MeCN to afford Compound 11, 80%. $C_{21}H_{38}F_2N_3O_8PSi_2$. LRMS (ESI-) 584.4. $^1$H NMR spectrum as TEA salt (DMSO-$d_6$): 0.04 (s, 9H), 0.10 (s, 3H), 0.13 (s, 3H), 0.88 (s, 9H), 1.00 (p, 2H), 1.16 (bs, 9H), 3.07 (bs, 6H), 3.80 (m, 1H), 3.99 (m, 2H), 4.22 (t, 2H), 4.40 (q, 1H), 6.06-7.20 (d, 1H), 6.18 (t, 1H), 7.09 (d, 1H), 8.38 (d, 1H), 9.35 (bs, 1H), 10.80 (s, 1H)

Compound 12: Compound 11 (1.033 grams, 1.5 mmol**)** was dissolved in 10 mL of pyridine and added to an oven dried round bottomed flask. The flask was fitted with septum and repeatedly evacuated and purged with nitrogen gas. To the clear solution was added 150 μL of (2-trimethylsilyl)ethanol (150, 1 mmol) followed by 250 uL of Trimethylacetyl chloride (2 eq., 2 mmol). The reaction stirred for 4 hours while monitoring consumption of alcohol by TLC. After consumption of alcohol, propargyl amine (240 μL, 5.6 mmol), carbon tetrachloride (150 μL, 2.25 mmol), and triethylamine (418 μL, 4.5 mmol) were added to the reaction solution. The yellow turbid solution stirred for one hour and was concentrated to a yellow residue. The residue was co-evaporated with toluene to remove residual pyridine and the resulting residue was purified by flash chromatography to obtain fully protected phosphoramidate, 38%. The fully protected phosphoramidate (422 mg,

0.57 mmol) was dissolved in anhydrous THF and added to a round bottomed flask, cooled with a water bath under $N_2$ atmosphere. To this solution was added TBAF (1 M in THF, 4.0 eq., 2.2 mL). The reaction mixture was stirred overnight and concentrated to a white residue. The residue was diluted with 1 M triethylammonium bicarbonate buffer and purified with reverse phase chromatography 100%-0% 50 mM triethylamine bicarbonate. The resulting salt was subjected to cation exchange with Dowex 50wx8 ($Na^+$ form) to yield Compound 13, 93%. $C_{12}H_{15}F_2N_4O_6P$. LRMS (ESI-) 379.4. $^1$H NMR ($D_2O$): 2.57 (d, 1H), 3.64 (dd, 2H), 4.13 (m, 1H), 4.21 (d, 1H), 4.28 (d, 1H), 4.51 (m, 1H) 6.14 (d, 1H), 6.27 (t, 1H), 7.91 (d, 1H). $^{31}$P NMR: ($D_2O$, proton decoupled) 7.87.

NAP-FF-GEM, Compound 8: A solution of Compound 12 (357 mg, 0.53 mmol) in dimethylsulfoxide (3 mL) and Compound 1 (139 mg, 0.35 mmol) in $H_2O$ (1.5 mL) were stirred in reaction vessel to create a homogenous suspension. The reaction vessel was purged with Argon and $CuSO_4 \cdot 5\ H_2O$ (9 mg, 0.035 mmol) and sodium ascorbate (14 mg, 0.07 mmol) were added to the suspension. The reaction vessel was covered to protect from light and stirred for 48 hours at room temperature. Upon reaction completion, the reaction solution was concentrated to a DMSO solution and purified via reverse phase chromatography (0-100% Acetonitrile in 50 mM triethylammonium bicarbonate buffer). Product containing fractions were pooled, lyophilized to powder, and purified via cation exchange with Dowex 50wx8 ($Na^+$ form). The synthesis of compound 1 was performed as previously reported.[244] The sodium salt was again purified through reverse phase chromatography to remove any extraneous salt (0-100% Acetonitrile in $H_2O$), 31%. LRMS

(ESI-) 1059.7. $C_{50}H_{58}F_2N_{10}O_{12}PNa$. $^{31}P$ NMR (DMSO-$d_6$) 6.59. $^{1}H$ NMR and HPLC chromatogram are located in **Appendices.**

## BIBLIOGRAPHY


(1) Balaban, A. T.; Klein, D. J. Is Chemistry "TheCentral Science"? How Are Different Sciences Related? Co-Citations,Reductionism, Emergence, and Posets. *Scientometrics* **2006**, *69* (3), 615–637. https://doi.org/10.1007/s11192-006-0173-2.

(2) Nicolaou, K. C. Organic Synthesis: The Art and Science of Replicating the Molecules of Living Nature and Creating Others like Them in the Laboratory. *Proc Math Phys Eng Sci* **2014**, *470* (2163). https://doi.org/10.1098/rspa.2013.0690.

(3) Bünzli, J.-C. G. Grand Challenges in Inorganic Chemistry: Toward Better Life Quality and a More Sustainable World. *Front Chem* **2013**, *1*. https://doi.org/10.3389/fchem.2013.00002.

(4) Katritzky, A. R.; Fara, D. C. How Chemical Structure Determines Physical, Chemical, and Technological Properties: An Overview Illustrating the Potential of Quantitative Structure−Property Relationships for Fuels Science. *Energy Fuels* **2005**, *19* (3), 922–935. https://doi.org/10.1021/ef040033q.

(5) Katritzky, A. R.; Kuanar, M.; Slavov, S.; Hall, C. D.; Karelson, M.; Kahn, I.; Dobchev, D. A. Quantitative Correlation of Physical and Chemical Properties with Chemical Structure: Utility for Prediction. *Chem. Rev.* **2010**, *110* (10), 5714–5789. https://doi.org/10.1021/cr900238d.

(6) Lehn, J.-M. Perspectives in Supramolecular Chemistry—From Molecular Recognition towards Molecular Information Processing and Self-Organization. *Angewandte Chemie International Edition in English* **1990**, *29* (11), 1304–1319. https://doi.org/10.1002/anie.199013041.

(7) Tkatchenko, A.; Alfè, D.; Kim, K. S. First-Principles Modeling of Non-Covalent Interactions in Supramolecular Systems: The Role of Many-Body Effects. *J. Chem. Theory Comput.* **2012**, *8* (11), 4317–4322. https://doi.org/10.1021/ct300711r.

(8) Whitesides, G. M.; Boncheva, M. Beyond Molecules: Self-Assembly of Mesoscopic and Macroscopic Components. *Proc Natl Acad Sci U S A* **2002**, *99* (8), 4769–4774. https://doi.org/10.1073/pnas.082065899.

(9) Amabilino, D. B.; Smith, D. K.; Steed, J. W. Supramolecular Materials. *Chem. Soc. Rev.* **2017**, *46* (9), 2404–2420. https://doi.org/10.1039/C7CS00163K.

(10) Safinya, C. R. Supramolecular Assembly of Biological Molecules. In *Forces, Growth and Form in Soft Condensed Matter: At the Interface between Physics and Biology*; Skjeltorp, A. T., Belushkin, A. V., Eds.; NATO Science Series II: Mathematics, Physics and Chemistry; Springer Netherlands, 2005; pp 29–50.

(11) Fyfe, M. C. T.; Stoddart, J. F. Synthetic Supramolecular Chemistry. *Acc. Chem. Res.* **1997**, *30* (10), 393–401. https://doi.org/10.1021/ar950199y.

(12) Webber, M. J.; Appel, E. A.; Meijer, E. W.; Langer, R. Supramolecular Biomaterials. *Nature Materials* **2016**, *15* (1), 13–26. https://doi.org/10.1038/nmat4474.

(13) Mann, J. L.; Yu, A. C.; Agmon, G.; Appel, E. A. Supramolecular Polymeric Biomaterials. *Biomater. Sci.* **2017**, *6* (1), 10–37. https://doi.org/10.1039/C7BM00780A.
(14) Biomaterials | National Institute of Biomedical Imaging and Bioengineering https://www.nibib.nih.gov/science-education/science-topics/biomaterials (accessed Jul 15, 2019).
(15) Kulinets, I. 1 - Biomaterials and Their Applications in Medicine. In *Regulatory Affairs for Biomaterials and Medical Devices*; Amato, S. F., Ezzell, R. M., Eds.; Woodhead Publishing Series in Biomaterials; Woodhead Publishing, 2015; pp 1–10. https://doi.org/10.1533/9780857099204.1.
(16) Hench, L. L.; Polak, J. M. Third-Generation Biomedical Materials. *Science* **2002**, *295* (5557), 1014–1017. https://doi.org/10.1126/science.1067404.
(17) Badeau, B. A.; DeForest, C. A. Programming Stimuli-Responsive Behavior into Biomaterials. *Annual Review of Biomedical Engineering* **2019**, *21* (1), 241–265. https://doi.org/10.1146/annurev-bioeng-060418-052324.
(18) Holzapfel, B. M.; Reichert, J. C.; Schantz, J.-T.; Gbureck, U.; Rackwitz, L.; Nöth, U.; Jakob, F.; Rudert, M.; Groll, J.; Hutmacher, D. W. How Smart Do Biomaterials Need to Be? A Translational Science and Clinical Point of View. *Advanced Drug Delivery Reviews* **2013**, *65* (4), 581–603. https://doi.org/10.1016/j.addr.2012.07.009.
(19) Williams, D. F. The Biomaterials Conundrum in Tissue Engineering. *Tissue Engineering Part A* **2014**, *20* (7–8), 1129–1131. https://doi.org/10.1089/ten.tea.2013.0769.
(20) Li, Y.; Wang, Y.; Huang, G.; Gao, J. Cooperativity Principles in Self-Assembled Nanomedicine. *Chem. Rev.* **2018**, *118* (11), 5359–5391. https://doi.org/10.1021/acs.chemrev.8b00195.
(21) Webber, M. J. Engineering Responsive Supramolecular Biomaterials: Toward Smart Therapeutics. *Bioeng Transl Med* **2016**, *1* (3), 252–266. https://doi.org/10.1002/btm2.10031.
(22) Shigemitsu, H.; Hamachi, I. Design Strategies of Stimuli-Responsive Supramolecular Hydrogels Relying on Structural Analyses and Cell-Mimicking Approaches. *Acc. Chem. Res.* **2017**, *50* (4), 740–750. https://doi.org/10.1021/acs.accounts.7b00070.
(23) Appel, E. A.; Biedermann, F.; Rauwald, U.; Jones, S. T.; Zayed, J. M.; Scherman, O. A. Supramolecular Cross-Linked Networks via Host−Guest Complexation with Cucurbit[8]Uril. *J. Am. Chem. Soc.* **2010**, *132* (40), 14251–14260. https://doi.org/10.1021/ja106362w.
(24) J. Wilson, A. Non-Covalent Polymer Assembly Using Arrays of Hydrogen-Bonds. *Soft Matter* **2007**, *3* (4), 409–425. https://doi.org/10.1039/B612566B.
(25) Tavenor, N. A.; Murnin, M. J.; Horne, W. S. Supramolecular Metal-Coordination Polymers, Nets, and Frameworks from Synthetic Coiled-Coil Peptides. *J. Am. Chem. Soc.* **2017**, *139* (6), 2212–2215. https://doi.org/10.1021/jacs.7b00651.

(26) Rose, S.; Prevoteau, A.; Elzière, P.; Hourdet, D.; Marcellan, A.; Leibler, L. Nanoparticle Solutions as Adhesives for Gels and Biological Tissues. *Nature* **2014**, *505* (7483), 382–385. https://doi.org/10.1038/nature12806.
(27) Appel, E. A.; Tibbitt, M. W.; Webber, M. J.; Mattix, B. A.; Veiseh, O.; Langer, R. Self-Assembled Hydrogels Utilizing Polymer–Nanoparticle Interactions. *Nature Communications* **2015**, *6*, 6295. https://doi.org/10.1038/ncomms7295.
(28) Du, X.; Zhou, J.; Shi, J.; Xu, B. Supramolecular Hydrogelators and Hydrogels: From Soft Matter to Molecular Biomaterials. *Chem. Rev.* **2015**, *115* (24), 13165–13307. https://doi.org/10.1021/acs.chemrev.5b00299.
(29) De Greef, T. F. A.; Smulders, M. M. J.; Wolffs, M.; Schenning, A. P. H. J.; Sijbesma, R. P.; Meijer, E. W. Supramolecular Polymerization. *Chem. Rev.* **2009**, *109* (11), 5687–5754. https://doi.org/10.1021/cr900181u.
(30) Wang, J.; Liu, K.; Xing, R.; Yan, X. Peptide Self-Assembly: Thermodynamics and Kinetics. *Chem. Soc. Rev.* **2016**, *45* (20), 5589–5604. https://doi.org/10.1039/C6CS00176A.
(31) Li, J.; Xing, R.; Bai, S.; Yan, X. Recent Advances of Self-Assembling Peptide-Based Hydrogels for Biomedical Applications. *Soft Matter* **2019**, *15* (8), 1704–1715. https://doi.org/10.1039/C8SM02573H.
(32) Hendricks, M. P.; Sato, K.; Palmer, L. C.; Stupp, S. I. Supramolecular Assembly of Peptide Amphiphiles. *Acc. Chem. Res.* **2017**, *50* (10), 2440–2448. https://doi.org/10.1021/acs.accounts.7b00297.
(33) Davis, M. E.; Hsieh, P. C. H.; Takahashi, T.; Song, Q.; Zhang, S.; Kamm, R. D.; Grodzinsky, A. J.; Anversa, P.; Lee, R. T. Local Myocardial Insulin-like Growth Factor 1 (IGF-1) Delivery with Biotinylated Peptide Nanofibers Improves Cell Therapy for Myocardial Infarction. *PNAS* **2006**, *103* (21), 8155–8160. https://doi.org/10.1073/pnas.0602877103.
(34) Baek, K.; Noblett, A. D.; Ren, P.; Suggs, L. J. Design and Characterization of Nucleopeptides for Hydrogel Self-Assembly. *ACS Appl. Bio Mater.* **2019**. https://doi.org/10.1021/acsabm.9b00229.
(35) Jang, Y.; Champion, J. A. Self-Assembled Materials Made from Functional Recombinant Proteins. *Acc. Chem. Res.* **2016**, *49* (10), 2188–2198. https://doi.org/10.1021/acs.accounts.6b00337.
(36) C. Edwards-Gayle, C. J.; W. Hamley, I. Self-Assembly of Bioactive Peptides, Peptide Conjugates, and Peptide Mimetic Materials. *Organic & Biomolecular Chemistry* **2017**, *15* (28), 5867–5876. https://doi.org/10.1039/C7OB01092C.
(37) Qi, G.-B.; Gao, Y.-J.; Wang, L.; Wang, H. Self-Assembled Peptide-Based Nanomaterials for Biomedical Imaging and Therapy. *Advanced Materials* **2018**, *30* (22), 1703444. https://doi.org/10.1002/adma.201703444.
(38) Sadtler, K.; Singh, A.; Wolf, M. T.; Wang, X.; Pardoll, D. M.; Elisseeff, J. H. Design, Clinical Translation and Immunological Response of Biomaterials in Regenerative Medicine. *Nature Reviews Materials* **2016**, *1* (7), 16040. https://doi.org/10.1038/natrevmats.2016.40.

(39) Hainline, K. M.; Fries, C. N.; Collier, J. H. Progress towards the Clinical Translation of Bio-Inspired Peptide and Protein Assemblies. *Adv Healthc Mater* **2018**, *7* (5). https://doi.org/10.1002/adhm.201700930.
(40) Acar, H.; Srivastava, S.; Chung, E. J.; Schnorenberg, M. R.; Barrett, J. C.; LaBelle, J. L.; Tirrell, M. Self-Assembling Peptide-Based Building Blocks in Medical Applications. *Advanced Drug Delivery Reviews* **2017**, *110–111*, 65–79. https://doi.org/10.1016/j.addr.2016.08.006.
(41) Rad-Malekshahi, M.; Lempsink, L.; Amidi, M.; Hennink, W. E.; Mastrobattista, E. Biomedical Applications of Self-Assembling Peptides. *Bioconjugate Chem.* **2016**, *27* (1), 3–18. https://doi.org/10.1021/acs.bioconjchem.5b00487.
(42) Tibbitt, M. W.; Rodell, C. B.; Burdick, J. A.; Anseth, K. S. Progress in Material Design for Biomedical Applications. *PNAS* **2015**, *112* (47), 14444–14451. https://doi.org/10.1073/pnas.1516247112.
(43) Thomas Pashuck, E. Synthesis of Self-Assembling Peptide-Based Hydrogels for Regenerative Medicine Using Solid-Phase Peptide Synthesis. *Methods Mol. Biol.* **2018**, *1758*, 177–192. https://doi.org/10.1007/978-1-4939-7741-3_14.
(44) Mora-Solano, C.; Wen, Y.; Han, H.; Chen, J.; Chong, A. S.; Miller, M. L.; Pompano, R. R.; Collier, J. H. Active Immunotherapy for TNF-Mediated Inflammation Using Self-Assembled Peptide Nanofibers. *Biomaterials* **2017**, *149*, 1–11. https://doi.org/10.1016/j.biomaterials.2017.09.031.
(45) Wu, Y.; Norberg, P. K.; Reap, E. A.; Congdon, K. L.; Fries, C. N.; Kelly, S. H.; Sampson, J. H.; Conticello, V. P.; Collier, J. H. A Supramolecular Vaccine Platform Based on α-Helical Peptide Nanofibers. *ACS Biomater. Sci. Eng.* **2017**, *3* (12), 3128–3132. https://doi.org/10.1021/acsbiomaterials.7b00561.
(46) Chung, E. J.; Mlinar, L. B.; Sugimoto, M. J.; Nord, K.; Roman, B. B.; Tirrell, M. In Vivo Biodistribution and Clearance of Peptide Amphiphile Micelles. *Nanomedicine* **2015**, *11* (2), 479–487. https://doi.org/10.1016/j.nano.2014.08.006.
(47) J. Webber, M.; Langer, R. Drug Delivery by Supramolecular Design. *Chemical Society Reviews* **2017**, *46* (21), 6600–6620. https://doi.org/10.1039/C7CS00391A.
(48) J. Skilling, K.; Citossi, F.; D. Bradshaw, T.; Ashford, M.; Kellam, B.; Marlow, M. Insights into Low Molecular Mass Organic Gelators: A Focus on Drug Delivery and Tissue Engineering Applications. *Soft Matter* **2014**, *10* (2), 237–256. https://doi.org/10.1039/C3SM52244J.
(49) Zhang, S. Discovery and Design of Self-Assembling Peptides. *Interface Focus* **2017**, *7* (6). https://doi.org/10.1098/rsfs.2017.0028.
(50) Etheridge, M. L.; Campbell, S. A.; Erdman, A. G.; Haynes, C. L.; Wolf, S. M.; McCullough, J. The Big Picture on Nanomedicine: The State of Investigational and Approved Nanomedicine Products. *Nanomedicine* **2013**, *9* (1), 1–14. https://doi.org/10.1016/j.nano.2012.05.013.
(51) Min, Y.; Caster, J. M.; Eblan, M. J.; Wang, A. Z. Clinical Translation of Nanomedicine. *Chem. Rev.* **2015**, *115* (19), 11147–11190. https://doi.org/10.1021/acs.chemrev.5b00116.

(52) Zhang, S.; Holmes, T.; Lockshin, C.; Rich, A. Spontaneous Assembly of a Self-Complementary Oligopeptide to Form a Stable Macroscopic Membrane. *Proc Natl Acad Sci U S A* **1993**, *90* (8), 3334–3338.
(53) Du, X.; Zhou, J.; Li, X.; Xu, B. Self-Assembly of Nucleopeptides to Interact with DNAs. *Interface Focus* **2017**, *7* (6). https://doi.org/10.1098/rsfs.2016.0116.
(54) Caplan, M. R.; Schwartzfarb, E. M.; Zhang, S.; Kamm, R. D.; Lauffenburger, D. A. Control of Self-Assembling Oligopeptide Matrix Formation through Systematic Variation of Amino Acid Sequence. *Biomaterials* **2002**, *23* (1), 219–227. https://doi.org/10.1016/S0142-9612(01)00099-0.
(55) Cormier, A. R.; Pang, X.; Zimmerman, M. I.; Zhou, H.-X.; Paravastu, A. K. Molecular Structure of RADA16-I Designer Self-Assembling Peptide Nanofibers. *ACS Nano* **2013**, *7* (9), 7562–7572. https://doi.org/10.1021/nn401562f.
(56) Lee, M. F.; Ma, Z.; Ananda, A. A Novel Haemostatic Agent Based on Self-Assembling Peptides in the Setting of Nasal Endoscopic Surgery, a Case Series. *Int J Surg Case Rep* **2017**, *41*, 461–464. https://doi.org/10.1016/j.ijscr.2017.11.024.
(57) Pioche, M.; Camus, M.; Rivory, J.; Leblanc, S.; Lienhart, I.; Barret, M.; Chaussade, S.; Saurin, J.-C.; Prat, F.; Ponchon, T. A Self-Assembling Matrix-Forming Gel Can Be Easily and Safely Applied to Prevent Delayed Bleeding after Endoscopic Resections. *Endosc Int Open* **2016**, *4* (4), E415-419. https://doi.org/10.1055/s-0042-102879.
(58) Masuhara, H.; Fujii, T.; Watanabe, Y.; Koyama, N.; Tokuhiro, K. Novel Infectious Agent-Free Hemostatic Material (TDM-621) in Cardiovascular Surgery. *Ann Thorac Cardiovasc Surg* **2012**, *18* (5), 444–451.
(59) Aggeli, A.; Boden, N.; Cheng, Y.-L.; Findlay, J. B. C.; Knowles, P. F.; Kovatchev, P.; Turnbull, P. J. H.; Horváth, L.; Marsh, D. Peptides Modeled on the Transmembrane Region of the Slow Voltage-Gated IsK Potassium Channel: Structural Characterization of Peptide Assemblies in the β-Strand Conformation. *Biochemistry* **1996**, *35* (50), 16213–16221. https://doi.org/10.1021/bi960891g.
(60) Aggeli, A.; Bell, M.; Boden, N.; Keen, J. N.; Knowles, P. F.; McLeish, T. C.; Pitkeathly, M.; Radford, S. E. Responsive Gels Formed by the Spontaneous Self-Assembly of Peptides into Polymeric Beta-Sheet Tapes. *Nature* **1997**, *386* (6622), 259–262. https://doi.org/10.1038/386259a0.
(61) Aggeli, A.; Bell, M.; Carrick, L. M.; Fishwick, C. W. G.; Harding, R.; Mawer, P. J.; Radford, S. E.; Strong, A. E.; Boden, N. PH as a Trigger of Peptide β-Sheet Self-Assembly and Reversible Switching between Nematic and Isotropic Phases. *J. Am. Chem. Soc.* **2003**, *125* (32), 9619–9628. https://doi.org/10.1021/ja021047i.
(62) Brunton, P. A.; Davies, R. P. W.; Burke, J. L.; Smith, A.; Aggeli, A.; Brookes, S. J.; Kirkham, J. Treatment of Early Caries Lesions Using Biomimetic Self-Assembling Peptides – a Clinical Safety Trial. *British Dental Journal* **2013**, *215* (4), E6–E6. https://doi.org/10.1038/sj.bdj.2013.741.
(63) Kirkham, J.; Firth, A.; Vernals, D.; Boden, N.; Robinson, C.; Shore, R. C.; Brookes, S. J.; Aggeli, A. Self-Assembling Peptide Scaffolds Promote Enamel

Remineralization. *J Dent Res* **2007**, *86* (5), 426–430. https://doi.org/10.1177/154405910708600507.
(64) Cheng, L.; Jiang, Y.; Hu, Y.; Li, J.; Xu, H. H. K.; He, L.; Ren, B.; Zhou, X. Biomaterials in Caries Prevention and Treatment. In *Interface Oral Health Science 2016*; Sasaki, K., Suzuki, O., Takahashi, N., Eds.; Springer Singapore, 2017; pp 101–110.
(65) Paine, M. L.; Snead, M. L. Protein Interactions during Assembly of the Enamel Organic Extracellular Matrix. *J. Bone Miner. Res.* **1997**, *12* (2), 221–227. https://doi.org/10.1359/jbmr.1997.12.2.221.
(66) Schlee, M.; Schad, T.; Koch, J. H.; Cattin, P. C.; Rathe, F. Clinical Performance of Self-Assembling Peptide P11-4 in the Treatment of Initial Proximal Carious Lesions: A Practice-Based Case Series. *Journal of Investigative and Clinical Dentistry* **2018**, *9* (1), e12286. https://doi.org/10.1111/jicd.12286.
(67) Ceci, M.; Mirando, M.; Beltrami, R.; Chiesa, M.; Colombo, M.; Poggio, C. Effect of Self-Assembling Peptide P11-4 on Enamel Erosion: AFM and SEM Studies. *Scanning* **2016**, *38* (4), 344–351. https://doi.org/10.1002/sca.21276.
(68) Bowerman, C. J.; Nilsson, B. L. Review Self-Assembly of Amphipathic β-Sheet Peptides: Insights and Applications. *Peptide Science* **2012**, *98* (3), 169–184. https://doi.org/10.1002/bip.22058.
(69) Kim, S.; Kim, J. H.; Lee, J. S.; Park, C. B. Beta-Sheet-Forming, Self-Assembled Peptide Nanomaterials towards Optical, Energy, and Healthcare Applications. *Small* **2015**, *11* (30), 3623–3640. https://doi.org/10.1002/smll.201500169.
(70) Rajagopal, K.; Schneider, J. P. Self-Assembling Peptides and Proteins for Nanotechnological Applications. *Current Opinion in Structural Biology* **2004**, *14* (4), 480–486. https://doi.org/10.1016/j.sbi.2004.06.006.
(71) Hutchinson, J. A.; Burholt, S.; Hamley, I. W. Peptide Hormones and Lipopeptides: From Self-assembly to Therapeutic Applications. *J Pept Sci* **2017**, *23* (2), 82–94. https://doi.org/10.1002/psc.2954.
(72) Caplan, M. R.; Moore, P. N.; Zhang, S.; Kamm, R. D.; Lauffenburger, D. A. Self-Assembly of a β-Sheet Protein Governed by Relief of Electrostatic Repulsion Relative to van Der Waals Attraction. *Biomacromolecules* **2000**, *1* (4), 627–631. https://doi.org/10.1021/bm005586w.
(73) Lee, H.; Dehez, F.; Chipot, C.; Lim, H.-K.; Kim, H. Enthalpy–Entropy Interplay in π-Stacking Interaction of Benzene Dimer in Water. *J. Chem. Theory Comput.* **2019**, *15* (3), 1538–1545. https://doi.org/10.1021/acs.jctc.8b00880.
(74) Anand, U.; Mukherjee, M. Exploring the Self-Assembly of a Short Aromatic Aβ(16–24) Peptide. *Langmuir* **2013**, *29* (8), 2713–2721. https://doi.org/10.1021/la304585a.
(75) Timur Senguen, F.; R. Lee, N.; Gu, X.; M. Ryan, D.; M. Doran, T.; A. Anderson, E.; L. Nilsson, B. Probing Aromatic, Hydrophobic, and Steric Effects on the Self-Assembly of an Amyloid-β Fragment Peptide. *Molecular BioSystems* **2011**, *7* (2), 486–496. https://doi.org/10.1039/C0MB00080A.

(76) Castelletto, V.; Ryumin, P.; Cramer, R.; Hamley, I. W.; Taylor, M.; Allsop, D.; Reza, M.; Ruokolainen, J.; Arnold, T.; Hermida-Merino, D.; et al. Self-Assembly and Anti-Amyloid Cytotoxicity Activity of Amyloid Beta Peptide Derivatives. *Scientific Reports* **2017**, *7*, 43637. https://doi.org/10.1038/srep43637.
(77) Brahmachari, S.; Arnon, Z. A.; Frydman-Marom, A.; Gazit, E.; Adler-Abramovich, L. Diphenylalanine as a Reductionist Model for the Mechanistic Characterization of β-Amyloid Modulators. *ACS Nano* **2017**, *11* (6), 5960–5969. https://doi.org/10.1021/acsnano.7b01662.
(78) Davies, R. P. W.; Liu, B.; Maude, S.; Carrick, L. M.; Nyrkova, I.; McLeish, T. C.; Harris, S. A. Peptide Strand Length Controls the Energetics of Self-Assembly and Morphology of β-Sheet Fibrils. *Peptide Science* **2018**, *110* (1), e23073. https://doi.org/10.1002/bip.23073.
(79) Marini, D. M.; Hwang, W.; Lauffenburger, D. A.; Zhang, S.; Kamm, R. D. Left-Handed Helical Ribbon Intermediates in the Self-Assembly of a β-Sheet Peptide. *Nano Lett.* **2002**, *2* (4), 295–299. https://doi.org/10.1021/nl015697g.
(80) Buchner, G. S.; Kubelka, J. Isotope-Edited Infrared Spectroscopy. *Methods Mol. Biol.* **2012**, *895*, 347–358. https://doi.org/10.1007/978-1-61779-927-3_20.
(81) Sawaya, M. R.; Sambashivan, S.; Nelson, R.; Ivanova, M. I.; Sievers, S. A.; Apostol, M. I.; Thompson, M. J.; Balbirnie, M.; Wiltzius, J. J. W.; McFarlane, H. T.; et al. Atomic Structures of Amyloid Cross-β Spines Reveal Varied Steric Zippers. *Nature* **2007**, *447* (7143), 453–457. https://doi.org/10.1038/nature05695.
(82) Berryman, J. T.; Radford, S. E.; Harris, S. A. Systematic Examination of Polymorphism in Amyloid Fibrils by Molecular-Dynamics Simulation. *Biophysical Journal* **2011**, *100* (9), 2234–2242. https://doi.org/10.1016/j.bpj.2011.02.060.
(83) Verel, R.; Tomka, I. T.; Bertozzi, C.; Cadalbert, R.; Kammerer, R. A.; Steinmetz, M. O.; Meier, B. H. Polymorphism in an Amyloid-Like Fibril-Forming Model Peptide. *Angewandte Chemie International Edition* **2008**, *47* (31), 5842–5845. https://doi.org/10.1002/anie.200800021.
(84) Miller, Y.; Ma, B.; Nussinov, R. Zinc Ions Promote Alzheimer Aβ Aggregation via Population Shift of Polymorphic States. *PNAS* **2010**, *107* (21), 9490–9495. https://doi.org/10.1073/pnas.0913114107.
(85) Reches, M.; Gazit, E. Casting Metal Nanowires Within Discrete Self-Assembled Peptide Nanotubes. *Science* **2003**, *300* (5619), 625–627. https://doi.org/10.1126/science.1082387.
(86) Görbitz, C. H. Nanotube Formation by Hydrophobic Dipeptides. *Chemistry – A European Journal* **2001**, *7* (23), 5153–5159. https://doi.org/10.1002/1521-3765(20011203)7:23<5153::AID-CHEM5153>3.0.CO;2-N.
(87) Tamamis, P.; Adler-Abramovich, L.; Reches, M.; Marshall, K.; Sikorski, P.; Serpell, L.; Gazit, E.; Archontis, G. Self-Assembly of Phenylalanine Oligopeptides: Insights from Experiments and Simulations. *Biophysical Journal* **2009**, *96* (12), 5020–5029. https://doi.org/10.1016/j.bpj.2009.03.026.

(88) Chelli, R.; Gervasio, F. L.; Procacci, P.; Schettino, V. Stacking and T-Shape Competition in Aromatic−Aromatic Amino Acid Interactions. *J. Am. Chem. Soc.* **2002**, *124* (21), 6133–6143. https://doi.org/10.1021/ja0121639.
(89) Rutledge, L. R.; Wetmore, S. D. Remarkably Strong T-Shaped Interactions between Aromatic Amino Acids and Adenine: Their Increase upon Nucleobase Methylation and a Comparison to Stacking. *J. Chem. Theory Comput.* **2008**, *4* (10), 1768–1780. https://doi.org/10.1021/ct8002332.
(90) Jeon, J.; Mills, C. E.; Shell, M. S. Molecular Insights into Diphenylalanine Nanotube Assembly: All-Atom Simulations of Oligomerization. *J. Phys. Chem. B* **2013**, *117* (15), 3935–3943. https://doi.org/10.1021/jp308280d.
(91) Reches, M.; Gazit, E. Self-Assembly of Peptide Nanotubes and Amyloid-like Structures by Charged-Termini-Capped Diphenylalanine Peptide Analogues. *Israel Journal of Chemistry* **2005**, *45* (3), 363–371. https://doi.org/10.1560/5MC0-V3DX-KE0B-YF3J.
(92) Mahler, A.; Reches, M.; Rechter, M.; Cohen, S.; Gazit, E. Rigid, Self-Assembled Hydrogel Composed of a Modified Aromatic Dipeptide. *Advanced Materials* **2006**, *18* (11), 1365–1370. https://doi.org/10.1002/adma.200501765.
(93) Yang, Z.; Gu, H.; Zhang, Y.; Wang, L.; Xu, B. Small Molecule Hydrogels Based on a Class of Antiinflammatory Agents. *Chem. Commun.* **2004**, *0* (2), 208–209. https://doi.org/10.1039/B310574A.
(94) Jayawarna, V.; Ali, M.; Jowitt, T. A.; Miller, A. F.; Saiani, A.; Gough, J. E.; Ulijn, R. V. Nanostructured Hydrogels for Three-Dimensional Cell Culture Through Self-Assembly of Fluorenylmethoxycarbonyl–Dipeptides. *Advanced Materials* **2006**, *18* (5), 611–614. https://doi.org/10.1002/adma.200501522.
(95) M. Palomo, J. Solid-Phase Peptide Synthesis: An Overview Focused on the Preparation of Biologically Relevant Peptides. *RSC Advances* **2014**, *4* (62), 32658–32672. https://doi.org/10.1039/C4RA02458C.
(96) Isidro-Llobet, A.; Álvarez, M.; Albericio, F. Amino Acid-Protecting Groups. *Chem. Rev.* **2009**, *109* (6), 2455–2504. https://doi.org/10.1021/cr800323s.
(97) Smith, A. M.; Williams, R. J.; Tang, C.; Coppo, P.; Collins, R. F.; Turner, M. L.; Saiani, A.; Ulijn, R. V. Fmoc-Diphenylalanine Self Assembles to a Hydrogel via a Novel Architecture Based on π–π Interlocked β-Sheets. *Advanced Materials* **2008**, *20* (1), 37–41. https://doi.org/10.1002/adma.200701221.
(98) Raeburn, J.; Pont, G.; Chen, L.; Cesbron, Y.; Lévy, R.; Adams, D. J. Fmoc-Diphenylalanine Hydrogels: Understanding the Variability in Reported Mechanical Properties. *Soft Matter* **2012**, *8* (4), 1168–1174. https://doi.org/10.1039/C1SM06929B.
(99) Ulijn, R. V.; Moore, B. D.; Janssen, A. E. M.; Halling, P. J. A Single Aqueous Reference Equilibrium Constant for Amide Synthesis–Hydrolysis. *J. Chem. Soc., Perkin Trans. 2* **2002**, *0* (5), 1024–1028. https://doi.org/10.1039/B108041E.
(100) Tang, C.; Smith, A. M.; Collins, R. F.; Ulijn, R. V.; Saiani, A. Fmoc-Diphenylalanine Self-Assembly Mechanism Induces Apparent PKa Shifts. *Langmuir* **2009**, *25* (16), 9447–9453. https://doi.org/10.1021/la900653q.

(101) Chen, L.; Morris, K.; Laybourn, A.; Elias, D.; Hicks, M. R.; Rodger, A.; Serpell, L.; Adams, D. J. Self-Assembly Mechanism for a Naphthalene−Dipeptide Leading to Hydrogelation. *Langmuir* **2010**, *26* (7), 5232–5242. https://doi.org/10.1021/la903694a.
(102) Yang, Z.; Liang, G.; Ma, M.; Gao, Y.; Xu, B. Conjugates of Naphthalene and Dipeptides Produce Molecular Hydrogelators with High Efficiency of Hydrogelation and Superhelical Nanofibers. *J. Mater. Chem.* **2007**, *17* (9), 850–854. https://doi.org/10.1039/B611255B.
(103) Adams, D. J.; Butler, M. F.; Frith, W. J.; Kirkland, M.; Mullen, L.; Sanderson, P. A New Method for Maintaining Homogeneity during Liquid–Hydrogel Transitions Using Low Molecular Weight Hydrogelators. *Soft Matter* **2009**, *5* (9), 1856–1862. https://doi.org/10.1039/B901556F.
(104) Tena-Solsona, M.; Escuder, B.; Miravet, J. F.; Casttelleto, V.; Hamley, I. W.; Dehsorkhi, A. Thermodynamic and Kinetic Study of the Fibrillization of a Family of Tetrapeptides and Its Application to Self-Sorting. What Takes So Long? *Chem. Mater.* **2015**, *27* (9), 3358–3365. https://doi.org/10.1021/acs.chemmater.5b00580.
(105) Ramos Sasselli, I.; Halling, P. J.; Ulijn, R. V.; Tuttle, T. Supramolecular Fibers in Gels Can Be at Thermodynamic Equilibrium: A Simple Packing Model Reveals Preferential Fibril Formation versus Crystallization. *ACS Nano* **2016**, *10* (2), 2661–2668. https://doi.org/10.1021/acsnano.5b07690.
(106) Houton, K. A.; Morris, K. L.; Chen, L.; Schmidtmann, M.; Jones, J. T. A.; Serpell, L. C.; Lloyd, G. O.; Adams, D. J. On Crystal versus Fiber Formation in Dipeptide Hydrogelator Systems. *Langmuir* **2012**, *28* (25), 9797–9806. https://doi.org/10.1021/la301371q.
(107) Orbach, R.; Mironi-Harpaz, I.; Adler-Abramovich, L.; Mossou, E.; Mitchell, E. P.; Forsyth, V. T.; Gazit, E.; Seliktar, D. The Rheological and Structural Properties of Fmoc-Peptide-Based Hydrogels: The Effect of Aromatic Molecular Architecture on Self-Assembly and Physical Characteristics. *Langmuir* **2012**, *28* (4), 2015–2022. https://doi.org/10.1021/la204426q.
(108) Ma, M.; Kuang, Y.; Gao, Y.; Zhang, Y.; Gao, P.; Xu, B. Aromatic−Aromatic Interactions Induce the Self-Assembly of Pentapeptidic Derivatives in Water To Form Nanofibers and Supramolecular Hydrogels. *J. Am. Chem. Soc.* **2010**, *132* (8), 2719–2728. https://doi.org/10.1021/ja9088764.
(109) Carr, C.; Tyler, A. N.; Cohen, J. B. Myristic Acid Is the NH2-Terminal Blocking Group of the 43-KDa Protein of Torpedo Nicotinic Post-Synaptic Membranes. *FEBS Lett.* **1989**, *243* (1), 65–69.
(110) Thompson, N. L.; Brian, A. A.; McConnell, H. M. Covalent Linkage of a Synthetic Peptide to a Fluorescent Phospholipid and Its Incorporation into Supported Phospholipid Monolayers. *Biochimica et Biophysica Acta (BBA) - Biomembranes* **1984**, *772* (1), 10–19. https://doi.org/10.1016/0005-2736(84)90512-1.
(111) Berndt, P.; Fields, G. B.; Tirrell, M. Synthetic Lipidation of Peptides and Amino Acids: Monolayer Structure and Properties. *J. Am. Chem. Soc.* **1995**, *117* (37), 9515–9522. https://doi.org/10.1021/ja00142a019.

(112) Hartgerink, J. D.; Beniash, E.; Stupp, S. I. Self-Assembly and Mineralization of Peptide-Amphiphile Nanofibers. *Science* **2001**, *294* (5547), 1684–1688. https://doi.org/10.1126/science.1063187.
(113) Traub, W.; Arad, T.; Weiner, S. Three-Dimensional Ordered Distribution of Crystals in Turkey Tendon Collagen Fibers. *PNAS* **1989**, *86* (24), 9822–9826. https://doi.org/10.1073/pnas.86.24.9822.
(114) George, A.; Bannon, L.; Sabsay, B.; Dillon, J. W.; Malone, J.; Veis, A.; Jenkins, N. A.; Gilbert, D. J.; Copeland, N. G. The Carboxyl-Terminal Domain of Phosphophoryn Contains Unique Extended Triplet Amino Acid Repeat Sequences Forming Ordered Carboxyl-Phosphate Interaction Ridges That May Be Essential in the Biomineralization Process. *J. Biol. Chem.* **1996**, *271* (51), 32869–32873. https://doi.org/10.1074/jbc.271.51.32869.
(115) Pierschbacher, M. D.; Ruoslahti, E. Cell Attachment Activity of Fibronectin Can Be Duplicated by Small Synthetic Fragments of the Molecule. *Nature* **1984**, *309* (5963), 30. https://doi.org/10.1038/309030a0.
(116) Korevaar, P. A.; Newcomb, C. J.; Meijer, E. W.; Stupp, S. I. Pathway Selection in Peptide Amphiphile Assembly. *J. Am. Chem. Soc.* **2014**, *136* (24), 8540–8543. https://doi.org/10.1021/ja503882s.
(117) Tantakitti, F.; Boekhoven, J.; Wang, X.; Kazantsev, R. V.; Yu, T.; Li, J.; Zhuang, E.; Zandi, R.; Ortony, J. H.; Newcomb, C. J.; et al. Energy Landscapes and Functions of Supramolecular Systems. *Nature Materials* **2016**, *15* (4), 469–476. https://doi.org/10.1038/nmat4538.
(118) Mallamace, F.; Corsaro, C.; Mallamace, D.; Vasi, S.; Vasi, C.; Baglioni, P.; Buldyrev, S. V.; Chen, S.-H.; Stanley, H. E. Energy Landscape in Protein Folding and Unfolding. *PNAS* **2016**, *113* (12), 3159–3163. https://doi.org/10.1073/pnas.1524864113.
(119) Ortony, J. H.; Newcomb, C. J.; Matson, J. B.; Palmer, L. C.; Doan, P. E.; Hoffman, B. M.; Stupp, S. I. Internal Dynamics of a Supramolecular Nanofibre. *Nature Materials* **2014**, *13* (8), 812–816. https://doi.org/10.1038/nmat3979.
(120) da Silva, R. M. P.; van der Zwaag, D.; Albertazzi, L.; Lee, S. S.; Meijer, E. W.; Stupp, S. I. Super-Resolution Microscopy Reveals Structural Diversity in Molecular Exchange among Peptide Amphiphile Nanofibres. *Nature Communications* **2016**, *7*, 11561. https://doi.org/10.1038/ncomms11561.
(121) Xu, J.; Ma, H.; Liu, Y. Stochastic Optical Reconstruction Microscopy (STORM). *Curr Protoc Cytom* **2017**, *81*, 12.46.1-12.46.27. https://doi.org/10.1002/cpcy.23.
(122) Paramonov, S. E.; Jun, H.-W.; Hartgerink, J. D. Self-Assembly of Peptide−Amphiphile Nanofibers: The Roles of Hydrogen Bonding and Amphiphilic Packing. *J. Am. Chem. Soc.* **2006**, *128* (22), 7291–7298. https://doi.org/10.1021/ja060573x.
(123) Kaiser, E. T.; Kézdy, F. J. Secondary Structures of Proteins and Peptides in Amphiphilic Environments. (A Review). *PNAS* **1983**, *80* (4), 1137–1143. https://doi.org/10.1073/pnas.80.4.1137.

(124) Kaiser, E. T.; Kézdy, F. J. Amphiphilic Secondary Structure: Design of Peptide Hormones. *Science* **1984**, *223* (4633), 249–255. https://doi.org/10.1126/science.6322295.
(125) Velichko, Y. S.; Stupp, S. I.; de la Cruz, M. O. Molecular Simulation Study of Peptide Amphiphile Self-Assembly. *J. Phys. Chem. B* **2008**, *112* (8), 2326–2334. https://doi.org/10.1021/jp074420n.
(126) Brizard, A.; Dolain, C.; Huc, I.; Oda, R. Asp-Gly Based Peptides Confined at the Surface of Cationic Gemini Surfactant Aggregates. *Langmuir* **2006**, *22* (8), 3591–3600. https://doi.org/10.1021/la053516a.
(127) Miravet, J. F.; Escuder, B.; Segarra-Maset, M. D.; Tena-Solsona, M.; Hamley, I. W.; Dehsorkhi, A.; Castelletto, V. Self-Assembly of a Peptide Amphiphile: Transition from Nanotape Fibrils to Micelles. *Soft Matter* **2013**, *9* (13), 3558–3564. https://doi.org/10.1039/C3SM27899A.
(128) Tsonchev, S.; Niece, K. L.; Schatz, G. C.; Ratner, M. A.; Stupp, S. I. Phase Diagram for Assembly of Biologically-Active Peptide Amphiphiles. *J. Phys. Chem. B* **2008**, *112* (2), 441–447. https://doi.org/10.1021/jp076273z.
(129) Ulery, B. D.; Nair, L. S.; Laurencin, C. T. Biomedical Applications of Biodegradable Polymers. *J Polym Sci B Polym Phys* **2011**, *49* (12), 832–864. https://doi.org/10.1002/polb.22259.
(130) Law, B.; Weissleder, R.; Tung, C.-H. Peptide-Based Biomaterials for Protease-Enhanced Drug Delivery. *Biomacromolecules* **2006**, *7* (4), 1261–1265. https://doi.org/10.1021/bm050920f.
(131) West, J. L.; Hubbell, J. A. Polymeric Biomaterials with Degradation Sites for Proteases Involved in Cell Migration. *Macromolecules* **1999**, *32* (1), 241–244. https://doi.org/10.1021/ma981296k.
(132) Collier, J. H.; Segura, T. Evolving the Use of Peptides as Biomaterials Components. *Biomaterials* **2011**, *32* (18), 4198–4204. https://doi.org/10.1016/j.biomaterials.2011.02.030.
(133) Swanekamp, R. J.; Welch, J. J.; Nilsson, B. L. Proteolytic Stability of Amphipathic Peptide Hydrogels Composed of Self-Assembled Pleated β-Sheet or Coassembled Rippled β-Sheet Fibrils. *Chem. Commun.* **2014**, *50* (70), 10133–10136. https://doi.org/10.1039/C4CC04644G.
(134) Giano, M. C.; Pochan, D. J.; Schneider, J. P. Controlled Biodegradation of Self-Assembling β-Hairpin Peptide Hydrogels by Proteolysis with Matrix Metalloproteinase-13. *Biomaterials* **2011**, *32* (27), 6471–6477. https://doi.org/10.1016/j.biomaterials.2011.05.052.
(135) Gefen, T.; Vaya, J.; Khatib, S.; Rapoport, I.; Lupo, M.; Barnea, E.; Admon, A.; Heller, E. D.; Aizenshtein, E.; Pitcovski, J. The Effect of Haptens on Protein-Carrier Immunogenicity. *Immunology* **2015**, *144* (1), 116–126. https://doi.org/10.1111/imm.12356.
(136) Holmes, T. C.; Lacalle, S. de; Su, X.; Liu, G.; Rich, A.; Zhang, S. Extensive Neurite Outgrowth and Active Synapse Formation on Self-Assembling Peptide

Scaffolds. *PNAS* **2000**, *97* (12), 6728–6733. https://doi.org/10.1073/pnas.97.12.6728.
(137) Webber, M. J.; Stupp, S. I. Emerging Peptide Nanomedicine to Regenerate Tissues and Organs. *J Intern Med* **2010**, *267* (1), 71–88. https://doi.org/10.1111/j.1365-2796.2009.02184.x.
(138) Silva, G. A.; Czeisler, C.; Niece, K. L.; Beniash, E.; Harrington, D. A.; Kessler, J. A.; Stupp, S. I. Selective Differentiation of Neural Progenitor Cells by High-Epitope Density Nanofibers. *Science* **2004**, *303* (5662), 1352–1355. https://doi.org/10.1126/science.1093783.
(139) Hsieh, P. C. H.; Davis, M. E.; Gannon, J.; MacGillivray, C.; Lee, R. T. Controlled Delivery of PDGF-BB for Myocardial Protection Using Injectable Self-Assembling Peptide Nanofibers. *J Clin Invest* **2006**, *116* (1), 237–248. https://doi.org/10.1172/JCI25878.
(140) Jung, J. P.; Nagaraj, A. K.; Fox, E. K.; Rudra, J. S.; Devgun, J. M.; Collier, J. H. Co-Assembling Peptides as Defined Matrices for Endothelial Cells. *Biomaterials* **2009**, *30* (12), 2400–2410. https://doi.org/10.1016/j.biomaterials.2009.01.033.
(141) Yano, A.; Onozuka, A.; Matin, K.; Imai, S.; Hanada, N.; Nisizawa, T. RGD Motif Enhances Immunogenicity and Adjuvanicity of Peptide Antigens Following Intranasal Immunization. *Vaccine* **2003**, *22* (2), 237–243. https://doi.org/10.1016/S0264-410X(03)00561-9.
(142) Davis, M. E.; Motion, J. P. M.; Narmoneva, D. A.; Takahashi, T.; Hakuno, D.; Kamm, R. D.; Zhang, S.; Lee, R. T. Injectable Self-Assembling Peptide Nanofibers Create Intramyocardial Microenvironments for Endothelial Cells. *Circulation* **2005**, *111* (4), 442–450. https://doi.org/10.1161/01.CIR.0000153847.47301.80.
(143) Cheng, G.; Castelletto, V.; Jones, R. R.; Connon, C. J.; Hamley, I. W. Hydrogelation of Self-Assembling RGD-Based Peptides. *Soft Matter* **2011**, *7* (4), 1326–1333. https://doi.org/10.1039/C0SM00408A.
(144) M. Ryan, D.; M. Doran, T.; L. Nilsson, B. Stabilizing Self-Assembled Fmoc–F 5 –Phe Hydrogels by Co-Assembly with PEG-Functionalized Monomers. *Chemical Communications* **2011**, *47* (1), 475–477. https://doi.org/10.1039/C0CC02217A.
(145) Mahmoud, Z. N.; Gunnoo, S. B.; Thomson, A. R.; Fletcher, J. M.; Woolfson, D. N. Bioorthogonal Dual Functionalization of Self-Assembling Peptide Fibers. *Biomaterials* **2011**, *32* (15), 3712–3720. https://doi.org/10.1016/j.biomaterials.2010.12.002.
(146) Clerici, F.; Erba, E.; Gelmi, M. L.; Pellegrino, S. Non-Standard Amino Acids and Peptides: From Self-Assembly to Nanomaterials. *Tetrahedron Letters* **2016**, *57* (50), 5540–5550. https://doi.org/10.1016/j.tetlet.2016.11.022.
(147) Orain, D.; Ellard, J.; Bradley, M. Protecting Groups in Solid-Phase Organic Synthesis. *J. Comb. Chem.* **2002**, *4* (1), 1–16. https://doi.org/10.1021/cc0001093.
(148) Alsina, J.; Albericio, F. Solid-Phase Synthesis of C-Terminal Modified Peptides. *Biopolymers* **2003**, *71* (4), 454–477. https://doi.org/10.1002/bip.10492.

(149) Chen, W.; Yang, H.; Wang, R.; Cheng, R.; Meng, F.; Wei, W.; Zhong, Z. Versatile Synthesis of Functional Biodegradable Polymers by Combining Ring-Opening Polymerization and Postpolymerization Modification via Michael-Type Addition Reaction. *Macromolecules* **2010**, *43* (1), 201–207. https://doi.org/10.1021/ma901897y.
(150) Farmer, T. J.; Comerford, J. W.; Pellis, A.; Robert, T. Post-Polymerization Modification of Bio-Based Polymers: Maximizing the High Functionality of Polymers Derived from Biomass. *Polymer International* **2018**, *67* (7), 775–789. https://doi.org/10.1002/pi.5573.
(151) Gauthier, M. A.; Gibson, M. I.; Klok, H.-A. Synthesis of Functional Polymers by Post-Polymerization Modification. *Angewandte Chemie International Edition* **2009**, *48* (1), 48–58. https://doi.org/10.1002/anie.200801951.
(152) Hamsici, S.; Sardan Ekiz, M.; Cinar Ciftci, G.; Tekinay, A. B.; Guler, M. O. Gemcitabine Integrated Nano-Prodrug Carrier System. *Bioconjugate Chem.* **2017**, *28* (5), 1491–1498. https://doi.org/10.1021/acs.bioconjchem.7b00155.
(153) Makam, P.; Gazit, E. Minimalistic Peptide Supramolecular Co-Assembly: Expanding the Conformational Space for Nanotechnology. *Chem. Soc. Rev.* **2018**, *47* (10), 3406–3420. https://doi.org/10.1039/C7CS00827A.
(154) Guler, M. O.; Pokorski, J. K.; Appella, D. H.; Stupp, S. I. Enhanced Oligonucleotide Binding to Self-Assembled Nanofibers. *Bioconjugate Chem.* **2005**, *16* (3), 501–503. https://doi.org/10.1021/bc050053b.
(155) Hudalla, G. A.; Sun, T.; Gasiorowski, J. Z.; Han, H.; Tian, Y. F.; Chong, A. S.; Collier, J. H. Gradated Assembly of Multiple Proteins into Supramolecular Nanomaterials. *Nature Materials* **2014**, *13* (8), 829–836. https://doi.org/10.1038/nmat3998.
(156) Soutif, J.-C.; Brosse, J.-C. Chemical Modification of Polymers I. Applications and Synthetic Strategies. *Reactive Polymers* **1990**, *12* (1), 3–29. https://doi.org/10.1016/0923-1137(90)90058-C.
(157) Pieters, B. J. G. E.; Eldijk, M. B. van; Nolte, R. J. M.; Mecinović, J. Natural Supramolecular Protein Assemblies. *Chem. Soc. Rev.* **2015**, *45* (1), 24–39. https://doi.org/10.1039/C5CS00157A.
(158) Zhou, X.-R.; Ge, R.; Luo, S.-Z. Self-Assembly of PH and Calcium Dual-Responsive Peptide-Amphiphilic Hydrogel. *Journal of Peptide Science* **2013**, *19* (12), 737–744. https://doi.org/10.1002/psc.2569.
(159) Zelzer, M.; Todd, S. J.; Hirst, A. R.; McDonald, T. O.; Ulijn, R. V. Enzyme Responsive Materials: Design Strategies and Future Developments. *Biomater. Sci.* **2012**, *1* (1), 11–39. https://doi.org/10.1039/C2BM00041E.
(160) Pochan, D. J.; Schneider, J. P.; Kretsinger, J.; Ozbas, B.; Rajagopal, K.; Haines, L. Thermally Reversible Hydrogels via Intramolecular Folding and Consequent Self-Assembly of a de Novo Designed Peptide. *J. Am. Chem. Soc.* **2003**, *125* (39), 11802–11803. https://doi.org/10.1021/ja0353154.
(161) Maslovskis, A.; Guilbaud, J.-B.; Grillo, I.; Hodson, N.; Miller, A. F.; Saiani, A. Self-Assembling Peptide/Thermoresponsive Polymer Composite Hydrogels: Effect

of Peptide–Polymer Interactions on Hydrogel Properties. *Langmuir* **2014**, *30* (34), 10471–10480. https://doi.org/10.1021/la502358b.
(162) Kwon, S.; Kim, B. J.; Lim, H.-K.; Kang, K.; Yoo, S. H.; Gong, J.; Yoon, E.; Lee, J.; Choi, I. S.; Kim, H.; et al. Magnetotactic Molecular Architectures from Self-Assembly of β-Peptide Foldamers. *Nature Communications* **2015**, *6*, 8747. https://doi.org/10.1038/ncomms9747.
(163) Ni, R.; Liu, J.; Chau, Y. Ultrasound-Facilitated Assembly and Disassembly of a PH-Sensitive Self-Assembly Peptide. *RSC Adv.* **2018**, *8* (51), 29482–29487. https://doi.org/10.1039/C8RA04391D.
(164) Roth-Konforti, M. E.; Comune, M.; Halperin-Sternfeld, M.; Grigoriants, I.; Shabat, D.; Adler-Abramovich, L. UV Light-Responsive Peptide-Based Supramolecular Hydrogel for Controlled Drug Delivery. *Macromol Rapid Commun* **2018**, *39* (24), e1800588. https://doi.org/10.1002/marc.201800588.
(165) Zhang, Y.; Yang, Z.; Yuan, F.; Gu, H.; Gao, P.; Xu, B. Molecular Recognition Remolds the Self-Assembly of Hydrogelators and Increases the Elasticity of the Hydrogel by 106-Fold. *J. Am. Chem. Soc.* **2004**, *126* (46), 15028–15029. https://doi.org/10.1021/ja044401g.
(166) Xu, X.-D.; Chen, C.-S.; Lu, B.; Cheng, S.-X.; Zhang, X.-Z.; Zhuo, R.-X. Coassembly of Oppositely Charged Short Peptides into Well-Defined Supramolecular Hydrogels. *J. Phys. Chem. B* **2010**, *114* (7), 2365–2372. https://doi.org/10.1021/jp9102417.
(167) Sato, K.; Ji, W.; Palmer, L. C.; Weber, B.; Barz, M.; Stupp, S. I. Programmable Assembly of Peptide Amphiphile via Noncovalent-to-Covalent Bond Conversion. *J Am Chem Soc* **2017**, *139* (26), 8995–9000. https://doi.org/10.1021/jacs.7b03878.
(168) Perfumo, A.; Banat, I. M.; Marchant, R. Going Green and Cold: Biosurfactants from Low-Temperature Environments to Biotechnology Applications. *Trends in Biotechnology* **2018**, *36* (3), 277–289. https://doi.org/10.1016/j.tibtech.2017.10.016.
(169) Naughton, P. J.; Marchant, R.; Naughton, V.; Banat, I. M. Microbial Biosurfactants: Current Trends and Applications in Agricultural and Biomedical Industries. *Journal of Applied Microbiology 0* (0). https://doi.org/10.1111/jam.14243.
(170) Sikorska, E.; Dawgul, M.; Greber, K.; Iłowska, E.; Pogorzelska, A.; Kamysz, W. Self-Assembly and Interactions of Short Antimicrobial Cationic Lipopeptides with Membrane Lipids: ITC, FTIR and Molecular Dynamics Studies. *Biochimica et Biophysica Acta (BBA) - Biomembranes* **2014**, *1838* (10), 2625–2634. https://doi.org/10.1016/j.bbamem.2014.06.016.
(171) Kirkham, S.; Castelletto, V.; Hamley, I. W.; Inoue, K.; Rambo, R.; Reza, M.; Ruokolainen, J. Self-Assembly of the Cyclic Lipopeptide Daptomycin: Spherical Micelle Formation Does Not Depend on the Presence of Calcium Chloride. *Chemphyschem* **2016**, *17* (14), 2118–2122. https://doi.org/10.1002/cphc.201600308.

(172) Straus, S. K.; Hancock, R. E. W. Mode of Action of the New Antibiotic for Gram-Positive Pathogens Daptomycin: Comparison with Cationic Antimicrobial Peptides and Lipopeptides. *Biochimica et Biophysica Acta (BBA) - Biomembranes* **2006**, *1758* (9), 1215–1223. https://doi.org/10.1016/j.bbamem.2006.02.009.
(173) Mahlapuu, M.; Håkansson, J.; Ringstad, L.; Björn, C. Antimicrobial Peptides: An Emerging Category of Therapeutic Agents. *Front Cell Infect Microbiol* **2016**, *6*. https://doi.org/10.3389/fcimb.2016.00194.
(174) Ong, P. Y.; Ohtake, T.; Brandt, C.; Strickland, I.; Boguniewicz, M.; Ganz, T.; Gallo, R. L.; Leung, D. Y. M. Endogenous Antimicrobial Peptides and Skin Infections in Atopic Dermatitis. *N. Engl. J. Med.* **2002**, *347* (15), 1151–1160. https://doi.org/10.1056/NEJMoa021481.
(175) Ottosson, H.; Nylén, F.; Sarker, P.; Miraglia, E.; Bergman, P.; Gudmundsson, G. H.; Raqib, R.; Agerberth, B.; Strömberg, R. Potent Inducers of Endogenous Antimicrobial Peptides for Host Directed Therapy of Infections. *Scientific Reports* **2016**, *6*, 36692. https://doi.org/10.1038/srep36692.
(176) Tian, X.; Sun, F.; Zhou, X.-R.; Luo, S.-Z.; Chen, L. Role of Peptide Self-Assembly in Antimicrobial Peptides. *Journal of Peptide Science* **2015**, *21* (7), 530–539. https://doi.org/10.1002/psc.2788.
(177) Chu, H.; Pazgier, M.; Jung, G.; Nuccio, S.-P.; Castillo, P. A.; Jong, M. F. de; Winter, M. G.; Winter, S. E.; Wehkamp, J.; Shen, B.; et al. Human α-Defensin 6 Promotes Mucosal Innate Immunity Through Self-Assembled Peptide Nanonets. *Science* **2012**, *337* (6093), 477–481. https://doi.org/10.1126/science.1218831.
(178) Song, C.; Weichbrodt, C.; Salnikov, E. S.; Dynowski, M.; Forsberg, B. O.; Bechinger, B.; Steinem, C.; Groot, B. L. de; Zachariae, U.; Zeth, K. Crystal Structure and Functional Mechanism of a Human Antimicrobial Membrane Channel. *PNAS* **2013**, *110* (12), 4586–4591. https://doi.org/10.1073/pnas.1214739110.
(179) Gour, S.; Kumar, V.; Singh, A.; Gadhave, K.; Goyal, P.; Pandey, J.; Giri, R.; Yadav, J. K. Mammalian Antimicrobial Peptide Protegrin-4 Self Assembles and Forms Amyloid-like Aggregates: Assessment of Its Functional Relevance. *Journal of Peptide Science* **2019**, *25* (3), e3151. https://doi.org/10.1002/psc.3151.
(180) Lombardi, L.; Shi, Y.; Falanga, A.; Galdiero, E.; de Alteriis, E.; Franci, G.; Chourpa, I.; Azevedo, H. S.; Galdiero, S. Enhancing the Potency of Antimicrobial Peptides through Molecular Engineering and Self-Assembly. *Biomacromolecules* **2019**, *20* (3), 1362–1374. https://doi.org/10.1021/acs.biomac.8b01740.
(181) Chang, R.; Subramanian, K.; Wang, M.; Webster, T. J. Enhanced Antibacterial Properties of Self-Assembling Peptide Amphiphiles Functionalized with Heparin-Binding Cardin-Motifs. *ACS Appl. Mater. Interfaces* **2017**, *9* (27), 22350–22360. https://doi.org/10.1021/acsami.7b07506.
(182) Rodrigues de Almeida, N.; Han, Y.; Perez, J.; Kirkpatrick, S.; Wang, Y.; Sheridan, M. C. Design, Synthesis, and Nanostructure-Dependent Antibacterial Activity of Cationic Peptide Amphiphiles. *ACS Appl. Mater. Interfaces* **2019**, *11* (3), 2790–2801. https://doi.org/10.1021/acsami.8b17808.

(183) Zou, R.; Zhu, X.; Tu, Y.; Wu, J.; Landry, M. P. Activity of Antimicrobial Peptide Aggregates Decreases with Increased Cell Membrane Embedding Free Energy Cost. *Biochemistry* **2018**, *57* (18), 2606–2610. https://doi.org/10.1021/acs.biochem.8b00052.
(184) Chen, X.; Hirt, H.; Li, Y.; Gorr, S.-U.; Aparicio, C. Antimicrobial GL13K Peptide Coatings Killed and Ruptured the Wall of Streptococcus Gordonii and Prevented Formation and Growth of Biofilms. *PLOS ONE* **2014**, *9* (11), e111579. https://doi.org/10.1371/journal.pone.0111579.
(185) Ye, Z.; Zhu, X.; Acosta, S.; Kumar, D.; Sang, T.; Aparicio, C. Self-Assembly Dynamics and Antimicrobial Activity of All l - and d -Amino Acid Enantiomers of a Designer Peptide. *Nanoscale* **2019**, *11* (1), 266–275. https://doi.org/10.1039/C8NR07334A.
(186) Xu, D.; Chen, W.; Tobin-Miyaji, Y. J.; Sturge, C. R.; Yang, S.; Elmore, B.; Singh, A.; Pybus, C.; Greenberg, D. E.; Sellati, T. J.; et al. Fabrication and Microscopic and Spectroscopic Characterization of Cytocompatible Self-Assembling Antimicrobial Nanofibers. *ACS Infect. Dis.* **2018**, *4* (9), 1327–1335. https://doi.org/10.1021/acsinfecdis.8b00069.
(187) Gilliet, M.; Lande, R. Antimicrobial Peptides and Self-DNA in Autoimmune Skin Inflammation. *Curr. Opin. Immunol.* **2008**, *20* (4), 401–407. https://doi.org/10.1016/j.coi.2008.06.008.
(188) Tjabringa, G. S.; Rabe, K. F.; Hiemstra, P. S. The Human Cathelicidin LL-37: A Multifunctional Peptide Involved in Infection and Inflammation in the Lung. *Pulm Pharmacol Ther* **2005**, *18* (5), 321–327. https://doi.org/10.1016/j.pupt.2005.01.001.
(189) Kahlenberg, J. M.; Kaplan, M. J. Little Peptide, Big Effects: The Role of LL-37 in Inflammation and Autoimmune Disease. *J Immunol* **2013**, *191* (10). https://doi.org/10.4049/jimmunol.1302005.
(190) Scott, M. G.; Davidson, D. J.; Gold, M. R.; Bowdish, D.; Hancock, R. E. W. The Human Antimicrobial Peptide LL-37 Is a Multifunctional Modulator of Innate Immune Responses. *The Journal of Immunology* **2002**, *169* (7), 3883–3891. https://doi.org/10.4049/jimmunol.169.7.3883.
(191) Lee, E. Y.; Takahashi, T.; Curk, T.; Dobnikar, J.; Gallo, R. L.; Wong, G. C. L. Crystallinity of Double-Stranded RNA-Antimicrobial Peptide Complexes Modulates Toll-Like Receptor 3-Mediated Inflammation. *ACS Nano* **2017**, *11* (12), 12145–12155. https://doi.org/10.1021/acsnano.7b05234.
(192) Lee, E. Y.; Zhang, C.; Domizio, J. D.; Jin, F.; Connell, W.; Hung, M.; Malkoff, N.; Veksler, V.; Gilliet, M.; Ren, P.; et al. Helical Antimicrobial Peptides Assemble into Protofibril Scaffolds That Present Ordered DsDNA to TLR9. *Nature Communications* **2019**, *10* (1), 1012. https://doi.org/10.1038/s41467-019-08868-w.
(193) Baron, R.; McCammon, J. A. Molecular Recognition and Ligand Association. *Annual Review of Physical Chemistry* **2013**, *64* (1), 151–175. https://doi.org/10.1146/annurev-physchem-040412-110047.

(194) Portoghese, P. S. From Models to Molecules: Opioid Receptor Dimers, Bivalent Ligands, and Selective Opioid Receptor Probes. *J. Med. Chem.* **2001**, *44* (14), 2259–2269. https://doi.org/10.1021/jm010158+.
(195) Lodish, H.; Berk, A.; Zipursky, S. L.; Matsudaira, P.; Baltimore, D.; Darnell, J. Overview of Extracellular Signaling. *Molecular Cell Biology. 4th edition* **2000**.
(196) Keire, D. A.; Bowers, C. W.; Solomon, T. E.; Reeve, J. R. Structure and Receptor Binding of PYY Analogs. *Peptides* **2002**, *23* (2), 305–321. https://doi.org/10.1016/S0196-9781(01)00602-7.
(197) Yi, J.; Warunek, D.; Craft, D. Degradation and Stabilization of Peptide Hormones in Human Blood Specimens. *PLOS ONE* **2015**, *10* (7), e0134427. https://doi.org/10.1371/journal.pone.0134427.
(198) Hutchinson, J. A.; Burholt, S.; Hamley, I. W.; Lundback, A.-K.; Uddin, S.; Gomes dos Santos, A.; Reza, M.; Seitsonen, J.; Ruokolainen, J. The Effect of Lipidation on the Self-Assembly of the Gut-Derived Peptide Hormone PYY3–36. *Bioconjugate Chem.* **2018**, *29* (7), 2296–2308. https://doi.org/10.1021/acs.bioconjchem.8b00286.
(199) Hutchinson, J. A.; Hamley, I. W.; Torras, J.; Alemán, C.; Seitsonen, J.; Ruokolainen, J. Self-Assembly of Lipopeptides Containing Short Peptide Fragments Derived from the Gastrointestinal Hormone PYY3–36: From Micelles to Amyloid Fibrils. *The Journal of Physical Chemistry B* **2019**. https://doi.org/10.1021/acs.jpcb.8b11097.
(200) Henderson, N. C.; Sethi, T. The Regulation of Inflammation by Galectin-3. *Immunological Reviews* **2009**, *230* (1), 160–171. https://doi.org/10.1111/j.1600-065X.2009.00794.x.
(201) Stegmayr, J.; Zetterberg, F.; Carlsson, M. C.; Huang, X.; Sharma, G.; Kahl-Knutson, B.; Schambye, H.; Nilsson, U. J.; Oredsson, S.; Leffler, H. Extracellular and Intracellular Small-Molecule Galectin-3 Inhibitors. *Scientific Reports* **2019**, *9* (1), 2186. https://doi.org/10.1038/s41598-019-38497-8.
(202) Restuccia, A.; Fettis, M. M.; Farhadi, S. A.; Molinaro, M. D.; Kane, B.; Hudalla, G. A. Evaluation of Self-Assembled Glycopeptide Nanofibers Modified with N,N′-Diacetyllactosamine for Selective Galectin-3 Recognition and Inhibition. *ACS Biomater. Sci. Eng.* **2018**, *4* (10), 3451–3459. https://doi.org/10.1021/acsbiomaterials.8b00611.
(203) Shang, Y.; Zhi, D.; Feng, G.; Wang, Z.; Mao, D.; Guo, S.; Liu, R.; Liu, L.; Zhang, S.; Sun, S.; et al. Supramolecular Nanofibers with Superior Bioactivity to Insulin-Like Growth Factor-I. *Nano Lett.* **2019**, *19* (3), 1560–1569. https://doi.org/10.1021/acs.nanolett.8b04406.
(204) Bathina, S.; Das, U. N. Brain-Derived Neurotrophic Factor and Its Clinical Implications. *Arch Med Sci* **2015**, *11* (6), 1164–1178. https://doi.org/10.5114/aoms.2015.56342.
(205) Edelbrock, A. N.; Àlvarez, Z.; Simkin, D.; Fyrner, T.; Chin, S. M.; Sato, K.; Kiskinis, E.; Stupp, S. I. Supramolecular Nanostructure Activates TrkB Receptor Signaling of Neuronal Cells by Mimicking Brain-Derived Neurotrophic Factor.

*Nano Lett.* **2018**, *18* (10), 6237–6247. https://doi.org/10.1021/acs.nanolett.8b02317.
(206) Hendrikse, S. I. S.; Spaans, S.; Meijer, E. W.; Dankers, P. Y. W. Supramolecular Platform Stabilizing Growth Factors. *Biomacromolecules* **2018**, *19* (7), 2610–2617. https://doi.org/10.1021/acs.biomac.8b00219.
(207) Leach, D. G.; Young, S.; Hartgerink, J. D. Advances in Immunotherapy Delivery from Implantable and Injectable Biomaterials. *Acta Biomaterialia* **2019**, *88*, 15–31. https://doi.org/10.1016/j.actbio.2019.02.016.
(208) Hainline, K. M.; Fries, C. N.; Collier, J. H. Progress Toward the Clinical Translation of Bioinspired Peptide and Protein Assemblies. *Advanced Healthcare Materials* **2018**, *7* (5), 1700930. https://doi.org/10.1002/adhm.201700930.
(209) He, X.; Abrams, S. I.; Lovell, J. F. Peptide Delivery Systems for Cancer Vaccines. *Advanced Therapeutics* **2018**, *1* (5), 1800060. https://doi.org/10.1002/adtp.201800060.
(210) Yang, C.; Shi, F.; Li, C.; Wang, Y.; Wang, L.; Yang, Z. Single Dose of Protein Vaccine with Peptide Nanofibers As Adjuvants Elicits Long-Lasting Antibody Titer. *ACS Biomater. Sci. Eng.* **2018**, *4* (6), 2000–2006. https://doi.org/10.1021/acsbiomaterials.7b00488.
(211) Coffman, R. L.; Sher, A.; Seder, R. A. Vaccine Adjuvants: Putting Innate Immunity to Work. *Immunity* **2010**, *33* (4), 492–503. https://doi.org/10.1016/j.immuni.2010.10.002.
(212) Appavu, R.; Chesson, C. B.; Koyfman, A. Y.; Snook, J. D.; Kohlhapp, F. J.; Zloza, A.; Rudra, J. S. Enhancing the Magnitude of Antibody Responses through Biomaterial Stereochemistry. *ACS Biomater. Sci. Eng.* **2015**, *1* (7), 601–609. https://doi.org/10.1021/acsbiomaterials.5b00139.
(213) Black, M.; Trent, A.; Kostenko, Y.; Lee, J. S.; Olive, C.; Tirrell, M. Self-Assembled Peptide Amphiphile Micelles Containing a Cytotoxic T-Cell Epitope Promote a Protective Immune Response In Vivo. *Advanced Materials* **2012**, *24* (28), 3845–3849. https://doi.org/10.1002/adma.201200209.
(214) Hwang, D. H.; Kim, J.-A.; Lee, J. Y. Mechanisms for the Activation of Toll-like Receptor 2/4 by Saturated Fatty Acids and Inhibition by Docosahexaenoic Acid. *Eur. J. Pharmacol.* **2016**, *785*, 24–35. https://doi.org/10.1016/j.ejphar.2016.04.024.
(215) Kalász, H.; Antal, I. Drug Excipients. *Curr. Med. Chem.* **2006**, *13* (21), 2535–2563.
(216) Liechty, W. B.; Kryscio, D. R.; Slaughter, B. V.; Peppas, N. A. Polymers for Drug Delivery Systems. *Annu Rev Chem Biomol Eng* **2010**, *1*, 149–173. https://doi.org/10.1146/annurev-chembioeng-073009-100847.
(217) Tian, R.; Chen, J.; Niu, R. The Development of Low-Molecular Weight Hydrogels for Applications in Cancer Therapy. *Nanoscale* **2014**, *6* (7), 3474–3482. https://doi.org/10.1039/C3NR05414D.
(218) Cheetham, A. G.; Chakroun, R. W.; Ma, W.; Cui, H. Self-Assembling Prodrugs. *Chem. Soc. Rev.* **2017**, *46* (21), 6638–6663. https://doi.org/10.1039/C7CS00521K.

(219) Wang, Y.; Cheetham, A. G.; Angacian, G.; Su, H.; Xie, L.; Cui, H. Peptide–Drug Conjugates as Effective Prodrug Strategies for Targeted Delivery. *Adv Drug Deliv Rev* **2017**, *110–111*, 112–126. https://doi.org/10.1016/j.addr.2016.06.015.
(220) Ma, P.; Mumper, R. J. Paclitaxel Nano-Delivery Systems: A Comprehensive Review. *J Nanomed Nanotechnol* **2013**, *4* (2), 1000164. https://doi.org/10.4172/2157-7439.1000164.
(221) Zhao, N.; Woodle, M. C.; Mixson, A. J. Advances in Delivery Systems for Doxorubicin. *J Nanomed Nanotechnol* **2018**, *9* (5). https://doi.org/10.4172/2157-7439.1000519.
(222) Ling, Y.; Gao, Y.; Shu, C.; Zhou, Y.; Zhong, W.; Xu, B. Using a Peptide Segment to Covalently Conjugate Doxorubicin and Taxol for the Study of Drug Combination Effect. *RSC Adv.* **2015**, *5* (123), 101475–101479. https://doi.org/10.1039/C5RA14156G.
(223) Li, J.; Kuang, Y.; Gao, Y.; Du, X.; Shi, J.; Xu, B. D-Amino Acids Boost the Selectivity and Confer Supramolecular Hydrogels of a Nonsteroidal Anti-Inflammatory Drug (NSAID). *J. Am. Chem. Soc.* **2013**, *135* (2), 542–545. https://doi.org/10.1021/ja310019x.
(224) Li, J.; Li, X.; Kuang, Y.; Gao, Y.; Du, X.; Shi, J.; Xu, B. Self-Delivery Multifunctional Anti-HIV Hydrogels for Sustained Release. *Advanced Healthcare Materials* **2013**, *2* (12), 1586–1590. https://doi.org/10.1002/adhm.201300041.
(225) Liu, H.; Li, Y.; Lyu, Z.; Wan, Y.; Li, X.; Chen, H.; Chen, H.; Li, X. Enzyme-Triggered Supramolecular Self-Assembly of Platinum Prodrug with Enhanced Tumor-Selective Accumulation and Reduced Systemic Toxicity. *J. Mater. Chem. B* **2014**, *2* (47), 8303–8309. https://doi.org/10.1039/C4TB01563K.
(226) Kanamala, M.; Wilson, W. R.; Yang, M.; Palmer, B. D.; Wu, Z. Mechanisms and Biomaterials in PH-Responsive Tumour Targeted Drug Delivery: A Review. *Biomaterials* **2016**, *85*, 152–167. https://doi.org/10.1016/j.biomaterials.2016.01.061.
(227) Matson, J. B.; Stupp, S. I. Drug Release from Hydrazone-Containing Peptide Amphiphiles. *Chem Commun (Camb)* **2011**, *47* (28), 7962–7964. https://doi.org/10.1039/c1cc12570b.
(228) Webber, M. J.; Matson, J. B.; Tamboli, V. K.; Stupp, S. I. Controlled Release of Dexamethasone from Peptide Nanofiber Gels to Modulate Inflammatory Response. *Biomaterials* **2012**, *33* (28), 6823–6832. https://doi.org/10.1016/j.biomaterials.2012.06.003.
(229) Matson, J. B.; Newcomb, C. J.; Bitton, R.; Stupp, S. I. Nanostructure-Templated Control of Drug Release from Peptide Amphiphile Nanofiber Gels. *Soft Matter* **2012**, *8* (13), 3586–3595. https://doi.org/10.1039/C2SM07420F.
(230) So, M. M.; Mansukhani, N. A.; Peters, E. B.; Albaghdadi, M. S.; Wang, Z.; Pérez, C. M. R.; Kibbe, M. R.; Stupp, S. I. Peptide Amphiphile Nanostructures for Targeting of Atherosclerotic Plaque and Drug Delivery. *Advanced Biosystems* **2018**, *2* (3), 1700123. https://doi.org/10.1002/adbi.201700123.

(231) Martin, C.; Dumitrascuta, M.; Mannes, M.; Lantero, A.; Bucher, D.; Walker, K.; Van Wanseele, Y.; Oyen, E.; Hernot, S.; Van Eeckhaut, A.; et al. Biodegradable Amphipathic Peptide Hydrogels as Extended-Release System for Opioid Peptides. *J. Med. Chem.* **2018**, *61* (21), 9784–9789. https://doi.org/10.1021/acs.jmedchem.8b01282.
(232) Research, A. A. for C. Lanreotide Slows Growth of Neuroendocrine Cancer. *Cancer Discov* **2014**, *4* (10), OF3–OF3. https://doi.org/10.1158/2159-8290.CD-NB2014-124.
(233) Salvatori, R.; Woodmansee, W. W.; Molitch, M.; Gordon, M. B.; Lomax, K. G. Lanreotide Extended-Release Aqueous-Gel Formulation, Injected by Patient, Partner or Healthcare Provider in Patients with Acromegaly in the United States: 1-Year Data from the SODA Registry. *Pituitary* **2014**, *17* (1), 13–21. https://doi.org/10.1007/s11102-012-0460-2.
(234) Valéry, C.; Paternostre, M.; Robert, B.; Gulik-Krzywicki, T.; Narayanan, T.; Dedieu, J.-C.; Keller, G.; Torres, M.-L.; Cherif-Cheikh, R.; Calvo, P.; et al. Biomimetic Organization: Octapeptide Self-Assembly into Nanotubes of Viral Capsid-like Dimension. *PNAS* **2003**, *100* (18), 10258–10262. https://doi.org/10.1073/pnas.1730609100.
(235) Wolin, E. M. The Expanding Role of Somatostatin Analogs in the Management of Neuroendocrine Tumors. *Gastrointest Cancer Res* **2012**, *5* (5), 161–168.
(236) Steinberg, M. Degarelix: A Gonadotropin-Releasing Hormone Antagonist for the Management of Prostate Cancer. *Clin Ther* **2009**, *31 Pt 2*, 2312–2331. https://doi.org/10.1016/j.clinthera.2009.11.009.
(237) Broqua, P.; Riviere, P. J.-M.; Conn, P. M.; Rivier, J. E.; Aubert, M. L.; Junien, J.-L. Pharmacological Profile of a New, Potent, and Long-Acting Gonadotropin-Releasing Hormone Antagonist: Degarelix. *J. Pharmacol. Exp. Ther.* **2002**, *301* (1), 95–102. https://doi.org/10.1124/jpet.301.1.95.
(238) Maji, S. K.; Schubert, D.; Rivier, C.; Lee, S.; Rivier, J. E.; Riek, R. Amyloid as a Depot for the Formulation of Long-Acting Drugs. *PLoS Biol* **2008**, *6* (2). https://doi.org/10.1371/journal.pbio.0060017.
(239) Zhou, N.; Gao, X.; Lv, Y.; Cheng, J.; Zhou, W.; Liu, K. Self-Assembled Nanostructures of Long-Acting GnRH Analogs Modified at Position 7. *J. Pept. Sci.* **2014**, *20* (11), 868–875. https://doi.org/10.1002/psc.2678.
(240) Bomar, M. G.; Samuelsson, S. J.; Kibler, P.; Kodukula, K.; Galande, A. K. Hemopressin Forms Self-Assembled Fibrillar Nanostructures under Physiologically Relevant Conditions. *Biomacromolecules* **2012**, *13* (3), 579–583. https://doi.org/10.1021/bm201836f.
(241) Dao, H. M.; Chen, J.; Tucker, B. S.; Thomas, V.; Jun, H.-W.; Li, X.-C.; Jo, S. Hemopressin-Based PH-Sensitive Hydrogel: A Potential Bioactive Platform for Drug Delivery. *ACS Biomater. Sci. Eng.* **2018**, *4* (7), 2435–2442. https://doi.org/10.1021/acsbiomaterials.8b00423.
(242) Toniolo, E. F.; Maique, E. T.; Ferreira, W. A.; Heimann, A. S.; Ferro, E. S.; Ramos-Ortolaza, D. L.; Miller, L.; Devi, L. A.; Dale, C. S. Hemopressin, an

Inverse Agonist of Cannabinoid Receptors, Inhibits Neuropathic Pain in Rats. *Peptides* **2014**, *56*, 125–131. https://doi.org/10.1016/j.peptides.2014.03.016.
(243) Serra, L.; Doménech, J.; Peppas, N. A. Drug Transport Mechanisms and Release Kinetics from Molecularly Designed Poly(Acrylic Acid-g-Ethylene Glycol) Hydrogels. *Biomaterials* **2006**, *27* (31), 5440–5451. https://doi.org/10.1016/j.biomaterials.2006.06.011.
(244) West, H. T.; Csizmar, C. M.; Wagner, C. R. Tunable Supramolecular Assemblies from Amphiphilic Nucleoside Phosphoramidate Nanofibers by Enzyme Activation. *Biomacromolecules* **2018**, *19* (7), 2650–2656. https://doi.org/10.1021/acs.biomac.8b00254.
(245) Perham Richard Nelson; Phillips David Chilton; Radda George Karoly. Self-Assembly of Biological Macromolecules. *Philosophical Transactions of the Royal Society of London. B, Biological Sciences* **1975**, *272* (915), 123–136. https://doi.org/10.1098/rstb.1975.0075.
(246) Kentsis, A.; Borden, K. L. B. Physical Mechanisms and Biological Significance of Supramolecular Protein Self-Assembly. *Curr. Protein Pept. Sci.* **2004**, *5* (2), 125–134.
(247) Schek, H. T.; Gardner, M. K.; Cheng, J.; Odde, D. J.; Hunt, A. J. Microtubule Assembly Dynamics at the Nanoscale. *Current Biology* **2007**, *17* (17), 1445–1455. https://doi.org/10.1016/j.cub.2007.07.011.
(248) Nogales, E.; Wang, H.-W. Structural Mechanisms Underlying Nucleotide-Dependent Self-Assembly of Tubulin and Its Relatives. *Curr. Opin. Struct. Biol.* **2006**, *16* (2), 221–229. https://doi.org/10.1016/j.sbi.2006.03.005.
(249) Hartman, J. J.; Mahr, J.; McNally, K.; Okawa, K.; Iwamatsu, A.; Thomas, S.; Cheesman, S.; Heuser, J.; Vale, R. D.; McNally, F. J. Katanin, a Microtubule-Severing Protein, Is a Novel AAA ATPase That Targets to the Centrosome Using a WD40-Containing Subunit. *Cell* **1998**, *93* (2), 277–287. https://doi.org/10.1016/S0092-8674(00)81578-0.
(250) Luptovčiak, I.; Komis, G.; Takáč, T.; Ovečka, M.; Šamaj, J. Katanin: A Sword Cutting Microtubules for Cellular, Developmental, and Physiological Purposes. *Front Plant Sci* **2017**, *8*. https://doi.org/10.3389/fpls.2017.01982.
(251) Barry, R.; Gitai, Z. Self-Assembling Enzymes and the Origins of the Cytoskeleton. *Curr Opin Microbiol* **2011**, *14* (6), 704–711. https://doi.org/10.1016/j.mib.2011.09.015.
(252) Webb, B.; Ackerman, L.; Barber, D. Filament Assembly by Phosphofructokinase-1, the Gatekeeper of Glycolysis. *Biophysical Journal* **2014**, *106* (2), 682a. https://doi.org/10.1016/j.bpj.2013.11.3777.
(253) Webb, B. A.; Dosey, A. M.; Wittmann, T.; Kollman, J. M.; Barber, D. L. The Glycolytic Enzyme Phosphofructokinase-1 Assembles into Filaments. *J Cell Biol* **2017**, *216* (8), 2305–2313. https://doi.org/10.1083/jcb.201701084.
(254) Si, K.; Giustetto, M.; Etkin, A.; Hsu, R.; Janisiewicz, A. M.; Miniaci, M. C.; Kim, J.-H.; Zhu, H.; Kandel, E. R. A Neuronal Isoform of CPEB Regulates Local Protein Synthesis and Stabilizes Synapse-Specific Long-Term Facilitation in

Aplysia. *Cell* **2003**, *115* (7), 893–904. https://doi.org/10.1016/S0092-8674(03)01021-3.
(255) Fioriti, L.; Myers, C.; Huang, Y.-Y.; Li, X.; Stephan, J. S.; Trifilieff, P.; Colnaghi, L.; Kosmidis, S.; Drisaldi, B.; Pavlopoulos, E.; et al. The Persistence of Hippocampal-Based Memory Requires Protein Synthesis Mediated by the Prion-like Protein CPEB3. *Neuron* **2015**, *86* (6), 1433–1448. https://doi.org/10.1016/j.neuron.2015.05.021.
(256) Drisaldi, B.; Colnaghi, L.; Fioriti, L.; Rao, N.; Myers, C.; Snyder, A. M.; Metzger, D. J.; Tarasoff, J.; Konstantinov, E.; Fraser, P. E.; et al. SUMOylation Is an Inhibitory Constraint That Regulates the Prion-like Aggregation and Activity of CPEB3. *Cell Reports* **2015**, *11* (11), 1694–1702. https://doi.org/10.1016/j.celrep.2015.04.061.
(257) Krumova, P.; Meulmeester, E.; Garrido, M.; Tirard, M.; Hsiao, H.-H.; Bossis, G.; Urlaub, H.; Zweckstetter, M.; Kügler, S.; Melchior, F.; et al. Sumoylation Inhibits α-Synuclein Aggregation and Toxicity. *The Journal of Cell Biology* **2011**, *194* (1), 49–60. https://doi.org/10.1083/jcb.201010117.
(258) Weisel, J. W.; Litvinov, R. I. Mechanisms of Fibrin Polymerization and Clinical Implications. *Blood* **2013**, *121* (10), 1712–1719. https://doi.org/10.1182/blood-2012-09-306639.
(259) Wolberg, A. S.; Campbell, R. A. Thrombin Generation, Fibrin Clot Formation and Hemostasis. *Transfus Apher Sci* **2008**, *38* (1), 15–23. https://doi.org/10.1016/j.transci.2007.12.005.
(260) Ulijn, R. V. Enzyme-Responsive Materials: A New Class of Smart Biomaterials. *J. Mater. Chem.* **2006**, *16* (23), 2217–2225. https://doi.org/10.1039/B601776M.
(261) Toledano, S.; Williams, R. J.; Jayawarna, V.; Ulijn, R. V. Enzyme-Triggered Self-Assembly of Peptide Hydrogels via Reversed Hydrolysis. *J. Am. Chem. Soc.* **2006**, *128* (4), 1070–1071. https://doi.org/10.1021/ja056549l.
(262) Yang, Z.; Liang, G.; Wang, L.; Xu, B. Using a Kinase/Phosphatase Switch to Regulate a Supramolecular Hydrogel and Forming the Supramolecular Hydrogel in Vivo. *J. Am. Chem. Soc.* **2006**, *128* (9), 3038–3043. https://doi.org/10.1021/ja057412y.
(263) Gao, L.; Wu, J.; Gao, D. Enzyme-Controlled Self-Assembly and Transformation of Nanostructures in a Tetramethylbenzidine/Horseradish Peroxidase/H2O2 System. *ACS Nano* **2011**, *5* (8), 6736–6742. https://doi.org/10.1021/nn2023107.
(264) Gao, Y.; Yang, Z.; Kuang, Y.; Ma, M.-L.; Li, J.; Zhao, F.; Xu, B. Enzyme-Instructed Self-Assembly of Peptide Derivatives to Form Nanofibers and Hydrogels. *Peptide Science* **2010**, *94* (1), 19–31. https://doi.org/10.1002/bip.21321.
(265) Webber, M. J.; Newcomb, C. J.; Bitton, R.; Stupp, S. I. Switching of Self-Assembly in a Peptide Nanostructure with a Specific Enzyme. *Soft Matter* **2011**, *7* (20), 9665–9672. https://doi.org/10.1039/c1sm05610g.
(266) Dong, L.; Qian, J.; Hai, Z.; Xu, J.; Du, W.; Zhong, K.; Liang, G. Alkaline Phosphatase-Instructed Self-Assembly of Gadolinium Nanofibers for Enhanced

T2-Weighted Magnetic Resonance Imaging of Tumor. *Anal. Chem.* **2017**, *89* (13), 6922–6925. https://doi.org/10.1021/acs.analchem.7b00621.
(267) Brenner, C.; Bieganowski, P.; Pace, H. C.; Huebner, K. The Histidine Triad Superfamily of Nucleotide-binding Proteins. *Journal of Cellular Physiology* **1999**, *181* (2), 179–187. https://doi.org/10.1002/(SICI)1097-4652(199911)181:2<179::AID-JCP1>3.0.CO;2-8.
(268) Brenner, C. Hint, Fhit, and GalT: Function, Structure, Evolution, and Mechanism of Three Branches of the Histidine Triad Superfamily of Nucleotide Hydrolases and Transferases. *Biochemistry* **2002**, *41* (29), 9003–9014. https://doi.org/10.1021/bi025942q.
(269) Motzik, A.; Amir, E.; Erlich, T.; Wang, J.; Kim, B.-G.; Han, J. M.; Kim, J. H.; Nechushtan, H.; Guo, M.; Razin, E.; et al. Post-Translational Modification of HINT1 Mediates Activation of MITF Transcriptional Activity in Human Melanoma Cells. *Oncogene* **2017**, *36* (33), 4732–4738. https://doi.org/10.1038/onc.2017.81.
(270) Genovese, G.; Ghosh, P.; Li, H.; Rettino, A.; Sioletic, S.; Cittadini, A.; Sgambato, A. The Tumor Suppressor HINT1 Regulates MITF and β-Catenin Transcriptional Activity in Melanoma Cells. *Cell Cycle* **2012**, *11* (11), 2206–2215. https://doi.org/10.4161/cc.20765.
(271) Schöler, J.; Ferralli, J.; Thiry, S.; Chiquet-Ehrismann, R. The Intracellular Domain of Teneurin-1 Induces the Activity of Microphthalmia-Associated Transcription Factor (MITF) by Binding to Transcriptional Repressor HINT1. *J. Biol. Chem.* **2015**, *290* (13), 8154–8165. https://doi.org/10.1074/jbc.M114.615922.
(272) Zimoń, M.; Baets, J.; Almeida-Souza, L.; De Vriendt, E.; Nikodinovic, J.; Parman, Y.; Battaloğlu, E.; Matur, Z.; Guergueltcheva, V.; Tournev, I.; et al. Loss-of-Function Mutations in HINT1 Cause Axonal Neuropathy with Neuromyotonia. *Nat. Genet.* **2012**, *44* (10), 1080–1083. https://doi.org/10.1038/ng.2406.
(273) Peeters, K.; Chamova, T.; Tournev, I.; Jordanova, A. Axonal Neuropathy with Neuromyotonia: There Is a HINT. *Brain* **2017**, *140* (4), 868–877. https://doi.org/10.1093/brain/aww301.
(274) Garzón, J.; Herrero-Labrador, R.; Rodríguez-Muñoz, M.; Shah, R.; Vicente-Sánchez, A.; Wagner, C. R.; Sánchez-Blázquez, P. HINT1 Protein: A New Therapeutic Target to Enhance Opioid Antinociception and Block Mechanical Allodynia. *Neuropharmacology* **2015**, *89*, 412–423. https://doi.org/10.1016/j.neuropharm.2014.10.022.
(275) Chou, T.-F.; Baraniak, J.; Kaczmarek, R.; Zhou, X.; Cheng, J.; Ghosh, B.; Wagner, C. R. Phosphoramidate Pronucleotides: A Comparison of the Phosphoramidase Substrate Specificity of Human and Escherichia Coli Histidine Triad Nucleotide Binding Proteins. *Mol. Pharmaceutics* **2007**, *4* (2), 208–217. https://doi.org/10.1021/mp060070y.
(276) Chou, T.-F.; Bieganowski, P.; Shilinski, K.; Cheng, J.; Brenner, C.; Wagner, C. R. 31P NMR and Genetic Analysis Establish HinT as the Only Escherchia Coli Purine Nucleoside Phosphoramidase and as Essential for Growth under High Salt

Conditions. *J. Biol. Chem.* **2005**, *280* (15), 15356–15361. https://doi.org/10.1074/jbc.M500434200.
(277) Zhou, X.; Chou, T.-F.; Aubol, B. E.; Park, C. J.; Wolfenden, R.; Adams, J.; Wagner, C. R. Kinetic Mechanism of Human Histidine Triad Nucleotide Binding Protein 1 (Hint1). *Biochemistry* **2013**, *52* (20). https://doi.org/10.1021/bi301616c.
(278) Wagner, C. R.; Iyer, V. V.; McIntee, E. J. Pronucleotides: Toward the in Vivo Delivery of Antiviral and Anticancer Nucleotides. *Medicinal Research Reviews* **2000**, *20* (6), 417–451. https://doi.org/10.1002/1098-1128(200011)20:6<417::AID-MED1>3.0.CO;2-Z.
(279) Clark, J. L.; Hollecker, L.; Mason, J. C.; Stuyver, L. J.; Tharnish, P. M.; Lostia, S.; McBrayer, T. R.; Schinazi, R. F.; Watanabe, K. A.; Otto, M. J.; et al. Design, Synthesis, and Antiviral Activity of 2‘-Deoxy-2‘-Fluoro-2‘-C-Methylcytidine, a Potent Inhibitor of Hepatitis C Virus Replication. *J. Med. Chem.* **2005**, *48* (17), 5504–5508. https://doi.org/10.1021/jm0502788.
(280) Shah, R.; Maize, K. M.; Zhou, X.; Finzel, B. C.; Wagner, C. R. Caught before Released: Structural Mapping of the Reaction Trajectory for the Sofosbuvir Activating Enzyme, Human Histidine Triad Nucleotide Binding Protein 1 (HHint1). *Biochemistry* **2017**, *56* (28), 3559–3570. https://doi.org/10.1021/acs.biochem.7b00148.
(281) Zhang, Y.; Kuang, Y.; Gao, Y.; Xu, B. Versatile Small-Molecule Motifs for Self-Assembly in Water and the Formation of Biofunctional Supramolecular Hydrogels. *Langmuir* **2011**, *27* (2), 529–537. https://doi.org/10.1021/la1020324.
(282) Yan, C.; J. Pochan, D. Rheological Properties of Peptide -Based Hydrogels for Biomedical and Other Applications. *Chemical Society Reviews* **2010**, *39* (9), 3528–3540. https://doi.org/10.1039/B919449P.
(283) Wang, S.-Sun. P-Alkoxybenzyl Alcohol Resin and p-Alkoxybenzyloxycarbonylhydrazide Resin for Solid Phase Synthesis of Protected Peptide Fragments. *J. Am. Chem. Soc.* **1973**, *95* (4), 1328–1333. https://doi.org/10.1021/ja00785a602.
(284) Himo, F.; Lovell, T.; Hilgraf, R.; Rostovtsev, V. V.; Noodleman, L.; Sharpless, K. B.; Fokin, V. V. Copper(I)-Catalyzed Synthesis of Azoles. DFT Study Predicts Unprecedented Reactivity and Intermediates. *J. Am. Chem. Soc.* **2005**, *127* (1), 210–216. https://doi.org/10.1021/ja0471525.
(285) Newcomb, C. J.; Moyer, T. J.; Lee, S. S.; Stupp, S. I. Advances in Cryogenic Transmission Electron Microscopy for the Characterization of Dynamic Self-Assembling Nanostructures. *Curr Opin Colloid Interface Sci* **2012**, *17* (6), 350–359. https://doi.org/10.1016/j.cocis.2012.09.004.
(286) Shah, R.; Strom, A.; Zhou, A.; Maize, K. M.; Finzel, B. C.; Wagner, C. R. Design, Synthesis, and Characterization of Sulfamide and Sulfamate Nucleotidomimetic Inhibitors of HHint1. *ACS Med. Chem. Lett.* **2016**, *7* (8), 780–784. https://doi.org/10.1021/acsmedchemlett.6b00169.

(287) Singh, V.; Snigdha, K.; Singh, C.; Sinha, N.; Thakur, A. K. Understanding the Self-Assembly of Fmoc–Phenylalanine to Hydrogel Formation. *Soft Matter* **2015**, *11* (26), 5353–5364. https://doi.org/10.1039/C5SM00843C.
(288) Rajbhandary, A.; Raymond, D. M.; Nilsson, B. L. Self-Assembly, Hydrogelation, and Nanotube Formation by Cation-Modified Phenylalanine Derivatives. *Langmuir* **2017**, *33* (23), 5803–5813. https://doi.org/10.1021/acs.langmuir.7b00686.
(289) Zhou, J.; Du, X.; Li, J.; Yamagata, N.; Xu, B. Taurine Boosts Cellular Uptake of Small D-Peptides for Enzyme-Instructed Intracellular Molecular Self-Assembly. *J Am Chem Soc* **2015**, *137* (32), 10040–10043. https://doi.org/10.1021/jacs.5b06181.
(290) Du, X.; Li, J.; Gao, Y.; Kuang, Y.; Xu, B. Catalytic Dephosphorylation of Adenosine Monophosphate (AMP) to Form Supramolecular Nanofibers/Hydrogels. *Chem. Commun.* **2012**, *48* (15), 2098–2100. https://doi.org/10.1039/C2CC16723A.
(291) Aulisa, L.; Dong, H.; Hartgerink, J. D. Self-Assembly of Multidomain Peptides: Sequence Variation Allows Control over Cross-Linking and Viscoelasticity. *Biomacromolecules* **2009**, *10* (9), 2694–2698. https://doi.org/10.1021/bm900634x.
(292) Kumar, V. A.; Shi, S.; Wang, B. K.; Li, I.-C.; Jalan, A. A.; Sarkar, B.; Wickremasinghe, N. C.; Hartgerink, J. D. Drug-Triggered and Cross-Linked Self-Assembling Nanofibrous Hydrogels. *J. Am. Chem. Soc.* **2015**, *137* (14), 4823–4830. https://doi.org/10.1021/jacs.5b01549.
(293) Lee, K. Y.; Mooney, D. J. Alginate: Properties and Biomedical Applications. *Prog Polym Sci* **2012**, *37* (1), 106–126. https://doi.org/10.1016/j.progpolymsci.2011.06.003.
(294) Martínez-Martínez, M.; Rodríguez-Berna, G.; Gonzalez-Alvarez, I.; Hernández, M. J.; Corma, A.; Bermejo, M.; Merino, V.; Gonzalez-Alvarez, M. Ionic Hydrogel Based on Chitosan Cross-Linked with 6-Phosphogluconic Trisodium Salt as a Drug Delivery System. *Biomacromolecules* **2018**, *19* (4), 1294–1304. https://doi.org/10.1021/acs.biomac.8b00108.
(295) Karikari, A. S.; Mather, B. D.; Long, T. E. Association of Star-Shaped Poly(d,l-Lactide)s Containing Nucleobase Multiple Hydrogen Bonding. *Biomacromolecules* **2007**, *8* (1), 302–308. https://doi.org/10.1021/bm060869v.
(296) Kang, Y.; Pitto-Barry, A.; Willcock, H.; Quan, W.-D.; Kirby, N.; Sanchez, A. M.; O'Reilly, R. K. Exploiting Nucleobase-Containing Materials – from Monomers to Complex Morphologies Using RAFT Dispersion Polymerization. *Polym. Chem.* **2014**, *6* (1), 106–117. https://doi.org/10.1039/C4PY01074D.
(297) Moura, M. J.; Faneca, H.; Lima, M. P.; Gil, M. H.; Figueiredo, M. M. In Situ Forming Chitosan Hydrogels Prepared via Ionic/Covalent Co-Cross-Linking. *Biomacromolecules* **2011**, *12* (9), 3275–3284. https://doi.org/10.1021/bm200731x.
(298) Yang, J.-A.; Yeom, J.; Hwang, B. W.; Hoffman, A. S.; Hahn, S. K. In Situ-Forming Injectable Hydrogels for Regenerative Medicine. *Progress in Polymer Science* **2014**, *39* (12), 1973–1986. https://doi.org/10.1016/j.progpolymsci.2014.07.006.

(299) Flaherty, D.; Balse, P.; Li, K.; Moore, B. M.; Doughty, M. B. Synthesis of 2-Azido-1,N6-Etheno and 2-Azido Analogs of Deoxyadenosine as Nucleotide Photoaffinity Probes. *Nucleosides and Nucleotides* **1995**, *14* (1–2), 65–76. https://doi.org/10.1080/15257779508014653.
(300) Gelain, F.; Horii, A.; Zhang, S. Designer Self-Assembling Peptide Scaffolds for 3-D Tissue Cell Cultures and Regenerative Medicine. *Macromolecular Bioscience* **2007**, *7* (5), 544–551. https://doi.org/10.1002/mabi.200700033.
(301) Onogi, S.; Shigemitsu, H.; Yoshii, T.; Tanida, T.; Ikeda, M.; Kubota, R.; Hamachi, I. *In Situ* Real-Time Imaging of Self-Sorted Supramolecular Nanofibres. *Nature Chemistry* **2016**, *8* (8), 743–752. https://doi.org/10.1038/nchem.2526.
(302) Yang, L.; Zhang, C.; Ren, C.; Liu, J.; Zhang, Y.; Wang, J.; Huang, F.; Zhang, L.; Liu, J. Supramolecular Hydrogel Based on Chlorambucil and Peptide Drug for Cancer Combination Therapy. *ACS Appl. Mater. Interfaces* **2019**, *11* (1), 331–339. https://doi.org/10.1021/acsami.8b18425.
(303) Jung, J. P.; Jones, J. L.; Cronier, S. A.; Collier, J. H. Modulating the Mechanical Properties of Self-Assembled Peptide Hydrogels via Native Chemical Ligation. *Biomaterials* **2008**, *29* (13), 2143–2151. https://doi.org/10.1016/j.biomaterials.2008.01.008.
(304) Mammadov, R.; Mammadov, B.; Toksoz, S.; Aydin, B.; Yagci, R.; Tekinay, A. B.; Guler, M. O. Heparin Mimetic Peptide Nanofibers Promote Angiogenesis. *Biomacromolecules* **2011**, *12* (10), 3508–3519. https://doi.org/10.1021/bm200957s.
(305) Uzunalli, G.; Mammadov, R.; Yesildal, F.; Alhan, D.; Ozturk, S.; Ozgurtas, T.; Guler, M. O.; Tekinay, A. B. Angiogenic Heparin-Mimetic Peptide Nanofiber Gel Improves Regenerative Healing of Acute Wounds. *ACS Biomater. Sci. Eng.* **2017**, *3* (7), 1296–1303. https://doi.org/10.1021/acsbiomaterials.6b00165.
(306) Guttenplan, A. P. M.; Young, L. J.; Matak-Vinkovic, D.; Kaminski, C. F.; Knowles, T. P. J.; Itzhaki, L. S. Nanoscale Click-Reactive Scaffolds from Peptide Self-Assembly. *J Nanobiotechnology* **2017**, *15*. https://doi.org/10.1186/s12951-017-0300-7.
(307) Li, X.; Kuang, Y.; Lin, H.-C.; Gao, Y.; Shi, J.; Xu, B. Supramolecular Nanofibers and Hydrogels of Nucleopeptides. *Angewandte Chemie International Edition* **2011**, *50* (40), 9365–9369. https://doi.org/10.1002/anie.201103641.
(308) Wang, H.; Feng, Z.; Qin, Y.; Wang, J.; Xu, B. Nucleopeptide Assemblies Selectively Sequester ATP in Cancer Cells to Increase the Efficacy of Doxorubicin. *Angewandte Chemie International Edition* **2018**, *57* (18), 4931–4935. https://doi.org/10.1002/anie.201712834.
(309) Li, X.; Du, X.; Gao, Y.; Shi, J.; Kuang, Y.; Xu, B. Supramolecular Hydrogels Formed by the Conjugates of Nucleobases , Arg-Gly-Asp (RGD) Peptides , and Glucosamine. *Soft Matter* **2012**, *8* (28), 7402–7407. https://doi.org/10.1039/C2SM25725D.

(310) Vernille, J. P.; Kovell, L. C.; Schneider, J. W. Peptide Nucleic Acid (PNA) Amphiphiles: Synthesis, Self-Assembly, and Duplex Stability. *Bioconjugate Chem.* **2004**, *15* (6), 1314–1321. https://doi.org/10.1021/bc049831a.
(311) DiMaio, J. T. M.; Doran, T. M.; Ryan, D. M.; Raymond, D. M.; Nilsson, B. L. Modulating Supramolecular Peptide Hydrogel Viscoelasticity Using Biomolecular Recognition. *Biomacromolecules* **2017**, *18* (11), 3591–3599. https://doi.org/10.1021/acs.biomac.7b00925.
(312) Peters, G. M.; Davis, J. T. Supramolecular Gels Made from Nucleobase, Nucleoside and Nucleotide Analogs. *Chem. Soc. Rev.* **2016**, *45* (11), 3188–3206. https://doi.org/10.1039/C6CS00183A.
(313) Skilling, K. J.; Stocks, M. J.; Kellam, B.; Ashford, M.; Bradshaw, T. D.; Burroughs, L.; Marlow, M. Nucleoside-Based Self-Assembling Drugs for Localized Drug Delivery. *ChemMedChem* **2018**, *13* (11), 1098–1101. https://doi.org/10.1002/cmdc.201800063.
(314) Couvreur, P.; Stella, B.; Reddy, L. H.; Hillaireau, H.; Dubernet, C.; Desmaële, D.; Lepêtre-Mouelhi, S.; Rocco, F.; Dereuddre-Bosquet, N.; Clayette, P.; et al. Squalenoyl Nanomedicines as Potential Therapeutics. *Nano Lett.* **2006**, *6* (11), 2544–2548. https://doi.org/10.1021/nl061942q.
(315) Liang, H.; Zhang, Z.; Yuan, Q.; Liu, J. Self-Healing Metal-Coordinated Hydrogels Using Nucleotide Ligands. *Chem. Commun.* **2015**, *51* (82), 15196–15199. https://doi.org/10.1039/C5CC06824J.
(316) Wang, Y.; Desbat, B.; Manet, S.; Aimé, C.; Labrot, T.; Oda, R. Aggregation Behaviors of Gemini Nucleotide at the Air–Water Interface and in Solutions Induced by Adenine–Uracil Interaction. *Journal of Colloid and Interface Science* **2005**, *283* (2), 555–564. https://doi.org/10.1016/j.jcis.2004.09.003.
(317) Lane, A. N.; Chaires, J. B.; Gray, R. D.; Trent, J. O. Stability and Kinetics of G-Quadruplex Structures. *Nucleic Acids Res* **2008**, *36* (17), 5482–5515. https://doi.org/10.1093/nar/gkn517.
(318) Buerkle, L. E.; Recum, H. A. von; Rowan, S. J. Toward Potential Supramolecular Tissue Engineering Scaffolds Based on Guanosine Derivatives. *Chem. Sci.* **2012**, *3* (2), 564–572. https://doi.org/10.1039/C1SC00729G.
(319) Peters, G. M.; Skala, L. P.; Plank, T. N.; Oh, H.; Reddy, G. N. M.; Marsh, A.; Brown, S. P.; Raghavan, S. R.; Davis, J. T. G4-Quartet·M(+) Borate Hydrogels. *J. Am. Chem. Soc.* **2015**, *137* (17), 5819–5827. https://doi.org/10.1021/jacs.5b02753.
(320) Way, A. E.; Korpusik, A. B.; Dorsey, T. B.; Buerkle, L. E.; von Recum, H. A.; Rowan, S. J. Enhancing the Mechanical Properties of Guanosine-Based Supramolecular Hydrogels with Guanosine-Containing Polymers. *Macromolecules* **2014**, *47* (5), 1810–1818. https://doi.org/10.1021/ma402618z.
(321) Peters, G. M.; Skala, L. P.; Davis, J. T. A Molecular Chaperone for G4-Quartet Hydrogels. *J. Am. Chem. Soc.* **2016**, *138* (1), 134–139. https://doi.org/10.1021/jacs.5b08769.

(322) Datta, D.; Tiwari, O.; Ganesh, K. N. New Archetypes in Self-Assembled Phe-Phe Motif Induced Nanostructures from Nucleoside Conjugated-Diphenylalanines. *Nanoscale* **2018**, *10* (7), 3212–3224. https://doi.org/10.1039/C7NR08436F.
(323) Du, X.; Li, J.; Gao, Y.; Kuang, Y.; Xu, B. Catalytically Dephosphorylate Adenosine Monophosphate (AMP) to Form Supramolecular Nanofibers/Hydrogels. *Chem Commun (Camb)* **2012**, *48* (15), 2098–2100. https://doi.org/10.1039/c2cc16723a.
(324) Schnitzler, J. G.; Bernelot Moens, S. J.; Tiessens, F.; Bakker, G. J.; Dallinga-Thie, G. M.; Groen, A. K.; Nieuwdorp, M.; Stroes, E. S. G.; Kroon, J. Nile Red Quantifier: A Novel and Quantitative Tool to Study Lipid Accumulation in Patient-Derived Circulating Monocytes Using Confocal Microscopy. *J Lipid Res* **2017**, *58* (11), 2210–2219. https://doi.org/10.1194/jlr.D073197.
(325) Rexeisen, E. L.; Fan, W.; Pangburn, T. O.; Taribagil, R. R.; Bates, F. S.; Lodge, T. P.; Tsapatsis, M.; Kokkoli, E. Self-Assembly of Fibronectin Mimetic Peptide-Amphiphile Nanofibers. *Langmuir* **2010**, *26* (3), 1953–1959. https://doi.org/10.1021/la902571q.
(326) Rai, U.; Thrimawithana, T. R.; Dharmadana, D.; Valery, C.; Young, S. A. Release Kinetics of Somatostatin from Self-Assembled Nanostructured Hydrogels. *Peptide Science* **2018**, *110* (2), e23085. https://doi.org/10.1002/bip.23085.
(327) Pizzey, C. L.; Pomerantz, W. C.; Sung, B.-J.; Yuwono, V. M.; Gellman, S. H.; Hartgerink, J. D.; Yethiraj, A.; Abbott, N. L. Characterization of Nanofibers Formed by Self-Assembly of β-Peptide Oligomers Using Small Angle x-Ray Scattering. *J. Chem. Phys.* **2008**, *129* (9), 095103. https://doi.org/10.1063/1.2955745.
(328) Blanchet, C. E.; Svergun, D. I. Small-Angle X-Ray Scattering on Biological Macromolecules and Nanocomposites in Solution. *Annual Review of Physical Chemistry* **2013**, *64* (1), 37–54. https://doi.org/10.1146/annurev-physchem-040412-110132.
(329) Palmer, L. C.; Leung, C.-Y.; Kewalramani, S.; Kumthekar, R.; Newcomb, C. J.; Olvera de la Cruz, M.; Bedzyk, M. J.; Stupp, S. I. Long-Range Ordering of Highly Charged Self-Assembled Nanofilaments. *J. Am. Chem. Soc.* **2014**, *136* (41), 14377–14380. https://doi.org/10.1021/ja5082519.
(330) Koenigs, M. M. E.; Pal, A.; Mortazavi, H.; Pawar, G. M.; Storm, C.; Sijbesma, R. P. Tuning Cross-Link Density in a Physical Hydrogel by Supramolecular Self-Sorting. *Macromolecules* **2014**, *47* (8), 2712–2717. https://doi.org/10.1021/ma500446g.
(331) Jaspers, M.; Pape, A. C. H.; Voets, I. K.; Rowan, A. E.; Portale, G.; Kouwer, P. H. J. Bundle Formation in Biomimetic Hydrogels. *Biomacromolecules* **2016**, *17* (8), 2642–2649. https://doi.org/10.1021/acs.biomac.6b00703.
(332) Loh, W.; Brinatti, C.; Tam, K. C. Use of Isothermal Titration Calorimetry to Study Surfactant Aggregation in Colloidal Systems. *Biochimica et Biophysica Acta (BBA) - General Subjects* **2016**, *1860* (5), 999–1016. https://doi.org/10.1016/j.bbagen.2015.10.003.

(333) Kabiri, M.; Unsworth, L. D. Application of Isothermal Titration Calorimetry for Characterizing Thermodynamic Parameters of Biomolecular Interactions: Peptide Self-Assembly and Protein Adsorption Case Studies. *Biomacromolecules* **2014**, *15* (10), 3463–3473. https://doi.org/10.1021/bm5004515.
(334) Carducci, F.; Yoneda, J. S.; Itri, R.; Mariani, P. On the Structural Stability of Guanosine-Based Supramolecular Hydrogels. *Soft Matter* **2018**, *14* (15), 2938–2948. https://doi.org/10.1039/C8SM00299A.
(335) Fonseca Guerra, C.; Bickelhaupt, F. M.; Snijders, J. G.; Baerends, E. J. Hydrogen Bonding in DNA Base Pairs: Reconciliation of Theory and Experiment. *J. Am. Chem. Soc.* **2000**, *122* (17), 4117–4128. https://doi.org/10.1021/ja993262d.
(336) Escuder, B.; LLusar, M.; Miravet, J. F. Insight on the NMR Study of Supramolecular Gels and Its Application to Monitor Molecular Recognition on Self-Assembled Fibers. *J. Org. Chem.* **2006**, *71* (20), 7747–7752. https://doi.org/10.1021/jo0612731.
(337) Kabiri, M.; Bushnak, I.; McDermot, M. T.; Unsworth, L. D. Toward a Mechanistic Understanding of Ionic Self-Complementary Peptide Self-Assembly: Role of Water Molecules and Ions. *Biomacromolecules* **2013**, *14* (11), 3943–3950. https://doi.org/10.1021/bm401077b.
(338) Morel, B.; Varela, L.; Conejero-Lara, F. The Thermodynamic Stability of Amyloid Fibrils Studied by Differential Scanning Calorimetry. *J. Phys. Chem. B* **2010**, *114* (11), 4010–4019. https://doi.org/10.1021/jp9102993.
(339) Yu, G.; Yan, X.; Han, C.; Huang, F. Characterization of Supramolecular Gels. *Chem. Soc. Rev.* **2013**, *42* (16), 6697–6722. https://doi.org/10.1039/C3CS60080G.
(340) Jordheim, L. P.; Durantel, D.; Zoulim, F.; Dumontet, C. Advances in the Development of Nucleoside and Nucleotide Analogues for Cancer and Viral Diseases. *Nature Reviews Drug Discovery* **2013**, *12* (6), 447–464. https://doi.org/10.1038/nrd4010.
(341) Parker, W. B. Enzymology of Purine and Pyrimidine Antimetabolites Used in the Treatment of Cancer. *Chemical Reviews* **2009**, *109* (7), 2880–2893. https://doi.org/10.1021/cr900028p.
(342) Shelton, J.; Lu, X.; Hollenbaugh, J. A.; Cho, J. H.; Amblard, F.; Schinazi, R. F. Metabolism, Biochemical Actions, and Chemical Synthesis of Anticancer Nucleosides, Nucleotides, and Base Analogs. *Chemical Reviews* **2016**, *116* (23), 14379–14455. https://doi.org/10.1021/acs.chemrev.6b00209.
(343) De Clercq, E. The Nucleoside Reverse Transcriptase Inhibitors, Nonnucleoside Reverse Transcriptase Inhibitors, and Protease Inhibitors in the Treatment of HIV Infections (AIDS). *Adv. Pharmacol.* **2013**, *67*, 317–358. https://doi.org/10.1016/B978-0-12-405880-4.00009-3.
(344) Feng, J. Y. Addressing the Selectivity and Toxicity of Antiviral Nucleosides. *Antivir Chem Chemother* **2018**, *26*, 2040206618758524. https://doi.org/10.1177/2040206618758524.

(345) Galmarini, C. M.; Mackey, J. R.; Dumontet, C. Nucleoside Analogues and Nucleobases in Cancer Treatment. *The Lancet Oncology* **2002**, *3* (7), 415–424. https://doi.org/10.1016/S1470-2045(02)00788-X.
(346) Dasanu, C. A. Gemcitabine: Vascular Toxicity and Prothrombotic Potential. *Expert Opinion on Drug Safety* **2008**, *7* (6), 703–716. https://doi.org/10.1517/14740330802374262.
(347) Galmarini, C. M.; Mackey, J. R.; Dumontet, C. Nucleoside Analogues: Mechanisms of Drug Resistance and Reversal Strategies. *Leukemia* **2001**, *15* (6), 875–890. https://doi.org/10.1038/sj.leu.2402114.
(348) Kim, M. P.; Gallick, G. E. Gemcitabine Resistance in Pancreatic Cancer: Picking the Key Players. *Clin Cancer Res* **2008**, *14* (5), 1284–1285. https://doi.org/10.1158/1078-0432.CCR-07-2247.
(349) Zhang, J.; Visser, F.; King, K. M.; Baldwin, S. A.; Young, J. D.; Cass, C. E. The Role of Nucleoside Transporters in Cancer Chemotherapy with Nucleoside Drugs. *Cancer and Metastasis Reviews* **2007**, *26* (1), 85–110. https://doi.org/10.1007/s10555-007-9044-4.
(350) Sahasranaman, S.; Howard, D.; Roy, S. Clinical Pharmacology and Pharmacogenetics of Thiopurines. *Eur. J. Clin. Pharmacol.* **2008**, *64* (8), 753–767. https://doi.org/10.1007/s00228-008-0478-6.
(351) Arnér, E. S. J.; Eriksson, S. Mammalian Deoxyribonucleoside Kinases. *Pharmacology & Therapeutics* **1995**, *67* (2), 155–186. https://doi.org/10.1016/0163-7258(95)00015-9.
(352) Van Rompay, A. R.; Johansson, M.; Karlsson, A. Phosphorylation of Nucleosides and Nucleoside Analogs by Mammalian Nucleoside Monophosphate Kinases. *Pharmacology & Therapeutics* **2000**, *87* (2), 189–198. https://doi.org/10.1016/S0163-7258(00)00048-6.
(353) Van Rompay, A. R.; Johansson, M.; Karlsson, A. Substrate Specificity and Phosphorylation of Antiviral and Anticancer Nucleoside Analogues by Human Deoxyribonucleoside Kinases and Ribonucleoside Kinases. *Pharmacology & Therapeutics* **2003**, *100* (2), 119–139. https://doi.org/10.1016/j.pharmthera.2003.07.001.
(354) Achanta, G.; Pelicano, H.; Feng, L.; Plunkett, W.; Huang, P. Interaction of P53 and DNA-PK in Response to Nucleoside Analogues: Potential Role as a Sensor Complex for DNA Damage. *Cancer Res.* **2001**, *61* (24), 8723–8729.
(355) Jackson, S. P.; Bartek, J. The DNA-Damage Response in Human Biology and Disease. *Nature* **2009**, *461* (7267), 1071–1078. https://doi.org/10.1038/nature08467.
(356) Jordheim, L. P.; Dumontet, C. Review of Recent Studies on Resistance to Cytotoxic Deoxynucleoside Analogues. *Biochimica et Biophysica Acta (BBA) - Reviews on Cancer* **2007**, *1776* (2), 138–159. https://doi.org/10.1016/j.bbcan.2007.07.004.
(357) Heinemann, V. Gemcitabine: Progress in the Treatment of Pancreatic Cancer. *Oncology* **2001**, *60* (1), 8–18. https://doi.org/10.1159/000055290.

(358) Larsen, F. O.; Hansen, S. W. Severe Neurotoxicity Caused by Gemcitabine Treatment. *Acta Oncol* **2004**, *43* (6), 590–591. https://doi.org/10.1080/02841860410018494.
(359) Peters, G. J.; Clavel, M.; Noordhuis, P.; Geyssen, G. J.; Laan, A. C.; Guastalla, J.; Edzes, H. T.; Vermorken, J. B. Clinical Phase I and Pharmacology Study of Gemcitabine (2', 2'-Difluorodeoxycytidine) Administered in a Two-Weekly Schedule. *J Chemother* **2007**, *19* (2), 212–221. https://doi.org/10.1179/joc.2007.19.2.212.
(360) Moysan, E.; Bastiat, G.; Benoit, J.-P. Gemcitabine versus Modified Gemcitabine: A Review of Several Promising Chemical Modifications. *Mol. Pharm.* **2013**, *10* (2), 430–444. https://doi.org/10.1021/mp300370t.
(361) Higuchi, T.; Yokobori, T.; Takahashi, R.; Naito, T.; Kitahara, H.; Matsumoto, T.; Kakinuma, C.; Hagiwara, S.; Kuwano, H.; Shirabe, K.; et al. FF-10832 Enables Long Survival via Effective Gemcitabine Accumulation in Lethal Murine Peritoneal Dissemination Model. *Cancer Sci.* **2019**. https://doi.org/10.1111/cas.14123.
(362) Vandana, M.; Sahoo, S. K. Long Circulation and Cytotoxicity of PEGylated Gemcitabine and Its Potential for the Treatment of Pancreatic Cancer. *Biomaterials* **2010**, *31* (35), 9340–9356. https://doi.org/10.1016/j.biomaterials.2010.08.010.
(363) Park, J. Y.; Cho, Y. L.; Chae, J. R.; Moon, S. H.; Cho, W. G.; Choi, Y. J.; Lee, S. J.; Kang, W. J. Gemcitabine-Incorporated G-Quadruplex Aptamer for Targeted Drug Delivery into Pancreas Cancer. *Molecular Therapy - Nucleic Acids* **2018**, *12*, 543–553. https://doi.org/10.1016/j.omtn.2018.06.003.
(364) Slusarczyk, M.; Lopez, M. H.; Balzarini, J.; Mason, M.; Jiang, W. G.; Blagden, S.; Thompson, E.; Ghazaly, E.; McGuigan, C. Application of ProTide Technology to Gemcitabine: A Successful Approach to Overcome the Key Cancer Resistance Mechanisms Leads to a New Agent (NUC-1031) in Clinical Development. *J. Med. Chem.* **2014**, *57* (4), 1531–1542. https://doi.org/10.1021/jm401853a.
(365) Firer, M. A.; Gellerman, G. Targeted Drug Delivery for Cancer Therapy: The Other Side of Antibodies. *J Hematol Oncol* **2012**, *5*, 70. https://doi.org/10.1186/1756-8722-5-70.
(366) Karampelas, T.; Argyros, O.; Sayyad, N.; Spyridaki, K.; Pappas, C.; Morgan, K.; Kolios, G.; Millar, R. P.; Liapakis, G.; Tzakos, A. G.; et al. GnRH-Gemcitabine Conjugates for the Treatment of Androgen-Independent Prostate Cancer: Pharmacokinetic Enhancements Combined with Targeted Drug Delivery. *Bioconjugate Chem.* **2014**, *25* (4), 813–823. https://doi.org/10.1021/bc500081g.
(367) Kruspe, S.; Hahn, U. An Aptamer Intrinsically Comprising 5-Fluoro-2′-Deoxyuridine for Targeted Chemotherapy. *Angewandte Chemie International Edition* **2014**, *53* (39), 10541–10544. https://doi.org/10.1002/anie.201405778.
(368) Hammam, K.; Saez-Ayala, M.; Rebuffet, E.; Gros, L.; Lopez, S.; Hajem, B.; Humbert, M.; Baudelet, E.; Audebert, S.; Betzi, S.; et al. Dual Protein Kinase and Nucleoside Kinase Modulators for Rationally Designed Polypharmacology. *Nature Communications* **2017**, *8* (1), 1420. https://doi.org/10.1038/s41467-017-01582-5.

(369) Okon, A.; Matos de Souza, M. R.; Shah, R.; Amorim, R.; da Costa, L. J.; Wagner, C. R. Anchimerically Activatable Antiviral ProTides. *ACS Med. Chem. Lett.* **2017**, *8* (9), 958–962. https://doi.org/10.1021/acsmedchemlett.7b00277.
(370) Slusarczyk, M.; Serpi, M.; Pertusati, F. Phosphoramidates and Phosphonamidates (ProTides) with Antiviral Activity. *Antivir Chem Chemother* **2018**, *26*, 2040206618775243. https://doi.org/10.1177/2040206618775243.
(371) Abraham, T. W.; Wagner, C. R. A Phosphoramidite-Based Synthesis of Phosphoramidate Amino Acid Diesters of Antiviral Nucleosides. *Nucleosides and Nucleotides* **1994**, *13* (9), 1891–1903. https://doi.org/10.1080/15257779408010671.
(372) Wagner, C. R.; McIntee, E. J.; Schinazi, R. F.; Abraham, T. W. Aromatic Amino Acid Phosphoramidate Di- and Triesters of 3′-Azido-3′-Deoxythymidine (AZT) Are Non-Toxic Inhibitors of HIV-1 Replication. *Bioorganic & Medicinal Chemistry Letters* **1995**, *5* (16), 1819–1824. https://doi.org/10.1016/0960-894X(95)00302-A.
(373) Iyer, V. V.; Griesgraber, G. W.; Radmer, M. R.; McIntee, E. J.; Wagner, C. R. Synthesis, in Vitro Anti-Breast Cancer Activity, and Intracellular Decomposition of Amino Acid Methyl Ester and Alkyl Amide Phosphoramidate Monoesters of 3‘-Azido-3‘-Deoxythymidine (AZT). *J. Med. Chem.* **2000**, *43* (11), 2266–2274. https://doi.org/10.1021/jm000110g.
(374) Wagner, C. R.; Ballato, G.; Akanni, A. O.; McIntee, E. J.; Larson, R. S.; Chang, S.; Abul-Hajj, Y. J. Potent Growth Inhibitory Activity of Zidovudine on Cultured Human Breast Cancer Cells and Rat Mammary Tumors. *Cancer Res* **1997**, *57* (12), 2341–2345.
(375) Ghosh, B.; Benyumov, A. O.; Ghosh, P.; Jia, Y.; Avdulov, S.; Dahlberg, P. S.; Peterson, M.; Smith, K.; Polunovsky, V. A.; Bitterman, P. B.; et al. Nontoxic Chemical Interdiction of the Epithelial-to-Mesenchymal Transition by Targeting Cap-Dependent Translation. *ACS Chem. Biol.* **2009**, *4* (5), 367–377. https://doi.org/10.1021/cb9000475.
(376) Kim, J.; Chou, T.; Griesgraber, G. W.; Wagner, C. R. Direct Measurement of Nucleoside Monophosphate Delivery from a Phosphoramidate Pronucleotide by Stable Isotope Labeling and LC−ESI--MS/MS. *Mol. Pharmaceutics* **2004**, *1* (2), 102–111. https://doi.org/10.1021/mp0340338.
(377) Li, S.; Jia, Y.; Jacobson, B.; McCauley, J.; Kratzke, R.; Bitterman, P. B.; Wagner, C. R. Treatment of Breast and Lung Cancer Cells with a N-7 Benzyl Guanosine Monophosphate Tryptamine Phosphoramidate Pronucleotide (4Ei-1) Results in Chemosensitization to Gemcitabine and Induced ElF4E Proteasomal Degradation. *Mol Pharm* **2013**, *10* (2), 523–531. https://doi.org/10.1021/mp300699d.
(378) Murakami, E.; Tolstykh, T.; Bao, H.; Niu, C.; Steuer, H. M. M.; Bao, D.; Chang, W.; Espiritu, C.; Bansal, S.; Lam, A. M.; et al. Mechanism of Activation of PSI-7851 and Its Diastereoisomer PSI-7977. *J. Biol. Chem.* **2010**, *285* (45), 34337–34347. https://doi.org/10.1074/jbc.M110.161802.

(379) Blagden, S. P.; Rizzuto, I.; Suppiah, P.; O'Shea, D.; Patel, M.; Spiers, L.; Sukumaran, A.; Bharwani, N.; Rockall, A.; Gabra, H.; et al. Anti-Tumour Activity of a First-in-Class Agent NUC-1031 in Patients with Advanced Cancer: Results of a Phase I Study. *British Journal of Cancer* **2018**, *119* (7), 815. https://doi.org/10.1038/s41416-018-0244-1.
(380) Sofia, M. J.; Bao, D.; Chang, W.; Du, J.; Nagarathnam, D.; Rachakonda, S.; Reddy, P. G.; Ross, B. S.; Wang, P.; Zhang, H.-R.; et al. Discovery of a β-d-2′-Deoxy-2′-α-Fluoro-2′-β-C-Methyluridine Nucleotide Prodrug (PSI-7977) for the Treatment of Hepatitis C Virus. *J. Med. Chem.* **2010**, *53* (19), 7202–7218. https://doi.org/10.1021/jm100863x.
(381) May, J. P.; Ernsting, M. J.; Undzys, E.; Li, S.-D. Thermosensitive Liposomes for the Delivery of Gemcitabine and Oxaliplatin to Tumors. *Mol. Pharmaceutics* **2013**, *10* (12), 4499–4508. https://doi.org/10.1021/mp400321e.
(382) Utama, R. H.; Drechsler, M.; Förster, S.; Zetterlund, P. B.; Stenzel, M. H. Synthesis of PH-Responsive Nanocapsules via Inverse Miniemulsion Periphery RAFT Polymerization and Post-Polymerization Reaction. *ACS Macro Lett.* **2014**, *3* (9), 935–939. https://doi.org/10.1021/mz5005019.
(383) Utama, R. H.; Jiang, Y.; Zetterlund, P. B.; Stenzel, M. H. Biocompatible Glycopolymer Nanocapsules via Inverse Miniemulsion Periphery RAFT Polymerization for the Delivery of Gemcitabine. *Biomacromolecules* **2015**, *16* (7), 2144–2156. https://doi.org/10.1021/acs.biomac.5b00545.
(384) Zhang, Y.; Bush, X.; Yan, B.; Chen, J. A. Gemcitabine Nanoparticles Promote Antitumor Immunity against Melanoma. *Biomaterials* **2019**, *189*, 48–59. https://doi.org/10.1016/j.biomaterials.2018.10.022.
(385) Li, J.; Mooney, D. J. Designing Hydrogels for Controlled Drug Delivery. *Nature Reviews Materials* **2016**, *1* (12), 16071. https://doi.org/10.1038/natrevmats.2016.71.
(386) Sobot, D.; Mura, S.; Yesylevskyy, S. O.; Dalbin, L.; Cayre, F.; Bort, G.; Mougin, J.; Desmaële, D.; Lepetre-Mouelhi, S.; Pieters, G.; et al. Conjugation of Squalene to Gemcitabine as Unique Approach Exploiting Endogenous Lipoproteins for Drug Delivery. *Nature Communications* **2017**, *8*, 15678. https://doi.org/10.1038/ncomms15678.
(387) Bastiancich, C.; Lemaire, L.; Bianco, J.; Franconi, F.; Danhier, F.; Préat, V.; Bastiat, G.; Lagarce, F. Evaluation of Lauroyl-Gemcitabine-Loaded Hydrogel Efficacy in Glioblastoma Rat Models. *Nanomedicine* **2018**, *13* (16), 1999–2013. https://doi.org/10.2217/nnm-2018-0057.
(388) Lepeltier, E.; Bourgaux, C.; Maksimenko, A.; Meneau, F.; Rosilio, V.; Sliwinski, E.; Zouhiri, F.; Desmaële, D.; Couvreur, P. Self-Assembly of Polyisoprenoyl Gemcitabine Conjugates: Influence of Supramolecular Organization on Their Biological Activity. *Langmuir* **2014**, *30* (22), 6348–6357. https://doi.org/10.1021/la5007132.
(389) Wolinsky, J. B.; Colson, Y. L.; Grinstaff, M. W. Local Drug Delivery Strategies for Cancer Treatment: Gels, Nanoparticles, Polymeric Films, Rods, and Wafers.

*Journal of Controlled Release* **2012**, *159* (1), 14–26. https://doi.org/10.1016/j.jconrel.2011.11.031.
(390) Ren, C.; Xu, C.; Li, D.; Ren, H.; Hao, J.; Yang, Z. Gemcitabine Induced Supramolecular Hydrogelations of Aldehyde-Containing Short Peptides. *RSC Advances* **2014**, *4* (66), 34729–34732. https://doi.org/10.1039/C4RA05808A.
(391) Corre, S. S. L.; Berchel, M.; Couthon-Gourvès, H.; Haelters, J.-P.; Jaffrès, P.-A. Atherton–Todd Reaction: Mechanism, Scope and Applications. *Beilstein J. Org. Chem.* **2014**, *10* (1), 1166–1196. https://doi.org/10.3762/bjoc.10.117.
(392) Atherton, F. R.; Openshaw, H. T.; Todd, A. R. 174. Studies on Phosphorylation. Part II. The Reaction of Dialkyl Phosphites with Polyhalogen Compounds in Presence of Bases. A New Method for the Phosphorylation of Amines. *J. Chem. Soc.* **1945**, *0* (0), 660–663. https://doi.org/10.1039/JR9450000660.
(393) Atherton, F. R.; Todd, A. R. 129. Studies on Phosphorylation. Part III. Further Observations on the Reaction of Phosphites with Polyhalogen Compounds in Presence of Bases and Its Application to the Phosphorylation of Alcohols. *J. Chem. Soc.* **1947**, No. 0, 674–678. https://doi.org/10.1039/JR9470000674.
(394) Guerlavais-Dagland, T.; Meyer, A.; Imbach, J.-L.; Morvan, F. Fluoride-Labile Protecting Groups for the Synthesis of Base-Sensitive Methyl-SATE Oligonucleotide Prodrugs. *European Journal of Organic Chemistry* **2003**, *2003* (12), 2327–2335. https://doi.org/10.1002/ejoc.200300069.
(395) Zhang, Y.; Kuang, Y.; Gao, Y.; Xu, B. Versatile Small Molecule Motifs for Self-Assembly in Water and Formation of Biofunctional Supramolecular Hydrogels. *Langmuir* **2011**, *27* (2), 529–537. https://doi.org/10.1021/la1020324.
(396) Traut, T. W. Physiological Concentrations of Purines and Pyrimidines. *Mol Cell Biochem* **1994**, *140* (1), 1–22. https://doi.org/10.1007/BF00928361.
(397) Yao, Q.; Huang, Z.; Liu, D.; Chen, J.; Gao, Y. Enzyme-Instructed Supramolecular Self-Assembly with Anticancer Activity. *Advanced Materials 0* (0), 1804814. https://doi.org/10.1002/adma.201804814.
(398) Li, J.; Shi, J.; Medina, J. E.; Zhou, J.; Du, X.; Wang, H.; Yang, C.; Liu, J.; Yang, Z.; Dinulescu, D. M.; et al. Selectively Inducing Cancer Cell Death by Intracellular Enzyme-Instructed Self-Assembly (EISA) of Dipeptide Derivatives. *Adv Healthc Mater* **2017**, *6* (15). https://doi.org/10.1002/adhm.201601400.
(399) Wang, C.; Wang, J.; Zhang, X.; Yu, S.; Wen, D.; Hu, Q.; Ye, Y.; Bomba, H.; Hu, X.; Liu, Z.; et al. In Situ Formed Reactive Oxygen Species–Responsive Scaffold with Gemcitabine and Checkpoint Inhibitor for Combination Therapy. *Science Translational Medicine* **2018**, *10* (429), eaan3682. https://doi.org/10.1126/scitranslmed.aan3682.

# APPENDICES

$^{1}$H-NMR and HPLC Chromatograms for Phosphoramidate Pro-gelators **2-8**

NAP-FF-AMP (**2**)

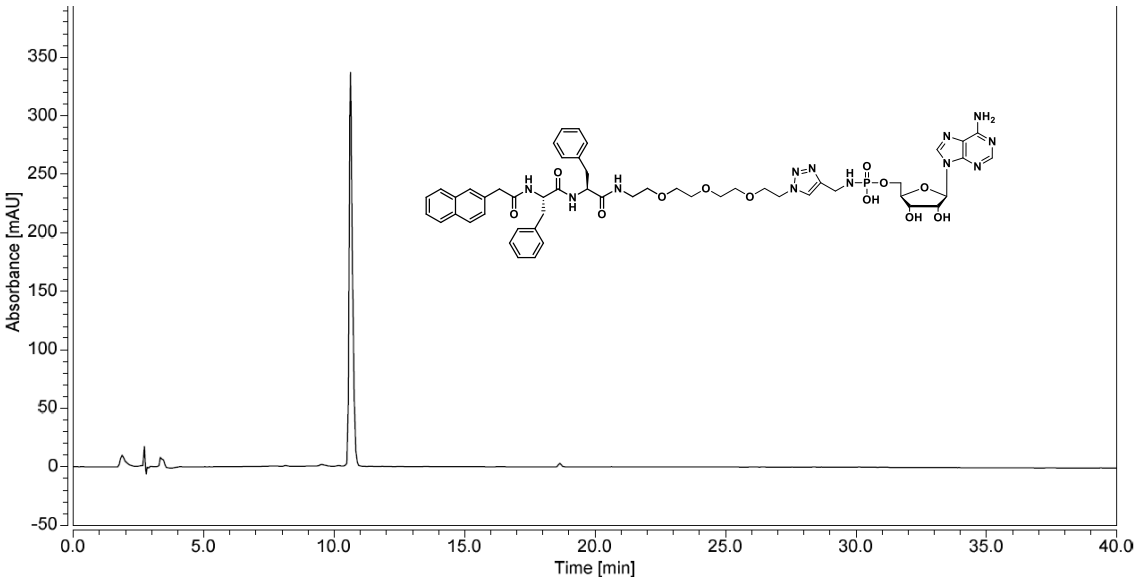


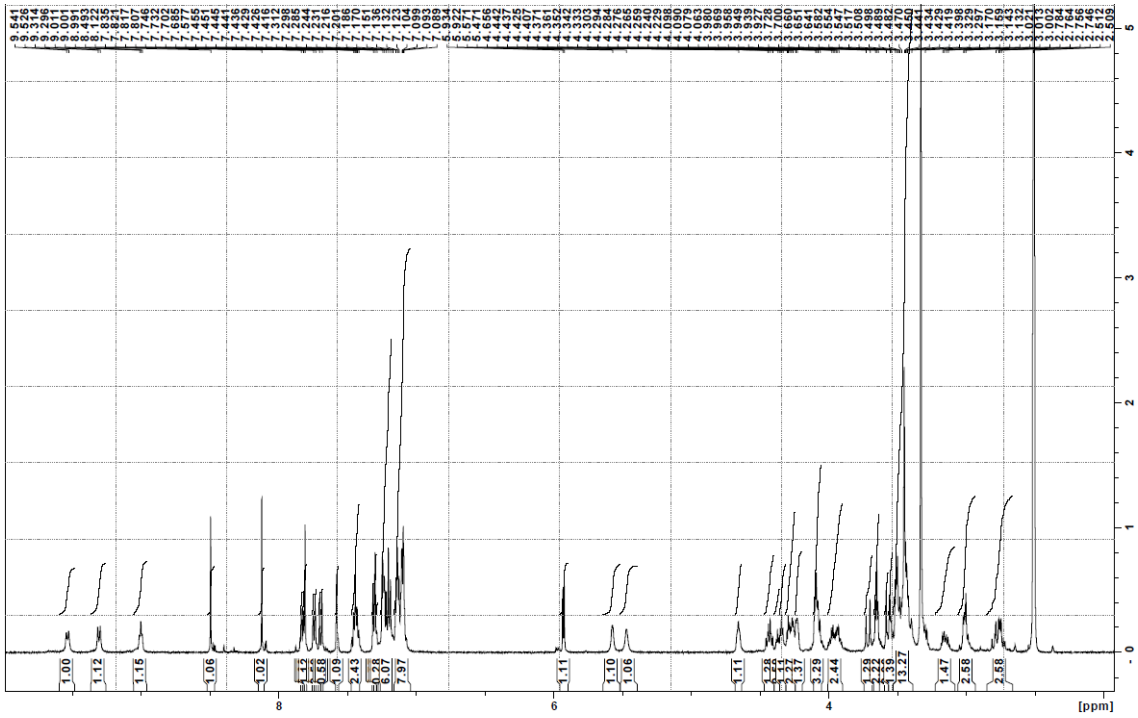

NAP-FF-UMP (**3**)

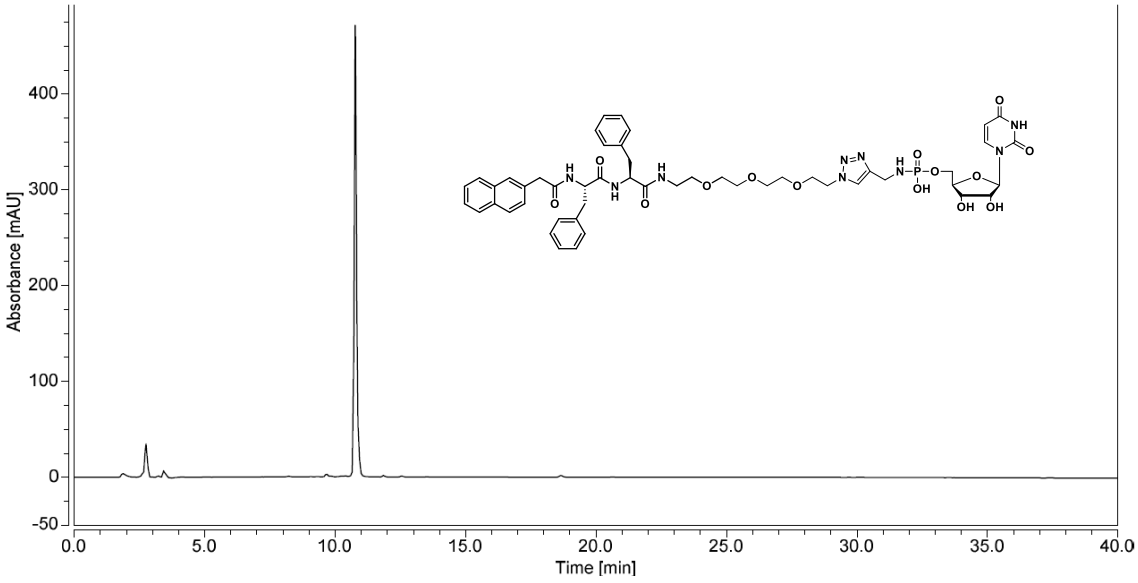


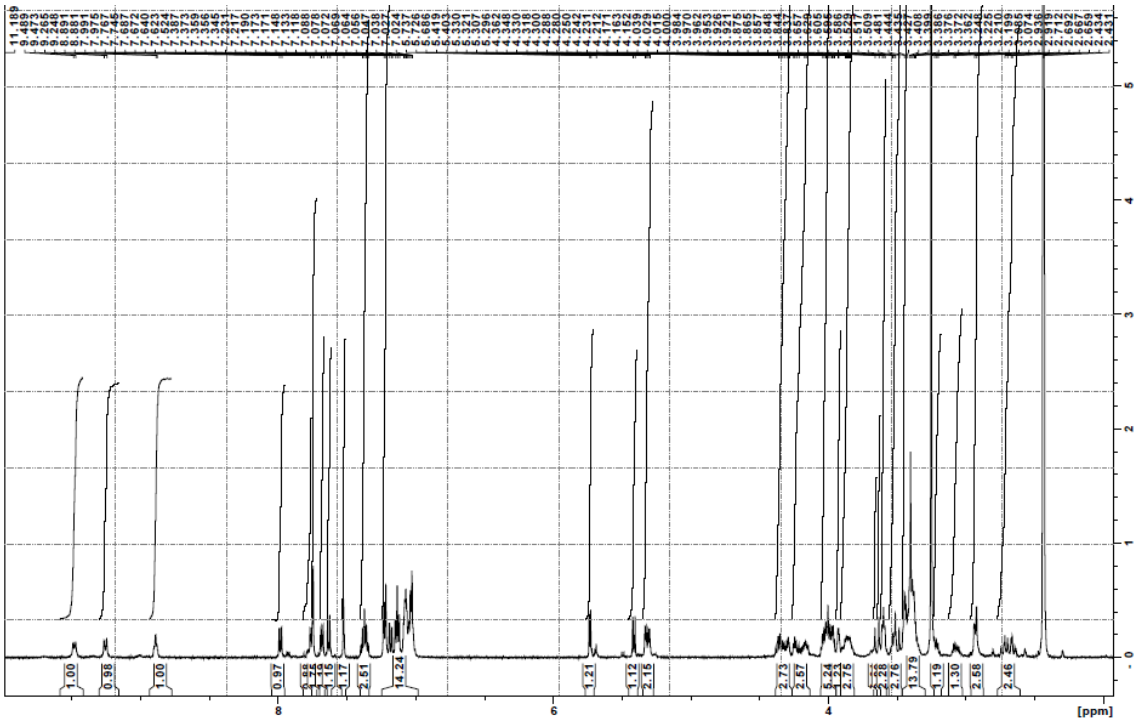

NAP-FF-GMP (**4**)

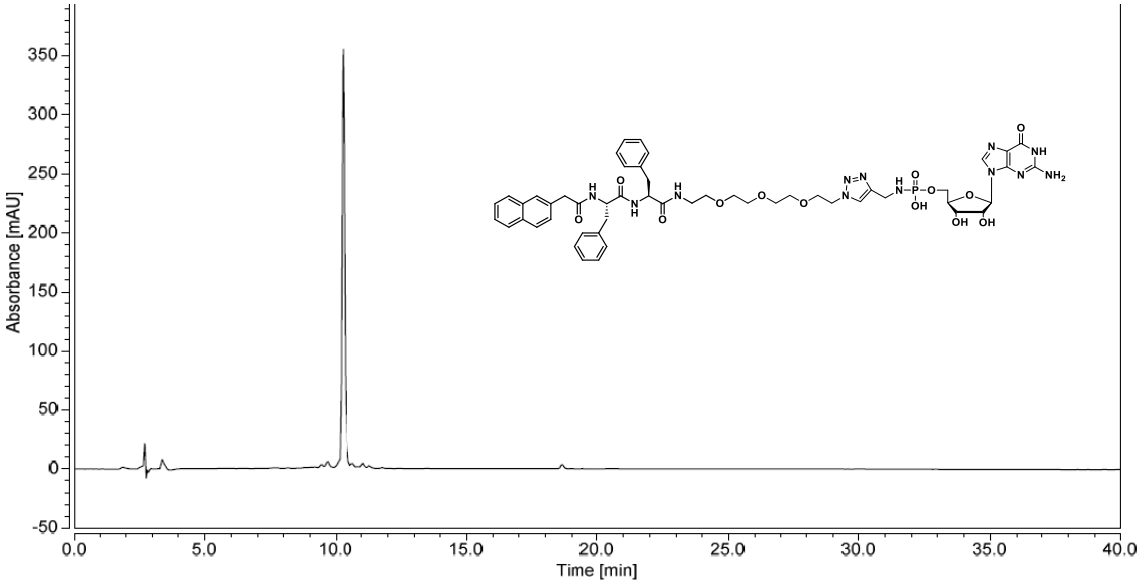


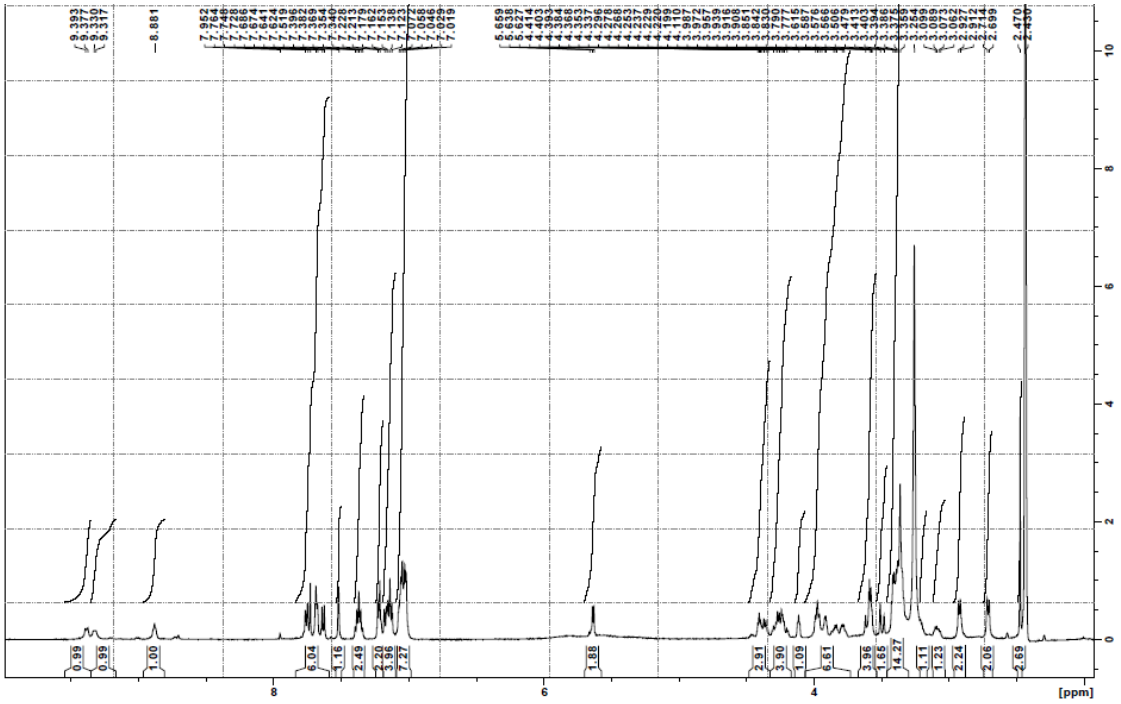

NAP-FF-CMP (**5**)

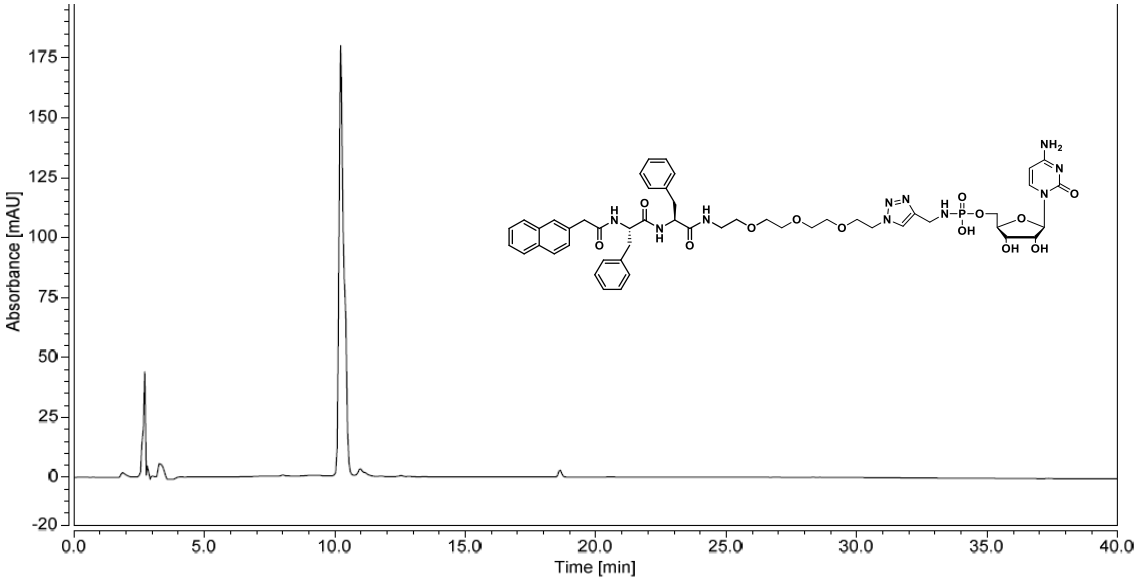


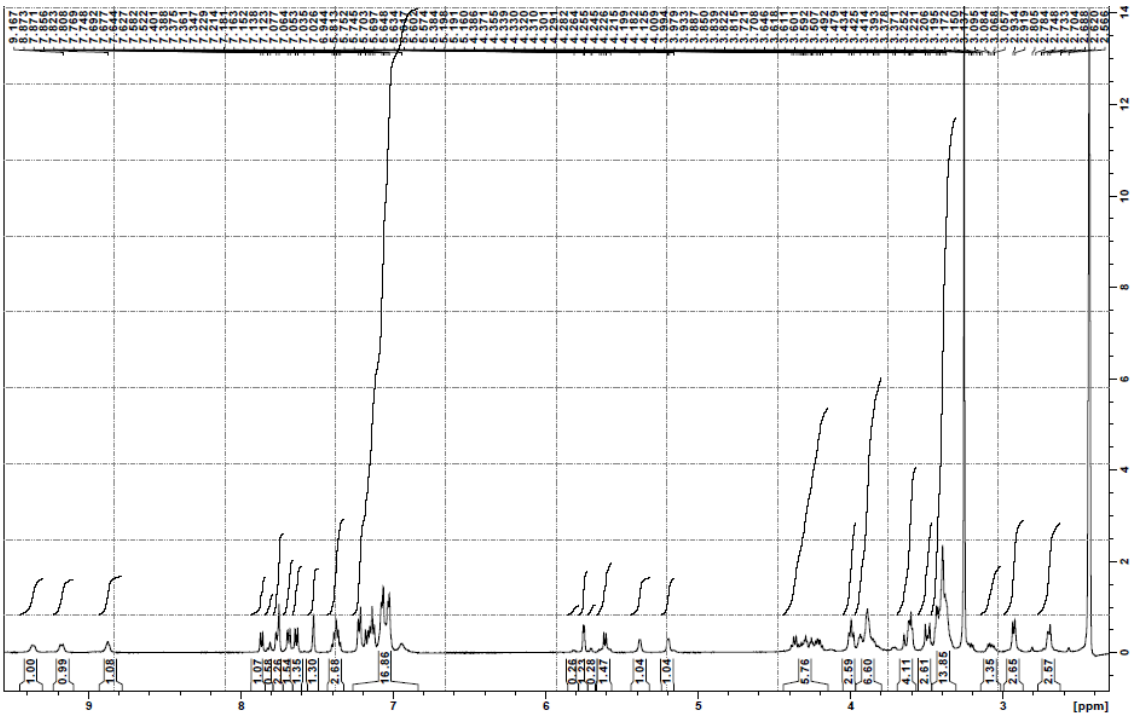

NAP-FF-INV-UMP (**6**)

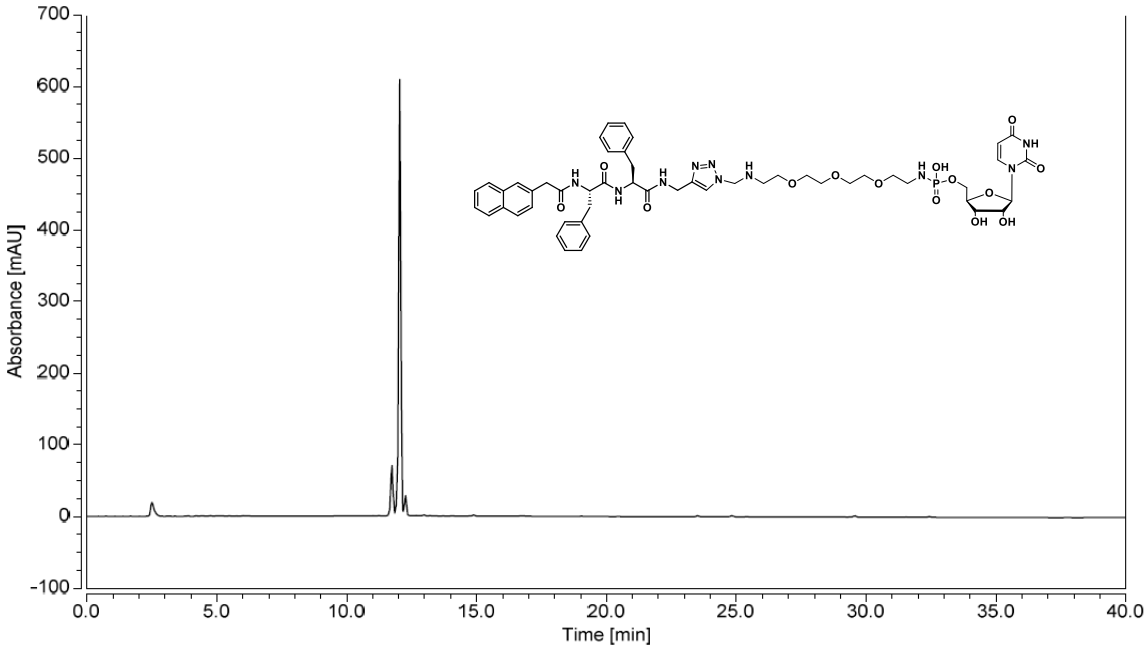


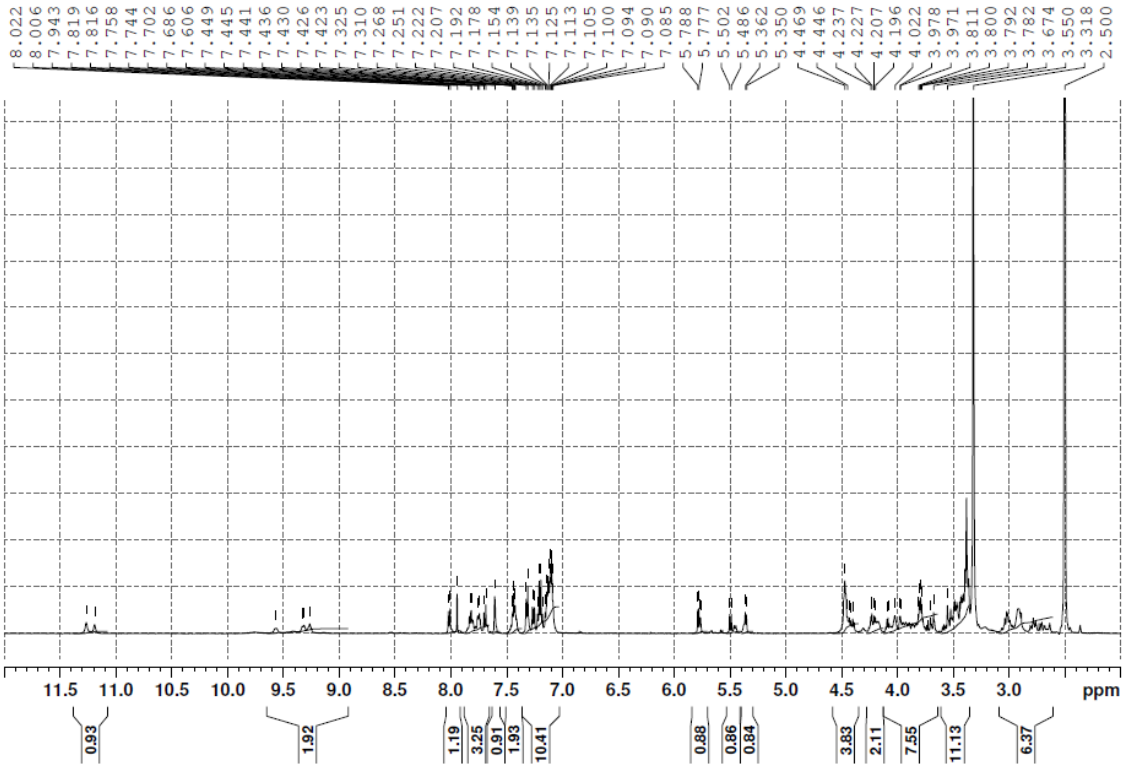

NAP-FF-EtAd (**7**)

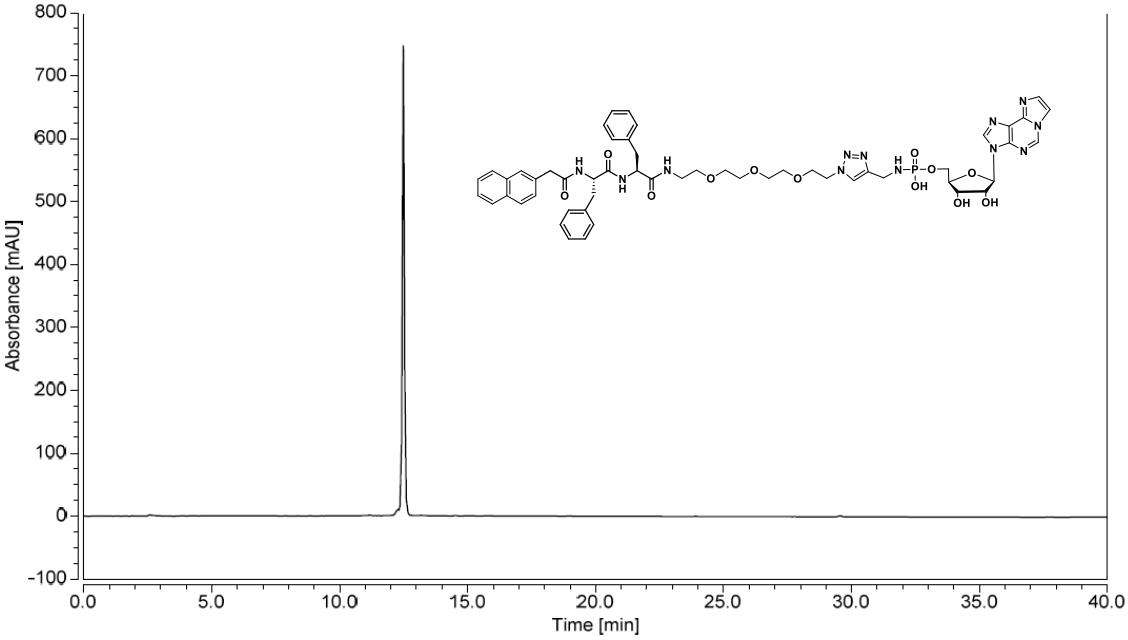


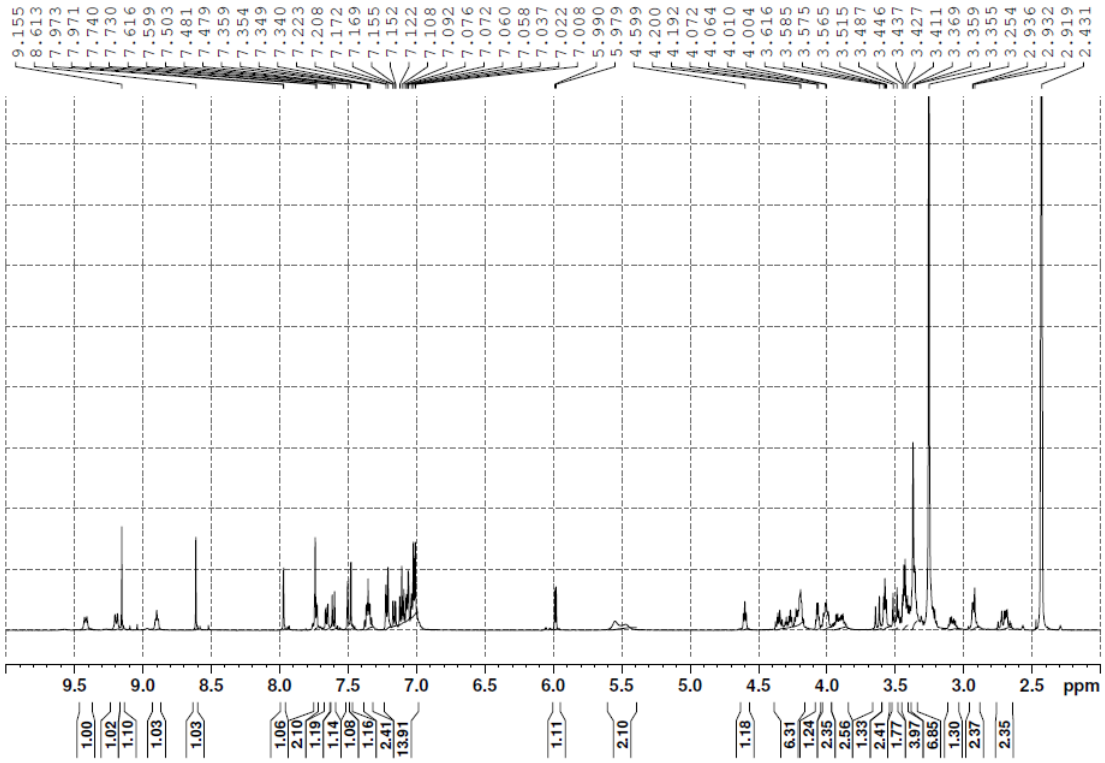

NAP-FF-GEM (**8**)